

THERMODYNAMICS OF GROUPS III-V
AND II-VI COMPOUND SEMICONDUCTORS

BY

KOW-MING CHANG

A DISSERTATION PRESENTED TO THE GRADUATE SCHOOL
OF THE UNIVERSITY OF FLORIDA IN
PARTIAL FULFILLMENT OF THE REQUIREMENTS
FOR THE DEGREE OF DOCTOR OF PHILOSOPHY

UNIVERSITY OF FLORIDA

1985

Copyright 1985

by

Kow-Ming Chang

This project
is
dedicated
to
my parents
for their continual love,
encouragement, and support
throughout the years

ACKNOWLEDGMENTS

The author wishes to express his sincere gratitude to Dr. T.J. Anderson for his guidance, encouragement and friendship throughout the author's graduate program. He is also grateful to the other members of the advisory committee: Dr. L.E. Johns, Dr. J.P. O'Connell, Dr. G.B. Westermann-Clark and Dr. R.T. DeHoff for their valuable time and advice. Special thanks are due to Dr. J.P. O'Connell for his many helpful discussions of this work.

The author wishes to extend his thanks to Ron and Tracy for their help in constructing experimental equipment for this study. He also wishes to extend his appreciation to Ms. Cindy Zimmerman for typing this manuscript.

The author gratefully acknowledges the financial assistance of National Science Foundation for a portion of this study under Grant No. DMR-8012684.

Warm, personal thanks go to the author's family, especially his wife, Yu-Fen, who provided moral support and understanding necessary for this undertaking. Many thanks are also due his daughter, Jennifer, who provided the author with many hours of relaxation.

TABLE OF CONTENTS

	<u>Page</u>
ACKNOWLEDGMENTS.....	iv
ABSTRACT.....	viii
CHAPTERS	
I INTRODUCTION.....	1
1.1 Thermodynamic Properties of the Elemental, III-V, and II-VI Semiconductors.....	1
1.2 Phase Diagrams.....	8
1.3 Previous Calculations of Phase Diagrams.....	15
1.4 Proposed Approach.....	24
II SOLID-LIQUID EQUILIBRIA IN QUATERNARY ($A_xB_yC_{1-x-y}$) $_mC_n$ AND (A_xB_{1-x}) $_m(C_yD_{1-y})_n$ SYSTEMS.....	27
2.1 Solid-Liquid Equilibrium in the (A_xB_{1-x}) $_m(C_yD_{1-y})_n$ System	28
2.1.1 Basic Equilibrium Conditions.....	28
2.1.2 Thermodynamic Properties of the (A_xB_{1-x}) $_m(C_yD_{1-y})_n$ Quaternary Solid Solution.....	31
2.1.3 Liquid Equations for the (A_xB_{1-x}) $_m(C_yD_{1-y})_n$ Quaternary Solid Solution.....	36
2.1.4 Special Cases of the (A_xB_{1-x}) $_m(C_yD_{1-y})_n$ System.....	40
2.2 Solid-Liquid Equilibrium in the ($A_xB_yC_{1-x-y}$) $_mD_n$ System.....	44
2.2.1 Basic Equilibrium Conditions.....	44
2.2.2 Thermodynamic Properties of the ($A_xB_yC_{1-x-y}$) $_mD_n$ Quaternary Solid Solution....	46
2.2.3 Liquidus Equations for the ($A_xB_yC_{1-x-y}$) $_mD_n$ Quaternary Solid Solution.....	49
2.2.4 Special Case of the ($A_xB_yC_{1-x-y}$) $_mD_n$ System.....	51
III THE REDUCED STANDARD STATE CHEMICAL POTENTIAL FOR COMPOUND SEMICONDUCTORS.....	54
3.1 Theory.....	56

	3.1.1 Pressure Dependence of θ_{IC}	56
	3.1.2 Temperature Dependence of θ_{IC}	58
	3.2 Results and Discussion.....	65
IV	THERMODYNAMICS OF BINARY SYSTEMS.....	91
	4.1 Theory.....	93
	4.2 Solution Models.....	97
	4.3 Computational Procedures.....	112
	4.4 Data Base.....	116
	4.4.1 Al-Sb System.....	116
	4.4.2 Ga-Sb System.....	119
	4.4.3 In-Sb System.....	119
	4.4.4 Al-Ga System.....	120
	4.4.5 Ga-In System.....	122
	4.4.6 Al-In System.....	123
	4.5 Results for a Combined Data Set.....	123
	4.6 Data Cross-Prediction in III-Sb Systems.....	143
	4.7 Improved Methods for Data Cross-Prediction.....	156
	4.8 Calculation of Confidence Ellipses.....	181
V	THERMODYNAMICS OF PSEUDOBINARY SYSTEMS.....	191
	5.1 Theory.....	192
	5.1.1 Treatment of Liquid Solution as a Three Component System (Method 1).....	192
	5.1.2 Treatment of Liquid Solution as a Two Component System (Method 2).....	195
	5.2 Computational Procedure.....	197
	5.3 Data Base.....	199
	5.3.1 AlSb-GaSb System.....	199
	5.3.2 AlSb-InSb System.....	200
	5.3.3 GaSb-InSb System.....	201
	5.4 Results and Discussion.....	202
VI	PREDICTIONS OF THE $III_xIII_{1-x}Sb$ TERNARY PHASE DIAGRAMS.....	231
	6.1 Introduction.....	231
	6.2 Calculation of the Phase Diagram.....	233
	6.3 Computational Procedure.....	240
	6.4 Results and Discussion.....	242
VII	THERMODYNAMICS OF THE $Al_xGa_yIn_{1-x-y}Sb$ SYSTEM.....	273
	7.1 Calculation of the Phase Diagram.....	274
	7.2 Computer Program.....	277
	7.3 Results and Discussion.....	280
VIII	SOLID-STATE ELECTROCHEMICAL STUDY OF THE STANDARD GIBBS ENERGY OF FORMATION OF ALUMINUM OXIDE USING A CALCIUM FLUORIDE SOLID ELECTROLYTE.....	292

8.1	Introduction.....	292
8.2	Theory.....	294
8.3	Experiment.....	295
8.4	Materials.....	297
8.5	Procedure.....	300
8.6	Results.....	300
8.7	Discussion.....	302
IX	CONCLUSIONS AND RECOMMENDATIONS.....	313
9.1	Conclusions.....	313
9.2	Recommendations.....	320
	9.2.1 Theory.....	320
	9.2.2 Experiments.....	322
APPENDIX	SAMPLE PROGRAM FOR CALCULATING Al-Ga-In-Sb PHASE DIAGRAM.....	326
REFERENCES.....		328
BIOGRAPHICAL SKETCH.....		344

Abstract of Dissertation Presented to the Graduate School
of the University of Florida in Partial Fulfillment of the
Requirements for the Degree of Doctor of Philosophy

THERMODYNAMICS OF GROUPS III-V
AND II-VI COMPOUND SEMICONDUCTORS

BY

KOW-MING CHANG

December, 1985

Chairman: Dr. Timothy J. Anderson
Major Department: Chemical Engineering

An important consideration for the advancement of process technology surrounding groups III-V and II-VI compound semiconductor materials is an understanding of their thermodynamic behavior, particularly with respect to solid-liquid equilibrium. General, rigorous and unified thermodynamic relationships that can be used to describe phase equilibrium in quaternary systems of the types $(A_xB_yC_{1-x-y})_mD_n$ and $(A_xB_{1-x})_m(C_yD_{1-y})_n$ have been developed. This formulation is easily applied to binary and ternary systems by assigning the value of m, n, x or y to one or zero.

The formulation of the problem requires the evaluation of two types of quantities: one type represents the reduced standard state chemical potential difference and the other represents the ratio of the deviation from ideal solution behavior in the liquid phase to that in the solid phase. The former parameter is a function of the

temperature and pressure of the system and choice of standard state while the latter parameter is a complex function of the temperature, pressure and composition and is normally expressed in terms of solution models. Both quantities can be calculated from well-characterized binary and pseudobinary thermodynamic properties.

Novel thermodynamic sequences have been developed to calculate the pure component standard state chemical potential change and are applied to group III-V and II-VI semiconductors. A number of solution models have been investigated for their ability to represent both the liquid and solid phase thermodynamic properties of the binary and pseudobinary systems. The NRTL equation for liquid solution and simple solution model for solid solution best represent all of the experimental data for the III-Sb, III-III' (except Al-In) and IIISb-III'Sb systems. The best fit parameters for these solid solutions were used to investigate the possibility of the solid phase immiscibility gap in each system. The phase diagrams of the III-III'-Sb and Al-Ga-In-Sb systems are calculated with only binary and pseudobinary parameters and compared with the available measurements. In addition, an improved method is presented to predict the binary phase diagram and ternary system behavior. Finally, the use of a solid state galvanic cell employing CaF_2 as an oxygen ion conductor in high temperature Al systems has been demonstrated for the first time.

CHAPTER I INTRODUCTION

1.1 Thermodynamic Properties of the Elemental, III-V, and II-VI Semiconductors

There are several families of semiconductor materials; the most studied are the elemental semiconductors Si and Ge, formed from atoms located in column IV A of the periodic table. Compound semiconductors are formed from various combinations of atoms located in columns III A and V A, and columns II B and VI A. Silicon is used almost exclusively in the fabrication of semiconductor devices and modern microcircuits, mainly as the results of its ease of preparation, pure single crystal availability, good surface passivation treatments and good electrical properties (1). For some device applications, however, silicon is not the optimum material since its inherent electronic properties and physical parameters are not variable. As a consequence, many important device applications are not possible with silicon (e.g., high speed and frequency devices, light emitting diodes, lasers and infrared photodetectors). Because of this inflexibility, a considerable amount of current investigation has focused on the pure, doped or mixed (multicomponent) III-V and II-VI compound semiconductors to meet the material demands of the devices that cannot be satisfied by silicon.

The III-V materials considered here are formed from one or more of the group III A elements, Al, Ga, or In, and from one or more of the group V A elements, P, As, or Sb. The II-VI semiconductors examined in the study are formed from the elements Cd and Hg in the group II B column and from the element Te in the group VI A column. The motivation for this research is found in two major advantages offered by compound semiconductor materials. The first advantage that compound semiconductors offer is an improvement in the electrical properties. Table I-1 shows electron mobilities, μ_e , observed for the III-V and II-VI binary compounds as well as for Si and Ge. The electron mobility describes the ease with which electrons drift in a material and is defined as the ratio of the average electron drift velocity to the electric field strength, provided Boltzmann statistics are valid to describe the transport. For certain devices (e.g., ultra-high speed, high frequency and low-power logic devices (2)), several compound semiconductors provide significantly larger electron mobilities than elemental semiconductors. As can be seen in Table 1-1, as much as an order of magnitude improvement can be found by using compound semiconductors InSb, InAs and GaAs instead of either Si or Ge.

Also shown in Table 1-1 are the bandgap energy and band structure for each semiconductor. The bandgap energy is the energy difference between the lowest possible conduction band electron state and the highest possible valence band state. Two types of materials have to be distinguished, namely, materials where the wave vectors of the valence band maximum and the conduction band minimum coincide

Table 1-1. Band structure, electron mobility, lattice parameter and bandgap energy for some semiconductor materials at 300°K.

Material	Band Structure	μ_e (cm ² /v.sec)	a (Å)	E _g (eV)
Si	Indirect	1350	5.43	1.11
Ge	Indirect	3900	5.66	0.67
AlSb	Indirect	200	6.14	1.60
GaSb	Direct	5000	6.09	0.70
InSb	Direct	100000	6.48	0.18
AlP	Indirect	80	5.46	2.45
GaP	Indirect	130	5.45	2.26
InP	Direct	4000	5.87	1.28
AlAs	Indirect	180	5.66	2.16
GaAs	Direct	8500	5.65	1.43
InAs	Direct	22600	6.06	0.36
CdTe	Direct	1050	6.48	1.58

Source: Reference (3).

(direct bandgap materials) and materials where this is not the case (indirect bandgap materials). The fundamental band to band transition of direct and indirect bandgap materials leads to different dependencies of the absorption coefficient on photon energy in the region of the bandgap. For a direct semiconductor, the energy of an incident photon ($h\nu$) is transferred directly to minority carrier electron-hole pairs generated at the extrema of the conduction band and valence band. For an indirect semiconductor, however, extra crystal momentum is required to generate the electron-hole pairs. Consequently, the absorption process in the indirect material involves multiple particles, with a considerable decrease in the minority carrier generation rate. For optical devices, e.g., high speed photodetectors and lasers, it is advantageous to utilize a direct band semiconductor to acquire high quantum efficiency.

The second advantage of III-V compound semiconductors over elemental semiconductors is to provide more degrees of freedom in the physical, electrical, and optical properties available to the device engineer. One degree of freedom is in the choice of the binary compound base system that is formed by combining a group III atom with a group V atom to give nine nearly stoichiometric binary compounds. These materials provide, for example, diode sources at several different wavelengths. The other degree of freedom is realized as a result of the ability to form completely miscible substitutional solid solutions independently on both the group III and group V sublattices. For instance, if a single group V element is used, the substitution of one atom on the group III sublattice by

another group III' element results in a III-III'-V ternary solid solution, e.g., $\text{Al}_x\text{Ga}_{1-x}\text{Sb}$. Of course, further substitution of a group III atom by a group III" element gives a quaternary solid solution of the type III-III'-III"-V. In a similar manner, if two different elements are used on each group III and group V sublattice, a quaternary solid solution of the type III-III'-V-V' is obtained, e.g., $\text{Ga}_x\text{In}_{1-x}\text{As}_y\text{P}_{1-y}$.

Figure 1-1 plots the lattice parameter, a , of III-V binary compounds versus the observed room temperature bandgap energy, E_g . The bandgap energy corresponds to the cutoff wavelength ($\lambda(\mu\text{m}) = 1.24/E_g(\text{eV})$) of detection devices. The cutoff wavelength is the longest wavelength to which a detector can respond, i.e., the upper limit of the detectable wavelength range. With solid solution formation, the properties of the III-V solid solutions can be varied continuously between the binary compound limits. Each solid circle symbol in Figure 1-1 represents the values of E_g and a for the particular compound listed. The continuous substitution of a cation for another cation or an anion for another anion is represented by a line (ternary domain). A solid line indicates a direct bandgap transition, while a dashed line indicates an indirect bandgap transition. The substitution of both a cation and anion leads to an enclosed area (quaternary domain) of permissible lattice parameters and corresponding bandgap energies. It is now clear that the physical, electrical, and optical properties of the solid solutions are expanded into a wider spectrum than those in elemental semiconductors.

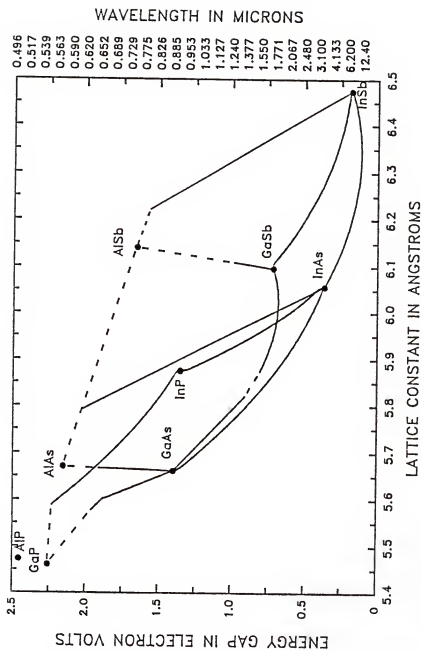


Figure 1-1. Lattice constant, bandgap energy, and corresponding diode emission wavelength for III-V compounds and solid solutions at room temperature: —, direct bandgap; ---, indirect bandgap; •, binary compounds.

Essentially, the entire area enclosed in Figure 1-1 is accessible to the device designer when ternary and quaternary III-V solid solutions are employed. This is particularly important in the design of heterojunction devices in order to specify both the material's bandgap energy (to produce the desired optical properties) and the lattice constant (lattice matching of the active layer to the substrate material is necessary to produce defect free epitaxial layers). For example, ternary $\text{Ga}_x\text{In}_{1-x}\text{P}$ of a particular composition and, therefore, a particular bandgap energy between two binary limits, can be lattice-matched (nearly free for all $\text{Ga}_x\text{Al}_{1-x}\text{V}$) to GaAs or AlAs. Lattice mismatch at the region of the heteroboundary may cause two degrading effects. First, it can introduce deep energy levels into the bandgap which can serve as traps. These traps will function as recombination centers which in turn shortens the minority carrier lifetime and hence limits the efficiency of devices (e.g., infrared diode lasers and photodetectors). Second, lattice mismatch can increase interface charge density and hence increase the interface scattering centers which in turn reduce the carrier mobility across the junction. Also, these centers will increase the free carrier response time.

Similarly, II-VI materials can provide more degrees of freedom in the appropriate properties of the material. For longer wavelength devices, however, one has to rely on II-VI or IV-VI (narrow energy bandgap) compound semiconductors. As an example, photodetectors operating up to about $12\text{ }\mu\text{m}$ are required for thermal imaging systems in the third atmospheric window (4). The cutoff wavelength region

from $\lambda = 0.5 \text{ } \mu\text{m}$ (AlP) to $\lambda = 7.3 \text{ } \mu\text{m}$ (InSb) can be covered by devices on the basis of elemental and III-V semiconductors. The basic problem is to find a suitable semiconductor with an energy gap of about 0.103 eV which corresponds to the desired 12 μm long-wavelength cutoff of detector response. No elemental or III-V semiconductors with an energy gap suitable for an intrinsic detector responding at wavelengths longer than 7.3 μm is available. It is necessary to use a multicomponent II-VI system for which the properties could be tuned in the 7.3-12 μm interval by adjusting the alloy composition.

The $\text{Cd}_x\text{Hg}_{1-x}\text{Te}$ ternary alloy is such a material. This ternary consists of a mixture of the semiconductor CdTe ($E_g = 1.58 \text{ eV}$) and the semimetal HgTe ($E_g = -0.3 \text{ eV}$)(4). The energy gap as well as the lattice constant depend almost linearly on the mole fraction x between two pure compound values, so that it passes through zero at an intermediate composition ($x \approx 0.15$) and is 0.1 eV at $x \approx 0.2$. Materials suitable for intrinsic infrared detectors can be obtained simply by mixing CdTe and HgTe. Although some of these alloys have been studied at particular compositions, the widespread use of these materials is still limited due to technological difficulties.

1.2 Phase Diagrams

The analysis of many solid state processes, e.g., bulk crystal growth, liquid phase epitaxy and laser recrystallization, require the knowledge of the related phase diagrams. They provide information about the solid-liquid equilibrium boundary condition, the distribution of a component between phases, the miscibility of the

participating compounds and the solid phase solubility. The latter is particularly important for device applications because the electronic properties of compound crystals depend on the nature and range of the homogeneity domain. The carrier type and concentration of an intrinsic material are directly related to the deviation from stoichiometry. In order to specify and control these properties during the crystal fabrication and annealing processes, the phase diagrams offer indispensable information. Usually, the equilibrium conditions are given in multidimensional P - T - X diagrams. In practice, however, these are projected unto temperature-composition (T - X) diagrams or unto pressure-temperature (P - T) diagrams.

The III-V and II-VI compound semiconductors of interest here crystallize in the zincblende structure. This is a very open and low density structure where each atom is tetrahedrally-coordinated to its neighbors. The covalent bond, which is dominant in most of these materials, arises from the sharing of the outer four electrons with its four nearest neighbors. Because of this strong bonding, there is a tendency for the two components to cluster together. This appears on the phase diagram as a negative deviation from ideality and formation of a congruently melting compound. A majority of the binary phase diagrams have been experimentally determined (5) (except for the Al-P and Al-As systems). Shown in Figure 1-2 is a generalized binary phase field of these materials. The solid phase is characterized by a single equimolar compound showing a negligible range of stoichiometry. In truth, the binary compounds considered here are not strictly line compounds; some nonstoichiometry

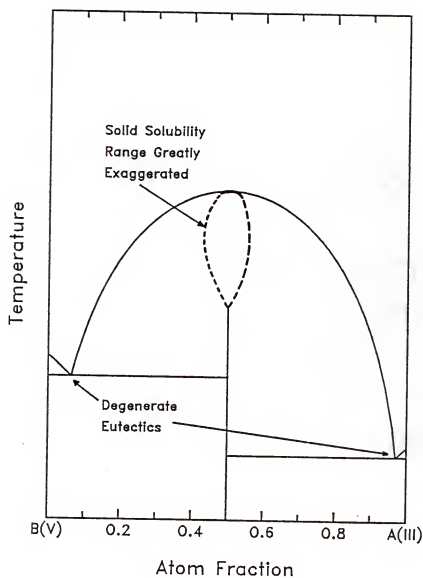


Figure 1-2. Generalized group III-V (or II-VI) binary phase diagram.

is present. The defect calculations of Van Vechten (6), Hurle (7), and Edelein and Mathiot (8) indicate the range of nonstoichiometry is less than 3×10^{-4} , 3×10^{-3} , and 3×10^{-5} mole fraction in GaP, GaAs, and GaSb, respectively. In general, the melting temperature of the congruently melting compound is higher than that of the elements (except for the InSb-Sb case). The systems also exhibit simple eutectic behavior and are often nearly degenerate.

The temperature-composition phase diagram of a generalized ternary A-B-C system is shown in Figure 1-3 using triangular coordinates to represent composition. A single liquidus surface covers nearly the entire phase diagram and the solidus sheet of $(A_x B_{1-x})_{1+\delta} C_{1-\delta}$ is simplified to zero thickness ($\delta = 0$). Furthermore, the solidus sheet would be slightly inclined if the maximum melting temperatures of the alloys are located at nonstoichiometric compositions. These simplifications are nevertheless of great importance to the growth and properties of the alloys. For example, it is preferable to prepare stoichiometric crystals by equilibration with the melt at lower temperatures where the extent of defects is less and therefore inhomogeneities are less severe. Also shown in this figure is the pseudobinary phase diagram which is isomorphous for all systems (except for the GaAs-GaSb system). Experimentally ternary liquidus-solidus data exist for most of the pseudobinary systems while results outside the pseudobinary phase field exist only for a few technologically important systems. The phase diagrams of quaternary and higher systems have received very little attention.

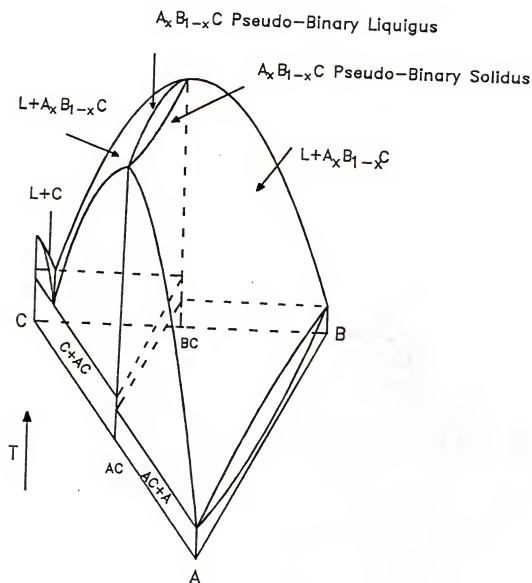


Figure 1-3. Generalized group III-V ternary phase diagram of interest.

To experimentally determine the possible 18 ternary and 15 quaternary phase diagrams of III-V compounds would be an expensive and time-consuming process. In addition, some systems have extremely high vapor pressures (As, P, and Hg dissociation pressures at the melting temperature are 30.8, 0.33, and 12.5 atm for GaP, InAs, and HgTe, respectively (5,9)). Some of the elements are highly reactive (e.g., Al). For these reasons, the development of solution models capable of interpolation and extrapolation of the existing experimental data and prediction of phase diagrams for systems of a greater number of components is desirable.

Figure 1-4 shows a representation of the Ga-In-Sb ternary phase diagram useful for obtaining information related to liquid phase epitaxial growth. Here the lines labeled 573°K through 948°K are liquidus isotherms, i.e., these lines represent isotherma (horizontal) sections through the ternary liquidus at each of the indicated temperatures. Any composition on the 773°K liquidus is in equilibrium with $\text{Ga}_x\text{In}_{1-x}\text{Sb}$ solid at 773°K. The value of the solid composition parameter x in equilibrium with the liquid are given by the isosolidus lines. Two such lines are shown in Figure 1-4, $x = 0.98$ and 0.95 . Each line represents values of the liquid mixture mole fractions in equilibrium with a solid with the specific value of x with which the curve is labeled. Thus, for example, the ternary diagram indicates that for the growth of an $\text{Ga}_{.91}\text{In}_{.19}\text{Sb}$ alloy at 773°K the liquid must have a composition such that the elemental mole fractions are $x_{\text{Ga}} = 0.335$, $x_{\text{In}} = 0.483$, and $x_{\text{Sb}} = 0.182$.

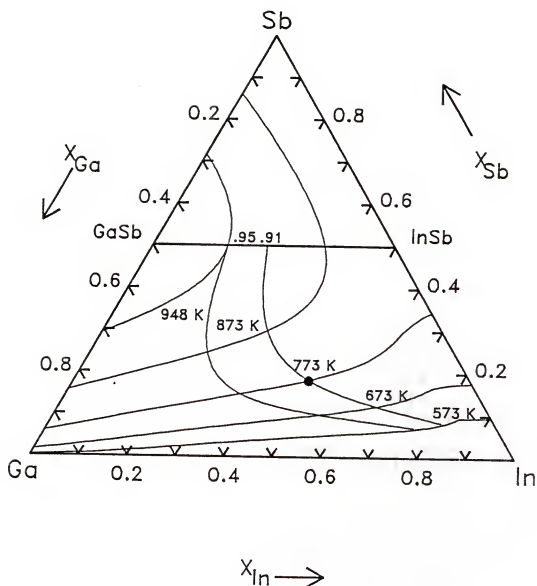


Figure 1-4. Isothermal liquidus and isosolidus concentration curves in the Ga-In-Sb system, •: Ga_{.91}In_{.19}Sb alloy at 773°K.

1.3 Previous Calculations of Phase Diagrams

The calculational techniques for estimating III-V and II-VI phase diagrams have been widely studied by several investigators in the past three decades. Vieland's method (9) has been almost exclusively used to characterize the standard state properties. In this procedure, the chemical potential of pure compound IC, $\mu_{IC}^{0,S}$, as expressed in terms of the chemical potentials of the components in the stoichiometric liquid mixture, $\mu_I^{S1}(T)$ and $\mu_C^{S1}(T)$, the entropy of fusion, ΔS_{IC}^F , the compound melting temperature, T_{IC}^F , and the difference in constant pressure molar heat capacity between the compound IC and its supercooled liquid mixture, ΔC_p . The resulting expression is

$$\begin{aligned} \mu_{IC}^{0,S}(T) = & \mu_I^{S1}(T) + \mu_C^{S1}(T) - \Delta S_{IC}^F (T_{IC}^F - T) \\ & + \Delta C_p (T_{IC}^F - T - T \ln(T_{IC}^F/T)) \end{aligned} \quad (1-1)$$

where $I = A, B$. The term, ΔC_p , is usually taken to be zero or a constant. With this expression for μ_{IC}^0 and with $\Delta C_p = 0$, the equilibrium equations, for a liquid-solid equilibrium in a ternary system $A_x B_{1-x} C$, are given by

$$\gamma_{AC} x_{AC} = \frac{\gamma_A^S \gamma_C^S}{\gamma_A^L \gamma_C^L} x_A x_C \exp\left[-\frac{\Delta S_{AC}^F}{RT} (T_{AC}^F - T)\right] \quad (1-2)$$

$$\gamma_{BC} x_{BC} = \frac{\gamma_B^S \gamma_C^S}{\gamma_B^L \gamma_C^L} x_B x_C \exp\left[-\frac{\Delta S_{BC}^F}{RT} (T_{BC}^F - T)\right] \quad (1-3)$$

where γ is the activity coefficient of the indicated element (A, B, or C) in the liquid or of the compound (AC or BC) in the solid at the temperature of interest, T , and x is the mole fraction of the indicated element in the liquid solution or of the compound in the solid solution. The superscript sl denotes the binary stoichiometric liquid, i.e., $A_{0.5}C_{0.5}$ in Equation (1-2) and $B_{0.5}C_{0.5}$ in Equation (1-3). Typically, the adjustable parameters in a solution model for liquid or solid solution have been obtained by fitting only the available binary or pseudobinary phase diagram. The solution model expression for the activity coefficient has been used not only to represent the component activities along the liquidus curves, but also the stoichiometric liquid activities needed in Equations (1-2) and (1-3).

The simple solution model has been most extensively applied to describe the dependence of the excess integral molar Gibbs energy, G^{XS} , on temperature and composition in binary (10-19), quasibinary (20-24), ternary (24-40) and quaternary (41-47) III-V phase diagram calculations. Considering a simple multicomponent system, the excess integral molar Gibbs energy of solution is expressed by

$$G^{XS} = \frac{1}{2} \sum_{k=1}^n \sum_{\substack{j=1 \\ k \neq j}}^n w_{kj} x_k x_j \quad (1-4)$$

where the interchange energies, $w_{kj} = w_{jk}$ are functions of temperature and pressure and are independent of composition. For condensed phases, the pressure dependence of w_{ij} can be neglected and

w_{ij} is usually permitted a linear temperature dependence, $a + bT$. Strictly regular (random mixing, $S^{XS} = 0$, which is excess entropy of mixing) and athermal ($\Delta H_m = 0$, which is enthalpy of mixing) solutions are two limiting cases of the simple solution. For strictly regular solutions, $w_{xj} = a$ and deviations from ideal solution behavior arise from heat effects, while for athermal solutions, $w_{kj} = bT$ and deviations from ideality arise from entropy rather than heat effects. The activity coefficients are found by the thermodynamic relationship

$$RT \ln \gamma_i = \left[\frac{\partial(N_T G^{XS})}{\partial N_i} \right]_{T,P,\{N_{j \neq i}\}} \quad (1-5)$$

to give

$$RT \ln \gamma_i = \sum_{\substack{j=1 \\ i \neq j}}^n w_{ij} x_j^2 + \sum_{\substack{j=1 \\ i \neq j,k}}^{n-1} \sum_{k=1}^{j-1} x_k x_j (w_{ij} + w_{ik} - w_{kj}) \quad (1-6)$$

where N_T is the total number of moles in the system, N_i is the number of moles of component i , and n is the total number of components.

In general, the simple solution model can be used quite well to describe the symmetric binary systems (e.g., Ga-Sb system). Inspection of Equation (1-4) with $n = 2$ shows that the excess integral molar Gibbs energy is a symmetric function of composition for binary systems. For highly asymmetric system, e.g., Al-Sb system, Anderson et al. (18) and Joullie and Gautier (19) used different values of the interaction parameter on either side of the compound melting point, while Cheng and Pearson (48) added a

concentration-dependent term to the interaction parameter w_{kj} . In a similar manner, a composition-dependent w_{ij} has been used to describe the Ga-In (21) and the Ga-As and Ga-P systems (49). However, the use of two different values w_{kj} for a binary compound in the prediction of a ternary phase diagram will give a discontinuity in the liquidus at quasibinary composition. Also, incorporation of this concentration-dependent term in the calculations contradicts the requirement of the simple solution model where the interaction parameters are functions of temperature and pressure only. For this case, the parameters determined by curve fitting have no thermodynamic significance. In addition, the use of this extra term to calculate the ternary phase diagram will lead to the thermodynamic inconsistency in the ternary activity expressions which invalidate the Gibbs-Duhem requirements.

Although the simple solution model provides a good analytical representation of the binary phase diagrams, it does not yield good values for liquid solution thermodynamic properties when using the same parameters as those determined from a fit of the binary liquidus. For example, values of the enthalpy of mixing predicted from these liquidus fits is always positive, while the available experimental data all show negative values. Indeed, it is expected that the enthalpy of mixing is always negative due to the strong attractive interactions. This is also expressed on the III-V phase diagrams as a negative deviation from ideality and a tendency toward compound formation. Similarly, Thurmond (11) and Arthur (12) found that the interaction coefficients obtained from a fit of the

experimental liquidus or vapor pressure in the arsenide and phosphide systems did not produce the same dependence on T. Panish and Ilegems (16) pointed out that these discrepancies may be due to (a) errors resulting from assumed values for ΔS_{IC}^F and the $\Delta C_p = 0$ approximation in Vieland's liquidus equation (1-1), (b) deviations from simple solution behavior, or (c) uncertainties in the interpretation of the vapor pressure data because some of the quantities necessary in the calculations are not accurately known (for example, reference state vapor pressures for pure liquid As and P). Knobloch et al. (50,51) and Peuschel et al. (52,53) have obtained excellent agreement between calculated and experimental activities and vapor pressures with the use of Krupkowski's asymmetrical formalism for activity coefficients, while Ilegems et al. (54) and Panish (55) demonstrate that a satisfactory agreement between liquidus results and vapor pressures is obtained when an accurate expression for the liquidus is used.

In addition, several other models have been used with Vieland's Equation (1-1) to calculate binary or ternary phase diagrams. Among these are the quasichemical equilibrium model (56,57), truncated Margules expansions (49,58,59), Gaussian formalism (60), orthogonal series expansions (61), Darken's formalism (62), and various associated solution models (63-68). The associated solution model usually is based on the following assumptions: (a) the molecular-like stoichiometric species of unlike atoms called "clusters," "associates," or "complexes" exist in the liquid state; (b) the associated complexes are in a dynamic equilibrium with the non-associated atoms which can be described by a mass action law; (c) the

associated complexes behave as an independent particle, (d) all species are statistically distributed; (e) the excess thermodynamic properties consist of both the physical interactions and chemical reaction contributions. This model has been widely used in strongly interacting systems with their asymmetric properties, which could not be expressed by many of the other models mentioned here. It becomes a complicated problem, however, to generalize this model to multicomponent systems due to a large number of parameters involved in the calculation. For example, it would then be possible to describe a given ΔH_m curve with very different sets of parameters within the experimental error due to the existence of multiple solution. Although a few studies combined the liquid phase properties with the liquidus in the parameter estimation (59,68,69), almost all of these models have used only one set of thermodynamic properties to estimate the model parameters. Some of these results will be discussed in connection with the results of this work in Chapter III and subsequent chapters.

Several attempts have been successfully made to calculate ternary and quaternary phase diagrams with the various solution models by fitting the available binary and pseudobinary phase diagrams. For example, the liquid phase activity coefficients of a simple solution can be calculated with Equation (1-6) in which the binary parameters are obtained by fitting the binary experimental data. To obtain the solid solution activity coefficients, as required for Equations (1-2) and (1-3), the solid solution is usually treated as pseudobinary and as pseudoternary and pseudoquaternary

mixtures for ternary and quaternary systems, respectively. The solid interchange energies which give the best fits to the experimental pseudobinary phase field are generally used. Where the binary liquidus or pseudobinary liquidus and solidus are not available solution model parameters have been estimated from available ternary phase diagram data (16). Foster and Woods (20,70-72) indicate that six pseudobinary sections can be satisfactorily fitted on the assumption that the liquid phase is ideal while the solid phase is athermal. Panish and Ilegems (16) obtained somewhat poorer fits on the assumption that both liquid and solid solutions are strictly regular. Brebrick and Panlener (23) investigated the ideal, strictly regular, athermal, and quasiregular models for each phase and concluded that the strictly regular liquid with the simple solid is the simplest formulation giving satisfactory fits for each of the seven systems with the best experimental data base.

Attempts have been made to calculate the solid and liquid interaction parameters from the physical properties of the constituents. Ilegems (27), Foster (73), and Panish et al. (16) have suggested that the solid phase interaction parameter can be approximately determined from the magnitude of the lattice parameter mismatch between two end compounds, although no analytical expressions were presented to quantify the contribution to the excess Gibbs energy. For example, the solid interaction parameters might be taken to be zero for the AlSb-GaSb, AlP-GaP, and AlAs-GaAs ternary systems since the lattice parameters of the binary compounds are nearly identical. Using the theory of Phillips and Van Vechten (74)

of chemical bonding for calculation of the solid interaction parameters and employing the molar volumes, Hildebrand's solubility parameters (75) and electronegativities (76,77) of the constituent elements for calculation of the liquid interaction parameters, Stringfellow (78,79) calculated the binary and ternary phase diagrams of III-V systems. The agreement with the experimentally determined phase boundaries, however, was poor in several cases. Stringfellow (80) presents a simpler, more accurate semi-empirical model, called the delta-lattice-parameter (DLP) model, based on Phillips' theory (81) to predict the solid interaction parameters for III-V systems. The results of the calculations are in good agreement with those determined by fitting the experimental phase diagram. This model, however, is not always appropriate for II-VI and other systems because DLP model has neglected mismatches in the ionicities and dehydridization factors of two binary compounds (81). Fedders and Muller (82) have recently derived an estimate of the solid interaction parameter from another point of view which ascribes the mixing enthalpy to bond distortions associated with the alloy formation, and relates these to the macroscopic elastic properties of the crystal. They concluded that the results based on elastic crystal parameters yield a similar form for the thermodynamic properties as those estimated by DLP model based on optical crystal parameters.

The predicted results of the ternary and quaternary III-V phase diagrams from the various solution models mentioned above show that no single model can describe the whole ternary or quaternary system

as well as the binary limits and agree with the experimental results. For example, Gratton and Woolley (24) have shown that the simple solution model for Ga-In-Sb system can give values of liquidus isotherms in good agreement with the available experimental data, while the predicted solidus isotherms and isoconcentration lines are very different from the experimental data. In general, the calculated liquidus isotherms are in satisfactory agreement with experimental data, and are insensitive to a small variation in the model parameters. The calculated solidus isotherms, however, are more sensitive to the values of the interaction parameters, and are in fair to poor agreement with experimental data.

In order to obtain a better match of the calculated ternary phase diagram to the experimental one, some investigators (16,19,21,26) have obtained the binary interaction parameters by fitting experimental ternary data. Similarly, this procedure has been adopted in the calculation of some quaternary phase diagrams (43,44,46,83). Stringfellow (80) has reviewed some of the solution models and discussed the discrepancy between the calculated and experimental thermodynamic properties. He concluded that the simple solution model is the most useful approach for phase diagram calculations, but it cannot accurately predict the solution thermodynamic properties. Although the associated solution model as proposed by Liao et al. (68) and Szapiro (84) is a more physical model, it is very complicated and introduces excessive numbers of adjustable parameters, 15 parameters in the ternary calculation and 8 in the binary calculation.

In summary, Vieland's equation (1-1) has been widely used with the various solution models to calculate the binary and multicomponent III-V phase diagrams. This method usually provides a good description of the binary phase diagram, but the predicted results for multicomponent phase equilibria are typically only satisfactory in a small temperature range. In addition, the model parameters obtained by fitting the binary liquidus usually are different (either opposite sign or wrong magnitude) from those obtained by fitting the other experimental thermodynamic properties, e.g., vapor pressures, component activities, and enthalpies of mixing.

1.4 Proposed Approach

This work presents a systematic approach to calculating the binary and multicomponent phase diagrams from available binary or ternary thermodynamic data. Rigorous and unified thermodynamic results that can be used to describe phase equilibrium in quaternary systems of the types $(A_xB_{1-x})_m(C_yD_{1-y})_n$ and $(A_xB_yC_{1-x-y})_mD_n$ are derived in Chapter II. The formulae presented are general and can be easily applied with a specific value of x , y , m or n , to give the binary or ternary limit. The formulation of the problem contains two types of parameters. One designating the reduced standard state chemical potential change, θ_{IC} , that is a function of temperature and pressure and the choice of standard state, and the other representing the deviation of solution behavior from ideality, Γ_{IC} , that is a complex function of temperature, pressure and composition. Both

quantities can be calculated from well-characterized binary and quasibinary thermodynamic properties.

Chapter III discusses the reduced standard state chemical potential change, θ_{IC} , for compound semiconductors. Four different methods of determining θ_{IC} are presented; each requiring a different experimental data base. The techniques are applied to the Al-Sb, Ga-Sb, In-Sb, Hg-Te, and Cd-Te systems and values for θ_{IC} are suggested. A consistent model representation of the available thermodynamic properties as well as the phase diagram in conjunction with the recommended θ_{IC} values is discussed in Chapters IV and V. Chapter IV presents the results for several III-V and III-III' binary systems. The binary data sets, as well as the cross-prediction based on different data sets, are discussed here. The ability of selected solution models to describe all of the available thermodynamic data for the Al-Sb system is considered, while NRTL and simple solution models are compared for the Ga-Sb, In-Sb, Al-Ga, Al-In, and Ga-In systems. In addition, an improved method was presented to predict the liquidus of the binary systems by fixing one or two parameters based on the individual activity and enthalpy of mixing fits or the combined data set fit of the models at the individual melting point and eutectic point or both points of the binary compound. The techniques are applied to the Ga-Sb and In-Sb systems and extended to the Ga-In-Sb system.

In Chapter V, the pseudobinary data sets are discussed. Two different ways for calculating the solid interaction parameters are presented. The first method considers the pseudobinary liquid

mixture as a three component system. Results are obtained by fitting the pseudobinary liquidus and solidus with the formulae of a ternary solution, in which the liquid phase mole fraction of the group III elements and group V elements are required each to sum to 0.5. The second method considers that there only exist two components in the pseudobinary liquid. The calculation is done by fitting the pseudobinary solidus and liquidus data with the formulae for binary isomorphous phase equilibrium. The definition of Θ_{IC} and Γ_{IC} is not the same in both cases.

In Chapter VI, the ternary data sets are discussed. Also, the available liquidus and solidus isotherms of the Ga-In-Sb, Al-Ga-Sb, and Al-In-Sb systems are compared with the results predicted with the use of the NRTL and simple solution models and parameters determined from binary data alone. In Chapter VII, the phase diagram of Al-Ga-In-Sb system is calculated for the first time by the simple solution model with only binary and quasibinary parameters. Chapter VIII demonstrates for the first time the use of a solid state galvanic cell employing CaF_2 as an oxygen ion conductor in high temperature Al systems. Finally, Chapter IX presents a summary of the results of this work and recommendations for future studies.

CHAPTER II
SOLID-LIQUID EQUILIBRIUM IN QUATERNARY $(A_xB_yC_{1-x-y})_mC_n$
AND $(A_xB_{1-x})_m(C_yD_{1-y})_n$ SYSTEMS

There are three basic types of quaternary group III-V solid solutions: 3III:1V or 1III:3V $A_xB_yC_{1-x-y}D$ alloys composed of three binaries with a common anion or cation, respectively (pseudoternary) and 2III:2V $A_xB_{1-x}C_yD_{1-y}$ type in which both the anion and the cation sublattices are mixed. The calculation of quaternary phase diagrams from available binary or ternary thermodynamic data has been presented in the literature (85-87). A general treatment of quaternary solid-liquid equilibrium, however, has not been presented. In previous work, the phase equilibrium equations were arrived at by extending Vilend's approach to binary systems and solution treatments were confined to regular solution or quasi-chemical models. In this chapter, general, rigorous and unified thermodynamic results describing solid-liquid phase equilibrium in quaternary systems of the types $(A_xB_yC_{1-x-y})_mD_n$ and $(A_xB_{1-x})_m(C_yD_{1-y})_n$ are presented.

There are two general methods of determining the equilibrium state. Firstly, if the Gibbs energies of all the phases in the system are known as a function of the appropriate variables (temperature (T), pressure (P), species composition (x)), then the compositions at equilibrium correspond to the minimum Gibbs energy of

the system at a given temperature and pressure. Secondly, if the phases and species present in a system are known, the equilibrium state for such a system is determined by equating the temperature and pressure in each phase and the chemical potential for each species transferable between phases. Of course, the results obtained for a system by these two approaches must be consistent. For convenience of computation, the latter approach is taken here. The direct determination of phase diagrams is easier and more direct than the measurement of the Gibbs energy of solution phases for metallic systems. The number of binary III-V and II-VI systems for which phase boundaries have been well determined is much greater than that for which the thermodynamic properties of solution phases are known. The binary phase diagrams provide a data base for estimating parameters in solution models which are then useful for describing the thermodynamic behavior of higher order systems.

2.1 Solid-Liquid Equilibrium in the $(A_xB_{1-x})_m(C_yD_{1-y})_n$ System

2.1.1 Basic Equilibrium Conditions

Consider a quaternary solid solution which consists of two group III elements, A(1) and B(2), and two group V elements, C(3) and D(4), in equilibrium with the liquid phase. The conditions of solid-liquid equilibrium are given by

$$T^S = T^L \quad (2-1)$$

$$p^S = p^L \quad (2-2)$$

$$\mu_1^s = \mu_1^l \quad (2-3)$$

$$\mu_2^s = \mu_2^l \quad (2-4)$$

$$\mu_3^s = \mu_3^l \quad (2-5)$$

$$\text{and} \quad \mu_4^s = \mu_4^l \quad (2-6)$$

These equations are difficult to work with since the chemical potentials of the solid phase elements cannot be measured (e.g., the mole numbers component 1 cannot be varied over large ranges without also varying the mole 3 or 4 component mole numbers). The quaternary solid solution may be considered as if it were composed of four binary solid compounds with components A_mC_n (13), A_mD_n (14), B_mC_n (23) and B_mD_n (24). Algebraic manipulation of Equations (2-3) to (2-6), with the following definition of the chemical potential of the solid compound component, gives the following set of equilibrium conditions.

$$\mu_{A_mC_n}^s \equiv \mu_{13}^s \equiv m\mu_1^s + n\mu_3^s = m\mu_1^l + n\mu_3^l \quad (2-7)$$

$$\mu_{14}^s = m\mu_1^l + n\mu_4^l \quad (2-8)$$

$$\mu_{23}^s = m\mu_2^l + n\mu_3^l \quad (2-9)$$

$$\text{and} \quad \mu_{24}^s = m\mu_2^l + n\mu_4^l \quad (2-10)$$

The chemical potential of component i in phase j in Equations (2-7) through (2-10) is given by

$$\begin{aligned}\mu_i^j &= \mu_i^{0,j} + RT \ln x_i^j \gamma_i^j \\ &= \mu_i^{0,j} + RT \ln a_i^j\end{aligned}\quad (2-11)$$

where $\mu_i^{0,j}$ is the standard state chemical potential of component i in the phase j , and is a function only of temperature, pressure, and choice of standard state, γ_i^j is the activity coefficient of the component i in phase j and is a function of temperature, pressure and composition, x_i^j is the mole fraction of component i in phase j , and a_i^j is the activity of the component i in the phase j and is the product of composition and activity coefficient.

Furthermore, it can be verified that one of these four equations ((2-9) to (2-10)) is not independent by observing that their left and right members obey the evident relationship

$$\mu_{13}^S + \mu_{24}^S = \mu_{14}^S + \mu_{23}^S \quad (2-12)$$

Equation (2-12) provides a constraint for the chemical potentials of the four binary species in the quaternary mixture and results from the stoichiometry constraint imposed on the solid solution (equal number of group III and V atoms). By imposing the constraint of stoichiometry on the solid, it has been assumed that the homogeneity range of the binary compound is narrow enough to produce negligible variation in the Gibbs energy with composition, i.e.,

$$m\mu_1^S + n\mu_3^S = \mu_{13}^S = g(T,P) \neq f(m,n) \quad (2-13)$$

It is apparent from Eq. (2-13) that the chemical potential of an elemental component in the solid compound can be a strong function of composition m or n along the locus of points of nonstoichiometry, but the sum of the chemical potentials in the binary solid is nearly constant at a given temperature and pressure. The variation of the Gibbs energy of the solid for such nearly stoichiometric compounds CdTe and HgTe had been studied in previous work. Results indicate that neglecting this variation does not lead to significant errors. The maximum value of this variation would be only 0.1 kcal/mol for HgTe and 1 cal/mol for CdTe with homogeneity range of 0.5 at % and 0.001 at %, respectively. The homogeneity ranges suggested for IV-V compounds are all less than 0.001 at %.

2.1.2 Thermodynamic Properties of the $(A_xB_{1-x})_m(C_yD_{1-y})_n$ Quaternary Solid Solution

Denoting n_1^S , n_2^S , n_3^S and n_4^S as the number of moles of elements in the solid and n_{13} , n_{14} , n_{23} and n_{24} as the number of moles of the binary components forming the quaternary solid solution, a single material balance gives the relationship

$$n_1^S = mn_{13} + mn_{14} \quad (2-14)$$

$$n_2^S = mn_{23} + mn_{24} \quad (2-15)$$

$$n_3^S = nn_{13} + nn_{23} \quad (2-16)$$

$$n_4^S = nn_{14} + nn_{24} \quad (2-17)$$

It is obvious from Equations (2-14) through (2-17) that the sum of the first and second equation equals that of the third and fourth times m/n , i.e.,

$$n(n_1^S + n_2^S) = m(n_3^S + n_4^S) \quad (2-18)$$

Equation (2-18) is a stoichiometric constraint placed on the solid solution, i.e., the sum of the moles of the group III elements must be equal to the sum of the moles of the group V elements. The solid phase elemental mole number in terms of the group III sublattice mole fraction x and group V sublattice mole fraction y are

$$n_1^S = mxn_t^S \quad (2-19)$$

$$n_2^S = m(1-x)n_t^S \quad (2-20)$$

$$n_3^S = nyn_t^S \quad (2-21)$$

$$n_4^S = n(1-y)n_t^S \quad (2-22)$$

Here n_t^S is the total number of moles of the solid solution.

$$\begin{aligned} n_t^S &= (n_1^S + n_2^S)/m = (n_3^S + n_4^S)/n \\ &= n_{13} + n_{14} + n_{23} + n_{24} \end{aligned} \quad (2-23)$$

The insertion of Equations (2-19) through (2-23) into Equations (2-14) through (2-17), followed by some algebraic manipulation, results in the following expressions:

$$x = x_{13} + x_{14} \quad (2-24)$$

$$1-x = x_{23} + x_{24} \quad (2-25)$$

$$y = x_{13} + x_{23} \quad (2-26)$$

$$1-y = x_{14} + x_{24} \quad (2-27)$$

Inspection of the set of Equations (2-24) through (2-27) shows that the sum of the first and second equations equals that of the third and fourth. Thus, one of the four Equations (2-14) through (2-17) and (2-24) through (2-27) is redundant and any one of the n_{ij} 's or x_{ij} 's may be arbitrary chosen. For example, taking n_{13} or x_{13} as the arbitrary value, Equations (2-14) through (2-17) and (2-24) through (2-27) then reduce to the following:

$$n_{14} = x n_t - n_{13} \quad (2-28)$$

$$n_{23} = y n_t - n_{13} \quad (2-29)$$

$$n_{24} = (1-x-y)n_t + n_{13} \quad (2-30)$$

and

$$x_{14} = x - x_{13} \quad (2-31)$$

$$x_{23} = y - x_{13} \quad (2-32)$$

$$x_{24} = (1-x-y) + x_{13} \quad (2-33)$$

Clearly, an infinite set of values of n_{13} , n_{14} , n_{23} and n_{24} or x_{13} , x_{14} , x_{23} and x_{24} is obtained by specifying x , y and n_t or x and y in Equations (2-28) through (2-30) or Equations (2-31) through (2-33), respectively. This is a characteristic feature of a quaternary solid solution with mixing on both sublattices. Therefore, it can be deduced that the molar Gibbs energy, g^S , of the solid solution is given as a function of x_{14} , x_{23} , x_{24} , T and P , i.e.,

$$g^S = g^S(x_{14}, x_{23}, x_{24}, T, P) \quad (2-34)$$

or, alternatively, as a function of x , y , x_{13} , T and P , i.e.,

$$g^S = g^S(x, y, x_{13}, T, P) \quad (2-35)$$

The molar Gibbs energy of the quaternary solid solution with respect to binary components is given by

$$g^S = x_{13}\mu_{13}^S + x_{14}\mu_{14}^S + x_{23}\mu_{23}^S + x_{24}\mu_{24}^S \quad (2-36)$$

Alternatively, the molar Gibbs energy of the quaternary solid solution with respect to elements is given by

$$g^S = x\mu_1^S + (1-x)\mu_2^S + y\mu_3^S + (1-y)\mu_4^S \quad (2-37)$$

Substituting Equations (2-31) through (2-33) into Equation (2-36) and

rearranging, we have the following expression:

$$g^S = x_{13}(\mu_{13}^S - \mu_{14}^S - \mu_{23}^S + \mu_{24}^S) + x\mu_{14}^S + y\mu_{23}^S + (1-x-y)\mu_{24}^S \quad (2-38)$$

while algebraic transformation of Equation (2-37) leads to

$$g^S = x(m\mu_1^S + n\mu_4^S) + y(m\mu_2^S + n\mu_3^S) + (1-x-y)(m\mu_2^S + n\mu_4^S) \quad (2-39)$$

comparing Equations (2-38) and (2-39) which must be identical for all choices of the value x , y and x_{13} yields the relationships between chemical potentials

$$\mu_{14}^S \equiv m\mu_1^S + n\mu_4^S \quad (2-40)$$

$$\mu_{24}^S \equiv m\mu_2^S + n\mu_4^S \quad (2-41)$$

$$\mu_{23}^S \equiv m\mu_2^S + n\mu_3^S \quad (2-42)$$

$$\mu_{13}^S \equiv m\mu_1^S + n\mu_3^S \quad (2-43)$$

and

$$\mu_{13}^S + \mu_{24}^S - \mu_{14}^S - \mu_{23}^S \equiv 0 \quad (2-44)$$

Not surprisingly, the constraint of Equation (2-44) is thermodynamically equivalent to Equation (2-12). Note that Equations (2-40) through (2-44) are satisfied regardless of the choice of the arbitrary n_{ij} or x_{ij} .

2.1.3 Liquidus Equations for the $(A_xB_{1-x})_m(C_yD_{1-y})_n$ Quaternary Solid Solution

In order to put Equations (2-7) through (2-10) into a workable and convenient form the two quantities mentioned in Chapter I (θ_{ij} , the reduced standard state chemical potential difference, and r_{ij} , the ratio of liquid phase to solid phase activity coefficients) are introduced. Substituting Equation (2-11) for each term in Equations (2-7) to (2-10) yields

$$x_{13} = r_{13}(x_1^1)^m(x_3^1)^n \exp(-\theta_{13}) \quad (2-45)$$

$$x_{14} = r_{14}(x_1^1)^m(x_4^1)^n \exp(-\theta_{14}) \quad (2-46)$$

$$x_{23} = r_{23}(x_2^1)^m(x_3^1)^n \exp(-\theta_{23}) \quad (2-46)$$

and

$$x_{24} = r_{24}(x_2^1)^m(x_4^1)^n \exp(-\theta_{24}) \quad (2-47)$$

where θ_{ij} and r_{ij} are defined by

$$\theta_{ij} \equiv \frac{\mu_{ij}^{o,s} - m\mu_i^{o,l} - n\mu_j^{o,l}}{RT} ; ij = 13, 14, 23, 24 \quad (2-49)$$

and

$$r_{ij} \equiv \frac{(\gamma_i^1)^m(\gamma_j^1)^n}{\gamma_{ij}^s} ; ij = 13, 14, 23, 24 \quad (2-50)$$

It is obvious that the subscripts i and j in Equations (2-45) to

(2-50) refer to liquid phase components, while the subscript ij refers to a solid component. For convenience, the mole fraction superscript indicating the phase is dropped. Moreover, by purely algebraic operations, Equations (2-45) through (2-48) are transformed into

$$x_{13} = \Gamma_{13}^{1/m} x_{13}^{(m-1)/m} x_1 x_3^{n/m} e^{-\theta_{13}/m} \equiv P_{13} x_1 \quad (2-51)$$

$$x_{14} = \Gamma_{14}^{1/m} x_{14}^{(m-1)/m} x_1 x_4^{n/m} e^{-\theta_{14}/m} \equiv P_{14} x_1 \quad (2-52)$$

$$x_{23} = \Gamma_{23}^{1/m} x_{23}^{(m-1)/m} x_2 x_3^{n/m} e^{-\theta_{23}/m} \equiv P_{23} x_2 \quad (2-53)$$

and

$$x_{24} = \Gamma_{24}^{1/m} x_{24}^{(m-1)/m} x_2 x_4^{n/m} e^{-\theta_{24}/m} \equiv P_{24} x_2 \quad (2-54)$$

where P_{ij} is identified as

$$P_{ij} \equiv \Gamma_{ij}^{1/m} x_{ij}^{(m-1)/m} x_j^{n/m} \exp(-\theta_{ij}/m); \quad ij = 13, 14, 23, 24 \quad (2-55)$$

Substituting Equations (2-51) and (2-52) into Equation (2-24) gives

$$x = (P_{13} + P_{14}) x_1 \quad (2-56)$$

The distribution coefficient of component 1, K_1 , is defined by

$$K_1 \equiv \frac{x}{x_1} = P_{13} + P_{14} \quad (2-57)$$

Substituting Equations (2-53) and (2-54) into Equation (2-25) gives

$$1 - x = (P_{23} + P_{24})x_2 \quad (2-58)$$

Substituting Equation (2-56) into Equation (2-58) followed by some algebraic manipulation results in the following implicit expression for the liquid 1 composition in equilibrium

$$x_1 = \frac{1 - (1 - x_3 - x_4)(P_{23} + P_{24})}{(P_{13} + P_{14}) - (P_{23} + P_{24})} \quad (2-59)$$

Similarly, one can find

$$x_2 = \frac{1 - (1 - x_3 - x_4)(P_{13} + P_{14})}{(P_{23} + P_{24}) - (P_{13} + P_{14})} \quad (2-60)$$

Substituting Equation (2-59) into Equation (2-56) or Equation (2-60) into Equation (2-58) gives

$$x = \frac{(P_{13} + P_{14})[1 - (1 - x_3 - x_4)(P_{23} + P_{24})]}{(P_{13} + P_{14}) - (P_{23} + P_{24})} \quad (2-61)$$

Substituting Equations (2-52) and (2-54) into Equation (2-26) gives

$$y = P_{13}x_1 + P_{23}x_2 \quad (2-62)$$

Substituting Equations (2-59) and (2-60) into Equation (2-62) gives

$$y = \frac{(P_{13} - P_{23}) - (1 - x_3 - x_4)(P_{13}P_{24} - P_{14}P_{23})}{(P_{13} + P_{14}) - (P_{23} + P_{24})} \quad (2-63)$$

If we choose x_{13} as an arbitrary value and substitute Equations (2-31) to (2-33) into Equations (2-59), (2-61) and (2-63), we find

$$x_1 = x_1(T, P, x, y, x_{13}, x_1, x_3, x_4) \quad (2-64)$$

$$x = x(T, P, x, y, x_{13}, x_1, x_3, x_4) \quad (2-65)$$

and

$$y = y(T, P, x, y, x_{13}, x_1, x_3, x_4) \quad (2-66)$$

In addition to these three equations, we have one constraint Equation (2-12). Moreover, by using ordinary algebraic operations, Equation (2-12) is transformed into

$$x_{13} = \frac{\Gamma_{14}\Gamma_{23}}{\Gamma_{13}\Gamma_{24}} \cdot \frac{X_{14}X_{23}}{X_{24}} \exp(\Theta_{14} + \Theta_{23} - \Theta_{13} - \Theta_{24}) \quad (2-67)$$

$$= x_{13}(x, y, x_{13}, T, P) \quad (2-68)$$

Applying the Gibbs' phase rule to solid-liquid equilibrium in a quaternary system, we find that the number of degrees of freedom is equal to four. It can be seen if T , P , x_3 and x_4 are specified, then x_1 , x , y and x_{13} can be completely determined by Equations (2-59), (2-61), (2-63) and (2-67) and the system becomes invariant.

It is now clear that the working Equations (2-59), (2-61), (2-63) and (2-67) describing the phases equilibria are implicitly

complex relations for T , P , x , y , x_{13} , x_1 , x_3 and x_4 and involve only two thermodynamic quantities θ_{ij} and Γ_{ij} .

2.1.4 Special Cases of the $(A_x B_{1-x})_m (C_y D_{1-y})_n$ System

In this section, several special cases that result from the above general working equations are discussed. These equations are easily applied to ternary and binary systems by assigning the value of m , n , x or y to one or zero. The ideal solution phase diagram is generated by letting the Γ_{ij} terms equal unit.

(1) $m = n = 1$:

The quaternary systems are now of the type $A_x B_{1-x} C_y D_{1-y}$ (e.g., $Ga_x In_{1-x} P_y As_{1-y}$, $Al_x Ga_{1-x} As_y Sb_{1-y}$ and $Al_x Ga_{1-x} P_y As_{1-y}$). The general working Equations (2-55), (2-59), (2-61), (2-63) and (2-67) are reduced to a simpler form and given by

$$P_{ij} \equiv \Gamma_{ij} x_j \exp(-\theta_{ij}) ; ij = 13, 14, 23, 24 \quad (2-69)$$

$$x_1 = \frac{1 - (1 - x_3 - x_4)(P_{23} + P_{24})}{(P_{13} + P_{14}) - (P_{23} + P_{24})} \quad (2-70)$$

$$x = \frac{(P_{13} + P_{14})[1 - (1 - x_3 - x_4)(P_{23} + P_{24})]}{(P_{13} + P_{14}) - (P_{23} + P_{24})} \quad (2-71)$$

$$y = \frac{(P_{13} - P_{23}) - (1 - x_3 - x_4)(P_{13}P_{24} - P_{14}P_{23})}{(P_{13} + P_{14}) - (P_{23} + P_{24})} \quad (2-72)$$

and

$$x_{13} = \frac{\Gamma_{14}\Gamma_{23}}{\Gamma_{13}\Gamma_{24}} \cdot \frac{x_{14}x_{23}}{x_{24}} \exp(\theta_{14} + \theta_{23} - \theta_{13} - \theta_{24}) \quad (2-73)$$

The distribution coefficient of component 1, K_1 , is given by

$$K_1 \equiv \frac{x}{x_1} = p_{13} + p_{14} = r_{13}x_3e^{-\theta_{13}} + r_{14}x_4e^{-\theta_{14}} \quad (2-74)$$

(2) $y = 1$ (i.e., $x_{14} = x_{24} = x_4 = 0$):

The general quaternary system $(A_xB_{1-x})_m(C_yD_{1-y})_n$ is now reduced to the general ternary system of the type $(A_xB_{1-x})_mC_n$. The results are given by

$$p_{ij} = r_{ij}^{1/m} x_{ij}^{(m-1)/m} x_j^{n/m} \exp(-\theta_{ij}/m) ; ij = 13, 23 \quad (2-75)$$

$$x_1 = \frac{1 - (1 - x_3)p_{23}}{p_{13} - p_{23}} \quad (2-76)$$

$$x = \frac{\frac{1}{p_{23}} - (1 - x_3)}{\frac{1}{p_{23}} - \frac{1}{p_{13}}} \quad (2-77)$$

The distribution coefficient of component 1, K_1 , is then

$$K_1 \equiv \frac{x}{x_1} = p_{13} \quad (2-78)$$

Note that $p_{14} = p_{24} = 0$, and x_{13} is equal to x in the formulation $(A_xB_{1-x})_mC_n$. In addition, we do not have a constraint Equation (2-12) for this ternary system. Inspection of the set of Equations (2-75) to (2-78) shows that the results are completely identical to those equations directly derived for the general ternary system. It should be obvious that the similar results were obtained for the case of $y = 0$.

(3) $m = n = 1, y = 1$ (i.e., $x_{14} = x_{24} = x_4 = 0$)

The general quaternary system is now ternary system of the type $A_xB_{1-x}C$ (e.g., $Ga_xIn_{1-x}Sb$, $Al_xGa_{1-x}Sb$, $Al_xIn_{1-x}Sb$ and $Al_xGa_{1-x}As$).

After some algebraic operations, the working equations are given by

$$x_1 = \frac{\frac{1}{x_3} - (1 - x_3)r_{23}e^{-\theta_{23}}}{r_{13}e^{-\theta_{13}} - r_{23}e^{-\theta_{23}}} \quad (2-79)$$

$$x = \frac{x_3(1 - x_3) - \frac{1}{r_{23}} \exp(\theta_{23})}{\frac{1}{r_{13}} \exp(\theta_{13}) - \frac{1}{r_{23}} \exp(\theta_{23})} \quad (2-80)$$

and the distribution coefficient of component 1, K_1 , is given by

$$K_1 \equiv \frac{x}{x_1} = r_{13}x_3 \exp(-\theta_{13}) = P_{13} \quad (2-81)$$

Note that x_{13} is equal to x in the formulation $A_xB_{1-x}C$. It is apparent that the similar results can be obtained for the case of $m = n = 1$ and $y = 0$.

(4) $x = 1$ (i.e., $x_{23} = x_{24} = x_2 = 0$):

The quaternary systems of the type $(A_xB_{1-x})_m(C_yD_{1-y})_n$ are reduced to the ternary systems of the type $A_m(C_yD_{1-y})_n$. The results are given by

$$P_{ij} = r_{ij}^{1/m} x_{ij}^{(m-1)/m} x_j^{n/m} \exp(-\theta_{ij}/m) ; ij = 13, 14 \quad (2-82)$$

$$x_1 = \frac{1}{p_{13} + p_{14}} \quad (2-83)$$

and

$$y = \frac{p_{13}}{p_{13} + p_{14}} \quad (2-84)$$

The distribution coefficient of component 1, K_1 , is given by

$$K_1 \equiv \frac{y}{x_1} = p_{13} \quad (2-85)$$

Note that $p_{23} = p_{24} = 0$, and x_{13} is equal to y in the formulation

$A_m(C_y D_{1-y})_n$.

(5) $x = y = 1$ (i.e., $x_{14} = x_{24} = x_{23} = 0$, $x_2 = x_4 = 0$):

The quaternary systems of the type $(A_x B_{1-x})_m (C_y D_{1-y})_n$ are reduced to the binary systems of the type $A_m C_n$ (13). The results are given by

$$p_{13} = r_{13}^{1/m} x_{13}^{(m-1)/m} x_3^{n/m} \exp(-\theta_{13}/m) \quad (2-86)$$

and

$$x_1 = \frac{1}{p_{13}} \quad (2-87)$$

Substituting Equations (2-86) into (2-87) and rearranging,

$$(a_1^1)^m (a_3^1)^n = \exp(\theta_{13}) \quad (2-88)$$

Here we use the fact that $x_{13} = y_{13}^S = 1$ and $p_{14} = p_{24} = p_{23} = 0$.

(6) $m = n = 1$, $x = y = 1$ (i.e., $x_{14} = x_{23} = x_{24} = 0$, $x_2 = x_4 = 0$):

The quaternary systems of the type $(A_x B_{1-x})_m (C_y D_{1-y})_n$ are reduced to the binary systems of the type AC (13). The results are given by

$$p_{13} = r_{13} x_3 \exp(-\theta_{13}) \quad (2-89)$$

and

$$x_1 = \frac{1}{p_{13}} \quad (2-90)$$

After rearranging Equations (2-89) and (2-90), we have

$$a_1^1 a_3^1 = \exp(\theta_{13}) \quad (2-91)$$

Here we use the fact that $x_{13} = y_{13}^S = 1$ and $p_{14} = p_{24} = p_{23} = 0$.

2.2 Solid-Liquid Equilibrium in the $(A_x B_y C_{1-x-y})_m D_n$ System

2.2.1 Basic Equilibrium Conditions

In this section, the quaternary solid solution is considered which is composed of three elements A (1), B (2) and C (3) of the group III or V column of the periodic table and one element D (4) of either the group V or III column, respectively, in equilibrium with the liquid phase. The equilibrium conditions are given by

$$T^S = T^L \quad (2-92)$$

$$p^S = p^I \quad (2-93)$$

$$\mu_1^S = \mu_1^I \quad (2-94)$$

$$\mu_2^S = \mu_2^I \quad (2-95)$$

$$\mu_3^S = \mu_3^I \quad (2-96)$$

$$\mu_4^S = \mu_4^I \quad (2-97)$$

Again, the effect of defects, i.e., nonstoichiometry, is neglected. With this treatment, the solid solution can be considered as a pseudoternary solid solution and represented by

$(A_m D_n)_x (B_m D_n)_y (C_m D_n)_{1-x-y}$, where binary compounds $A_m D_n$ (14), $B_m D_n$ (24) and $C_m D_n$ (34) are completely miscible within some temperature range. Equations (2-94) through (2-97) then reduce to the following:

$$\mu_{14}^S = m\mu_1^I + n\mu_4^I \quad (2-98)$$

$$\mu_{24}^S = m\mu_2^I + n\mu_4^I \quad (2-99)$$

$$\text{and} \quad \mu_{34}^S = m\mu_3^I + n\mu_4^I \quad (2-100)$$

The chemical potential of component i in phase j in Equations (2-98) through (2-100) is given by Equation (2-11). Unlike the previous quaternary system $(A_x B_{1-x})_m (C_y D_{1-y})_n$, there is no extra chemical potential constraint imposed on the solid solution of the quaternary system $(A_x B_y C_{1-x-y})_m D_n$.

2.2.2 Thermodynamic Properties of the $(A_xB_yC_{1-x-y})_mD_n$ Quaternary Solid Solution

Let n_1 , n_2 , n_3 and n_4 denote the number of moles of elements and n_{14} , n_{24} and n_{34} denote the number of moles of the binary components forming the quaternary solid solution. Then, mass balance provides

$$n_1 = mn_{14} \quad (2-101)$$

$$n_2 = mn_{24} \quad (2-102)$$

$$n_3 = mn_{34} \quad (2-103)$$

and
$$n_4 = n(n_{14} + n_{24} + n_{34}) \quad (2-104)$$

It is apparent from Equations (2-101) to (2-104) that the sum of the first three equations is equal to the fourth equation times m/n , i.e.,

$$n(n_1 + n_2 + n_3) = mn_4 \quad (2-105)$$

Equation (2-105) is a constraint of stoichiometry imposed on the solid solution, i.e., the sum of the moles of the group III elements must equal the sum of the moles of the Group V elements. Setting

$$n_1 = mxn_t \quad (2-106)$$

$$n_2 = myn_t \quad (2-107)$$

$$n_3 = m(1 - x - y)n_t \quad (2-108)$$

and
$$n_4 = n n_t \quad (2-109)$$

where
$$n_t = n_4/n = (n_1 + n_2 + n_3)/m$$

$$= n_{14} + n_{24} + n_{34} \quad (2-110)$$

is the total number of moles of the solid solutions. Substituting Equations (2-106) to (2-110) into Equations (2-101) to (2-104) gives

$$x = x_{14} \quad (2-111)$$

$$y = x_{24} \quad (2-112)$$

and
$$1 - x - y = x_{34} \quad (2-113)$$

It is now clear that the molar Gibbs energy, g^S , of the solid solution can be expressed as a function of x_{14} , x_{24} , T and P or x , y , T and P , i.e.,

$$g^S = g^S(x_{14}, x_{24}, T, P)$$

$$= g^S(x, y, T, P) \quad (2-114)$$

The molar Gibbs energy of the quaternary solid solution with respect to binary component is given by

$$g^S = x_{14} \mu_{14} + x_{24} \mu_{24} + x_{34} \mu_{34} \quad (2-115)$$

Also, the molar Gibbs free energy of the quaternary solid solution with respect to elements is given by

$$g^S = x\mu_1^S + y\mu_2^S + (1 - x - y)m\mu_3^S + n\mu_4^S \quad (2-116)$$

Substituting Equations (2-111) to (2-113) into Equation (2-115) gives

$$g^S = x\mu_{14}^S + y\mu_{24}^S + (1 - x - y)\mu_{34}^S \quad (2-117)$$

Rearranging Equation (2-116) gives

$$g^S = x(m\mu_1^S + n\mu_4^S) + y(m\mu_2^S + n\mu_4^S) + (1 - x - y)(m\mu_3^S + n\mu_4^S) \quad (2-118)$$

Comparing Equations (2-117) and (2-118) results in the following relationship between chemical potentials

$$\mu_{14}^S = m\mu_1^S + n\mu_4^S \quad (2-119)$$

$$\mu_{24}^S = m\mu_2^S + n\mu_4^S \quad (2-120)$$

$$\text{and} \quad \mu_{34}^S = m\mu_3^S + n\mu_4^S \quad (2-121)$$

In fact, as can be seen from Equations (2-119) to (2-121), the compound chemical potentials are consistent with Equations (2-98) to (2-100).

2.2.3 Liquidus Equations for the $(A_xB_yC_1-x-y)_mD_n$ Quaternary Solid Solution

Compared to the derivation of the quaternary system $(A_xB_{1-x})_m(C_yD_{1-y})_n$, the algebra in the following derivation is simpler and less tedious and proceeds according to the same pattern. Again, the two quantities θ_{ij} and Γ_{ij} are introduced as mentioned above to produce Equations (2-98) to (2-100) into a concise and convenient form. Substituting Equation (2-11) for each term in Equations (2-98) to (2-100) gives

$$x_{14} = \Gamma_{14} (x_1^1)^m (x_4^1)^n \exp(-\theta_{14}) \quad (2-122)$$

$$x_{24} = \Gamma_{24} (x_2^1)^m (x_4^1)^n \exp(-\theta_{24}) \quad (2-123)$$

$$\text{and} \quad x_{34} = \Gamma_{34} (x_3^1)^m (x_4^1)^n \exp(-\theta_{34}) \quad (2-124)$$

where θ_{ij} and Γ_{ij} are defined by Equations (2-49) and (2-50), respectively. For convenience, the superscript to indicate the phase on mole fractions will not be used in the following derivation. Moreover, by some algebraic manipulation, Equations (2-122) to (2-124) are transformed into

$$x_{14} = \Gamma_{14}^{1/m} x_{14}^{(m-1)/m} x_1 x_4^{n/m} \exp(-\theta_{14}/m) \equiv P_{14} x_1 \quad (2-125)$$

$$x_{24} = \Gamma_{24}^{1/m} x_{24}^{(m-1)/m} x_2 x_4^{n/m} \exp(-\theta_{24}/m) \equiv P_{24} x_2 \quad (2-126)$$

$$\text{and} \quad x_{34} = \Gamma_{34}^{1/m} x_{34}^{(m-1)/m} x_3 x_4^{n/m} \exp(-\theta_{34}/m) \equiv P_{34} x_3 \quad (2-127)$$

where P_{ij} is defined by Equation (2-55). Substituting Equations (2-125) to (2-127) into (2-111) to (2-113) gives

$$x = P_{14}x_1 \quad (2-128)$$

$$y = P_{24}x_2 \quad (2-129)$$

$$\text{and} \quad 1 - x - y = P_{34}x_3 \quad (2-130)$$

The distribution coefficient, K , is defined by

$$K \equiv \frac{\text{mole fraction in the solid solution}}{\text{mole fraction in the liquid solution}} \quad (2-131)$$

For example, the distribution coefficient of component 1, K_1 , is given by

$$K_1 \equiv \frac{x}{x_1} = P_{14} \quad (2-132)$$

Substituting Equations (2-128) and (2-129) into (2-130) followed by some algebraic manipulation results in the following implicit expression for the liquid 1 composition in equilibrium

$$x_1 = \frac{1 - (1 - x_4)P_{34}}{P_{14} - P_{34}} - x_2 \cdot \frac{P_{24} - P_{34}}{P_{14} - P_{34}} \quad (2-133)$$

Substituting Equation (2-133) back into Equation (2-125) gives

$$x = P_{14} \left[\frac{1 - (1 - x_4)P_{34}}{P_{14} - P_{34}} - x_2 \cdot \frac{P_{24} - P_{34}}{P_{14} - P_{34}} \right] \quad (2-134)$$

It is apparent from Equations (2-129), (2-133) and (2-134) that x_1 , x and y are an implicit function of T , P , x , y , x_1 , x_2 and x_4 , i.e.,

$$x_1 = x_1(T, P, x, y, x_1, x_2, x_4) \quad (2-135)$$

$$x = x(T, P, x, y, x_1, x_2, x_4) \quad (2-136)$$

and
$$y = y(T, P, x, y, x_1, x_2, x_4) \quad (2-137)$$

As indicated above, the number of degrees of freedom is equal to four for a quaternary system. It can be seen if T , P , x_2 and x_4 are specified, then x_1 , x and y can be completely determined by Equations (2-129), (2-133) and (2-134) and the system becomes invariant.

It also is apparent that these equations described the phases equilibria are implicitly complex relations for T , P , x , y , x_1 , x_2 and x_4 and involve only two quantities θ_{ij} and Γ_{ij} which can be calculated from the available binary or ternary thermodynamic data.

2.2.4 Special Case of the $(A_x B_y C_{1-x-y})_m D_n$ System

One can obtain all possible special cases by putting m , n , x or y to be equal to one or zero in the above general solutions. However, the results of equilibrium in the ternary and binary limit will be the same for both systems. Thus, only one special case will be presented in this section. The ideal solution phase diagram is generated by letting the Γ_{ij} terms equal unity.

(1) $m = n = 1$:

The quaternary solid solutions of this case are represented as $A_x B_y C_{1-x-y} D$ (e.g., $Al_x Ga_y In_{1-x-y} Sb$ and $InP_x As_y Sb_{1-x-y}$). Substituting Equation (2-55) into Equations (2-129), (2-133) and (2-134) followed by some algebraic manipulations results in the following implicit expressions for the liquid and solid compositions in equilibrium

$$x_1 = \frac{\frac{1}{x_4} - \Gamma_{34}(1 - x_4)e^{-\theta_{34}}}{\Gamma_{14}e^{-\theta_{14}} - \Gamma_{34}e^{-\theta_{34}}} - x_2 \left(\frac{\Gamma_{24}e^{-\theta_{24}} - \Gamma_{34}e^{-\theta_{34}}}{\Gamma_{14}e^{-\theta_{14}} - \Gamma_{34}e^{-\theta_{34}}} \right) \quad (2-138)$$

$$x = \frac{x_4(1 - x_4) - \frac{1}{\Gamma_{34}} \exp(\theta_{34})}{\frac{1}{\Gamma_{14}} \exp(\theta_{14}) - \frac{1}{\Gamma_{34}} \exp(\theta_{34})} - x_2 x_4 \Gamma_{14} e^{-\theta_{14}} \left(\frac{\Gamma_{24}e^{-\theta_{24}} - \Gamma_{34}e^{-\theta_{34}}}{\Gamma_{14}e^{-\theta_{14}} - \Gamma_{34}e^{-\theta_{34}}} \right) \quad (2-139)$$

and

$$y = \Gamma_{24} x_2 x_4 e^{-\theta_{24}} \quad (2-140)$$

The distribution coefficient of component i , K_i , is given by

$$K_i = \Gamma_{ij} x_j \exp(-\theta_{ij}) ; ij = 14, 24, 34 \quad (2-141)$$

In summary, the general, rigorous and unified thermodynamic results that can be used to describe phase equilibria in quaternary systems of the types $(A_x B_y C_{1-x-y})_m (C_y D_{1-y})_n$ and $(A_x B_y C_{1-x-y})_m D_n$ have been derived. The formulation of the problem contains two types of parameters, one relating the standard state chemical potential

change, and the other representing the deviation of solution behavior from ideality. Both quantities can be calculated from well-characterized binary and quasibinary thermodynamic properties. The special cases of equilibria in the ternary or binary limit are found by putting m , n , x or y equal to one or zero, while the ideal solution phase diagram is generated by letting the r_{ij} terms equal unity. The importance of determining θ_{IC} and therefore in characterizing the reference state is apparent in the working equations as this term appears in the argument of an exponential. The evaluation of the ability of the solution models to represent the experimental phase diagram as well as thermodynamic properties cannot proceed until a reliable value for θ_{IC} is ascertained. The standard state chemical potential calculation will be discussed in more detail in the next chapter, while the solution behavior will be examined in the subsequent chapters.

CHAPTER III
THE REDUCED STANDARD STATE CHEMICAL POTENTIAL
FOR COMPOUND SEMICONDUCTORS

As presented in Chapter II, the conditions for solid-liquid equilibrium require standard states to be selected and differences characterized. The accuracy of the value for the standard state chemical potential change influences the estimation of the model parameters and hence the data cross-prediction. The reduced standard state chemical potential difference for compound semiconductor IC, denoted by θ_{IC} , is defined by Equation (2-49) and rewritten as

$$\theta_{IC}(T,P) = [\mu_{IC}^{O,S}(T,P) - \mu_I^{O,l}(T,P) - \mu_C^{O,l}(T,P)]/RT. \quad (3-1)$$

The choice of reference state is entirely arbitrary and aided by the availability of an experimental definition of θ_{IC} or the ability to accurately estimate it. The standard state usually selected for compound semiconductors is the pure component of the same phase at the temperature of interest. It is for this reference state that the most progress has been made in determining a functionality for the activity coefficient that has a physical basis. However, for the problem considered here, there exists a portion of the phase field in which the pure component is unstable, or at best meta-stable, and presents the problem of characterizing its thermodynamic

properties. This problem is particularly apparent with the group III arsenides and phosphides. Other possible standard states that are experimentally accessible include

1. The pure components in the phase of interest but at the melting temperature for the compound IC.
2. The pure components of the same phase and at the temperature of interest for easily characterized element and the compound (e.g., I and IC) but at infinite dilution for the experimentally difficult element (e.g., C).
3. The difficult element (e.g., C) in the stoichiometric melt at the temperature of interest.

Unfortunately, there are no experimental data, which are needed in the calculation of θ_{IC} characterized by above standard states. It should be pointed out here, however, that the pure liquid reference state provides problems for the mercuride, arsenide, and phosphide systems, as mercury, arsenic, and phosphorous sublime well below the compound melting points. The use of an infinite dilution reference state would overcome this difficulty. Since the choice of standard state is coupled to the calculation of activity coefficients the corresponding functionality of the standard state is altered. The problem had, therefore, simply been shifted into modelling the activity coefficient.

This chapter addresses the problem of calculating θ_{IC} with the standard state to be the pure components in the same phase at the temperature of interest. Four different methods of determining θ_{IC} are presented, each requiring a different data base. The techniques

are applied to the Al-Sb, Ga-Sb, In-Sb, Hg-Te, and Cd-Te systems and values for θ_{IC} are suggested. In addition, the effect of the use of a solution model on the calculation of θ_{IC} with two of the methods is discussed.

3.1 Theory

3.1.1 Pressure Dependence of θ_{IC}

As discussed above, the standard state chemical potential of a pure substance is a function of both temperature and pressure. Because available thermodynamic data are generally measured at some reference pressure, P_r (usually 1 atm), it is convenient to separate the pressure dependence shown in Equation (3-1) as

$$\theta_{IC}(T,P) = [\mu_{IC}^{0,S}(T,P_r) - \mu_I^{0,l}(T,P_r) - \mu_C^{0,l}(T,P_r)]/RT + \frac{1}{RT} \int_{P_r}^P [V_{IC}^{0,S}(T,P) - V_I^{0,l}(T,P) - V_C^{0,l}(T,P)] dP \quad (3-2)$$

where $V_i^{0,j}$ is the molar volume of pure component i in phase j . The importance of this last term is not expected to be significant at low or moderate pressures ($p < 100$ atm) since the molar volume of a solid and liquid is generally small in magnitude and the molar volume difference between the compound and the two pure elements is usually even smaller. As an example, this last term in Equation (3-2) has been computed for GaSb, InSb, AlSb, and CdTe at 40 and 100 atm and is listed in Table 3-1. In these calculations, the molar volumes (88) were assumed to be independent of temperature and pressure. The

Table 3-1. The pressure dependence of θ_{IC} .

IC	T(K)	P-Pr(atm)	$\theta_{IC}(T,P) - \theta_{IC}(T,Pr)$	$\theta_{IC}(T,Pr)$
AlSb	1073	40	0.0021	-4.04
	1073	100	0.0052	-4.04
GaSb	873	40	0.0018	-3.06
	873	100	0.0044	-3.06
InSb	773	40	0.0032	-2.89
	773	100	0.0080	-2.89
CdTe	873	40	0.0022	-12.10
	873	100	0.0054	-12.10

magnitude of the pressure dependent term is compared to that of the first term in the right hand side of Equation 3-2 (determined from the first method described below) and is seen to be considerably smaller than the experimental error associated with calculating the first term. It is thus concluded that the pressure dependence of $\theta_{IC}(T,P)$ can be neglected for the systems considered here.

3.1.2 Temperature Dependence of θ_{IC}

With the reference state chosen to be the pure component at the temperature of interest, θ_{IC} is simply the molar Gibbs energy of the solid compound IC minus the molar Gibbs energy of each liquid element I and C, all reduced by RT . This difference can be determined from a variety of thermodynamic sequences for which thermodynamic information is available.

One such sequence, first suggested by Wagner (89) and applied to group III-V binary systems by Vieland (90), and then extended to multicomponent systems by Ilegems (91), is shown in Figure 3-1a. In this sequence, the solid compound IC at the liquidus temperature of interest, T , is first raised to the melting temperature, T_m , and then melted. The stoichiometric liquid is then subcooled to T and finally separated into the pure liquid elements. This sequence (termed method I) results in

$$\begin{aligned} \theta_{IC}^I = & \ln[a_I^{sl}(T)a_C^{sl}(T)] - \frac{\Delta H_f(IC)}{R} \left[\frac{1}{T} - \frac{1}{T_m} \right] \\ & + \frac{1}{RT} \int_T^{T_m} \int_T^{T_m} \frac{\Delta C_p(IC)}{T} dT^2 \end{aligned} \quad (3-3)$$

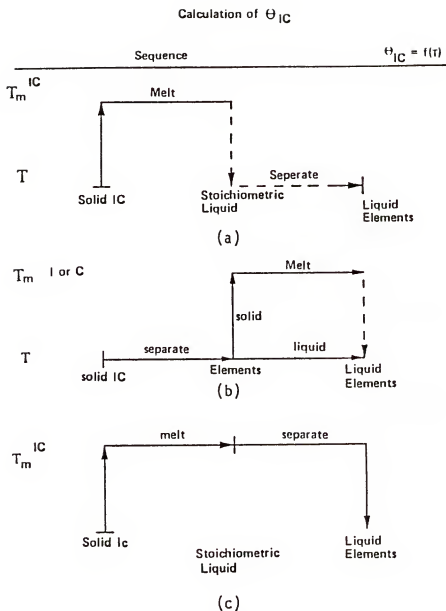


Figure 3-1. Three thermodynamic sequences for calculation of the reduced standard state chemical potential difference: (a) method I, (b) method II, and (c) method III.

Here, $a_i^S(T)$ is the activity of component i in the stoichiometric liquid at the liquidus temperature, T , $\Delta H_f(IC)$ is the molar enthalpy of fusion of the compound IC at the melting temperature, T_m , $\Delta C_p(IC)$ is the molar heat capacity difference between the stoichiometric liquid and the compound IC , and R is the gas constant. This representation suffers the draw back of requiring the Gibbs energy of mixing and C_p^S for the stoichiometric liquid mixture as a function of temperature in a range for which it is not stable and thus generally not observable. When Equation (3-3) is combined with either Equation (2-128) or (2-178) for the binary limit, it is termed the "fusion equation" for the liquidus (54,89-92).

In applying Equation (3-3), C_p^S is usually extrapolated from high temperature measurements or assumed equal to C_p of the compound IC (usually assume $\Delta C_p = 0$ or constant) while the activity product, $a_I^S(T)a_C^S(T)$, is estimated by interjection of a solution model with the parameters estimated from phase equilibrium data involving the liquid phase (i.e., solid-liquid or vapor-liquid equilibrium systems). However, this can produce consideration error, particularly at temperatures well removed from the compound melting-point temperature. In addition to this problem, in some systems there exists a multiplicity of experimental measurements often exhibiting marked discrepancy.

In order to put Equation (3-3) into a more convenient form in terms of the available data base the activity product term is expressed in terms of the measurable product at some temperature, T^* , greater than or equal to T_m and corrected to the temperature of

interest with the relatively temperature insensitive enthalpy of mixing, ΔH_{mix}^{S1} . Equation (3-3) then becomes

$$\begin{aligned} \theta_{IC}^I = & \ln[a_I^{S1}(T^*)a_C^{S1}(T^*)] - 2 \int_T^{T^*} \frac{\Delta H_{mix}^{S1}}{RT^2} dT - \frac{\Delta H_f(IC)}{R} \left(\frac{1}{T} - \frac{1}{T_m} \right) \\ & + \frac{1}{RT} \int_T^{T_m} \int_T^{T_m} \frac{\Delta C_p(IC)}{T} dT^2 \end{aligned} \quad (3-4)$$

The data base for method I is seen to consist of the measurable quantities $a_I^{S1}(T^*)$, $a_C^{S1}(T^*)$, $\Delta H_f(IC)$, T_m , and $C_p(IC)$ and the extrapolated quantities ΔH_{mix}^{S1} and C_p^{S1} . It is noted this expression contains liquid mixture information.

A second thermodynamic sequence useful for calculating θ_{IC} is depicted in Figure 3-1b and consists of performing the reverse of the direct compound formation reaction at the temperature of interest. If the elements are stable liquids at this temperature the Gibbs energy of formation of the compound, $\Delta G_f^0(T)$, is proportional to θ_{IC} . However, if one or both of the elements are solid at these conditions the following sequence, which is similar to that applied to the compound in the first method, is performed: the solid element is raised from T to the element melting temperature, T_m^i , melted, and finally subcooled to the original temperature of interest. In this case, however, the process is carried out for the pure element rather than the stoichiometric liquid. The resulting expression for θ_{IC} (method II) is

$$\theta_{IC}^{II} = \frac{\Delta G_f^\circ(T)}{RT} - \sum_{i=I,C} \frac{K_i}{RT} [\Delta H_f(i) (1 - \frac{T}{T_m^i}) - \int_T^{T_m^i} \int_T^{T_m^i} \frac{\Delta C_p(i)}{T} dT^2] \quad (3-5)$$

where $K_i = 0$ if species i is a liquid at T and $K_i = 1$ if species i is a solid at T . $\Delta H_f(i)$ is the enthalpy of fusion of species i , and $\Delta C_p(i)$ is the heat capacity difference between pure liquid and solid element i . It is noted that if the pure element i is a vapor at T the $\Delta H_f(i)$ and $\Delta C_p(i)$ terms indicate the vapor-liquid transition. For many compounds encountered there exist a range in temperature for which $K_i = 0$ for both elements (e.g., AlSb, GaSb) and therefore θ_{IC}^{II} is directly measurable. Substitution of Equation (3-5) into Equations (2-79) and (2-80) results in the "formation" expression for the liquidus (54,92-98). The data required for method II are the measurable $\Delta G_f^\circ(T)$ and possibly measurable $\Delta H_f(i)$, T_m^i and $C_p^S(i)$ and an extrapolated $C_p^L(i)$. The standard Gibbs energy of formation can be expressed in terms of the standard enthalpy and entropy of formation and is particularly useful for pinning down the values of θ_{IC} at low temperatures. The advantage of this formulation is that thermodynamic information for unstable or meta-stable systems is required only for the elements, for which a better estimate can usually be made, and not for the stoichiometric liquid.

The third sequence is shown in Figure 3-1c and is different from method I in that the pure liquid elements are separated from the stoichiometric mixture at the melting temperature and not the temperature of interest. The pure liquid elements are then cooled back to the original temperature, possibly becoming unstable or

meta-stable. The expression for θ_{IC} for method III is

$$\theta_{IC}^{III} = \frac{T_m}{T} \ln[a_i^s(T_m)a_c^s(T_m)] + \frac{\Delta S_f^{\circ}(IC, T_m)}{R} \left[\frac{T_m}{T} - 1 \right] + \frac{1}{RT} \int_T^{T_m} \int_T^{T_m} \frac{\Delta C_p}{T} dT^2 \quad (3-6)$$

where $a_i^s(T_m)$ is the activity of component i in the stoichiometric liquid at compound melting point, T_m , $\Delta S_f^{\circ}(IC, T_m)$ is the standard entropy of formation of the compound IC from the pure liquid elements at the melting temperature, and ΔC_p is the heat capacity difference between both pure liquids and the solid compound.

$$\Delta C_p = C_p^l(I) + C_p^l(C) - C_p(IC) \quad (3-7)$$

As in the case of method I, the stoichiometric activity product at melting temperature T_m in Equation (3-6) can be expressed in terms of the measured quantities $a_i^s(T^*)$, $a_c^s(T^*)$, and ΔH_{m1x}^s . If the elements are a liquid in the standard state specified by the formation reaction, the Neumann-Kopp rule (99) suggests ΔC_p is zero. For the standard formation reaction in which $K_i = 0$ at the compound melting temperature the standard entropy of formation can be obtained from the temperature derivative of $\Delta G_f^{\circ}(T)$ or, often more accurately, from a combination of the absolute values for $\Delta G_f^{\circ}(T_m)$ and $\Delta H_f^{\circ}(IC, T_m)$. For the situation in which $K_i = 1$ at T_m the value of the natural standard entropy of formation, $\Delta S_f^{\circ}(IC, T_m)$, must be corrected as

$$\Delta S_f^0(IC, T_m) = \Delta S_f^0(IC, T_m) - \sum_{i=I, C} K_i \left[\frac{\Delta H_f(i)}{T_m^i} + \int_{T_m^i}^{T_m} \frac{\Delta C_p(i)}{T} dT \right] \quad (3-8)$$

It is seen that $\Delta S_f^0(IC, T_m)$ is independent of temperature and requires extrapolation of $C_p^l(i)$ only over a limited temperature range

(T_m^i, T_m) . The data base for the application of Equation (3-6) is the measurable activity product at the melting temperature, T_m ,

$\Delta S_f^0(IC, T_m)$ (as discussed above), $C_p(IC)$ and $C_p^l(I \text{ or } C)$ and possibly an extrapolation $C_p^l(I \text{ or } C)$ and the measurable properties $C_p^s(I \text{ or } C)$ and $\Delta H_f(I \text{ or } C)$. If $\Delta C_p(T)$ function is known, then the temperature dependence is explicit in Equation (3-6). This has modelling advantages. Therefore, the advantage of method III lies in a separation of the principle temperature dependence and, at most, extrapolation of only the liquid element heat capacity.

A final process by which θ_{IC} can be directly determined from experimental results is an application of Equations (2-59), (2-61), (2-63), and (2-67). In its simplest form of the binary limit, the result is

$$\begin{aligned} \theta_{IC}^{IV} &= \ln[a_I(T^l, x_I^l) a_C(T^l, x_I^l)] \\ &= \ln[a_I(T^*, x_I^l) a_C(T^*, x_I^l)] - \int_{T^*}^{T^l} \frac{[\Delta \bar{H}_I(T, x_I^l) + \Delta \bar{H}_C(T, x_I^l)]}{RT^2} dT \quad (3-9) \end{aligned}$$

where $a_I(T^*, x_I^l) a_C(T^*, x_I^l)$ is the activity product at some measurement temperature, T^* , and the liquidus composition, x_I^l , and $\Delta \bar{H}_i(T, x_I^l)$ is the relative partial molar enthalpy for component i at the

temperature, T , and the liquidus composition, x_I^l . The data base required for this final procedure is the measurable phase diagram and the activity product along the liquidus line (or an isothermal activity product and the liquid phase enthalpy of mixing). In order to carry out the integration in Equation (3-9) we need to know the equation for the equilibrium composition, $x_I^l = f(T)$ (i.e., phase diagram), and also the relative partial molar enthalpy of component i ($i = I, C$) for these compositions. The disadvantage of this equation in practice is that the relative partial molar enthalpies which appear in the integration usually are not experimentally available, unlike the liquid phase integral enthalpy of mixing. As seen, this procedure utilizes binary mixture information and will produce two values of θ_{IC} at each liquidus temperature, one from each side of the compound, which are identical given a consistent data set. In the less likely event that multicomponent data are available, Equations (2-59), (2-61), (2-63), and (2-67) can be solved for θ_{AC} , θ_{AD} , θ_{BC} , and θ_{BD} simultaneously, requiring the activity and relative partial molar enthalpy of each component in the liquid and solid.

3.2 Results and Discussion

The above four procedures were applied to the semiconductor compounds Al-Sb, Ga-Sb, In-Sb, Cd-Te and Hg-Te as these systems are relatively well characterized. Indeed, many of the required thermodynamic properties have been investigated by several investigators and often show considerable discrepancy. A selected data set for the values of the thermodynamic properties of the

compounds and liquid mixture is shown in Table 3-2, while Table 3-3 summarizes reported measurements of $\Delta G_f^\circ(T)$ of the solid compound IC. The selected thermodynamic properties of the elements are given in Table 3-4. The value of $\Delta S_f^\circ(IC, T_m)$ listed in Table 3-2 is that either directly reported or calculated from Equation (3-8) and the elemental properties listed in Table 3-4. The low temperature values of $\Delta G_f^\circ(T)$ were calculated from the absolute entropy for the compound and elements and calorimetric values of $\Delta H_f^\circ(IC, T)$. The activity of Hg, Cd, and Te were determined from vapor pressure measurements and the relation

$$a_I^1(T, P, x_I) = [f_{I_m}^g(T, P, y_{I_m}) / f_{I_m}^{O,g}(T, P, y_{I_m} = 1)]^{1/m} \quad (3-10)$$

where $f_{I_m}^{O,g}(T, P, y_{I_m} = 1)$ is the fugacity of the pure species I_m . The value of m was unity for Cd and Hg and two for Te.

The solid line in Figure 3-2 illustrates the results of using Method I in conjunction with the selected data given in Tables 3-2 and 3-4 for the In-Sb system. This system is particularly instructive in that a considerable amount of experimental information is available. For purpose of comparison, the upper and lower experimental bounds of θ_{InSb} are also shown. The upper bound was calculated using the experimental values $\Delta H_{mix}^{S1} = 2261 \text{ J.mol}^{-1}$ (100), $\Delta H_f(InSb) = 37.67 \text{ kJ.mol}^{-1}$ (101), $T_m(InSb) = 794 \text{ K}$ (102) and the remaining properties $a_{In}^{S1}(973 \text{ K})$, $a_{Sb}^{S1}(973 \text{ K})$ and $\Delta C_p(InSb)$ was listed in Table 3-2. The lower experimental bound consisted of the data

Table 3-2. Selected values for the thermodynamic properties of the compound IC and liquid mixture.

Property	AlSb	GaSb	InSb	CdTe	HgTe
a_I^S	0.374 (103)	0.362 (104)	0.262 (105)	a	b
a_C^S	0.333 (103)	0.370 (104)	0.335 (105)	a	b
T(K)	1300 (103)	1003 (106)	973 (106)	a	b
$\Delta H_{mix}^S (\text{J.mol}^{-1})$	-4343 (103)	-1071 (107)	-6600 + 3.6T (108)	-37450 (109)	-10983 (109)
$\Delta H_f^S [\text{IC}] (\text{KJ.mol}^{-1})$	82.0 (110)	65.10 (102)	47.76 (102)	50.21 (109)	36.32 (109)
$T_f [\text{IC}] (\text{K})$	1338 (16,19)	985 (111)	798 (112)	1365 (113-116)	943 (109,115,117)
$C_p^S [\text{IC}] (\text{J.mol}^{-1}\text{K}^{-1})$	48.02 + 8.54 $\times 10^{-3}T$ (111)	45.07 + 12.05 $\times 10^{-3}T$ (111)	47.45 + 10.88 $\times 10^{-3}T$ (102)	c	47.78 + 13.64 $\times 10^{-3}T$ (117)
$C_p^S [\text{IC}] (\text{J.mol}^{-1}\text{K}^{-1})$	74.5 (111)	62.76 (111)	66.94 (102)	-	-
$\Delta S_f^S [\text{IC}, T(\text{IC})]$	-46.75 (111,118,119)	-28.158 (111,118)	-48.794 (111,118,120,121)	-43.288 (114)	-38.697 (109,117)

a $\ln[a_{Cd}^S(T)a_{Te}^S(T)] = 0.971 - 9398/T$; calculated from partial pressure measurements (122,123).

b $\ln[a_{Hg}^S(T)a_{Te}^S(T)] = 0.437 - 2086/T - \frac{2.033 \times 10^{-8}}{T} \exp(-7136/T) [-\frac{1.793}{T} + \frac{251}{T^2} + 0.00107]$;
calculated from partial pressure measurements (114,124,125).

c $C_p^S[\text{CdTe}] = 52.51 + 19.0 \times 10^{-3}T - 7.36 \times 10^{-5}/T^2 \text{ J.mol}^{-1}\text{K}^{-1}(99)$.

Table 3-3. The standard Gibbs energy of formation of the compound IC, $\Delta G_f^\circ(T)$.

Ic	$\Delta G_f^\circ(T)$	T (K)	Reference
	(kJ.mol ⁻¹ K ⁻¹)		
AlSb	-53.806 + 14.393T	778-895	(126)
	-65.019 + 26.861T	663-889	(127)
	-47.567	298	(99)
	-47.363	298	(128)
	-48.827	298	(129)
GaSb	-46.86 + 27.61T	633-833	(130)
	-50.292 + 30.88T	673-823	(131)
	-38.409	298	(102)
InSb	-35.221 + 25.54T	298-798	(104)
	-33.305 + 23.263T	663-763	(132)
	-37.656 + 28.7T	643-763	(120)
	-34.141 + 25.47T	663-763	(133)
	-34.392 + 24.77T	653-753	(131)
	-15.146	798	(134)
	-24.099	298	(135)
	-26.275	273	(136)
CdTe	-125.62 + 43.287T	298-1365	(109,114,118)
	-128.344 + 44.864T	594-1038	(122,123)
	-125.26 + 41.145T	633-710	(137)
	-121.478 + 37.584T	769-1010	(138)
	-113.993 + 32.898T	718-930	(139)
HgTe	-58.295 + 39.905T	778-943	(109)

Table 3-4. Selected values for the thermodynamic properties of the elements.

Element	T_m^I (K)	$\Delta H_f^I[I]$ (kJ.mol ⁻¹)	$C_p^S[I]$ (J.mol ⁻¹ K ⁻¹)	$C_p^L[I]$ (J.mol ⁻¹ K ⁻¹)
Al	933 (119,127)	10.46 (127)	20.67 + 12.38 x10 ⁻³ T (118)	31.8 (118)
Ga	302.9 (118)	55.85 (140)	25.899 (118)	27.82 (118)
In	429.76 (118)	3.26 (118)	21.51 + 17.57 x10 ⁻³ T (118)	30.08 - 1.36 x10 ⁻³ T (118)
Sb	904 (118,119)	19.874 (119,127)	22.32 + 0.913 x10 ⁻² T (118)	31.38 (118)
Cd	594 (118)	6.192	22.22 + 12.3 x10 ⁻³ T (118)	29.71 (118)
Hg	234.28 (118)	2.295 (118)	(118)	30.37 - 11.46 x10 ⁻³ T + 10.15 x10 ⁻⁶ T ² (118)
Te	722.65 (118)	17.489 (118)	19.16 + 21.97 x10 ⁻³ T (118)	37.656 (118)

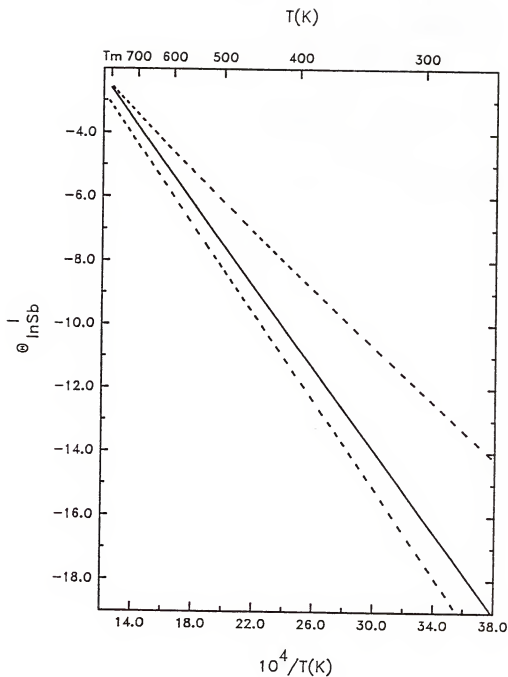


Figure 3-2. $\ln a_{\text{Sb}}$ versus reciprocal temperature. ---, upper and lower bound; —, selected property values listed in Tables 3-2 and 3-4.

base: $\Delta H_{mix}^{sl} = -3305 \text{ J.mol}^{-1}$ (141), $\Delta H_f(\text{InSb}) = 51.04 \text{ kJ.mol}^{-1}$ (134,142), $T_m(\text{InSb}) = 813 \text{ K}$ (143), $a_{In}^{sl}(923 \text{ K}) = 0.2211$ (144), $a_{Sb}^{sl}(923 \text{ K}) = 0.2594$ (104) and $\Delta C_p(\text{InSb}) = 2.5 \text{ J.mol}^{-1}\text{K}^{-1}$ (145). As can be seen, this procedure shows a small range in the experimental value of θ_{InSb}^I for temperature near $T_m(\text{InSb})$, but at lower temperatures a large range exists. This is not unexpected since in Equation (3-3) the last two terms are zero at $T_m(\text{InSb})$ and reflects a somewhat consistent activity data set while for decreasing temperature the experimentally inaccessible stoichiometric liquid properties increase in importance and are sensitive to the extrapolation procedure. These errors are serious with respect to Equations (2-59), (2-61), (2-63), and (2-67) when used to calculate the phase diagram since θ_{IC} appears as the argument of an exponential.

There have been four direct high temperature e.m.f. determinations of $\Delta G_f^\circ(\text{InSb}, T)$ using a molten salt electrolyte (106-109). Shown in Figure 3-3 are the values of θ_{InSb}^{II} calculated with method II and $\Delta G_f^\circ(\text{InSb}, T)$ results (120,131,133) (the results of (132) are nearly identical with (131)). Also shown are the values of θ_{InSb}^{II} calculated with the low temperature calorimetric determinations of $\Delta H_f^\circ(\text{InSb})$ (134,136,146) and the absolute entropy for the elements (118) and compound (111). These results are seen to be consistent with θ_{InSb}^I and the selected property values. The method is particularly useful in the range of temperature accessible with galvanic cells or calorimetry (allows the room temperature value of θ_{IC} to be "pinned down"). In addition a better estimate of $\Delta C_p(I)$ was available and,

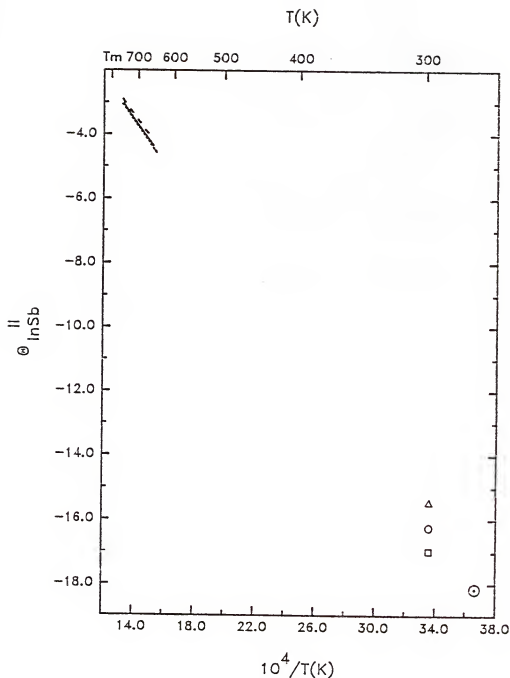


Figure 3-3. $\theta_{\text{InSb}}^{\text{II}}$ versus reciprocal temperature. ---, $\Delta G_f^\circ(\text{InSb}, T)$ of (133); —, $\Delta G_f^\circ(\text{InSb}, T)$ of (131); ..., $\Delta G_f^\circ(\text{InSb}, T)$ of (120); Δ and \circ , $\Delta H_f^\circ(\text{InSb}, 298 \text{ K})$ of (134); \square , $\Delta H_f^\circ(\text{InSb}, 298 \text{ K})$ of (136); \odot , $\Delta H_f^\circ(\text{InSb}, 273 \text{ K})$ of (146).

furthermore, was nearer zero (the $\Delta C_p(I)$ term in Equation (3-5) accounted for only 0.5% of the value of $\Theta_{InSb}^{II}(298\text{ K})$ compared to that of the selected value).

Shown in Figure 3-4 is the result for method III. The upper and lower experimental bounds are also depicted in Figure 3-4 and used the same activity product and $T_m(InSb)$ as for determining the bounds in Figure 3-2. The standard entropy of formation of InSb from the liquid elements at $T_m(InSb)$ was calculated from $\Delta H_f^o(InSb, 750\text{ K})(147)$ and $\Delta G_f^o(InSb, 798\text{ K})(135)$ for the upper bound while the lower bound employed the calorimetric value for $\Delta H_f^o(InSb, 723\text{ K})(121)$ and the standard Gibbs energy given in (133). The heat capacity for solid InSb of (147) and (148) was used for the upper and lower bound, respectively, along with the elemental properties given in Table 3-4. The dominant term in this calculation is the first one in Equation (3-6). Indeed, it is the only term in the limit of $T = T_m(InSb)$. Uncertainty in the activity product at the melting temperature gives rise to increasing uncertainty in Θ_{IC} as the temperature is lowered. However, this procedure is expected to be superior to method I given an activity measurement and equal uncertainty in $\Delta H_f(IC)$ and $\Delta S_f^o(IC, T_m)$ since the required heat capacities will generally be better defined and method I includes the uncertainties in the extrapolated activity product.

Finally, the reduced standard state chemical potential change was calculated from the reported phase diagram (112) and enthalpy of mixing (108) at the compositions for the available activity measurements (104,140,149). The results are summarized in Table 3-5.

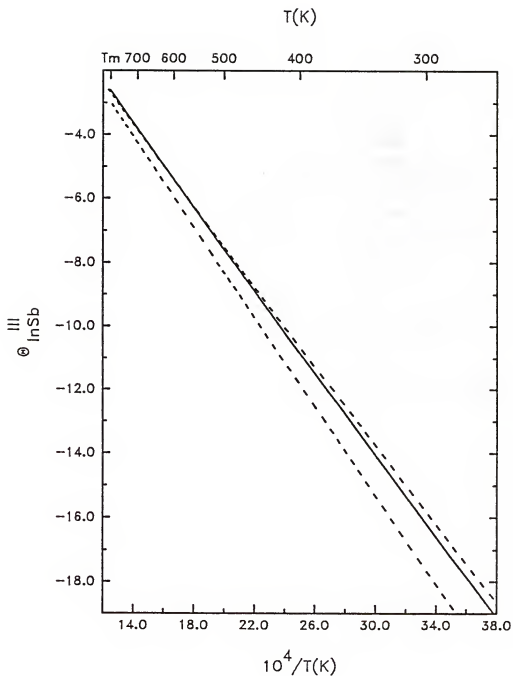


Figure 3-4. $\theta_{\text{InSb}}^{\text{III}}$ versus reciprocal temperature. ---, upper and lower bound; —, selected property values listed in Tables 3-2 and 3-4.

Table 3-5. Summary of θ_{InSb} values calculated by method [IV]* and by methods [I], [II] and [III] with the selected properties.

x_{In}	T (K)	$\theta_{\text{InSb}}^{\text{IV}}$	a_{In}^{I}	Reference	$\theta_{\text{InSb}}^{\text{I}}$	$\theta_{\text{InSb}}^{\text{II}}$	$\theta_{\text{InSb}}^{\text{III}}$
0.3	774.3	-3.41		104	-2.87	-2.84	-2.88
0.4	788.6	-3.12		104	-2.72	-2.69	-2.72
0.5	798.2	-3.01		104	-2.62	-2.59	-2.62
0.6	787.6	-3.14		104	-2.73	-2.70	-2.73
0.7	756.9	-3.56		104	-3.07	-3.04	-3.08
0.8	699.3	-4.42		104	-3.79	-3.76	-3.81
0.9	607.2	-6.24		104	-5.22	-5.19	-5.26
0.3	774.3	-2.87		120	-2.87	-2.84	-2.88
0.4	788.6	-2.69		120	-2.72	-2.69	-2.72
0.5	798.2	-2.55		120	-2.52	-2.59	-2.62
0.6	787.6	-2.66		120	-2.73	-2.70	-2.73
0.7	756.9	-3.04		120	-3.07	-3.04	-3.08
0.8	699.3	-3.87		120	-3.79	-3.76	-3.81
0.9	607.2	-5.61		120	-5.22	-5.19	-5.26
0.398	788.3	-2.90		121	-2.72	-2.69	-2.72
0.500	798.2	-2.60		121	-2.62	-2.59	-2.62
0.600	787.6	-2.75		121	-2.73	-2.70	-2.73
0.656	772.1	-2.78		121	-2.90	-2.87	-2.90
0.703	755.8	-3.16		121	-3.16	-3.05	-3.09
0.787	707.8	-3.96		121	-3.68	-3.64	-3.70
0.890	616.7	-5.81		121	-5.05	-5.03	-5.09

* The $\Delta H_{\text{mix}}[T, x_{\text{In}}]$ measurements of Rosa et al. (108) were smoothed with the Non-Random Two-Liquid Theory.

It is seen that the results of (104) and (148) are consistent with the selected value of Θ_{InSb} calculated by methods I, II, and III.

As another example, the Ga-Sb system was investigated with the four methods. Shown in Figure 3-5 are the upper and lower experimental bounds found with methods I and III and the selected experimental values found with methods II and IV. For method I the upper bound used $a_{\text{Ga}}^{\text{sl}}(1003 \text{ K})a_{\text{Sb}}^{\text{sl}}(1003 \text{ K}) = 0.1339$ (105), $T_{\text{m}}(\text{GaSb}) = 975 \text{ K}$ (149), $\Delta H_{\text{f}}(\text{GaSb}) = 50.21 \text{ kJ.mol}^{-1}$ (134), $\Delta H_{\text{mix}}^{\text{sl}} = -854 \text{ J.mol}^{-1}$ (150), and $\Delta C_{\text{p}}(\text{GaSb}) = 5.699 \text{ J.mol}^{-1}\text{K}^{-1}$ (111) while the lower bound employed $a_{\text{Ga}}^{\text{sl}}(1003 \text{ K})a_{\text{Sb}}^{\text{sl}}(1003 \text{ K}) = 0.0293$ (151), $T_{\text{m}}(\text{GaSb}) = 998 \text{ K}$ (152), $\Delta H_{\text{f}}(\text{GaSb}) = 66.94 \text{ kJ.mol}^{-1}$ (144), $\Delta H_{\text{mix}}^{\text{sl}} = 1071 \text{ J.mol}^{-1}$ (107) and $\Delta C_{\text{p}}(\text{GaSb}) = 2.895 \text{ J.mol}^{-1}\text{K}^{-1}$ (144). For method III the upper bound combined $\Delta H_{\text{f}}^{\circ}(\text{GaSb}, 750 \text{ K})$, $\Delta G_{\text{f}}^{\circ}(\text{GaSb}, 750 \text{ K})$ (153) and the elemental data listed in Table 3-4 to yield $\Delta S_{\text{f}}^{\circ}(\text{GaSb}, T_{\text{m}}) = -23.24 \text{ J.mol}^{-1}\text{K}^{-1}$ and used $\Delta C_{\text{p}} = 3.24 - 9.29 \times 10^{-4} T \text{ J.mol}^{-1}\text{K}^{-1}$. The lower bound employed $\Delta S_{\text{f}}^{\circ}(\text{GaSb}, T_{\text{m}}) = -28.16 \text{ J.mol}^{-1}\text{K}^{-1}$ and $\Delta C_{\text{p}} = 33.35 - 21.6821 \log(T) \text{ J.mol}^{-1}\text{K}^{-1}$ (118,147). For method II the high temperature e.m.f. results of $\Delta G_{\text{f}}^{\circ}(\text{GaSb}, T)$ from (130), and the low temperature results of $\Delta G_{\text{f}}^{\circ}(\text{GaSb}, 298 \text{ K})$ from (102) were used in conjunction with the elemental properties listed in Table 3-5. Finally, the fourth procedure used the interpolated phase diagram of (154) and enthalpy of mixing results of (155) along with the Ga activity measurements of (105). Again, there exists a large variation in the available Θ_{GaSb} assignments though an examination of the results of all four procedures suggests an appropriate

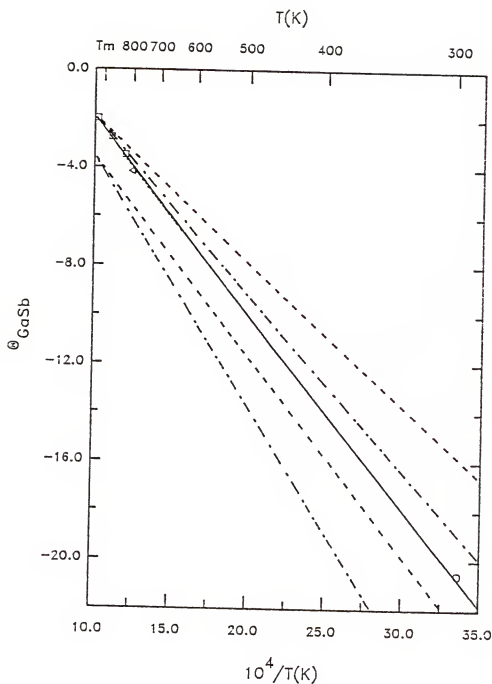


Figure 3-5. θ_{GaSb} versus reciprocal temperature. ---, upper and lower bound, method I; ..., $\Delta G^\circ(\text{GaSb}, T)$ of (130), method II; o, Ref. (146, 153); Δ , Ref. (131), method II; ---, upper and lower bound, method III; \square , Ref. (105, 154, 155), method IV; —, selected θ_{GaSb} .

temperature dependence of θ_{GaSb} . This selected value is shown in the solid line in Figure 3-5.

Assuming the following form for the temperature dependence of ΔC_p

$$\Delta C_p = d_1 + d_2 T + d_3 / T^2 \quad (3-10)$$

and for $\Delta H_{\text{mix}}^{\text{sl}}$

$$\Delta H_{\text{mix}}^{\text{sl}} = A + B T \quad (3-11)$$

the expression for θ_{IC} with the first three methods can be shown to have the functionality

$$\theta_{\text{IC}} = C_0 + C_1 T + C_2 / T + C_3 / T + C_4 \ln T \quad (3-12)$$

The dominant terms in this expression are the first and third terms with the remaining terms reflecting the magnitude of ΔC_p . Listed in Table 3-6 are the values of the constant C_{0-4} suggested by analysis of the available data when comparing the four calculational procedures. These selected θ_{IC} values are adopted in the calculation of phase diagrams in this work.

The four procedures discussed in this chapter are thermodynamically equivalent and, therefore, are useful in performing consistency tests on available data sets. As an example, the consistency of Ga (104) and In (105) activity measurements with the reported phase diagram and the enthalpy of mixing in liquid solution

Table 3-6. Suggested values of the constants for calculating θ_{IC} .

	AlSb	GaSb	InSb	CdTe	HgTe
C_0	-5.481	+5.37	-5.724	-6.334	-12.34
$C_1 \times 10^3$	-0.513	0	-0.706	-1.142	-1.510
C_2	-9,177	-7,950	-5,902	-14,930	-5,534
C_3	0 0	0	44,290	0	
C_4	1.522	0.1	1.656	1.787	2.436

with Sb (method IV) were compared with the available data sets required in methods I and II. In particular, the comparison with method II proved to be sensitive since the partial molar solution properties are required relative to the pure components rather than to the stoichiometric liquid.

As mentioned above, the Vieland's equation (method I) in conjunction with a solution model to represent the stoichiometric liquid activity coefficients has been used exclusively in the literature. In order to investigate the effect of the use of a solution model on the calculation of θ_{IC} , the NRTL equation and simple solution model were used with either Equation (3-3) or Equation (3-6) to fit data sets consisting of the liquidus temperature alone, liquidus temperature and activity (103), liquidus temperature and enthalpy of mixing (103), and all three types of data combined. The liquidus data used here are the same as those used in Chapter IV. With the parameters determined from the fit, values of θ_{IC} as a function of temperature can be calculated and compared with the recommended values listed in Table 3-6.

Shown in Figure 3-6 are the results obtained with the use of the NRTL equation with method I for the Al-Sb system. The nonrandomness parameter, α_{IC} , was considered a variable in each of the fits. Examination of the results for the fit of the liquidus temperature alone (usual procedure) indicates that both the activity product at the melting temperature and the temperature dependence of θ_{IC} are represented rather poorly, with the discrepancy increasing as the temperature decreases. This is not surprising since this result

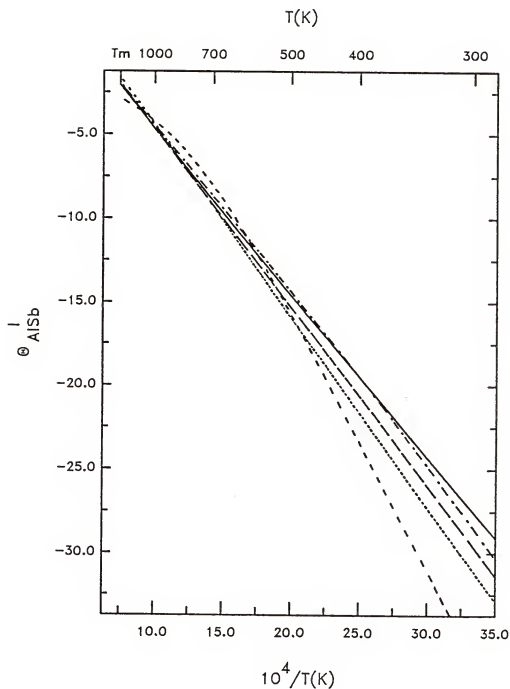


Figure 3-6. θ_{AlSn}^I versus reciprocal temperature, as calculated by the NRTL equation with method I: —, recommended value; ---, liquidus alone; —, liquidus and activity; ..., liquidus and enthalpy of mixing; -.-, combined data set.

reflects the nature of Equation (3-3), indicating that a solution model is required to represent activity coefficients for a stoichiometric liquid, which is unstable (or at best meta-stable) for temperatures below the solid compound melting point.

The results for the data base consisting of the liquidus along with the isothermal activity or with the enthalpy of mixing give significant improvement over the higher temperature range, but the results again become poor as the temperature is decreased. It is only for the case of the combined data set of the liquidus, activity, and enthalpy of mixing that the calculated values of θ_{IC} agree well with the suggested values over the entire temperature range. Therefore, it would be possible with the complete data set (if the correct T-X data are available) to calculate the values of θ_{IC} without the use of a solution model at all.

Figure 3-7 shows the results obtained with the use of the simple solution model along with method I for the Al-Sb system. The same general observations made for the NRTL equation hold for the simple solution model as well. The discrepancy between the calculated and recommended values is larger in some cases than that for the NRTL equation; this is apparently due to the inability of the simple solution model to represent the asymmetric thermodynamic property values.

The results of the use of the NRTL equation with method III are shown in Figure 3-8 for the Al-Sb system. Once again the nonrandomness parameter was considered as a variable for the calculation. The results with the various data bases show

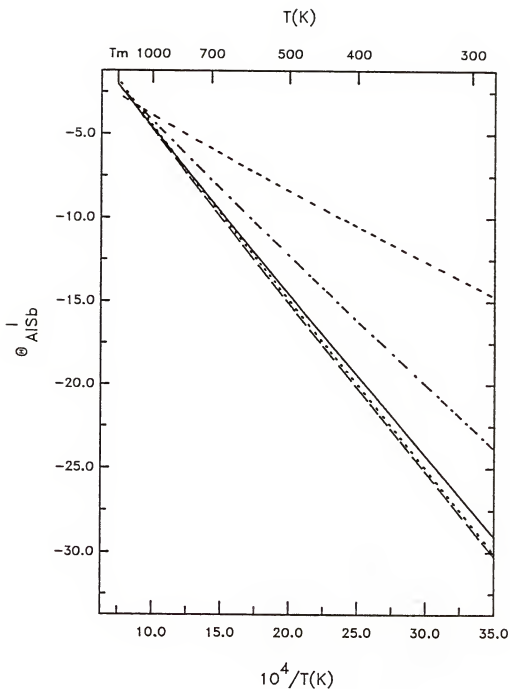


Figure 3-7. θ_{AlSb}^I versus reciprocal temperature, as calculated by the simple solution model with method I: ..., combined data set; ---, liquidus alone, —, liquidus and activity; -.-, liquidus and enthalpy of mixing; —, recommended value.

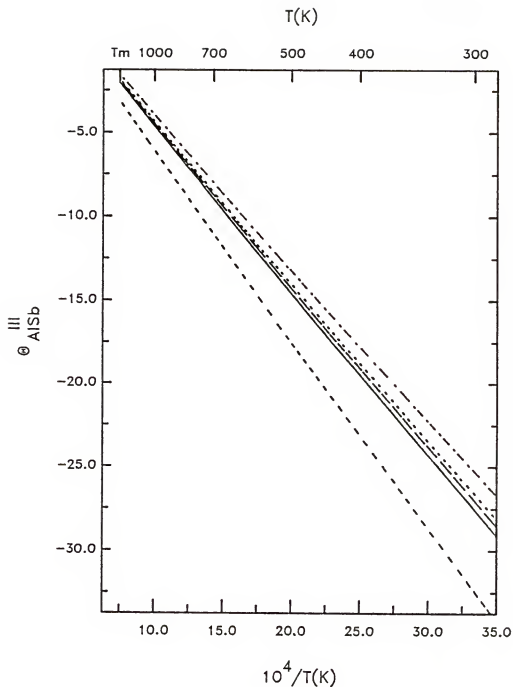


Figure 3-8. $\Theta_{\text{AlSb}}^{\text{III}}$ versus reciprocal temperature, as calculated by the NRTL equation with method III: —, combined data set; ---, liquidus alone; ..., liquidus and activity; -·-, liquidus and enthalpy of mixing; —, recommended value.

approximately the correct slope while the main differences appear in the activity product at the melting temperature. Those data sets with the isothermal activity measurements included provide better estimates of θ_{IC} at the melting point than when these data are not included. The results for the case of the data set of the liquidus alone again show that both the activity product at the melting temperature and the temperature dependence of θ_{IC} are represented rather poorly. The difference between any (except liquidus alone) of the calculated values and the recommended values is small, however, when compared with the differences found with method I. In addition, the temperature dependence of the calculated θ_{IC} is approximately correct with any (except liquidus alone) of the data sets. This result reflects the fact that Equation (3-6), in which the temperature dependence is explicit, requires the calculation of the stoichiometric liquid activity coefficients only at the solid compound melting temperature.

Shown in Figure 3-9 are the results obtained with the use of the simple solution model along with method III for the Al-Sb system. Once again, the slope of θ_{IC} versus the reciprocal temperature is approximately correct for any (except liquidus alone) of the data bases. Also, only those sets which contain isothermal activity measurements provide accurate values of the activity product at the melting temperature. As seen, the data set consisting of the liquidus temperature and enthalpy of mixing also gives good results. The discrepancy between the calculated and recommended values is not as large in some cases as for the NRTL equation; this

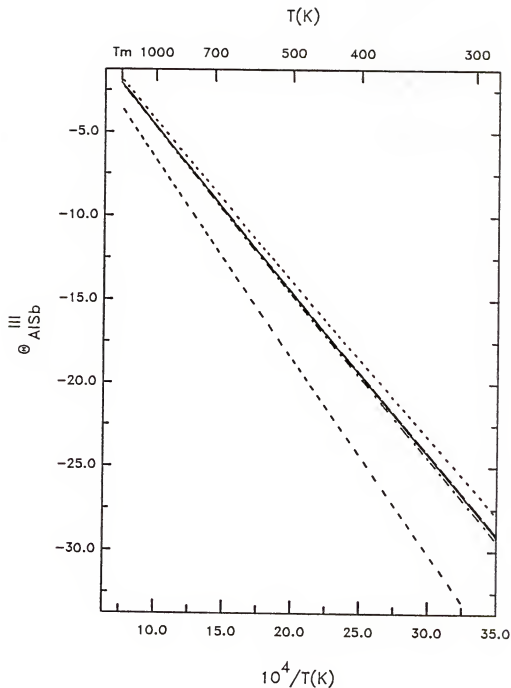


Figure 3-9. Θ_{AlSb}^{III} versus reciprocal temperature, as calculated by the simple solution model with method III: —, combined data set; ---, liquidus alone; -.-, liquidus and activity; ..., liquidus and enthalpy of mixing; —, recommended value.

is probably due to the explicit temperature dependence in θ_{IC} or the smaller number of adjustable parameters in the model.

There are two important features to notice about Figures 3-6 through 3-9. The first is that at the compound melting temperature, T_m , both Equation (3-3) and Equation (3-6) both reduce to the following expression:

$$\theta_{IC}(T_m) = \ln[a_I^{s1}(T_m)a_C^{s1}(T_m)] \quad (3-13)$$

It is, therefore, apparent that the disagreement between the calculated and suggested values of θ_{IC} at the compound melting temperature are due to the model's incorrect representation of the stoichiometric liquid activity coefficient. It is also noted that at the compound melting point the value of θ_{IC} , calculated with the same solution model but different methods, can be different due to different functionality, which affects the solution parameters determined from the fit, of the above three methods. The second feature is that the correct slope in the calculation of θ_{IC} versus the reciprocal temperature seems to depend on the method of calculation of θ_{IC} rather than on the model used in the calculation.

Shown in Figure 3-10 is a good example for comparison between the recommended value of θ_{IC} for the Al-Sb system and the value calculated by the simple solution model parameters (all other data as in Table 3-2 and 3-4) with method I obtained by several previous investigators. It is seen that widespread discrepancy exists among these results. As mentioned above, this is mainly due to the

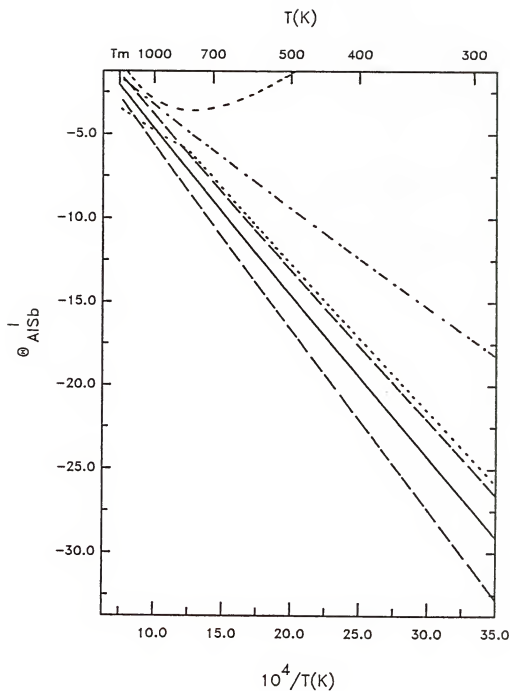


Figure 3-10. Θ_{AlSb}^I versus reciprocal temperature: —, selected property values listed in Tables 3-2 and 3-4; —, Ref. (19); ..., Ref. (18); -·-, Ref. (16); ---, Ref. (39).

inability of the solution model to represent the stoichiometric liquid activity coefficients for temperatures which are several hundred degrees below the compound melting point.

In summary, four different methods for calculating the reduced standard state chemical potential change have been suggested. For systems with extensive data bases these methods provide a means of testing their consistency with one method possibly being more reliable than the other methods for a given temperature range. These procedures have been applied to the Al-Sb, Ga-Sb, In-Sb, Cd-Te, and Hg-Te systems with reliable estimates for $\theta_{IC}(T)$ suggested. Also, the goodness of the use of solution models on the calculation of θ_{IC} with method I and method III has been compared and tested for the Al-Sb system. This comparison is particularly important when the complete data base is not available. It was shown that serious errors may result from the use of method I, particularly as the temperature is well removed from the compound melting temperature. These errors would expect to be even more serious in some III-V systems, e.g., Ga-As system, in which the compound melting point is much higher than the pure element melting point. The errors mainly resulted from an incorrect representation of the stoichiometric liquid activity product. The calculated temperature dependence was found to be approximately correct for any data base (except liquidus data alone) with the use of method III, however. The dominant error in this formalism was in the value of θ_{IC} calculated at the melting point. Inclusion of isothermal activity data served to pin down the value of the stoichiometric activity product at the melting point and

thus ensured a good representation of θ_{IC} over the entire temperature range. Method II is insensitive to the required experimental data base and thus the superior technique for calculating θ_{IC} . With this method of calculating θ_{IC} , however, one only has a direct experimental determination for some compounds over a limited temperature range (usually intermediate temperature range). This method is particularly useful in the low temperature range, in which the galvanic cell or calorimetric results are available and allow the room temperature value of θ_{IC} to be pinned down.

CHAPTER IV THERMODYNAMICS OF BINARY SYSTEMS

In Chapter II, a general formalism for the calculation of multicomponent phase diagrams was derived. It is emphasized again that predictive advantages are derived by splitting the phase diagram calculation into the two terms θ_{IC} and Γ_{IC} ; terms that can be calculated from available binary thermodynamic data. In the preceding chapter, four methods for calculation of θ_{IC} were considered; the selected values of θ_{IC} adopted in this work are given in Table 3-6. The practical calculation of the term Γ_{IC} necessarily involves solution models that are used to represent the component activity coefficients in each phase. As Γ_{IC} expresses the ratio of the deviation from ideality in the liquid phase to that in the solid phase, it is not possible to characterize the characteristics (e.g., magnitude, positive or negative deviation) of an individual phase from a given Γ_{IC} value. However, consideration of binary solid-liquid equilibrium, in which the solid phase consists of pure component IC, allows attention to be focused on the binary liquid phase nonidealities only.

This chapter assesses the thermochemistry and phase diagrams of three III-V (Al-Sb, Ga-Sb, and In-Sb) and three III-III' (Al-Ga, Ga-In, and Al-In) binary systems. All the III-V binary systems show a similar type of phase field as is plotted in Figure 1-2. The solid

phase is characterized by an equimolar compound (congruently melting) and shows a negligible range of stoichiometry. The melting temperature of the compound is higher than that of the elements (except for the Sb-InSb case). The systems also exhibit nearly degenerate eutectics that are usually located close to the pure components. The III-III' systems studied here form either eutectic (Al-Ga and Ga-In) or monotectic (Al-In) type phase diagrams. The eutectic alloys have eutectic compositions that are very close to pure Ga (nearly degenerate) and one solid phase shows negligible solubility of the other component. The monotectic alloy is characterized by a liquid miscibility gap and the monotectic reaction involves the decomposition of a liquid phase L_1 into a solid phase S_1 and a second liquid phase L_2 according to $L_1 \rightarrow S_1 + L_2$. The second liquid phase L_2 , which is immiscible in the original melt L_1 , subsequently solidifies at a temperature T_s below that of the monotectic reaction temperature T_m .

In this chapter, a consistent model representation of the available thermodynamic properties as well as the phase diagram in conjunction with the selected θ_{IC} values is discussed. The ability of several solution models to represent both liquid and solid phases nonidealities are addressed. A number of the solution models mentioned in Chapter 1 as well as several of the local composition models are considered. The binary data sets, as well as the problems associated with cross-prediction based on different data sets, are also discussed. In addition, an improvement has been made in the

procedure for calculating the liquidus curve from a fit of individual or combined data set of enthalpy of mixing and activity data.

4.1 Theory

The working equations for the binary III-V solid-liquid equilibria are given by either Equation (2-91) and repeated below

$$x_I(1-x_I) = \exp(\theta_{ISb})/\Gamma_{ISb}, \quad I = \text{Al, Ga, In} \quad (2-91)$$

where $\Gamma_{ISb} = \gamma_I^l \gamma_{Sb}^l$.

For a binary A-B eutectic system (e.g., Al-Ga, In-Ga), the conditions of solid-liquid equilibrium are given by

$$T^S = T^l = T \quad (4-1)$$

$$P^S = P^l = P \quad (4-2)$$

$$\mu_A^S(T, P, x_A^S) = \mu_A^l(T, P, x_A^l) \quad (4-3)$$

$$\mu_B^S(T, P, x_B^S) = \mu_B^l(T, P, x_B^l) \quad (4-4)$$

where, at temperature T and pressure P , the solid phase with mole fraction x_B^S of the B constituent is in equilibrium with the liquid phase with mole fraction x_B^l of the B constituent (as usual, $x_A^S = 1 - x_B^S$ and $x_A^l = 1 - x_B^l$). After substituting the chemical potential defined by Equation (2-11) into Equations (4-3) and (4-4) and rearranging, the following expressions are obtained:

$$x_A^l = \frac{1 - r_B \exp(-\theta_B)}{r_A \exp(-\theta_A) - r_B \exp(-\theta_B)} \quad (4-5)$$

and

$$x_a^s = \frac{1 - \frac{1}{r_B} \exp(\theta_B)}{\frac{1}{r_A} \exp(\theta_A) - \frac{1}{r_B} \exp(\theta_B)} \quad (4-6)$$

where θ_i and r_i are defined by the expression

$$\theta_i \equiv \frac{\mu_i^{o,s} - \mu_i^{o,l}}{RT}, \quad i = A, B \quad (4-7)$$

and

$$r_i \equiv \frac{\gamma_i^l}{\gamma_i^s} \quad (4-8)$$

As shown above, the θ_i and r_i terms again represent the reduced standard state chemical potential difference and the ratio of liquid to solid phase activity coefficients, but they are now defined in terms of properties for only component i .

Choosing the standard state as the pure component in the state indicated by the superscript at the temperature and pressure of interest, values for θ_i can be calculated from the following expression:

$$\theta_i(T) = \frac{\Delta H_f^i}{R} \left(\frac{1}{T_m^i} - \frac{1}{T} \right) + \frac{1}{RT} \int_T^{T_m^i} \int_T^{T_m^i} \frac{\Delta C_p^i}{T} dT^2 \quad (4-9)$$

where ΔH_f^i is the enthalpy of fusion of pure component i , T_m^i is the melting-point temperature of pure component i , and ΔC_p^i is the difference in heat capacity between pure liquid i and solid i . Upon inserting the selected values for these properties listed in Table 3-4, expressions for θ_i are found to be

$$\theta_{Al} = -5.355 - 7.448 \times 10^{-4} T - 969.4/T + 1.037 \ln T \quad (4-10)$$

$$\theta_{Ga} = 0.664 - 601.7/T + 0.2315 \ln T \quad (4-11)$$

$$\text{and } \theta_{In} = -5.389 - 1.138 \times 10^{-3} T - 159.8/T + 1.0307 \ln T \quad (4-12)$$

where T is the absolute temperature (K). These values along with the selected values of θ_{IC} listed in Table 3-4 are used in subsequent calculations of the phase diagrams and in the estimation of solution parameters from liquidus and solidus data.

Considering the case of negligible solid solubility in component i , the working equations expressing either pure solid A or B in equilibrium with the liquid solution are given by

$$\mu_i^l = \mu_i^s = \mu_i^{0,s} \quad (4-13)$$

Upon substituting the liquid chemical potential defined by Equation (2-11) into above equation and rearranging the expression, we obtain

$$\ln a_i^l = \theta_i \quad i = A \text{ or } B \quad (4-14)$$

Here θ_i is defined by Equation (4-7). Equation (4-14) gives the value of the activity of component i along the liquidus curve from pure i to the eutectic composition. Usually the value of the activity of component i at the eutectic composition, $\ln a_i^l(x_e, T_e) = \theta_i(T_e)$, is used as the boundary condition for integration of

$$\left. \frac{\partial \ln a_i^l}{\partial T} \right|_x \quad \text{or} \quad \left. \frac{\partial \ln a_i^l}{\partial x_i} \right|_T ,$$

from which the activity $a_i^l(x_i^l, T^l)$ of component i in the liquid phase on the liquidus line can be calculated.

For the case of the binary Al-In liquid-liquid equilibria, the activities of each constituent in the two phases are equal

$$x_{Al}^I \gamma_{Al}^I = x_{Al}^{II} \gamma_{Al}^{II} \quad (4-15)$$

$$x_{In}^I \gamma_{In}^I = x_{In}^{II} \gamma_{In}^{II} \quad (4-16)$$

where x_i^I and x_i^{II} are the molar fractions of the constituent i ($i = Al$ or In) in the two phases and γ_i^I and γ_i^{II} are the activity coefficients defined by a solution model. Note that the sum of the molar fractions must equal unity in each phase (i.e., $x_{Al}^I + x_{In}^I = 1$ and $x_{Al}^{II} + x_{In}^{II} = 1$). After rearranging Equations (4-15) and (4-16) the following expressions are obtained:

$$x_A^I = \frac{1 - r_B}{r_A - r_B} \quad (4-17)$$

and

$$x_A^{II} = \frac{1 - \frac{1}{r_B}}{\frac{1}{r_A} - \frac{1}{r_B}}, \quad A = Al, B = In \quad (4-18)$$

where r_i is defined by the expression

$$r_i \equiv \frac{\gamma_i^I}{\gamma_i^{II}}, \quad i = Al, In \quad (4-19)$$

It is apparent that Equations (4-17) and (4-18) are the same as Equations (4-5) and (4-6) with $\theta_i = 0$ and r_i defined by Equation (4-19). Equations (2-91), (4-5), (4-6), (4-14), (4-17), and (4-18) express the basic equilibrium conditions for group III-V and III-III' binary systems and are used in these studies.

4.2 Solution Models

In this section, several solution models for predicting thermodynamic properties of liquid mixtures are briefly reviewed. These include the regular solution theory of Hildebrand (156,157,158), the equation of Scatchard and Hamer (159,160), the quasichemical equation of Guggenheim (161), Jordan's regular associated solution model (64), and several of the local composition correlations (Wilson equation (162), the Non-Random Two-Liquid (NRTL)

theory (163) and the universal quasichemical (UNIQUAC) expressions (164)). If the models are physically significant, it should be possible to obtain other meaningful thermodynamic properties from the expression for the excess molar Gibbs energy, G^{XS} :

$$\begin{aligned} \ln \gamma_i &= \frac{\bar{g}_i^{XS}}{RT} = \left[\frac{\partial (N_T G^{XS}/RT)}{\partial n_i} \right]_{P, T, \{n_{j \neq i}\}} \\ &= \frac{G^{XS}}{RT} - \sum_{k=1}^n x_k \left[\frac{\partial (G^{XS}/RT)}{\partial x_k} \right]_{T, P, \{x_{l \neq k}\}} \end{aligned} \quad (4-20)$$

and

$$\Delta H^m = -RT^2 \left[\frac{\partial (G^{XS}/RT)}{\partial T} \right]_{P, \{x\}} \quad (4-21)$$

where \bar{g}_i^{XS} is the partial excess molar free energy of component i . In addition, the relationship between excess molar free energy and excess molar enthalpy and entropy is expressed as

$$G^{XS} = \Delta H^m - TS^{XS} = \sum_{i=1}^n x_i (\bar{H}_i^{XS} - T\bar{S}_i^{XS}) \quad (4-22)$$

Hence, a model for excess enthalpy, entropy, and activity coefficients can immediately be obtained for any model for G^{XS} . Thus, the excess molar Gibbs energy, G^{XS} , implicitly represents the complete thermodynamic property information. A summary of the model equations considered for the excess molar Gibbs free energy of a binary I-C liquid mixture is listed in Table 4-1, while the resulting expressions for the activity coefficients and enthalpy of mixing are

Table 4-1. Model equations for the excess molar Gibbs free energy of a binary I-C liquid mixture.

Solution Model	Parameter	Excess Molar Gibbs Free Energy	Eq. No.
Simple (quasi-regular)	$w = a+bT$		
Regular (strictly regular)	$w = a$	$G^{XS} = wx_I x_C$	(4-23)
Athermal	$w = bT$		
Scatchard-Hamer	$\beta = a+bT$ $\alpha = c+dT$	$G^{XS} = \beta V_I Z_C + \alpha Z_I^2 Z_C$	(4-24)
Regular Associated	$w = a+bT$ $K = c \exp(d/2RT)$	$G^{XS} = wx_I x_C + RTx_I \ln \left[\frac{x_I - x_C + p}{x_I(1+p)} \right] + RTx_C \ln \left[\frac{x_C - x_I + p}{x_C(1+p)} \right]$	(4-25)
Quasichemical	$w = a+bT$	$G^{XS} = wx_I x_C \left[1 - \frac{w}{2RT} x_I x_C + \dots \right]$	(4-26)
NRTL	$g_{CI} - g_I = a+bT$ $g_{IC} - g_{CC} = c+dT$	$G^{XS} = x_I x_{CI} (g_{CI} - g_{II}) + x_C x_{IC} (g_{IC} - g_{CC})$	(4-27)
Wilson	$\lambda_{IC} - \lambda_{II} = a+bT$ $\lambda_{IC} - \lambda_{CC} = c+dT$	$\frac{G^{XS}}{RT} = -x_I \ln(x_I + \lambda_{IC} x_C) - x_C \ln(x_C + \lambda_{CI} x_I)$	(4-28)
UNIQUAC	$u_{IC} - u_{CC} = a+bT$ $u_{CI} - u_{II} = c+dT$	$\frac{G^{XS}}{RT} = (x_I \ln \frac{\phi_I}{x_I} + x_C \ln \frac{\phi_C}{x_C}) + \frac{Z}{2} (q_I x_I \ln \frac{\theta_I}{\phi_I} + q_C x_C \ln \frac{\theta_C}{\phi_C})$ $- q_I x_I \ln(\theta_I + \theta_{CI}) - q_C x_C \ln(\theta_C + \theta_{IC})$	(4-29)

given in Table 4-2 and Table 4-3, respectively. Shown in Table 4-4 are the solution model equations considered for the excess molar Gibbs free energy, activity coefficients, and enthalpy of mixing of a binary I-C solid solution. The notations used in the above tables are the same as those used in the following discussion.

The concept of a regular liquid or solid solution was first introduced by Hildebrand (156-158) to describe mixtures, whose behavior show some experimental regularities. The theory is based on three simple assumptions: (1) All species are located at points on a lattice; (2) All interactions in the solution are between nearest neighbor pairs; (3) The configuration of the species is random. The expression for the excess Gibbs energy contains one adjustable parameter, the interchange energy $w = a$, which is strictly a constant. Therefore, the excess entropy is zero and the entropy of (strictly) regular solutions is identical to that of ideal solutions, in which the molecules are randomly mixed. This is in contrast to an athermal solution, for which the interchange energy is proportional to the temperature, i.e., $w = bT$, and thus the excess enthalpy is zero. In practical applications, w is empirically allowed to be a linear function of temperature, $w = a + bT$. With this approximation the expression for the excess Gibbs free energy is termed a simple solution. Because of its simplicity and ability to model many III-V systems well, the simple solution model is widely used in practice.

Guggenheim (161) presents the quasichemical equilibrium model (higher approximations of the lattice model) to improve the "random distribution" assumption in the lattice (or "strictly regular")

Table 4-2. Model equations for the activity coefficients of a binary I-C liquid mixture.

Solution Model	Equation for Species I*	Eq. No.
Simple Regular Athermal	$\ln \gamma_I = w x_C^2 / RT$	(4-30)
Scatchard-Hamer	$\ln \gamma_I = [(b + 2a)V_I Z_C^2 - 2aV_I Z_C^3] / RT$	(4-31)
Regular Associated	$\ln \gamma_I = \frac{w x_C^2}{RT} + \ln \left[\frac{x_I^{-x_C + p}}{x_I (1 + p)} \right]$	(4-32)
Quasichemical	$\ln \gamma_I = \frac{w}{RT} x_C^2 \left[1 - \frac{w}{ZRT} (2x_I x_C - x_C^2) \right]$	(4-33)
NRTL	$\ln \gamma_I = x_I^2 \left\{ \tau \frac{\exp(-\alpha_{IC} \tau_{CI})}{[x_I + x_C \exp(-\alpha_{IC} \tau_{CI})]^2} + \tau_{IC} \frac{\exp(-\alpha_{IC} \tau_{IC})}{[x_C + x_I \exp(-\alpha_{IC} \tau_{IC})]^2} \right\}$	(4-34)
Wilson	$\ln \gamma_I = -\ln(x_I + \Lambda_{IC} x_C) + x_C \left[\frac{\Lambda_{IC}}{x_I + \Lambda_{IC} x_C} - \frac{\Lambda_{CI}}{\Lambda_{CI} x_I + x_C} \right]$	(4-35)
UNIQUAC	$\ln \gamma_I = \ln \frac{\phi_I}{x_I} + \frac{Z}{2} q_I \ln \frac{\theta_I}{\phi_I} + \phi_C \left(1 - \frac{\gamma_I}{\gamma_C} \right)_C - q_I \ln (\theta_I + \theta_C \tau_{CI}) + \theta_C q_I \left(\frac{\tau_{CI}}{\theta_I + \theta_C \tau_{CI}} - \frac{\tau_{IC}}{\theta_C + \theta_I \tau_{CI}} \right)$	(4-36)

* The activity coefficient for species C is found by interchanging the subscripts I and C in each model equation (Equation (4-30) to Equation (4-36)).

Table 4-3. Equations for the enthalpy of mixing of a binary I-C liquid mixture.

Solution Model	Enthalpy of Mixing	Eq. No.
Simple	$\Delta H^m = a x_I x_C$	(4-37)
Regular	$\Delta H^m = a x_I x_C$	(4-38)
Athermal	$\Delta H^m = 0$	(4-39)
Scatchard-Hamer	$\Delta H^m = a V_I^2 Z_C + c V_I^2 Z_C$	(4-40)
Regular Associated	$\Delta H^m = a x_1 x_2 + \frac{4 x_I^2 x_C^2 D_1 D_2 \exp(D_2/2RT)}{(1+p)(1+D_1 \exp(D_2/2RT))^2 (p^2 - 4 x_I x_C - 1)}$	(4-41)
Quasichemical	$\Delta H^m = a x_I x_C - \frac{2 a w x_I^2 x_C^2}{ZRT}$	(4-42)
NRTL	$\Delta H^m = a x_I x_{CI} + c x_C x_{IC} - \frac{a^{\alpha} x_I^{\tau} x_{CI}^{\tau} x_C^2 \exp(-\alpha_{IC}^{\tau} x_{CI})}{[x_I + x_C \exp(-\alpha_{IC}^{\tau} x_{CI})]^2} - \frac{c^{\alpha} x_I^{\tau} x_C^2 \exp(-\alpha_{IC}^{\tau} x_{IC})}{[x_C + x_I \exp(-\alpha_{IC}^{\tau} x_{IC})]^2}$	(4-43)
Wilson	$\Delta H^m = x_I^{\lambda} \left[\frac{a^{\lambda} x_{IC}}{x_I + x_C} + \frac{c^{\lambda} x_{CI}}{x_C + x_I} \right]$	(4-44)
UNIQUAC	$\Delta H^m = \frac{c q_I^{\ominus} x_I^{\lambda} x_{CI}}{\vartheta_I + \vartheta_I^{\lambda} x_{CI}} + \frac{a q_C^{\ominus} x_C^{\lambda} x_{IC}}{\vartheta_C + \vartheta_I^{\lambda} x_{IC}}$	(4-45)

Table 4-4. The excess molar Gibbs free energy, activity coefficients, and enthalpy of mixing for a binary I-C solid solution.

Property	Model			
	Simple	Regular	Athermal	Ideal
G^{XS}	$\Omega x_I^S x_C^S$	$\Omega' x_I^S x_C^S$	$\Omega'' x_I^S x_C^S$	0
Parameter	$\Omega = a^S + b^S T$	$\Omega' = a^S$	$\Omega'' = b^S T$	-
$RT \ln \gamma_I^S$	$\Omega (x_C^S)^2$	$\Omega' (x_C^S)^2$	$\Omega'' (x_C^S)^2$	0
$RT \ln \gamma_C^S$	$\Omega (x_I^S)^2$	$\Omega' (x_I^S)^2$	$\Omega'' (x_I^S)^2$	0
ΔH_m^S	$a^S x_I^S x_C^S$	$a^S x_I^S x_C^S$	0	0

theory. The original model is based on the following main assumptions:

- (1) Each atom has Z nearest-neighbor atoms.
- (2) Nearest-neighbor interactions are pairwise with the composition and temperature independent interaction parameter, w , which is defined as

$$w = Z[w_{IC} - \frac{1}{2}(w_{II} + w_{CC})] \quad (4-46)$$

where w_{ij} is the energy of an i - j nearest-neighbor pair.

- (3) The distribution of atomic pairs is calculated using a mass action-like expression

$$N_{ii}N_{jj}/(N_{ij})^2 = \frac{1}{4} \exp(2w_{ij}/ZRT) \quad (4-47)$$

where i and j each represent I or C.

Again allowing the interchange energy to be a linear function of T , the resulting expression for the excess molar Gibbs free energy is given by Equation (4-46). The quadratic term (second term, which is contributed by the excess entropy term TS^{XS}) in Equation (4-26) is the first correction for nonrandom mixing. The S^{XS} term is always negative, as should be expected in this model from any reduction in nonrandomness. It has been shown that the correction for nonrandomness is very small (165,166,167). Hill (166) concluded that improvement of the quasichemical approximation does not provide an excess entropy term TS^{XS} of the same magnitude as H^{XS} . This difficulty, as well as the fact that S^{XS} is always negative, is a

property of the lattice model itself and not of approximations introduced in deriving thermodynamic functions from the model. A typical value of Z is 10 (a good average for a liquid) and is used in this study.

Both of the preceding models consider a solution consisting of components of similar size (otherwise they would not be interchangeable on the same lattice), omit all p - V effects (rigid lattice) and predict properties which are symmetric in composition about $x_1 = 1/2$. For III-V systems such symmetry is not always observed experimentally. Wohl (168) presents an expression for the excess Gibbs energy, which considers effective volume fractions and molecular interactions. The simple solution model (156-158), the Van Laar equation (169), the Margules equations (168), and the Scatchard-Hamer equations (159,160) can be derived from the Wohl expansion by a set of different assumptions. As shown in Equation (4-24), the equation of Scatchard and Hamer (159,160) involved two interaction parameters, α and β , which are allowed to possess a linear temperature dependence. The size effects are accounted for by employing the pure component molar volumes, v_i and volume fractions, $Z_i = x_i v_i / v$, where v is the ideal mixture molar volume. Note that the enthalpy of mixing given by Equation (4-40) allows for asymmetry in mole fraction but does not exhibit a temperature dependence, provided the small temperature dependence of the molar volumes is neglected.

The concept of associates was first introduced at the beginning of the 20th century by Dolezalek (170) and subsequently studied in

more detail by Lacmann (171-173). However, this early work on chemical models was only applied to mixtures of organic solvents. Of late, there have been several modern physical (viscosity), electrical (resistivity), optical (X-ray diffraction patterns), and magnetic (magnetic susceptibility) studies of group III-V melts, indicating that "complexes" or "associates" must exist in the liquid state. These properties indicate the presence of a strong interactions between unlike components in group III-V melts and fueled renewed interest in the application of associated solution models (chemical theories) to III-V melts. One of the earliest applications of the theory of associates to liquid alloys was published by Jordan (64). Jordan (64) considered the case in which the liquid phase consists of the three species I, C (unassociated species) and IC (associated species). These three species are assumed to be in a dynamic equilibrium according to $I_{(1)} + C_{(1)} \rightleftharpoons IC_{(1)}$. The thermodynamic behavior of such binary solutions with a single type of complex is described in terms of three interchange energies and represented by the ternary regular solution expressions. With certain simplifying assumptions, Jordan (64) arrived at the equation commonly known as the "regular associated solution" model. The model contains two adjustable parameters, an interchange energy, w , and an equilibrium constant, K , for the formation of IC from I and C. Also, this model allows the interchange energy to depend linearly on T , $w = a + bT$, and the equilibrium constant to depend exponentially on $1/T$, $K = c \exp(d/2RT)$. The resulting expressions for the excess Gibbs energy, the activity coefficients, and the enthalpy of mixing are

derived and given by Equations (4-25), (4-32), and (4-41), respectively. In Equation (4-32), P is defined by

$$P \equiv \left\{ 1 - \frac{4x_1x_C}{1 + K \exp(-w/2 RT)} \right\}^{1/2} \quad (4-48)$$

and D_1 is equal to $c \exp(-b/2 R)$ and D_2 equals $d - a$ in Equation (4-41). Note that this model allows for a weak-temperature dependence in the enthalpy of mixing and the expression is symmetric with respect to mole fraction.

Finally, three "local composition" formulations are considered. These models attempt to describe the nonideal-solution behavior due to strongly interacting molecules in the liquid phase, and are readily extended to multicomponent systems, while involving only binary interaction constants.

Since its introduction in 1964, the equation of Wilson (162) has received wide attention because of its ability to fit strongly nonideal, but miscible, systems. In the Wilson equation, the effects of differences in both molecular size and intermolecular forces are incorporated by an extension of the equation of Flory (174,175) and Huggins (176,177). Overall solution volume fractions ($\phi_i = x_i v_i / v$) are replaced by local volume fractions, ξ_i , which are related to local molecule segregations caused by differing energies of interaction between pairs of molecules. For the local volume fraction, Wilson proposed

$$\epsilon_i = \frac{v_i x_i \exp(-\lambda_{ii}/RT)}{\sum_{j=1}^n v_j x_j \exp(-\lambda_{ij}/RT)} \quad (4-49)$$

where energies of interaction $\lambda_{ij} = \lambda_{ji}$, but $\lambda_{ii} \neq \lambda_{jj}$. Following the treatment of Orye and Prausnitz (178), substitution of the binary form of Equation (4-49) into the equation of Flory and Huggins, and defining the binary constants as

$$\Lambda_{12} = \frac{v_2}{v_1} \exp\left[-\frac{(\lambda_{12} - \lambda_{11})}{RT}\right] \quad (4-50)$$

$$\Lambda_{21} = \frac{v_1}{v_2} \exp\left[-\frac{(\lambda_{12} - \lambda_{22})}{RT}\right] \quad (4-51)$$

leads to the excess Gibbs energy Equation (4-28) for a binary system. Studies indicate that $(\lambda_{12} - \lambda_{11})$ and $(\lambda_{12} - \lambda_{22})$ are linear functions of temperature. Values of v_i/v_j depend on temperature also, but the variation may be small compared to temperature effects on the exponential term and neglected in deriving the expressions for the activity coefficients and enthalpy of mixing.

The nonrandom two-liquid (NRTL) equation developed by Renon and Prausnitz (163) represents an accepted extension of Wilson's concept. Starting with an equation similar to Equation (4-49), but expressing local composition in terms of mole fractions rather than volume fractions, Renon and Prausnitz developed an equation for the local mole fraction of species j in a liquid cell occupied by a molecule of i at the center.

$$x_{ji} = \frac{x_j \exp(-\alpha_{ji} \tau_{ji})}{\sum_{l=1}^n x_l \exp(-\alpha_{li} \tau_{li})} \quad (4-52)$$

For the binary liquid system, τ_{IC} and τ_{CI} are adjustable parameters, and $\alpha_{IC}(=\alpha_{CI})$ is a third parameter that can be fixed or adjusted. The parameter α_{ji} characterizes the tendency of species j and species i to be distributed in a nonrandom fashion. When $\alpha_{ji} = 0$, local mole fractions are equal to overall solution mole fractions. Generally, α_{ji} is independent of temperature and depends on molecular properties. For organic liquids, values of α_{ji} usually lie between 0.2 and 0.47 (167). The τ coefficients for a binary system are given by

$$\tau_{IC} = (g_{IC} - g_{CC})/RT \quad (4-53)$$

$$\tau_{CI} = (g_{CI} - g_{II})/RT \quad (4-54)$$

where g_{ij} are energies of interaction between molecule pairs. Often $(g_{IC} - g_{CC})$ and $(g_{CI} - g_{II})$ are linear in temperature and not independent for a multicomponent mixture (179). Upon substituting Equation (4-48) into Scott's two-liquid cell theory (180), wherein only two-molecule interactions are considered, the NRTL representation of ΔG^{XS} for the liquid system is obtained. In general, the accuracy of the NRTL equation is comparable to that of the Wilson equation. Although α_{ij} is an adjustable parameter, there

is often little loss in accuracy by setting its value, typically between -1 and 1.

In an attempt to place the calculation of liquid phase activity coefficients on a simpler, yet more theoretical basis, Abrams and Prausnitz (164) derived a new expression for excess free energy. This model, called UNIQUAC (universal quasichemical), generalizes a previous analysis by Guggenheim (161) and allows the molecules to be of arbitrary size and shape. As in the Wilson and NRTL equations, local concentrations are used. However, rather than local volume fractions or local mole fractions, UNIQUAC uses the local area fraction θ_{ij} as the primary concentration variable. The local area fraction is determined by representing a molecule by a set of bonded segments. Each molecule is characterized by two structural parameters: the relative number of segments per molecule r (volume parameter) and the relative surface area of the molecule q (surface parameter). Following a procedure similar to that of Guggenheim (161) they derive an expression for excess Gibbs free energy given by Equation (4-29). The first four terms on the right-hand side are due to differences in molecule size and shape, while the last two terms are due to differences in intermolecular forces. Z is the lattice coordination number, again set equal to 10, and T_{IC} and T_{CI} are given by

$$T_{IC} = \exp\left[-\frac{U_{IC} - U_{CC}}{RT}\right] \quad (4-55)$$

and

$$\tau_{CI} = \exp\left[-\frac{U_{CI} - U_{II}}{RT}\right] \quad (4-56)$$

In addition, the segment fraction, ϕ_I , and area fraction, θ_I , are given by

$$\phi_I = x_I \gamma_I / (x_I \gamma_I + x_C \gamma_C) \quad (4-57)$$

and

$$\theta_I = x_I q_I / (x_I q_I + x_C q_C) \quad (4-58)$$

The expressions for the activity coefficients are given by Equation (4-36) in which l_i is given by

$$l_i = \left(\frac{Z}{2}\right)(\gamma_i - q_i) - (\gamma_i - 1), \quad i = I, C \quad (4-59)$$

As a result of the introduction of the Boltzman-type factor in the local composition models, the adjustable parameters occur in exponential terms. This alters not only the form of the activity coefficient equations, but also allows for temperature dependence and asymmetry in the enthalpy of mixing. The improvement of the local composition models is expected to occur because of this temperature dependence.

Each of the models mentioned above has adjustable parameters which can be estimated from experimental data. A maximum likelihood algorithm based on the Birtt-Luecke (181) method is used to estimate the model parameters. The technique maximizes the likelihood function for the problem and is equivalent to minimizing the x-square

distribution function of the following form:

$$(\underline{Z}_m - \underline{Z})^T \underline{R}^{-1} (\underline{Z}_m - \underline{Z}) \quad (4-60)$$

Here, \underline{Z}_m is the vector of measured variables (observed values), \underline{Z} is the vector of estimated variables (expected values), and \underline{R} is the error matrix, which specifies the variances of the measurements \underline{Z}_m . This algorithm may be thought of as an extension of ordinary least squares to the case where some (or all) of the independent variables, as well as the dependent variables, are subject to measurement error. In addition, it supplies a best estimate to the adjustable parameters and provides the estimated parameters variance and covariance matrix (error matrix) which allows the determination of the limit of confidence in these parameters and will give some insight into the problem of data cross-prediction.

4.3 Computational Procedure

The experimental liquidus points, solidus points, enthalpy of mixing, and group III activity were taken from tabulations, or more often, digitized from graphs. The basic equations are (2-91), (4-5), (4-6), (4-14), (4-17), (4-18), and those listed in Tables 4-2 through 4-4. The computational procedure is quite straightforward for either the combined or individual data sets except for the III-III' binary systems, in which isothermal solidus-liquidus or liquidus-liquidus pairs are usually not available. The procedures described below

were used to evaluate the liquid and solid solution model parameters for the Ga-In and Al-Ga systems in this study.

For convenience, the system of two implicit working Equations (4-5) and (4-6) can be written as

$$x_A^l = f(x_A^l, x_A^s, T) \quad (4-61)$$

$$x_A^s = g(x_A^l, x_A^s, T) \quad (4-62)$$

The computer calculation starts with an initial guess for the liquid and the solid solution model parameters. The first experimental liquidus temperature and composition is then inserted into Equation (4-62) along with the initial model parameters and the selected, reduced standard state chemical potential difference, and Equation (4-62) is solved for the corresponding equilibrium solidus composition. Thus, the problem is reduced to one constraint equation (4-61). This procedure is repeated for each of the liquidus points. Next, the experimental solidus composition and temperature are inserted one at a time into Equation (4-61) and this equation is solved for the corresponding equilibrium liquidus composition. Similarly, the problem is reduced to one constraint equation (4-62). The parameters for the Al-In system were obtained in a similar fashion by including both the liquid-liquid and liquid-pure solid Al equilibrium conditions. For example, considering the simple binary liquid mixture described by Equation (4-23), substitution of Equation (4-30) into Equations (4-15) and (4-16) gives the conditions for liquid-liquid equilibrium as

$$x_A^I \exp\left[\frac{(a+bT)(x_B^I)^2}{RT}\right] = x_A^{II} \exp\left[\frac{(a+bT)(x_B^{II})^2}{RT}\right] \quad (4-63)$$

and

$$x_B^I \exp\left[\frac{(a+bT)(x_A^I)^2}{RT}\right] = x_B^{II} \exp\left[\frac{(a+bT)(x_A^{II})^2}{RT}\right] \quad (4-64)$$

For pure solid Al in equilibrium with the binary melt substitution of Equation (4-20) into Equation (4-14) gives

$$x_A \exp\left[\frac{(a+bT)x_B^2}{RT}\right] = \exp(\theta_A), \quad A = \text{Al}, B = \text{In} \quad (4-65)$$

Simultaneous solution of these equilibrium relations (coupled with the conservation equations $x_A^I + x_B^I = 1$, $x_A^{II} + x_B^{II} = 1$ and $x_A + x_B = 1$) gives the complete phase diagram of this system.

The ability of the model to describe the combined data is characterized by the overall weighted sum of squares, σ_0^2 , which is provided by the maximum likelihood algorithm and calculated according to

$$\sigma_0^2 = \frac{(\underline{Z}_m - \underline{Z})\underline{R}^{-1}(\underline{Z}_m - \underline{Z})}{K - n} \quad (4-66)$$

Here, \underline{Z}_m is the vector of measured variables (observed values), \underline{Z} is the vector of estimated variables (expected values), K is the number of measurements, n is the number of parameters in the model, and \underline{R} is the error matrix, which specifies the variances of the measurements

\underline{Z}_m . The weighted sum of squares for the subset is calculated by a similar equation:

$$\begin{aligned}\sigma_e^2(\text{subset}) &= \frac{(\underline{X}_m - \underline{X})^T \underline{Y}^{-1} (\underline{X}_m - \underline{X})}{k - n} \\ &= \frac{\sum_{i=1}^k \sum_{j=1}^l [(X_{ij} - X_{mij})^2 / \gamma_{ij}]}{k - n}\end{aligned}\quad (4-67)$$

Here, \underline{X}_m is the vector of measured variables for the subset, \underline{X} is the vector of final variable estimates for the subset, \underline{Y} is the error matrix, which specifies the variances (a priori estimates) of the measurements \underline{X}_m , k is the number of measurements for the subset, n is the number of parameters in the model, l is the number of variables, and γ_{ij} is the i^{th} measurement error of the variable j (an element of \underline{Y}). Note that the conventional standard deviation, σ , is defined by

$$\sigma^2(\text{subset}) = \frac{(\underline{X}_m - \underline{X})^T (\underline{X}_m - \underline{X})}{k - n}\quad (4-68)$$

If the assumed measurement error, γ_{ij} , is considered to be the same in each variable, then the standard deviation σ can be related to the sigma estimate, σ_e , by

$$\sigma = \sqrt{\gamma_{ij}} \sigma_e\quad (4-69)$$

It is noted that the maximum likelihood approach used here requires that the covariances (off-diagonal elements of \underline{R} in Equation (4-66)

be zero. In this case \underline{R} becomes a diagonal matrix whose elements are variances (a priori estimates) of the variables \underline{Z}_m . Values of R_{ij} used in these studies for the liquidus temperature, solidus temperature, activity and enthalpy of mixing are 1.5 K, 1.5 K, 0.001, and $0.001 \cdot (RT_m)$, respectively. Here, R is the gas constant and T_m is the temperature at which the enthalpy of mixing is measured.

4.4 Data Base

4.4.1 Al-Sb System

The thermodynamic properties of the compound Al-Sb are well characterized with several determinations of ΔH_f (fusion), ΔH_f° (formation), ΔG_f° (formation) and both low and high temperature heat capacity. The selected values of these properties are listed in Tables 3-2 and 3-3. Several measurements of the liquidus (132,181-185) are depicted in Figure 4-1 and show some scatter. A single eutectic point (measured by a thermal cooling technique) near the Al-rich end was given by Dix et al. (186). Urasov (181) has measured the liquidus also by a thermal cooling technique over the entire composition range, as have Guertler and Berman (using DTA)(182). Linnebach and Benz (183,184) determined several Sb-rich liquidus points by direct observation method, while Glazov and Petrov (185) made several measurements (by DTA method) near the stoichiometric composition. The results of Glazov and Petrov (185) give a peak at the 1:1 Al-Sb composition, indicating that appreciable association may occur in the liquid. However, the data of Glazov and Petrov (185) are in relatively poor agreement with the measurements of

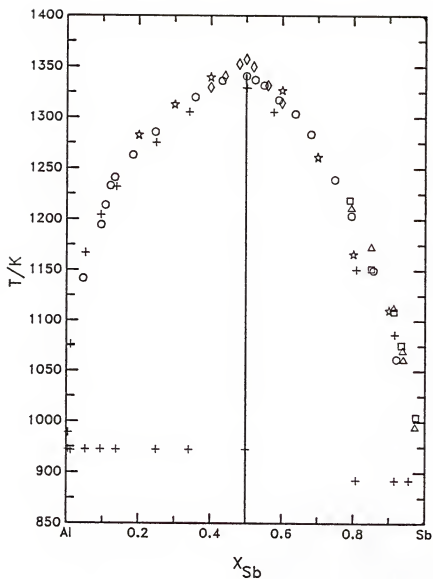


Figure 4-1. Phase diagram of the Al-Sb system: o, Ref. (181); +, Ref. (182); \square , Ref. (183), Δ , Ref. (184); \star , Ref. (132); \diamond , Ref. (185).

Urasov (181). The measurements of Guertler and Bergman (182) are in general lower than those obtained by Urasov (181) for $x_{\text{Sb}} \geq 0.1$, while the data of Linnebach and Benz (183,184) are somewhat higher than those obtained by Urasov (181). Based on comparison with the other thermochemical data selected by Hultgren et al. (111), the data of Urasov (181) are used in this study.

Only one experimental investigation of the liquid mixture thermochemical properties is reported. Predel and Schallner (103), using a molten salt galvanic cell, measured the Al activity as a function of composition and temperature. The enthalpy of mixing at 1400 K was also determined from the temperature dependency of the e.m.f. measurements in this work. These results have been employed for parameter estimation.

Values for the parameters γ_i and q_i are required for the UNIQUAC equation. As discussed by Abrams and Prausnitz (164), γ_i is a measure of the number of equivalent segments per molecule, and q_i is a measure of a molecule's external surface area relative to some reference molecule. It is clear from these considerations that γ_i should be unity for each component and q_i should be equal to the ratio of the square of the component radius to that of the standard. It is found that the result of UNIQUAC to represent the thermodynamic data of group III-V systems is rather insensitive to the values of γ_i and q_i . For convenience, aluminum was chosen as the standard (i.e., $q_{\text{Al}} = 1$). With the van der Waals radius used in Aselage et al. (187), a value of 4.84 \AA^2 was assigned for q_{Sb} .

4.4.2 Ga-Sb System

As summarized in Tables 3-2 and 3-3, the thermochemical data for the Ga-Sb system are well characterized. For this study, a data base for the Ga-Sb system consisting of the enthalpy of mixing and Ga activity as a function of composition was used to estimate the model parameters. The experimental liquidus measurements were used to compare the predicted phase diagram, which was calculated with parameters determined for the enthalpy of mixing and the Ga activity fits. Based on comparison with the various available experimental data (152,187), the results of the liquidus (39,48,130), enthalpy of mixing (131), and liquid-phase gallium activity (152) have been used in this study.

4.4.3 In-Sb System

As with Ga-Sb, the experimental information on the liquidus temperature, the enthalpy of mixing, and liquid phase component activity are available. The enthalpy of mixing (97) and the In activity (120,121,188) were used for parameter estimation, and the predicted phase diagram was compared to the available liquidus measurements. Both the Ga-Sb and In-Sb systems have been critically assessed by Aselage et al. (187), the liquidus (118), enthalpy of mixing (97), and liquid phase In activity (120,121,88) measurements selected by then have been used in this study.

4.4.4 Al-Ga System

The Al-Ga system has been investigated extensively as reviewed by Hultgren et al. (111). As shown in Figure 4-2, the liquidus has been determined by several investigators (189-195), while the work of Zoller (191) and Shunk (194) are the only investigations of the solidus line on the Al-rich side of the phase diagram. Based on comparison with the other thermochemical data selected by Hultgren et al. (111), the liquidus results of Predel and Stein (189) and the solidus data of Shunk (194) have been used in this study.

Predel and Stein (189) determined the enthalpy of mixing by calorimetry. The measurements of Lee and Yazawa (196) and Batalin et al. (197) are more positive than that of Predel and Stein (189). The results of Danilin and Yatsenko (190) are much lower (over 50% difference at $x_{Al} = 0.5$) than the other measurements. The data of Predel and Stein (189) has been included in the data base for the calculations.

The liquid phase activity of Al in Al-Ga mixtures has been determined with a molten salt galvanic cell by Lee and Yazawa (196), by Predel and Schallner (198) and by Eslami et al. (199). The data of Lee and Yazawa (196) are in good agreement with those selected by Hultgren et al. (111). The results of Predel and Schallner (198) show somewhat more positive deviation from ideality than the other measurements, while the data of Eslami et al. (199) exhibit less positive deviations than the other measurements. The data of Lee and

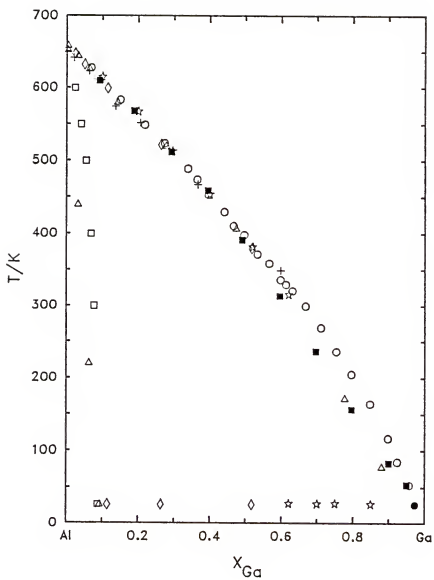


Figure 4-2. Phase diagram of the Al-Ga system: o, Ref. (189); ●, Ref. (113); □, Ref. (194); ■, Ref. (190); Δ, Ref. (191); ◇, Ref. (192); ☆, Ref. (193); +, Ref. (195).

Yazawa (196) and of Hultgren et al. (111) have been included in the data base.

4.4.5 Ga-In System

As with Al-Ga, a data base for the Ga-In system consisting of liquidus temperature, the enthalpy of mixing and liquid phase Ga activity as a function of temperature and composition was employed. The Ga-In liquidus has been measured by several investigators (200-205). Unfortunately, there are no reliable solidus and no measurements of thermodynamic quantities for the solid solution. Based on comparison with the other thermochemical data selected by Hultgren et al. (111), the liquidus data of Swirdely and Selis (200), and Hayes and Kubaschewski (204) have been used in this study.

The enthalpy of mixing has been accurately measured by Bros et al. (206,207) between 110° and 469°C. These data indicate that ΔH_m is independent of temperature within experimental error. The liquid phase component activity in Ga-In mixtures were also measured with a solid state electrochemical technique by Klinedinst et al. (208), by Pong and Donaghey (209), and by Svirbeley and Read (210) and with a Knudsen-Cell effusion technique by Macur et al. (211). Based on the consistency tests of Anderson (106), the results of Bros (206,207), and Klinedinst et al. (208) have been employed for parameter estimation.

4.4.6 Al-In System

The very limited information for the Al-In system has been reviewed by Hultgren et al. (111). Based on the discussion in Hultgren et al. (111), the liquid-liquid equilibrium data of Massart et al. (212), and the solid-liquid equilibrium data of Massart et al. (212) and Predel (213) have been used in this study. The selected values of the enthalpy of mixing and aluminum activity listed in Hultgren et al. (111) are also included in the data base for the calculations.

4.5 Results for a Combined Data Set

The combined data set consisting of liquidus temperature, enthalpy of mixing, group III liquid phase activity and the selected values for θ_I and θ_{IC} was used to estimate parameters in each model described above for the Al-Sb system, and to estimate NRTL and simple solution model parameters for the Al-In, Al-Ga, and Ga-In systems. The ability of a model to represent the combined data is characterized by the overall standard deviation defined by Equation (4-66). The standard deviations in the predicted liquidus temperature, the enthalpy of mixing and the group III liquid phase activity for each model mentioned above are calculated by Equation (4-68) and listed in Table 4-5 for parameters estimated with the combined Al-Sb data set. For comparison, the standard deviations of the individual Al-Sb data set fits are also listed in this table. A comparison of the deviations obtained from different models with the same data set gives an indication of relative adequacy of different

Table 4-5. Standard deviations for the combined and individual Al-Sb data base fits.

Model	Number of Parameters		Standard Deviation (σ)					
	Combined	Individual	Combined			Individual		
			T^1 (K)	ΔH^m (cal/mol)	a_{Al}	T^1 (K)	ΔH^m (cal/mol)	a_{Al}
NRTL	4	2	23.4	10.4	0.015	6.6	6.0	0.011
Wilson	4	2	34.1	39.0	0.016	17.6	35.2	0.011
UNIQUAC	4	2	33.6	40.6	0.016	19.4	36.3	0.011
Scatchard-Hamer	4	2	22.4	65.3	0.017	6.5	60.0	0.009
Quasichemical	2	1	38.6	76.3	0.013	32.3	71.7	0.011
Simple	2	1	36.3	73.4	0.015	31.4	72.8	0.010
Regular Associated	4	3	-	-	-	36.9	73.7	0.011

models. Convergence of the maximum likelihood algorithm to a unique set of parameters for the combined data set was not obtained for the regular associated solution model, apparently due to the inflexibility of the expression.

An examination of the results presented in Table 4-5 indicates that among the models considered here, the NRTL equation best represents the combined experimental data for the Al-Sb system. The inability of other models to represent either the combined or individual data set is clearly demonstrated in Table 4-5. It can be seen from Table 4-5 that all the predicted liquidus temperature (both combined and individual data set fits) lie far outside of the experimental error bounds (except for the individual data set fit with the NRTL and Scatchard-Hamer equations). Only the NRTL equation represents the individual data sets reasonably well in each case. As previously mentioned, this is expected for the highly asymmetric Al-Sb system. The improved exponential expression of local composition models in the enthalpy of mixing is evident in the results shown in Table 4-5.

The parameter sets determined with the combined data set for both the NRTL equation and the simple solution models are listed for the Al-Sb and Al-In systems in Table 4-6. The liquidus temperature, enthalpy of mixing, and liquid phase component activities calculated with the NRTL equation and the simple solution models are displayed in Figures 4-3 to 4-5 for the Al-Sb system and compared with the experimental data. Figure 4-3 shows that the calculated liquidus for Al-Sb system computed with the simple solution model parameters in

Table 4-6. NRTL and simple solution parameters obtained with the combined data base fit for the Al-Sb and Al-In systems.

System	Model	a (cal/mole)	b (cal/mole-K)	c (cal/mole)	d (cal/mole-K)	α_{IC}
Al-Sb	NRTL	-3282.3	1.612	-5756.7	1.353	-0.5
	Simple	-4413.6	0.736	-	-	-
Al-In	NRTL	3020.6	-0.149	1245.4	0.049	-0.3
	Simple	5595.6	-0.704	-	-	-

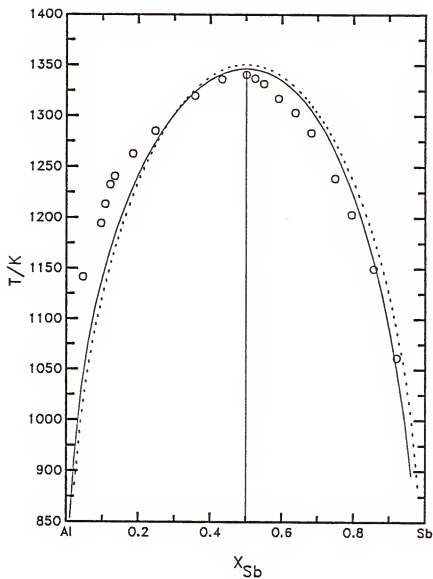


Figure 4-3. The Al-Sb phase diagram: o, Ref. (181); —, calculated from NRTL liquid solution parameters in Table 4-6; ---, calculated from simple liquid solution parameters in Table 4-6.

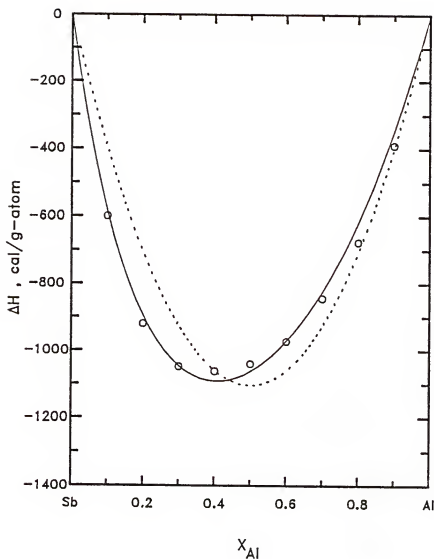


Figure 4-4. Enthalpy of mixing Al and Sb at $T = 1400$ K: o, Ref. (132); —, calculated from NRTL liquid solution parameters in Table 4-6; ---, calculated from simple solution parameters in Table 4-6.

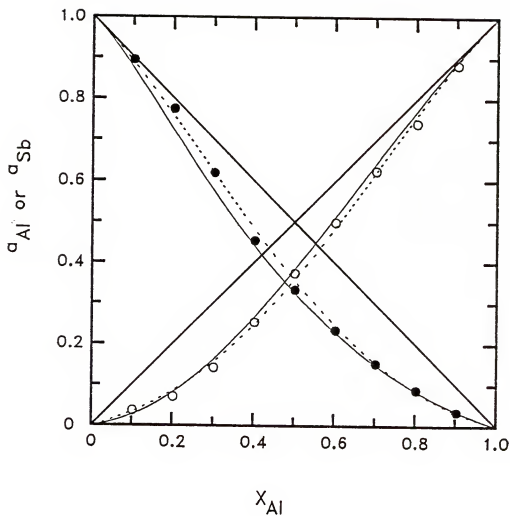


Figure 4-5. Al or Sb liquid phase component activity at $T = 1400 \text{ K}$: o, •, Ref. (132); —, calculated from NRTL liquid solution parameters in Table 4-6; ---, calculated from simple solution parameters in Table 4-6.

Table 4-6 are consistently higher than any measurement in the Sb-rich region (37 K at $x_{\text{Sb}} = 0.8$) and lower in the Al-rich portion (76 K at $x_{\text{Al}} = 0.9$). As shown in Figure 4-4, the enthalpy of mixing calculated with the NRTL equation is better than that obtained with the simple solution model. This substantial improvement is expected because the introduction of the Boltzman-type factor in the NRTL equation allows for asymmetry and temperature dependence in the enthalpy of mixing. Figure 4-5 shows that each of the models provides a good description of the component activities. Although the NRTL equation gives a good representation of the enthalpy of mixing and the component activities, the results of the calculated liquidus are similar to those obtained with the simple solution model. From these calculations the available thermochemical data (a_{Al}^{l} and ΔH_{m}) for the Al-Sb system is not consistent with the reported liquidus measurements, probably due to the inability of the model to represent the highly asymmetric liquidus data.

An attempt has been made for the first time to use a solution model to represent the phase diagram and thermochemical data of the Al-In system. As shown in Figure 4-6, the presence of a highly asymmetric miscibility gap in the Al-In liquid phase clearly indicates that the models considered here should have difficulty representing the liquid-liquid equilibrium data. Indeed, the calculated phase diagram with the NRTL equation is higher than those selected by Hultgren et al. (111) in the 15-70 mole percent In interval (30 K at $x_{\text{In}} = 0.4$). The results calculated with the simple solution model were even poorer than those obtained with the NRTL

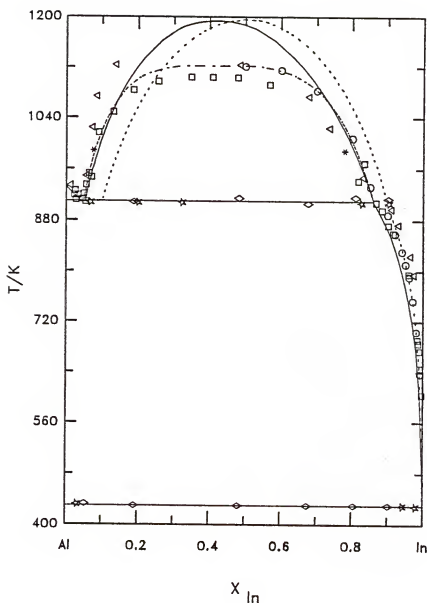


Figure 4-6. The Al-In phase diagram: o, Ref. (212); □, Ref. (213); Δ, Ref. (214); *, Ref. (215); ◇, Ref. (216); ☆, Ref. (217); ---, Ref. (113); —, calculated from NRTL liquid solution parameters in Table 4-6; ---, calculated from simple liquid solution parameters in Table 4-6.

equation. This is expected because the thermochemical properties expressed with the simple solution model are symmetric functions. As seen, the Al-rich eutectic point has been shifted from $x_{In} = 0.05$ (111) to $\sim x_{In} = 0.1$ (calculated value).

The enthalpy of mixing and liquid phase component activity calculated with the NRTL and simple solution models are plotted in Figures 4-7 and 4-8 for the Al-In system and compared with the selected data given by Hultgren et al. (111). As in the case of the Al-Sb system, the NRTL equation provides a good representation of the asymmetric data. It is shown in Chapter VI that the predicted Al-In-Sb ternary phase diagram are very sensitive to the parameters for this system.

Table 4-7 lists the parameter sets determined with the combined data set from the NRTL equation, the simple solution model and the strictly regular solution model for the Al-Ga and Ga-In systems. Note that no solidus data are used in the parameter estimation for the Ga-In system. Convergence of the maximum likelihood algorithm to a set of parameters was not obtained for the strictly regular liquid and simple (or strictly regular) solid solution model in the Ga-In system, probably due to the inability of the strictly regular solution to simultaneously represent the liquidus data and liquid phase thermochemical data. As shown in Table 4-7, the values of the overall standard deviations obtained with NRTL or simple liquid and simple solid solution are nearly identical. Also listed in this table is the overall standard deviation obtained with the strictly regular liquid and solid solution for the Al-Ga system. As can be

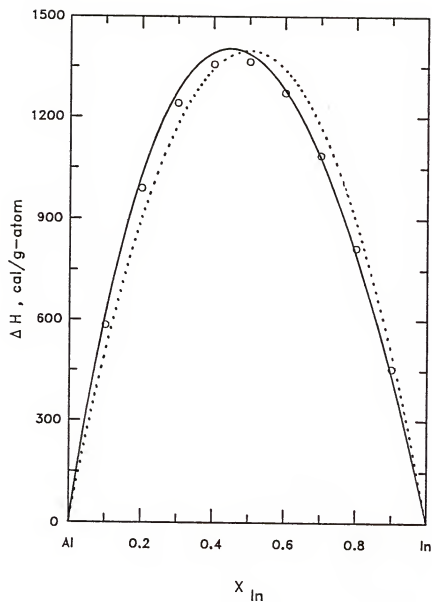


Figure 4-7. Enthalpy of mixing of Al and In at $T = 1173$ K: o, Ref. (113)(1173 K); —, calculated from NRTL liquid solution parameters in Table 4-6; ---, calculated from simple liquid solution parameters in Table 4-6.

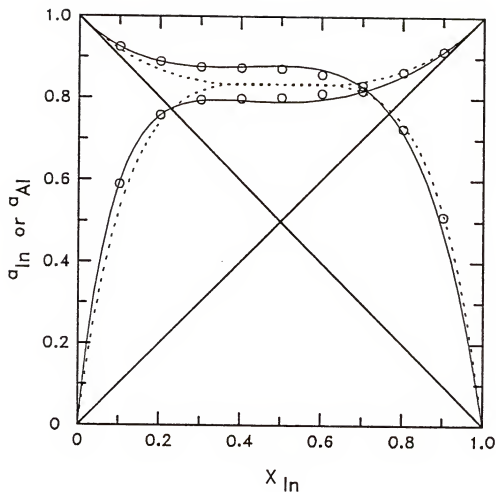


Figure 4-3. Al or In liquid phase component activity at $T = 1173 \text{ K}$: o, Ref. (113); —, calculated from NRTL liquid solution parameters in Table 4-6; ---, calculated from simple liquid solution parameters in Table 4-6.

Table 4-7. Solution model parameters obtained with the combined data base fit for the Al-Ga and Ga-In systems.

System	Phase	Model	a^1 (cal/mol)	b^1 (cal/mol-K)	c^1 or a^s (cal/mol)	d^1 or b^s (cal/mol-K)	α_{IC}	σ_0
Al-Ga	liquid	NRTL	-840.0	0.603	1640.1	-1.035	0.3	
	solid	simple	-	-	2284.8	-1.494	-	12.9
	liquid	simple	598.9	-0.318	-	-	-	
	solid	simple	-	-	2337.0	-1.597	-	13.4
	liquid	regular	511.7	-	-	-	-	
	solid	regular	-	-	1676.2	-	-	24.9
Ga-In	liquid	NRTL	697.3	-0.159	494.7	0.364	0.3	
	solid	simple	-	-	391.3	3.712	-	2.73
	liquid	simple	1029.9	0.290	-	-	-	
	solid	simple	-	-	-581.7	7.086	-	3.06

seen, nearly a factor of two increase in the magnitude of the overall standard deviation is found with the strictly regular liquid and solid solution. It is also seen in Table 4-7 that both the NRTL and simple liquid solution models give almost the same parameter sets of the solid solution for the Al-Ga system. However, two different parameter sets of the solid solution model for the Ga-In system are obtained with the two liquid solution models. The physical interpretation of these two parameter sets is quite different. For example, the parameter set $w^S = 391.3 + 3.712 T$ predicts positive values for the solid phase enthalpy of mixing and predicts a miscibility gap at $T = 51 \text{ K}$, while the parameter set $w^S = -581.7 + 7.086 T$ gives negative values for the solid phase enthalpy of mixing and predicts complete miscibility at all temperatures.

The calculated phase diagrams, liquid phase enthalpy of mixing and component activities are compared to the experimental data in Figures 4-9 to 4-11 for the Al-Ga system and in Figures 4-12 to 4-14 for the Ga-In system. It is apparent from Figures 4-9 to 4-14 that the NRTL or simple liquid and simple solid solution models provide an excellent fit to the reported phase diagram, liquid phase enthalpy of mixing and component activity. The common practice of applying the strictly regular solution model to a description of the liquid phase, however, gives only fair agreement with the experimental measurements. No previous work has been reported with the combined data set for these two systems. Unfortunately, because solid

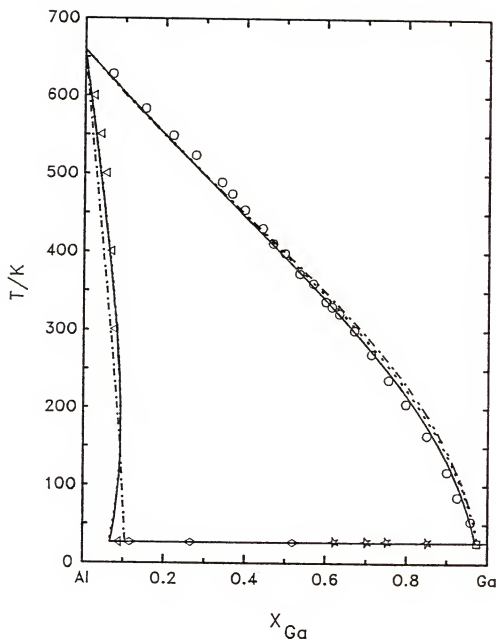


Figure 4-9. The Al-Ga phase diagram: o, Ref. (189); Δ, Ref. (113); Δ, Ref. (194); ◇, Ref. (192); ✕, Ref. (193); —, calculated from NRTL liquid solution and simple solid solution parameters in Table 4-7; ---, calculated from simple liquid and solid solution parameters in Table 4-7; -.-, calculated from regular liquid and solid solution parameters in Table 4-7.

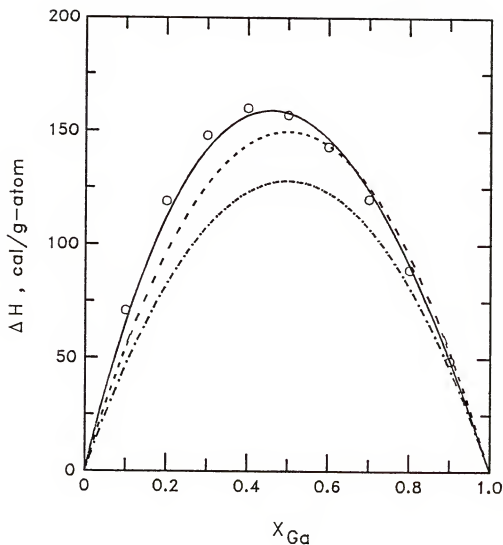


Figure 4-10. Enthalpy of mixing of Al and Ga at $T = 1023$ K: o, Ref. (113); —, calculated from NRTL liquid solution parameters in Table 4-7; ---, calculated from simple liquid solution parameters in Table 4-7; -·-, calculated from regular liquid solution parameter in Table 4-7.

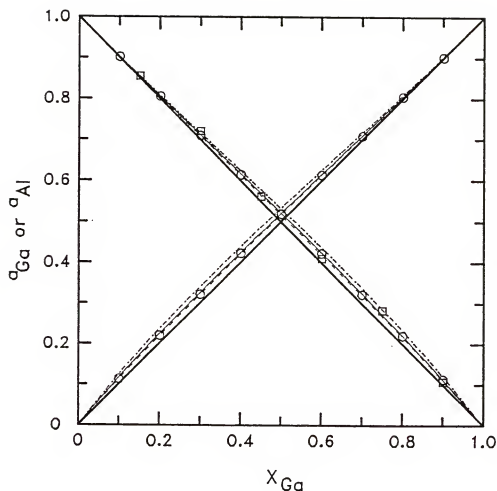


Figure 4-11. Al or Ga liquid phase component activity at $T = 1023 \text{ K}$: o, Ref. (113); □, Ref. (196); —, calculated from NRTL liquid solution parameters in Table 4-7; ---, calculated from simple liquid solution parameters in Table 4-7; -.-, calculated from regular liquid solution parameter in Table 4-7.

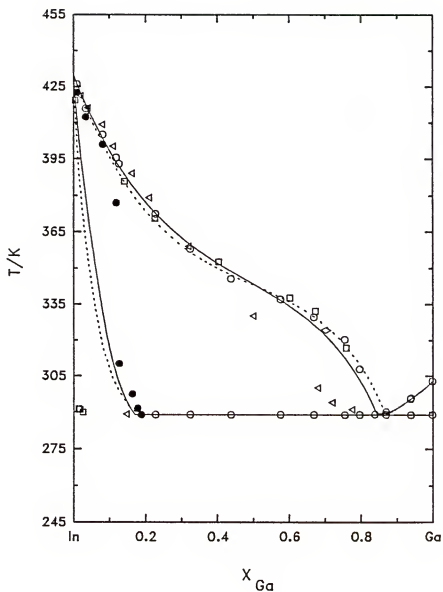


Figure 4-12. The Ga-In phase diagram: ●,○, Ref. (200); □, Ref. (201); Δ, Ref. (202); ◇, Ref. (204); —, calculated from NRTL liquid solution and simple solid solution parameters in Table 4-7; ---, calculated from simple liquid and solid solution parameters in Table 4-7.

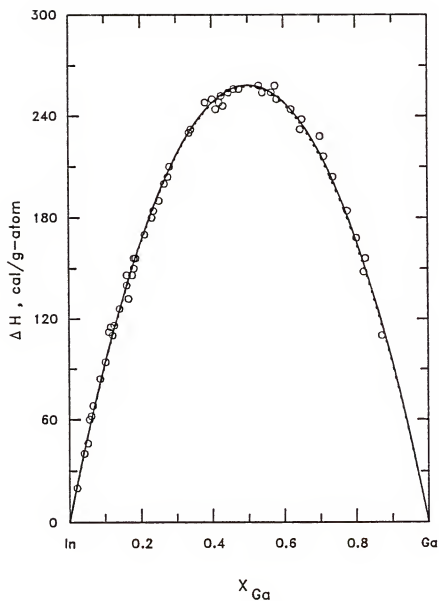


Figure 4-13. Enthalpy of mixing of Ga and In at $T = 742 \text{ K}$: o, Ref. (206,207); —, calculated from NRTL liquid solution parameters in Table 4-7; ---, calculated from simple liquid solution parameters in Table 4-7.

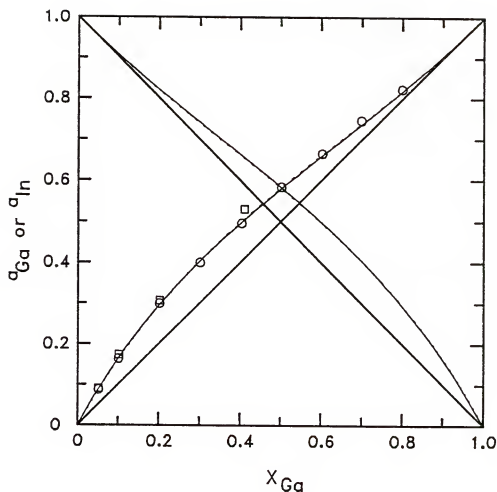


Figure 4-14. Ga or In liquid phase component activity at $T = 1123$ K: o, Ref. (208); □, Ref. (209)(1124 K); —, calculated from NRTL liquid solution parameters in Table 4-7; ---, calculated from simple liquid solution parameters in Table 4-7.

solution thermochemical data is lacking, the parameter set which best describes the solid solution behavior cannot be determined.

As mentioned previously, it may be possible to increase the number of adjustable parameters in the NRTL equation from four to five; this is accomplished by considering α_{IC} as a fifth parameter. However, it was found that the standard deviations exhibit a rather broad minimum (e.g., $-1 \leq \alpha_{IC} \leq 4$ and $\alpha_{IC} \neq 0$ for Al-Ga system) about the values of α_{IC} given in Tables 4-6 and 4-7. This indicates that the value of α_{IC} may be fixed at some value before fitting the data, which would be especially useful when the data base is small. In the limit that α_{IC} equals zero, the NRTL equation becomes equivalent to the simple solution model. Note that as α_{IC} is near zero (0^+ or 0^-), the standard deviation is still in the broad minimum. It was shown, however, that the predicted results of the ternary phase diagram were relatively poor with this set of parameters. Each of the models used to fit the combined data set was also used to fit each of the data sets (phase diagram, enthalpy of mixing, and component activity) individually. These results were used to investigate the cross-predictive abilities of the various models, and are discussed in the next section.

4.6 Data Cross-Prediction in III-Sb Systems

It is often found that a complete data base is unavailable for a particular system of interest. A common approach is to use a solution model to represent the experimental data and then to calculate the undetermined properties with the "best fit" model

parameters. The equation of a solution model also serves as a continuously smooth function by which interpolation between points in a data base and extrapolation of data are made possible. In the previous section, the ability of various solution models to represent a combined data set was examined. In this section, the possibility for cross-prediction with the parameters obtained from a single property data base fit is examined. If the model parameters are physically significant, the set of parameters used to represent the liquidus temperature for a specific system should be in close agreement with the parameters used to represent the liquid phase enthalpy of mixing and component activity. It is found that none of the models considered here possess this property. The very different values of the parameter sets indicate the lack of ability of the models to correctly describe the physical situation.

Firstly, a situation involving only a single type of data is considered. Skjold-Jørgensen et al. (218) and Hanks et al. (219) attempted to predict either VLE (vapor-liquid equilibrium) data from ΔH_m information or ΔH_m data from only one isothermal set of VLE information for several organic systems. They concluded that in some cases the cross prediction may be possible with the original local composition models (T-independent parameters). This is, however, not the general case. A significant improvement on cross-prediction can be made by the introduction of temperature dependent interaction parameters and, of course, requires a non-isothermal data base to estimate parameters. Several models mentioned above have been used to cross-predict properties for the systems considered in this

study. Figures 4-15 and 4-16 show the results obtained from model parameters determined by fitting the Al-Sb liquidus. As shown in Figure 4-15, the calculated activities in the Al-Sb system are always qualitatively correct with the exception of the values of a_{Al} ($x_{Al} \geq 0.55$) calculated from the Scatchard-Hamer equation, which exhibits positive deviation from ideal behavior. Note that the agreement is good for both the RAS and simple solution models, while the Wilson equations yield values which are considerably more negative than the experimental values. The results for the enthalpy of mixing predictions are less satisfactory. As plotted in Figure 4-16 for the Al-Sb system, the results of the RAS equation are correct in sign but wrong in magnitude, while the other models give results that are of the wrong sign.

Figure 4-17 shows the predicted Al or Ga activity obtained from parameters determined by fitting the Al-Ga liquidus. As can be seen, the agreement is excellent for the regular solution model, while the NRTL and simple solution models show results which are more positive than the experimental measurements. Figure 4-18 shows the enthalpy of mixing for Al-Ga system predicted with parameters determined by fitting the liquidus. The results of the NRTL and simple solution models are of the wrong sign, while the regular solution model gives results that are correct in sign but wrong in magnitude. In a similar fashion, Figure 4-19 shows the results for the enthalpy of mixing obtained from model parameters determined by fitting the Al activity (Al-Ga system). It is seen that all of the model predictions are of the correct sign but again wrong in magnitude.

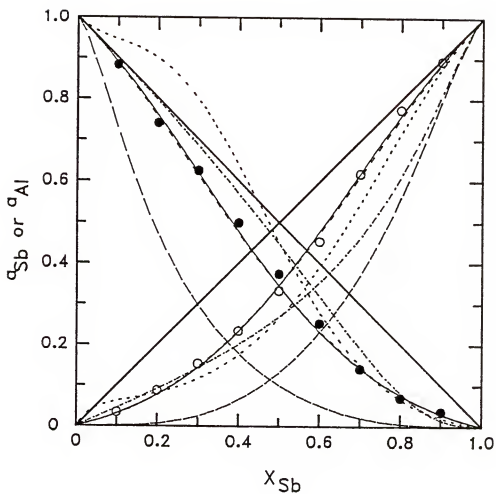


Figure 4-15. Component activities for the Al-Sb system as predicted with parameters determined by fitting the liquidus: —, RAS and simple solution (coincident); ---, NRTL; —·—, Wilson; ···, Scatchard-Hamer; ● and ○, Ref. (132).

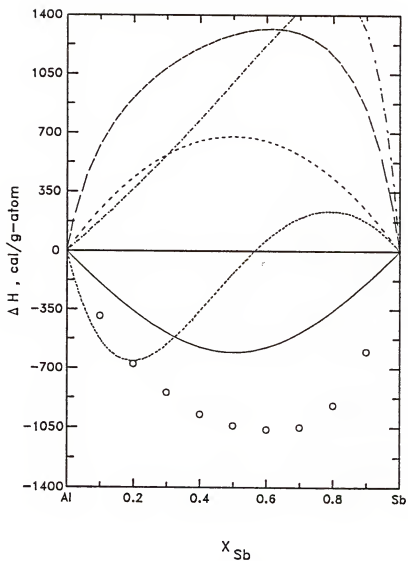


Figure 4-16. Enthalpy of mixing for the Al-Sb system as predicted with parameters determined by fitting the liquidus: —, RAS; ---, NRTL; —·—, Wilson; ···, simple solution; ····, Scatchard-Hamer; o, Ref. (132).

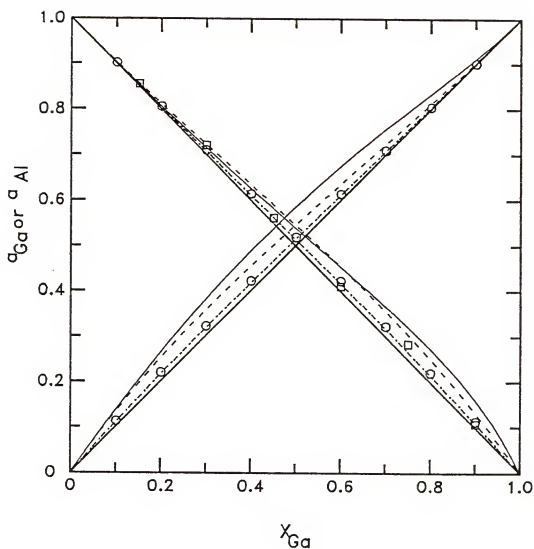


Figure 4-17. Al or Ga activity predicted with parameters determined by fitting the liquidus: —, NRTL; ---, simple solution; -·-, regular solution; o, Ref. (113); □, Ref. (196).

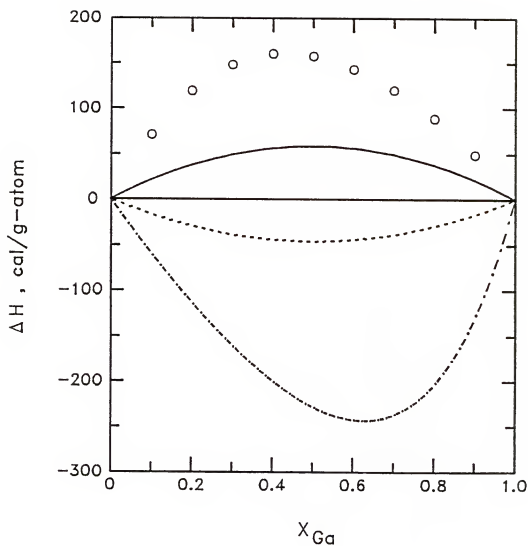


Figure 4-18. Enthalpy of mixing for the Al-Ga system as predicted with parameters determined by fitting the liquidus: ---, NRTL; ---, simple solution; —, regular solution; o, Ref. (113).

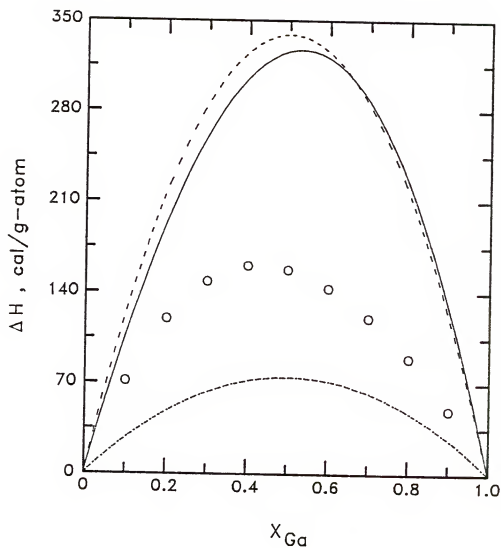


Figure 4-19. Enthalpy of mixing for the Al-Ga system as predicted with parameters determined by fitting the Al activity: —, NRTL; ---, simple solution; ---, regular solution; o, Ref. (113).

It is apparent from the above results that the model parameters determined by fitting the liquidus or activity individually show difficulty in describing the enthalpy of mixing.

Figure 4-20 presents the Al-Sb liquidus calculated with parameters determined using the enthalpy of mixing as a data base. The results obtained from the NRTL equation are quite different from the experimental phase diagram (the melting point differs by 124 K). Note that the data set used in generating Figure 4-20 is isothermal, so that the parameter temperature dependence could not be determined. It is apparent that values of the liquidus temperature are quite sensitive to the representation of the thermodynamic data.

The results shown above for the attempted cross-predictions from a single kind of data were, in general, unsatisfactory. This is not surprising since two of the data sets are needed to thermodynamically predict the third (187). Next, the case in which two of three individual data sets (T^l , ΔH_m , a_i^l) are available is considered; model parameters determined by a fit of the three possible pairs of data sets may then be used to predict the third. The results for the Al-Sb system are shown in Figures 4-21 to 4-23 for the predicted liquidus temperature, enthalpy of mixing, and component activity, respectively. It is seen that the agreement between the calculated values and experimental data is still poor. This is expected for the Al-Sb system because none of the models considered here can represent the combined data set well.

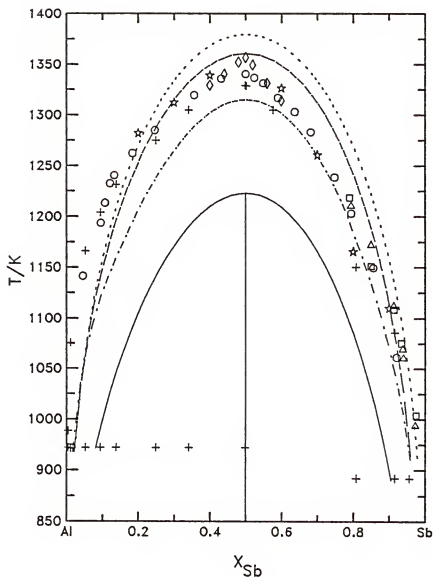


Figure 4-20. Al-Sb liquidus predicted from parameters estimated by fitting the enthalpy of mixing: —, NRTL; ---, UNIQUAC; -·-, Scatchard-Hamer; ---, simple solution; o, Ref. (181); +, Ref. (182); □, Ref. (183); Δ, Ref. (184); ☆, Ref. (132); ◊, Ref. (185).

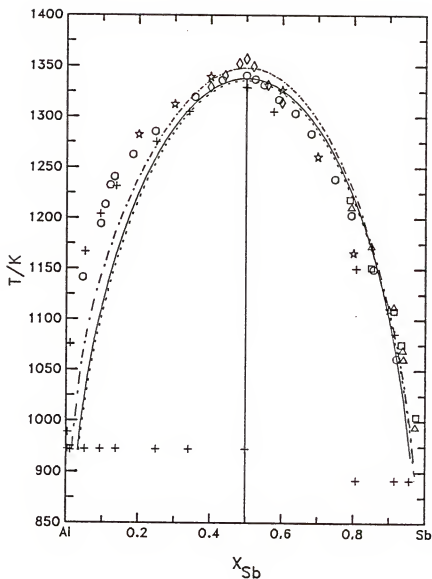


Figure 4-21. Al-Sb liquidus predicted from parameters estimated by fitting the Al activity and enthalpy of mixing: —, NRTL; ---, Scatchard-Hamer; -.-, simple solution; o, Ref. (181); +, Ref. (182); □, Ref. (183); Δ, Ref. (184); ☆, Ref. (132); ◇, Ref. (185).

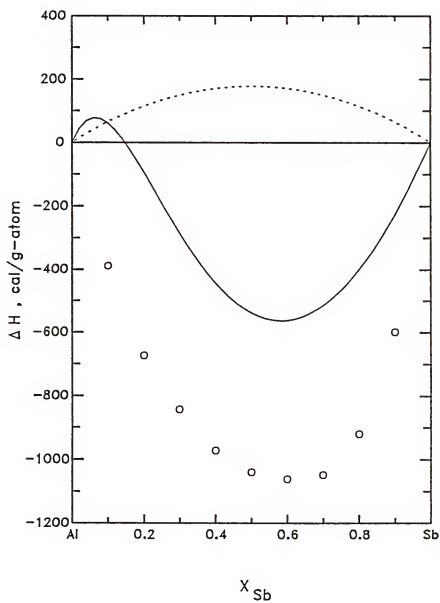


Figure 4-22. Enthalpy of mixing Al and Sb predicted from parameters estimated by fitting the liquidus and Al activity: —, NRTL; ---, simple solution; o, Ref. (132).

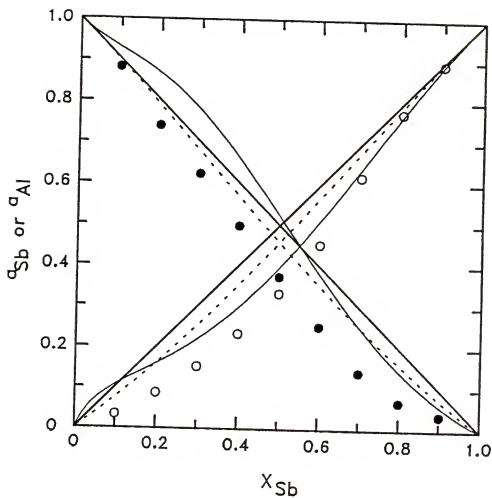


Figure 4-23. Al or Sb activity predicted from parameters estimated by fitting the liquidus and enthalpy of mixing: —, NRTL; ---, simple solution; o, ●, Ref. (132).

4.7 Improved Methods for Data Cross-Prediction

As mentioned previously, a model in which the parameters have a unique, physical significance may be expected to provide reasonable cross-predictions; this is obviously not the case for any of the models considered here. However, the results of the combined data set fits for some systems studied here show that a set of parameters could be found which accurately describe all of the available data. It is apparent that the problem lies in the nonuniqueness of the model parameters. It should be possible to improve cross-predict capabilities by fixing the model parameter values at well-determined experimental data points. Presented here is an improved method of predicting the liquidus of the binary systems by fixing one or two parameters based on the individual activity and enthalpy of mixing fits or the double data set fit of the models at the individual melting points and eutectic point or both points of the binary compound.

Case A: One Parameter Fixed at T_m^{IC} (Melting Temperature of the Compound IC)

Equation (2-91) at T_m^{IC} is reduced to the following result:

$$\theta_{IC}(T_m^{IC}) = \ln[a_I^{s1}(T_m^{IC}, x_I^1=0.5)] + \ln[a_C^{s1}(T_m^{IC}, x_C^1=0.5)] \quad (4-70)$$

Upon substitution, an expression for the activities into Equation (4-70), a relation between the parameters is obtained. For the case of the simple solution model with the interchange energy $w = a + bT$, the following expression results:

$$a = 2RT_m^{IC}[\theta_{IC}(T_m^{IC}) + \ln 4] - bT_m^{IC} \quad (4-71)$$

where R is the gas constant. Moreover, substituting Equation (4-71) back into the expression for the activity coefficient eliminates one adjustable parameter in the model. In a similar manner, the following relation results for the NRTL equation:

$$a = \frac{RT_m^{IC} \{ [\theta_{IC}(T_m^{IC}) + \ln 4] - \tau_{IC} \left[\frac{\exp(-\alpha_{IC}\tau_{IC})}{[1+\exp(-\alpha_{IC}\tau_{IC})]^2} + \frac{\exp(-2\alpha_{IC}\tau_{IC})}{[1+\exp(-\alpha_{IC}\tau_{IC})]^2} \right] \}}{\frac{\exp(-\alpha_{IC}\tau_{CI})}{[1+\exp(-\alpha_{IC}\tau_{CI})]^2} + \frac{\exp(-2\alpha_{IC}\tau_{CI})}{[1+\exp(-\alpha_{IC}\tau_{CI})]^2}} - bT_m^{IC} \quad (4-72)$$

where

$$\tau_{CI} = (a + bT_m^{IC}) / (RT_m^{IC}) \quad (4-73)$$

$$\tau_{IC} = (c + dT_m^{IC}) / (RT_m^{IC}) \quad (4-74)$$

It is apparent that the constraint Equation (4-72) is implicit in the parameters a , b , c and d and can be solved by numerical techniques.

Case B: One Parameter Fixed at T_e (Eutectic Temperature)

Either Equation (2-91) or (4-14) can be used as a constraint equation for this case. If Equation (2-91) is used, an equation similar to Equation (4-70) is obtained as follows:

$$\theta_{IC}(T_e) = \ln[a_I^1(T_e, x_I^1=x_e^1)] + \ln[a_C^1(T_e, x_C^1=1-x_e^1)] \quad (4-75)$$

where x_e^1 is the eutectic composition of the component I. For the case of the simple solution model, Equation (4-75) is reduced to the following result:

$$a = \frac{RT_e [\theta_{IC}(T_e) - \ln(x_e^1(1-x_e^1))]}{[(x_e^1)^2 + (1-x_e^1)^2]} - bT_e \quad (4-76)$$

On the other hand, if Equation (4-14) is applied, we have

$$\theta_C(T_e) = \ln[a_C(T_e, x_C^1=1-x_e^1)] \quad (4-77)$$

For the simple solution model, Equation (4-77) can then be expressed as

$$a = \frac{RT_e}{(x_e^1)^2} [\theta_C(T_e) - \ln(1-x_e^1)] - bT_e \quad (4-78)$$

Similarly, for the NRTL equation, if we introduce the expression for the activity coefficient given by Equation (4-34), Equations (4-75) and (4-77) can be written as

$$c = \frac{RT_e [\theta_{IC}(T_e) - \ln(x_1 x_2)] - \tau_{CI} \left[\frac{x_2^2 \exp(-\alpha_{IC} \tau_{IC})}{[x_2 + x_1 \exp(-\alpha_{IC} \tau_{CI})]^2} + \frac{x_1^2 \exp(-2\alpha_{IC} \tau_{CI})}{[x_2 + x_1 \exp(-\alpha_{IC} \tau_{CI})]^2} \right]}{\frac{x_2^2 \exp(-2\alpha_{IC} \tau_{IC})}{[x_1 + x_2 \exp(-\alpha_{IC} \tau_{IC})]^2} + \frac{x_1^2 \exp(-\alpha_{IC} \tau_{IC})}{[x_1 + x_2 \exp(-\alpha_{IC} \tau_{IC})]^2}} - dT_e \quad (4-79)$$

and

$$c = \frac{RT_e \{x_2 [\theta_C(T_e) - \ln x_1] - \tau_{CI} \frac{\exp(-\alpha_{IC} \tau_{IC})}{[x_2 + x_1 \exp(-\alpha_{IC} \tau_{CI})]^2}\}}{\frac{\exp(-2\alpha_{IC} \tau_{IC})}{[x_1 + x_2 \exp(-\alpha_{IC} \tau_{IC})]^2}} - dT_e \quad (4-80)$$

where $\tau_{CI} = (a + bT_e)/(RT_e)$ (4-81)

$$\tau_{IC} = (c + dT_e)/(RT_e) \quad (4-82)$$

$$x_1 = x_C^1 = 1 - x_e^1 \quad (4-83)$$

and $x_2 = x_I^1 = x_e^1$ (4-84)

Again, Equations (4-79) and (4-80) are implicit relations for the parameters a , b , c and d . With either constraint equation (4-79) or (4-80), one or two adjustable model parameters can be eliminated.

Case C: Two Parameters Fixed at T_m^{IC} and T_e

Two different equation sets are considered as constraint equations for this case. One is Equations (4-70) and (4-75) and the other is Equations (4-70) and (4-77). The computational procedure for this case is more complicated than that for case (A) or (B).

Table 4-8 shows all possible permutations of one or two parameters fixed at the individual melting point (T_m) and eutectic point (T_e) or both points of a binary IC compound for the simple solution model. The parameters sets determined with additional constraint equations (4-70), (4-75), or (4-77) for both the NRTL equation and the simple solution models are listed in

Table 4-8. Summary of cases studied with fixing one or two parameters from the equilibrium condition at the compound melting point and the Sb-rich eutectic point or both points for the simple solution model.

Number of Parameters Fixed	Case Number	Equation(s) Used			
		(2-91)	(4-70)	(4-75)	(4-77)
0	1	*			
1	2		*		
	3			*	
	4				*
2	5		*	*	
	6		*		*

Table 4-9. Results of cases listed in Table 4-8 with parameters estimated by fitting the group III activity and enthalpy of mixing for the In-Sb and Ga-Sb systems.

Case	In-Sb			Ga-Sb		
	a(cal/mole)	b(cal/mole-K)	σ_0	a(cal/mole)	b(cal/mole-K)	σ_0
1	-2662.6	-2.332	33.17	-982.7	-1.256	38.6
2	-2658.6	-1.568	34.3	-982.2	-1.489	38.7
3	-2657.8	-1.585	34.2	-982.2	-1.118	38.3
4	-2590.4	2.116	80.8	-967.7	1.061	101.6
5	-2968.8	-1.180	-	1570.6	-4.081	-
6	7225.3	-95.408	-	1680.9	-19.421	-

Table 4-10. NRTL parameters obtained with additional constraint Equations (4-72) and (4-79) for the In-Sb and Ga-Sb systems.

System	Data Base	Parameter Fixed	a (cal/mole)	b (cal/mole-K)	c (cal/mole)	d (cal/mole-K)	α_{IC}	σ_0
In-Sb	a_{In} and ΔH_{mix}	a	11366.8	-0.265	-9180.5	-3.093	0.042	13.45
		a and c	15384.1	-4.166	-14329.9	0.718	0.021	14.07
	a_{In}	a	7557.4	1.335	-2326.4	-4.190	0.225	17.98
	ΔH_{mix}	a and c	12204.7	-4.442	-1946.1	-3.254	0.319	17.16
Ga-Sb	a_{Ga} and ΔH_{mix}	a	14996.3	-12.153	-16437.0	9.789	0.018	8.58
		a and c	14422.1	-6.597	-14420.1	3.486	0.021	8.77
	a_{Ga}	a**	793.7	-3.539	-1553.9	1.348	-0.254	37.01
	ΔH_{mix}	a and c**	922.3	-13.919	-1454.1	9.748	-0.037	42.14
Ga-Sb	a_{Ga}	a	-2758.7	0	-2773.2	0	-0.890	27.54
	ΔH_{mix}	a*	-1525.8	0	-2680.7	0	-0.779	50.83
		a**	-1689.7	0	-2761.7	0	-0.814	27.98

* The enthalpy of mixing measured by Gambino and Bros (131) and ** by Predel and Stein (127).

Tables 4-9 and 4-10 for the Ga-Sb and In-Sb systems. It should be mentioned here that the convergence for the NRTL equation used in case (C) is slower than that in case (A) or (B). Also, no adjustable parameter exists for the simple solution model in case (C). The goodness of the fit for each case is also indicated by the overall standard deviation, σ_0 , which was calculated for the data set used in the parameter estimation for each model. As shown in Table 4-9, the standard deviation for case 1 (without any parameters fixed) is almost the same or even larger than that for cases 2 and 3 for which one parameter is fixed at either the compound melting temperature or Sb-rich eutectic point and calculated with the liquidus equation. This substantiates the characteristic nonuniqueness of the model parameters. Note that the standard deviation for case 4, for which the fixed parameter is calculated with Sb component-rich liquidus equation, is about 2.5 times higher than that for the cases 1, 2, and 3. As can be seen later, this discrepancy is mainly due to the incorrect representation of the activity coefficient, which is quite sensitive to the calculation of the liquidus. The standard deviation for cases 5 and 6 is not listed in Table 4-9 for the Ga-Sb and In-Sb systems because two constraint equations can be used to solve two adjustable parameters. Thus, no experimental measurements are needed to estimate the parameters. Of course, the standard deviation for each case can be evaluated by its definition but the calculation here is not performed here.

Because the NRTL equation has 4 (or 5) parameters (T-dependent), there exists more possible permutations of these parameters fixed at

T_m or T_e or both of a III-V binary compound for the NRTL equation than those for the simple solution model. Table 4-10 lists several cases for the Ga-Sb and In-Sb systems. Parameters b and d are zero for isothermal Ga activity and enthalpy of mixing of the Ga-Sb system. The nonrandomness parameter, α_{IC} , was considered as a variable on the calculation. The unit of the standard deviation for the enthalpy of mixing in each case is in cal/mole. As in the case of the simple solution model, the standard deviation for these cases shown in Table 4-10 is almost the same or even smaller than those given by Aselage et al. (187). This again shows the nonuniqueness characteristic of the model parameters.

The predicted phase diagram calculated with parameters listed in Table 4-9 (simple solution model) are displayed in Figures 4-24 and 4-25 for the In-Sb system and in Figures 4-26 and 4-27 for the Ga-Sb system. In a similar manner, the liquidus temperature calculated with parameters listed in Table 4-10 (NRTL equation) are plotted in Figures 4-28 to 4-30 for the In-Sb system and in Figures 4-31 to 4-33 for the Ga-Sb system. An examination of the results shown in these figures indicates that the parameter set determined with one or two parameters fixed at T_m^{IC} or T_m^{IC} and T_e with the liquidus equation can predict the phase diagrams well for the two antimonide systems. However, the prediction of the liquidus temperature with the parameter fixed at T_e with the component-rich liquidus equation leads to large errors as demonstrated in Figures 4-25 and 4-27. The error is probably due to an incorrect representation of the activity or a

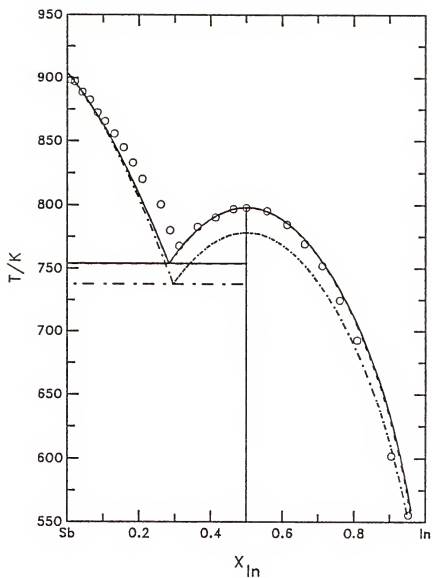


Figure 4-24. In-Sb liquidus predicted with simple solution parameters listed in Table 4-9: ---, case 1 (no parameters fixed); —, case 2; -·-, case 5; o, Ref. (118).

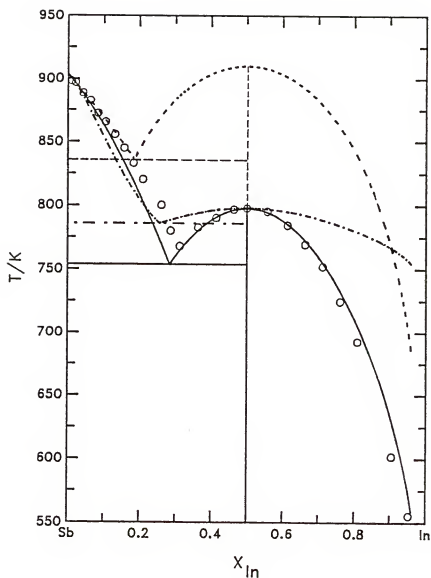


Figure 4-25. In-Sb liquidus predicted with simple solution parameters listed in Table 4-9: —, case 3; ---, case 4; -·-, case 6; o, Ref. (118).

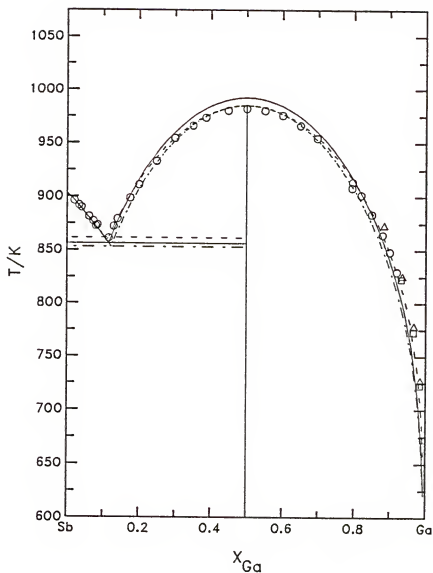


Figure 4-26. Ga-Sb liquidus predicted with NRTL parameters listed in Table 4-9: —, case 1 (no parameters fixed); ---, case 2; -·-, case 5; o, Ref. (130); Δ , Ref. (48); \square , Ref. (39).

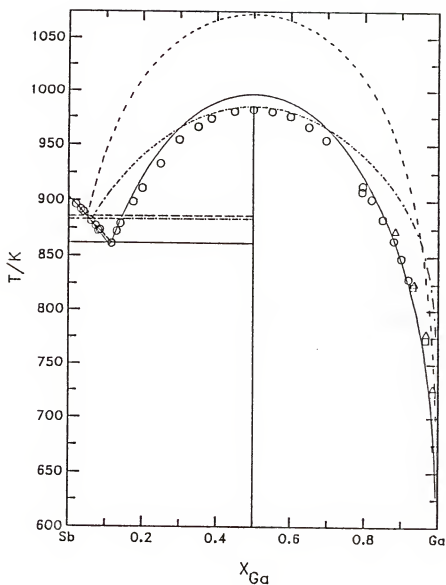


Figure 4-27. Ga-Sb liquidus predicted with NRTL parameters listed in Table 4-9: —, case 3; ---, case 4; -·-, case 6; o, Ref. (130); Δ, Ref. (48); □, Ref. (39).

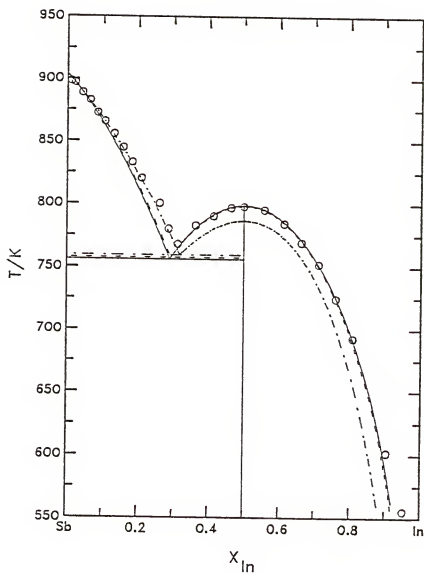


Figure 4-28. In-Sb liquidus predicted from a fit of the In-Sb enthalpy of mixing: ---, NRTL (no parameters fixed); __, NRTL (parameter a fixed at T_m^{InSb}); ---, NRTL (parameters a and c fixed at T_m^{InSb} and T_e , respectively); o, Ref. (118).

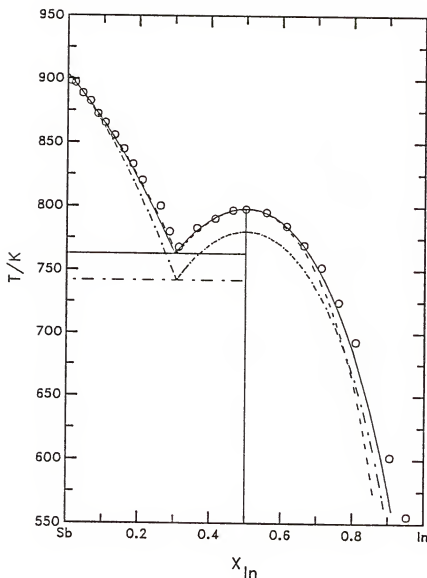


Figure 4-29. In-Sb liquidus predicted from a fit of the In activity: ---, NRTL (no parameters fixed); —, NRTL (parameter a fixed at T_m^{InSb}); ---, NRTL (parameters a and c fixed at T_m^{InSb} and T_e , respectively); o, Ref. (118).

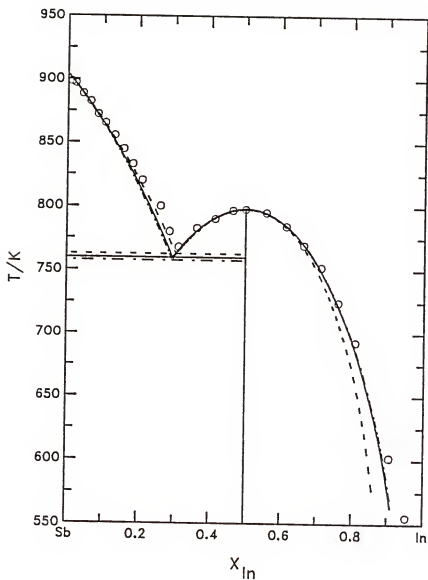


Figure 4-30. In-Sb liquidus predicted from a fit of the In activity and enthalpy of mixing: \longrightarrow , NRTL (parameter a fixed at T_m^{InSb}); $---$, NRTL (parameter b fixed at T_m^{InSb}); $-.-$, NRTL (parameters a and c fixed at T_m^{InSb} and T_e , respectively); \circ , Ref. (118).

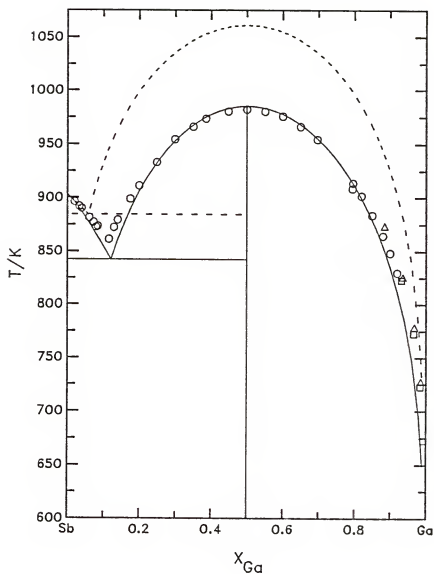


Figure 4-31. Ga-Sb liquidus predicted from a fit of the Ga-Sb enthalpy of mixing (131): ---, NRTL (without any parameter fixed); —, NRTL (parameter a fixed at T_m^{GaSb}); o, Ref. (130); Δ , Ref. (48); \square , Ref. (39).

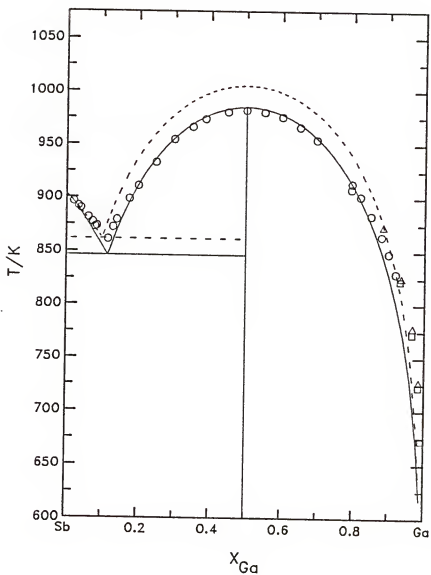


Figure 4-32. Ga-Sb liquidus predicted from a fit of the Ga activity: ---, NRTL (without any parameter fixed); —, NRTL (parameter a fixed at T_m^{GaSb}); o, Ref. (130); Δ , Ref. (48); \square , Ref. (39).

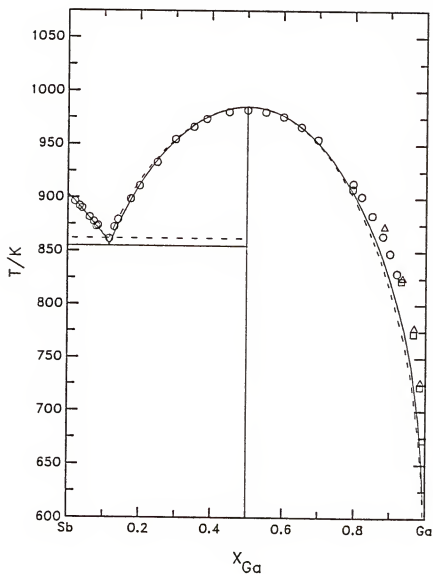


Figure 4-33. Ga-Sb liquidus predicted from a fit of the activity and enthalpy of mixing: —, NRTL (parameter a fixed at T_m^{GaSb}), ---, NRTL (parameters a and c fixed at T_m^{GaSb} and T_e , respectively); o, Ref. (130); Δ , Ref. (48); \square , Ref. (39).

bad value of θ_C . Note that the predicted liquidus temperature on the Sb-rich end for the In-Sb system in all cases is always lower than the experimental data. The discrepancy is a result of the predicted Sb activity being too low. This point is illustrated in Figures 4-34 and 4-36 for the simple solution model and NRTL equation, respectively. It is also shown in Figures 4-34 and 4-36 that the predicted In activity is too high. Thus, the good results for the predicted phase diagram are obtained because of the lower Sb activity being compensated by the higher In activity. Shown in Figures 4-35 and 4-47 as a dashed line is the phase diagram calculated by incorporating the Sb activity error (Δa_{Sb} in Table 4-11) into the Sb-rich end. As can be seen, the results of these calculations show excellent agreement with the experimental data. Table 4-11 shows the sensitivity (ΔT^1 vs Δa_{Sb}^1) of the calculation of the Sb-rich liquidus curve for the In-Sb system. It is clear from Table 4-11 that the calculated Sb-rich liquidus curve is very sensitive to the liquid Sb activity.

Note that the technique presented here makes it possible to predict the phase diagram from only isothermal enthalpy of mixing data or from component activity data alone. As shown above, the analysis with the techniques presented here allows the prediction of binary phase diagrams and shows excellent agreement with the experimental results. The calculational methods were extended to a description of the complete ternary system phase diagram and again good consistency with experimental liquidus and solidus data was found.

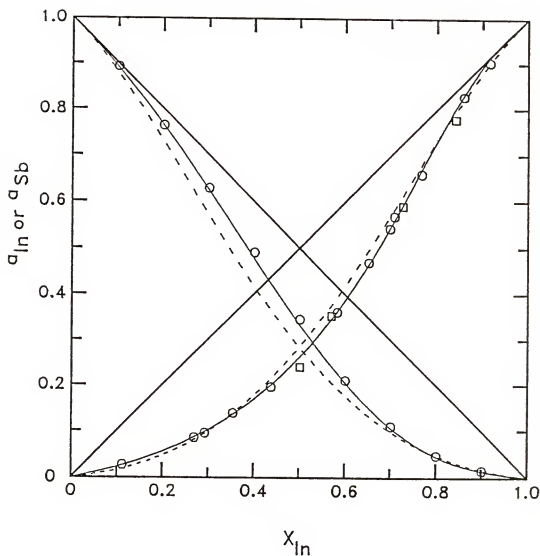


Figure 4-34. Component activities in the In-Sb system: —, NRTL, activity fit (parameters and c fixed at T_m^{InSb} and T_e , respectively), ---, simple solution model (case 1); o, Ref. (120); □, Ref. (188)(900 K).

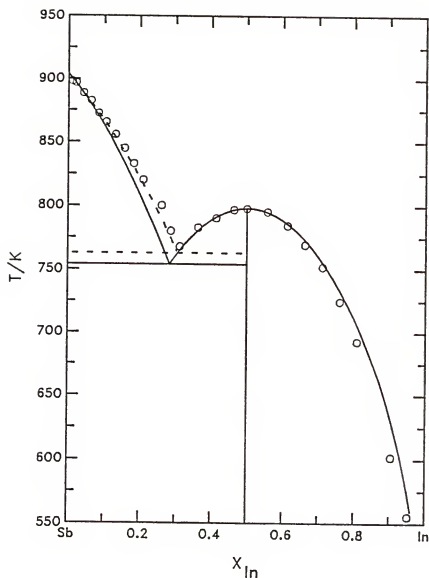


Figure 4-35. In-Sb liquidus predicted from a fit of the In activity and enthalpy of mixing: —, simple solution model (case 1); ---, simple solution model (case 1) incorporating activity error on the Sb-rich side; o, Ref. (118).

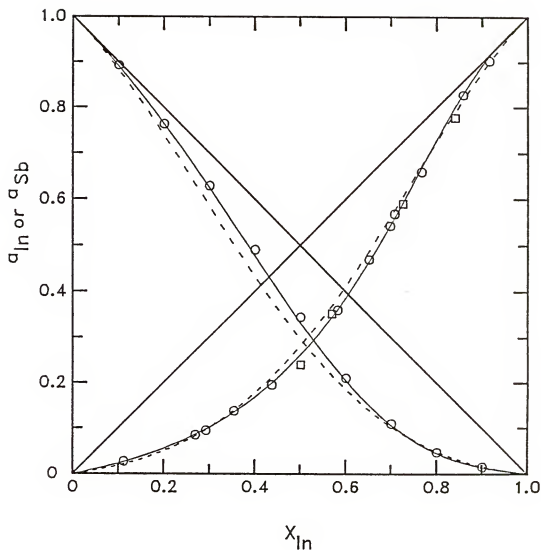


Figure 4-36. Component activities in the In-Sb system calculated by the NRTL equation: —, activity fit (parameters a and c fixed at $T_{\text{m}}^{\text{InSb}}$ and T_{e} , respectively); ---, enthalpy of mixing fit (parameter a fixed at $T_{\text{m}}^{\text{InSb}}$); o, Ref. (120); □, Ref. (188) (900 K).

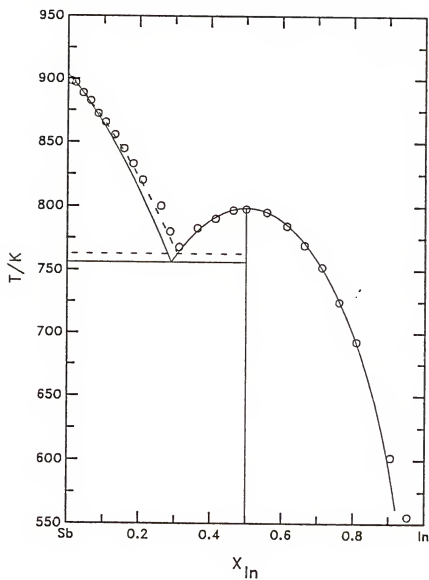


Figure 4-37. In-Sb liquidus predicted from a fit of the enthalpy of mixing: —, NRTL (parameter a fixed at T_m^{InSb}); ---, NRTL (parameter a fixed at T_m^{InSb}) incorporating activity error on the Sb-rich side; o, Ref. (118).

Table 4-11. Sensitivity analysis of the Sb-rich and liquidus change, ΔT , versus the liquid activity change, Δa_{Sb} , with the simple solution model for the In-Sb system.

x_{In}	Best Fit $a_{\text{Sb}} (1)$	Case 1 $a_{\text{Sb}} (2)$	Δa_{Sb} (1) - (2)	Predicted T(K) From Case 1 (3)	Predicted T with Incorporated Δa_{Sb} in Case 1 (4)	ΔT (4) - (3)
0.02	0.97964	0.97911	0.00053	896.702	896.880	0.178
0.06	0.93671	0.93222	0.00449	880.993	882.510	1.517
0.10	0.89072	0.87919	0.01153	862.979	866.937	3.958
0.14	0.84155	0.82085	0.02070	842.901	850.131	7.230
0.18	0.78909	0.75815	0.03093	820.349	831.616	11.267
0.22	0.73329	0.6212	0.04117	796.186	811.730	15.544
0.26	0.67421	0.62383	0.05038	770.357	790.192	19.835
0.30	0.6120	0.55444	0.05756	742.809	766.874	24.065
0.32	0.57982	0.51969	0.06013	728.553	754.522	25.969

4.8 Calculation of Confidence Ellipses

The "best fit" parameter covariance matrix provided by the maximum likelihood algorithm allows the calculation of parameter confidence ellipses. The covariance matrix (error matrix) specifies the variances and covariances of the parameters. The diagonal elements of the error matrix represent the variances of the parameters while the off-diagonal elements represent the covariances. The error matrix is symmetric, i.e., $\sigma_{ij} = \sigma_{ji}$. Given the maximum likelihood best estimates (expected or mean values) of the parameters \underline{c}^* (γ -dimensional real vector), and the parameter error (covariance) matrix \tilde{E} ($\gamma \times \gamma$ matrix), the probability that the true values of the parameters \underline{c} (γ -dimensional real vector) will be found within the hyperparabolic contour

$$\chi^2(\underline{c}) = \chi^2(\underline{c}^*) + k, \quad (4-85)$$

termed R_k , is given by

$$\Pr[\underline{c} \text{ inside } R_k] = \Pr[\chi^2(\underline{c}) \leq k] \quad (4-86)$$

As discussed by Meyer (220) for the bivariate normal distribution, the χ^2 table for $\chi^2(2)$ can be used to get the results in Table 4-12. Equation (4-85) represents a quadratic surface or hyperparaboloid in $(\gamma + 1)$ dimensional space and can be rewritten as

$$\chi^2(\underline{c}) - \chi_{\min}^2(\underline{c}^*) = (\underline{c} - \underline{c}^*)^T \tilde{E}^{-1} (\underline{c} - \underline{c}^*) = k \quad (4-87)$$

Table 4-12. The probability of finding the true value (a,b) within the elliptical contour $\chi^2(a,b) = \chi_{\min}^2 + k$ for several k values.

Pr(a,b) inside R_k	k
0.394	1
0.632	2
0.777	3
0.865	4
0.918	5
0.950	6
0.970	7
0.982	8
0.989	9

Source: Reference (220).

Here, we might say that the parameter set \underline{c} is contained within the region defined by R_k with $(100 \times k)\%$ confidence.

Note that the χ^2 -distribution is a normal distribution, which has two important features (221): (a) Any section through the distribution, say at $C_i = \text{constant}$, gives a normal distribution in $\gamma-1$ dimensions of the form (4-87), with covariance matrix $\tilde{E}_{\gamma-1}$ obtained by removing the i^{th} row and column of \tilde{E}^{-1} and inverting the resultant submatrix; (b) Any projection onto a lower space gives a marginal distribution which is again normal, of the form given by Equation (4-87), with the covariance matrix obtained by deleting appropriate rows and columns of \tilde{E} . Thus, it is easy to calculate the degree of the correlation between any two of the adjustable parameters in the model. As an example, the simple solution model, $w = a + bT$, has two adjustable parameters a and b . Equation (4-87) is reduced to the general equation of an ellipse, called the covariance ellipse:

$$\left(\frac{X_1}{\sigma_a}\right)^2 - 2\rho \frac{X_1 X_2}{\sigma_a \sigma_b} + \left(\frac{X_2}{\sigma_b}\right)^2 = (1 - \rho^2)k \quad (4-88)$$

In the above equation, $\rho (= \sigma_{ab}/\sigma_a \sigma_b)$ is the correlation coefficient between parameters a and b , and $X_1 (= a - a^*)$ and $X_2 (= b - b^*)$ are the deviations in a and b , respectively. This ellipse has a center of symmetry at (a^*, b^*) and its principal axes, a', b' , make an angle, θ , with the a, b axes. The angle is

$$\theta = \frac{1}{2} \tan^{-1} \left\{ \frac{2\rho\sigma_a\sigma_b}{\sigma_a^2 - \sigma_b^2} \right\} \quad (4-89)$$

If we consider σ_a , σ_b , a^* , b^* fixed and let ρ vary, different covariance ellipses result, but all are inscribed within a rectangle bounded by the lines

$$a = a^* \pm \sigma_a \quad (4-90)$$

$$b = b^* \pm \sigma_b \quad (4-91)$$

Two limiting cases are obtained from Equation (4-88). if $\rho = 0$, that is, a and b are uncorrelated, then Equation (4-88) is reduced to the following expression:

$$\left(\frac{x_1}{\sigma_a}\right)^2 + \left(\frac{x_2}{\sigma_b}\right)^2 = k \quad (4-92)$$

which is an ellipse in the a, b plane centered on (a^*, b^*) and with principal axes parallel to the coordinate axes. For $k = 1$, the semimajor and semiminor axes of the ellipse are σ_a, σ_b , respectively, if $\sigma_a > \sigma_b$. For the case $\rho = \pm 1$, we have perfect correlation between a and b ; Equation (4-88) becomes

$$\left(\frac{x_1}{\sigma_a}\right)^2 \mp 2\left(\frac{x_1}{\sigma_a}\right)\left(\frac{x_2}{\sigma_b}\right) + \left(\frac{x_2}{\sigma_b}\right)^2 = 0 \quad (4-93)$$

or

$$\frac{x_1}{\sigma_a} = \pm \frac{x_2}{\sigma_b} \quad (4-94)$$

which is the equation of a straight line along one of the two diagonals of the rectangle.

It is clear from the discussion above that both the shape and the magnitude of the ellipse provide information about the degree of the correlation between the estimated parameters and the bounds of the true values of the parameters, respectively. If the ellipse is quite narrow and elongated, this indicates a high degree of correlation between the parameters. In cases where the parameters a, b are uncorrelated, the principal axes of the ellipse are parallel to the coordinate axes. In other words, a and b can be determined independently. Note that this is true for the model with only two adjustable parameters (e.g., the simple solution model). However, this is not always true for the model with more adjustable parameters (e.g., NRTL equation with four or five adjustable parameters) because any two of the parameters may correlate to each other. The values of R_{ij} in Equation (4-66) have little effect on the estimated parameters, but they do change the parameter covariance matrix values calculated by the algorithm because the elements of the covariance matrix are functions of R_{ij} . For the same confidence level and measurement error, the smaller the confidence ellipse is, the better the model is. Note that the regions of the ellipse become smaller as the standard deviation becomes smaller or as the number of experimental measurements becomes larger.

Figure 4-38 shows the contours of the four-dimensional surface projected onto the b - d plane for the NRTL equation with two parameters a and c fixed at T_m^{IC} and T_e , respectively. The ellipses

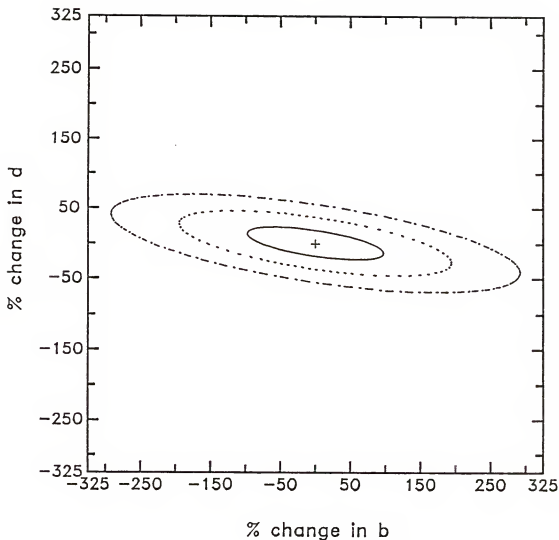


Figure 4-38. Covariance ellipses showing that sections of the four-dimensional surface are plotted versus b and d with different values of confidence level for the NRTL equation activity fit with two parameters a and c fixed at T_m^{InSb} and T_e , respectively, In-Sb system: —, 39%; ---, 87%; -·-, 99% confidence level.

shown for different values of confidence level are derived from the In-Sb activity fit. The correlation coefficient between b and d equals -0.589 . It is apparent from this figure that the elliptical region gets smaller when the confidence level becomes lower. In a similar manner, Figures 4-39 and 4-40 show the intersection of the 89% hyperellipsoid with the c - d and b - d planes, respectively. The ellipses shown are obtained from the In-Sb combined activity and enthalpy of mixing data set, activity, and enthalpy of mixing fits. As shown in Figure 4-39, the correlation coefficients between c and d are 0.27 , 0.56 , and -0.81 for the activity, enthalpy of mixing, and combined activity and enthalpy of mixing data set fits, respectively. Note that the elliptical region in Figure 4-39 gets smaller for the combined activity and enthalpy of mixing fit, while the correlation coefficient between c and d gets higher. It is clear from Figure 4-40 that the high degree of correlation between the parameters b and d is seen in the results from the activity and combined activity and enthalpy of mixing data set fits, while the correlation in the enthalpy of mixing expression between b and d is perfect (shown as straight line). The results shown above indicate that any two of the adjustable parameters for the NRTL equation within one or two parameters fixed at T_m^{IC} and T_e are strongly correlated or even perfectly correlated. In other words, these parameters cannot be determined independently.

In this chapter, a general formalism has been presented for the representation of the available thermodynamic properties and phase diagram for binary group III-V and III-III' systems. The approach

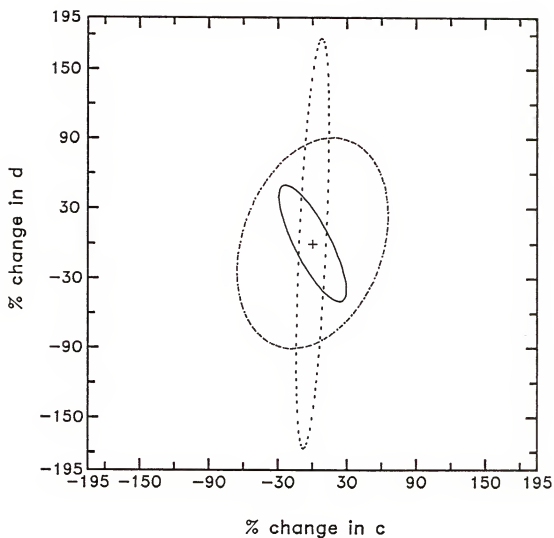


Figure 4-39. 89% covariance ellipses showing that sections of the five-dimensional surface are plotted versus c and d for the NRTL equation with one parameter a fixed at T_m^{InSb} , In-Sb system: —, activity and enthalpy of mixing fit; ---, activity fit; ---, enthalpy of mixing fit.

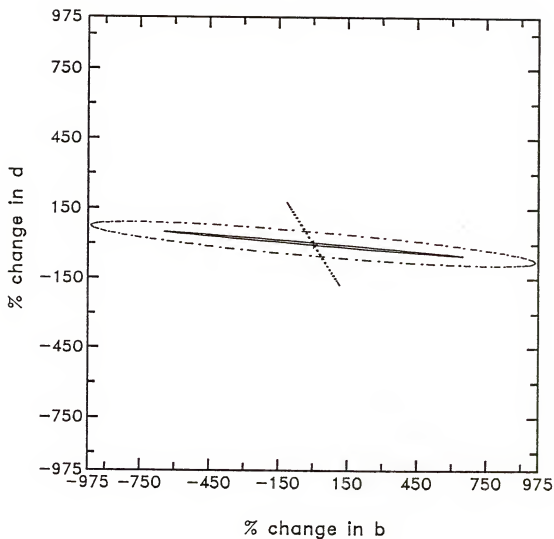


Figure 4-40. 89% covariance ellipses showing that sections of the five-dimensional surface are plotted versus b and d for the NRTL equation with one parameter a fixed at T_m^{InSb} , In-Sb system: —, activity and enthalpy of mixing fit; ---, activity fit; ···, enthalpy of mixing fit.

has been applied to the Al-Sb, Ga-Sb, In-Sb, Al-Ga, Al-In, and Ga-In systems. The results have shown that none of the solution models considered here can simultaneously represent all of the data (phase diagram, activity, enthalpy of mixing) in the Al-Sb and Al-In systems mainly due to highly asymmetric phase diagrams. It is probably necessary to include a special chemical term to properly describe systems with association in the liquid phase. However, both the NRTL equation and simple solution model are able to represent well the Al-Ga and Ga-In systems, for which complete and consistent data bases are available. The "best fit" results of these systems are presented in Chapter VI and Chapter VII, respectively.

The results of the attempted cross-predictions were unsatisfactory for the models considered here. It was found that the problem mainly lies in the nonuniqueness of the model parameters. Because of this specific feature an improved method was proposed to predict the phase diagram. The prediction of the phase diagram from the activity or enthalpy of mixing data alone is possible by means of this technique. This leads to very poor results with the original models, even when temperature dependent parameters are introduced. The problem of parameter correlation is also addressed. The correlation between the parameters usually is significant.

CHAPTER V THERMODYNAMICS OF PSEUDOBINARY SYSTEMS

As discussed in Chapter I, the objective is to calculate multicomponent phase diagrams from available binary phase diagrams and thermochemical data and pseudobinary phase diagrams. The problem is divided into two major tasks: evaluation of the reduced standard state chemical potential change for each binary semiconductor (θ_{IC}) and characterization of the solution behavior for both the liquid and solid phases ($r_{IC} = \gamma_I^L \gamma_C^L / \gamma_{IC}^S$). In the two previous chapters, the problem of calculating θ_{IC} and the use of solution models in the description of the binary liquid phase behavior were considered. The model parameters obtained from these binary studies can be used to estimate the liquid phase activity coefficients required for calculation of the multicomponent phase diagram. It is also necessary in performing such calculations to assign values to the solid solution activity coefficients. These values are usually determined from a solution model with parameters estimated from a fit of the pseudobinary phase diagram. A pseudobinary III-V system is one in which both the liquid and solid solutions have the same atomic numbers of group III and group V elements and is represented by the general formula $A_x B_{1-x} C$ or $(AC)_x (BC)_{1-x}$, where A and B are from the same column of the periodic table.

In this chapter, the solid solution behavior for the pseudobinary AlSb-GaSb, AlSb-InSb, and GaSb-InSb systems is addressed. Two different approaches for the calculation of the solid interaction parameters are presented. These parameters, in conjunction with a description of the binary liquid solution behavior, are then used to predict the remainder of the ternary phase diagrams in Chapter VI, the quaternary phase diagram in Chapter VII, and other thermodynamic properties. The simple solution model and NRTL equation are used to describe the liquid solution and the predicted phase diagram and liquid thermodynamic properties are compared with the experimental values. In addition, the selected models are used to predict solid phase component activities and enthalpy of mixing and to investigate the possibility of a solid phase immiscibility gap.

5.1 Theory

In this section, two different approaches are presented for calculation of solid interaction parameters for the pseudobinary solid solution $A_xB_{1-x}C(s)$. The resulting expressions for the liquidus and solidus are similar in both cases with only a constant difference in the numerators of the working equations. These two representations are thermodynamically correct; θ_{IC} and Γ_{IC} are defined differently in each case.

5.1.1 Treatment of Liquid Solution as a Three Component System (Method 1)

Consider the pseudobinary liquid mixture as a three component system. The governing equations describing phase equilibrium for a

three-component, two phases system of the type $A_xB_{1-x}C$ are given by Equations (2-79) and (2-80). In the pseudobinary system, these equations are further constrained by the requirement that in the liquid

$$x_A^1 + x_B^1 = x_C^1 = 0.5, \quad (5-1)$$

Substitution of the constraint Equation (5-1) into Equations (2-79) and (2-80) gives the implicit expressions for the pseudobinary liquid composition and the corresponding solid composition as follows:

$$x_A^1 = \frac{2 - 0.5 \Gamma_{BC} \exp(-\theta_{BC})}{\Gamma_{AC} \exp(-\theta_{AC}) - \Gamma_{BC} \exp(-\theta_{BC})}, \quad (5-2)$$

and

$$x_{AC}^s = x = \frac{0.25 - \frac{1}{\Gamma_{BC}} \exp(\theta_{BC})}{\frac{1}{\Gamma_{AC}} \exp(\theta_{AC}) - \frac{1}{\Gamma_{BC}} \exp(\theta_{BC})} \quad (5-3)$$

where x_A^1 is the liquid phase mole fraction of component A and x_{AC}^s or x is the solid phase mole fraction of component AC and is simply twice the component A mole fraction in the solid phase. The quantities θ_{IC} and Γ_{IC} are defined by Equations (2-49) and (2-50) with $m = n = 1$, respectively, i.e.,

$$\theta_{IC} \equiv \frac{\mu_{IC}^{0,s} - \mu_I^{0,1} - \mu_C^{0,1}}{RT}, \quad I = A \text{ or } B \quad (5-4)$$

and

$$\Gamma_{IC} = \frac{\gamma_I^l \gamma_C^l}{\gamma_{IC}^s}, \quad IC = AC \text{ or } BC \quad (5-5)$$

It is clear from the above results that the problem of quantitatively describing the group III-V pseudobinary solid-liquid phase diagram is reduced to the simpler problems of describing the standard state properties Θ_{IC} and the liquid and solid mixture properties Γ_{IC} . The problem of the calculation of Θ_{IC} has been investigated in Chapter III. The recommended values of Θ_{IC} used here are the same as those listed in Table 3-6.

The next problem is to determine values for Γ_{IC} (usually is a complex function of temperature, pressure and composition). A commonly used procedure (Panish and Ilegems (16)) for calculating values of Γ_{IC} is to estimate first the parameters of a liquid solution model from an analysis of the three experimental binary phase diagrams. These models are then extended to describe a ternary liquid without introduction of additional adjustable parameters. Finally, solid solution model parameters are estimated by analysis of the pseudobinary phase diagram with the ternary liquid solution behavior (γ_A^l , γ_B^l , and γ_C^l calculated with binary parameters only). In this study, the available measurements of liquid component activities and enthalpy of mixing are compared to the values of these properties predicted by the NRTL equation and simple solution model with their parameters estimated from the combined binary data alone. The simple solution model for the liquid phase is also used to estimate solid

solution model parameters from a data base consisting of the pseudobinary phase diagram. The results are then compared to the reported phase diagram. Since there are no adjustable parameters in the liquid phase, the solid solution behavior determined in this way has been found to be sensitive to the solidus data base and the assumed solid solution model and to be insensitive to the liquidus data base.

5.1.2 Treatment of Liquid Solution as a Two Component System (Method 2)

The treatment of liquid solution as a pseudobinary mixture of AC and BC in the calculation of the $A_xB_{1-x}C$ pseudobinary phase diagram has been addressed by several investigators (20,23). Upon equating the chemical potential of each component (AC and BC) in both phases, relationships similar to Equations (4-5) and (4-6) are derived, with the liquidus and solidus composition given by

$$x_{AC}^l = \frac{1 - r_{BC}' \exp(-\theta_{BC}')}{r_{AC}' \exp(-\theta_{AC}') - r_{BC}' \exp(-\theta_{BC}')} , \quad (5-6)$$

and

$$x_{AC}^s = \frac{1 - \frac{1}{r_{BC}'} \exp(\theta_{BC}')}{\frac{1}{r_{AC}'} \exp(\theta_{AC}') - \frac{1}{r_{BC}'} \exp(\theta_{BC}')} \quad (5-7)$$

Here, the θ_{AC}' and r_{AC}' terms again represent a reduced standard state chemical potential change and the relative liquid and solid deviation from ideal behavior, but they are defined somewhat differently

$$\theta'_{IC} = \frac{\mu_{IC}^{o,s} - \mu_{IC}^{o,l}}{RT} \quad , \quad IC = AC \text{ or } BC \quad (5-8)$$

and

$$\Gamma'_{IC} = \frac{\gamma_{IC}^l}{\gamma_{IC}^s} \quad , \quad IC = AC \text{ or } BC \quad (5-9)$$

Choosing the standard state as the pure component in the state shown in the superscript at the temperature and pressure of interest, values for θ'_{IC} can be calculated from the following expression

$$\theta'_{IC}(T) = \frac{\Delta H_f}{R} \left(\frac{1}{T_m} - \frac{1}{T} \right) + \frac{1}{RT} \int_T^{T_m} \int_T^{T_m} \frac{\Delta C_p}{T} dT^2 \quad (5-10)$$

where ΔH_f is the enthalpy of fusion of IC, T_m is the melting temperature of IC, and ΔC_p is the difference in heat capacity between the stoichiometric liquid IC and the compound IC. Introducing the selected values for these properties listed in Table 3-2 into Equation (5-10), we obtain

$$\theta'_{AlSb} = -0.154 - 8635.0/T + 0.918 \ln T \quad (5-11)$$

$$\theta'_{GaSb} = 2.540 - 7155.0/T + 0.685 \ln T \quad (5-12)$$

and

$$\theta'_{InSb} = -3.008 - 4683.6/T + 1.329 \ln T \quad (5-13)$$

where T is the absolute temperature (K). These values along with the

measurements of the pseudobinary phase diagram and liquid enthalpy of mixing are used to estimate solution model parameters. A major difference in this method is the presence of adjustable liquid mixture parameters. Apparently, the values of the solid interaction parameters depend on the models used to represent the liquid and solid phase and on the liquidus and solidus data base.

5.2 Computational Procedure

The experimental liquidus data (x_i^l, T_i^l), solidus data (x_j^s, T_j^s), and liquid enthalpy of mixing ($x_i^l, \Delta H^m$) were taken from tabulations or digitized from graphs. The binary liquid interaction parameters required for method 1 are given in Table 5-1. The basic equations are (5-2), (5-3), (5-6), (5-7), (4-34), (4-40), and those listed in Table 4-4. The fit of the enthalpy of mixing is quite straightforward because the working equation is an explicit constraint equation. However, the experimental equilibrium liquidus and solidus data are usually not available simultaneously. To make the one constraint problem still workable, the corresponding equilibrium data, either liquidus or solidus, must be calculated in advance. This can be done by rewriting the two implicit working Equations (5-2) and (5-3) or (5-6) and (5-7) as follows:

$$x_i^l = f(x_i^l, x_j^s, T) \quad i = A(\text{for method 1}); AC(\text{for method 2}) \quad (5-14)$$

$$x_j^s = f(x_i^l, x_j^s, T) \quad j = AC(\text{for method 1 and method 2}) \quad (5-15)$$

Table 5-1. Binary liquid solution model parameters for the simple and NRTL expressions.

System	Simple		NRTL				α_{IC}
	$a^1(\text{cal/mol})$	$b^1(\text{cal/mol K})$	$a^1(\text{cal/mol})$	$b^1(\text{cal/mol K})$	$c^1(\text{cal/mol})$	$d^1(\text{cal/mol K})$	
Al-Sb	-4413.6	0.736	-3282	1.612	-5757	1.353	-0.500
Ga-Sb*	-928.6	-1.394	3647	6.016	-1415	-5.324	0.157
In-Sb*	-2662.6	-1.708	6038	1.814	-1669	-3.622	0.315
Al-Ga	598.9	-0.318	-840	0.603	1640	-1.035	0.300
Al-In	5595.6	-0.704	3021	-0.149	1245	0.049	-0.300
Ga-In	1029.9	0.29	647	-0.159	495	0.364	0.300

* Reference (187).

It is clear that there are two independent Equations (5-14) and (5-15) with three unknowns (x_i^L , x_j^S , T). Thus, for a given experimental measurement (x_i^L , T) or (x_j^S , T), the corresponding equilibrium data point (x_j^S , T) or (x_i^L , T) can be calculated by the implicit equation (5-15) or (5-16). The computational procedures employed here are identical to those outlined in Chapter IV for the eutectic systems and not repeated here.

The ability of the model to describe the combined data is characterized by the overall weighted sum of squares, σ_0^2 , which was defined by the Equation (4-66). The standard deviation, σ , of the subset can be calculated by Equation (4-68). Values of R_{ij} (the assumed measurement error) used in these studies for the solidus temperature, liquidus temperature and enthalpy of mixing are 2.3 K, 2.3 K and $0.001 \cdot (RT_m)$, respectively. Here, R is the gas constant and T_m is the temperature at which the enthalpy of mixing is measured.

5.3 Data Base

5.3.1 AlSb-GaSb System

The combined data set for the AlSb-GaSb system consisted of liquid enthalpy of mixing, liquidus and solidus and was used in the parameter estimation procedure for the NRTL equation and simple solution model. The pseudobinary liquidus and solidus data of Koster and Thoma (221), Burdiyan and Borschevskii (222), Miller et al. (223) and Borschevskii et al. (224) are considerably scattered. Aulombard and Joullie (225) have measured the solidus over the entire composition range and the liquidus on GaSb-rich side. The solidus

data of Borshevskii et al. (224) are in relatively poor agreement with the measurements of Aulombard and Joullie (225), while the solidus measurements of Burdiyan and Borshevskii (222) are much lower than those obtained by Aulombard and Joullie (225). The liquidus data of Aulombard and Joullie (225) are in good agreement with the results of Miller et al. (223). Based on comparisons with the other available thermochemical data (225, 226), the liquidus and solidus results of Aulombard and Joullie (225) and the liquidus data of Miller et al. (223) have been used in this study.

The pseudobinary liquid enthalpy of mixing has been measured by Gerdes and Predel (226). However, there are no reported data of the pseudobinary liquid activity and no reliable data of the thermochemical properties of the pseudobinary solid solution. The results of Gerdes and Predel (226) have been included in the data base for these calculations.

5.3.2 AlSb-InSb System

As with AlSb-GaSb, a data base for the AlSb-InSb system consisting of liquid enthalpy of mixing, liquidus and solidus temperatures was employed. The pseudobinary liquidus and solidus data of Goryunova et al. (227), Koster and Thoma (221), and Wooley and Smith (228) are quite scattered. The liquidus measurements of Goryunova (227) are in general 20-40°K higher than those obtained by Koster and Thoma (221) in the 20-80 mole per cent AlSb interval. The solidus temperatures of Goryunova (227) show a scatter of about $\pm 15^{\circ}\text{C}$ between 0 and 60 mole percent AlSb and are about 20°C higher than the measurement of Wooley and Smith (228) at 15 mole percent AlSb. The

solidus data of Wooley and Smith (228) are lower than those obtained by Goryunova et al. (227) over the entire composition range. Due to the scatter of the available experimental data, several different data sets have been used and compared in this study.

As in the case of AlSb-GaSb, only pseudobinary liquid enthalpy of mixing for this system has been measured by Gerdes and Predel (226). There are no reported studies of the pseudobinary liquid activity or of the thermochemical properties of the pseudobinary solid solution. The measurements of Gerdes and Predel (226) have been employed for parameter estimation.

5.3.3 GaSb-InSb System

Unlike two systems above, the GaSb-InSb system is characterized by a variety of thermochemical data (the liquid Ga activity, liquid enthalpy of mixing, enthalpy of fusion, liquidus and solidus temperatures). The GaSb-InSb pseudobinary phase diagram has been determined by several investigators (221,228-233). Wooley et al. (228-230) have measured the liquidus and solidus temperatures over the entire composition range, as have Ufimtsev et al. (231). Gorshkov and Goryunova (232) determined several liquidus and solidus temperatures between 25 and 75 mole percent GaSb, while Koster and Thoma (221) investigated this system and reported a degenerate eutectic diagram without appreciable terminal solid solution. The results of Gorshkov and Goryunova (232) are in relatively poor agreement with measurements of Wooley et al. (228-230). The solidus data of Ufimtsev et al. (231) match well those of Wooley et al. (228-230), but their liquidus data fall consistently higher. One solidus

and two liquidus points are contributed by Blom and Plaskett (233); these agree well with the data of Wooley et al. (228-230). Based on comparisons with the other available thermochemical data (234), the results of Wooley et al. (228-230) and of Blom and Plaskett (233) have been used in this study.

The enthalpy of mixing has been measured by Gerdes and Predel (226) and by Ansara et al. (235), with the results in reasonable agreement. The measurements of either Vecher et al. (236) or Mechkovskii et al. (237) are significantly more positive than the other two determinations. The data of Gerdes and Predel (226) have been employed for parameter estimation. The liquid phase activity of Ga in the pseudobinary $\text{Ga}_x\text{In}_{1-x}\text{Sb}$ mixture has been determined by Anderson (152) with a solid state electrochemical technique. The a_{Ga}^1 measured by Anderson (152) and ΔH_m^1 reported by Gerdes and Predel (226) are compared to the values of these properties predicted by the NRTL and simple solution models with their parameters estimated from the combined binary data set alone. As with the AlSb-InSb and AlSb-GaSb systems, there are no reported studies of the component activity and enthalpy of mixing of the pseudobinary solid solution.

5.4 Results and Discussion

The simple solution model has been extensively used to describe group III-V pseudobinary $\text{A}_x\text{B}_{1-x}\text{C}$ solid solutions. In this model the IC (I = A or B) component activity coefficient is given by an expression similar to that listed in Table 4-4, and the molar excess Gibbs energy is represented by

$$\Delta G_m^{XS}(\text{AC-BC}) = (a^S + b^S T) x_{AC}^S (1 - x_{AC}^S) \quad (5-16)$$

The adjustable parameters a^S and b^S were estimated by using a maximum likelihood algorithm (181). It follows from Equation (5-16) that the enthalpy of mixing is given by

$$\Delta H_m^S = a^S x_{AC}^S (1 - x_{AC}^S) \quad (5-17)$$

Apparently, ΔH_m^S is independent of temperature for this model.

Several attempts have been made to calculate a^S from the physical, electronic, and optical properties of the constituents (78-82,238-247) and involving no fitted parameters. Any independent method of calculating the solid interaction parameters would give additional insight into their physical origin and allow the prediction of phase diagrams in systems where no experimental data are available. Unfortunately, the calculation of a^S did not always give good agreement with those obtained by fitting the phase diagram measurements of group III-V pseudobinary alloys.

In this study, we present two general approaches to calculate the solid interaction energy by fitting the available experimental data. For the first method, a data base consisting of liquidus temperature, solidus temperature, and the reduced standard state chemical potential difference given in Table 3-6 was used in the parameter estimation. The NRTL and simple solution model parameters required for this method were estimated for each of the six binary I-C systems. A data base consisting of the liquidus temperature,

group III activity and enthalpy of mixing was used. The parameter estimates are summarized in Table 5-1. The parameter values for the Ga-Sb and In-Sb systems are taken from Aselage et al. (187). For the other systems, parameter values are taken from Chapter 4 (Tables 4-6 and 4-7). A data base consisting of the liquidus and solidus data alone and of the combined liquidus, solidus and ΔH_m^I (AC-BC) measurements along with the θ'_{IC} given by Equations (5-11) to (5-13) was used in the parameter estimation for method 2. The parameter sets determined for a variety of solution models are listed in Table 5-2 for method 1 and in Tables (5-3) to (5-6) for method 2.

An examination of the results for the $Al_xGa_{1-x}Sb$ system presented in Tables 5-2 and 5-3 indicates that the predicted solid parameters a^s are positive in all cases considered here. This implies that a miscibility gap is present for this system. The critical temperature, T_c , at which the immiscibility gap appears, is determined by the following expression (167) for the simple solution model

$$T_c = \frac{a^s}{2R - b^s} \quad (5-18)$$

where R is the gas constant. As shown in Tables 5-2 and 5-3, the critical temperature predicted for this system is between 92 K and 583 K. The solid phase activity of AlSb in AlSb-GaSb mixtures has been determined with a solid state electrochemical technique by Samokhval et al. (129). Their results exhibit strongly negative deviation from ideal behavior. On the basis of these measurements,

Table 5-2. Solid solution model parameter estimates treating liquid as a three component mixture for the $\text{Al}_x\text{In}_{1-x}\text{Sb}$, $\text{Al}_x\text{Ga}_{1-x}\text{Sb}$ and $\text{Ga}_x\text{In}_{1-x}\text{Sb}$ systems.

System	Model		Parameter		Data Base
	Liquid	Solid	$a^S(\text{cal/mol})$	$b^S(\text{cal/mol K})$	
$\text{Al}_x\text{In}_{1-x}\text{Sb}$	simple	simple	-4,131	4.372	*
	simple	regular	332	0	*
$\text{Al}_x\text{Ga}_{1-x}\text{Sb}$	simple	simple	2,293	-1.469	*
	simple	regular	622	0	*
$\text{Ga}_x\text{In}_{1-x}\text{Sb}$	simple	simple	-1,146	3.275	*
	simple	regular	1,722	0	*

* Same as in Tables 5-3, 5-4, and 5-6.

Table 5-3. Solution model parameter estimates treating liquid as pseudobinary for the AlSb-GaSb system.

Model		Liquid		Solid		σ_o	$T_c(K)$
Liquid	Solid	a^l (cal/mol)	b^l (cal/mol K)	a^s (cal/mol)	b^s (cal/mol K)	Data Base	
simple	simple	-2,369	1,653	2,508	-1,857	*	3.8 430
regular	simple	-523	0	3,781	-2,992	*	3.7 543
ideal	simple	0	0	4,034	-2,943	*	5.2 583
regular	regular	-547	0	366	0	*	4.4 92
ideal	regular	0	0	688	0	*	5.7 173
NRTL	simple	fixed $\alpha_{AlSb-GaSb}^l = -1.0$		2,773	-2,065	*	2.1 459
simple	simple	-417	-0.090	3,859	-3,058	**	4.3 549
regular	simple	-420	0	3,873	-3,017	**	4.3 554
NRTL	simple	fixed $\alpha_{AlSb-GaSb}^l = 0.3$		2,730	-2,139	**	2.8 447

* Liquidus and solidus temperatures of Aulombard and Joulie (225), and liquidus temperatures of Miller et al. (223).

** Liquidus and solidus temperatures of Aulombard and Joulie (225), liquidus temperatures of Miller et al. (223), and liquid enthalpy of mixing of Gerdes and Predel (226).

Table 5-4. Solution model parameter estimates treating liquid as pseudobinary for the AlSb-InSb system.

Model		Liquid		Solid		Data Base	σ_0	T_c (K)
Liquid	Solid	a^l (cal/mol)	b^l (cal/mol K)	a^s (cal/mol)	b^s (cal/mol K)			
simple	simple	-10,791	10.015	-218	-0.27	*	9.3	-
regular	simple	649	0	1,750	-2.057	*	12.9	290
ideal	simple	0	0	3,827	-4.276	*	14.4	464
regular	regular	707	0	-329	0	*	12.7	-
ideal	regular	0	0	-519	0	*	14.8	-
NRTL	simple	fixed $\alpha_{\text{AlSb-InSb}}^l = 0.3$		-1,189	-0.474	*	8.7	-
simple	simple	-2,888	2.533	738	-1.184	**	7.6	143
regular	simple	-111	0	1,155	-1.574	**	7.6	208
ideal	simple	0	0	953	-1.349	**	7.4	179
regular	regular	-69	0	-433	0	**	7.5	-
ideal	regular	0	0	-416	0	**	7.8	-
NRTL	simple	fixed $\alpha_{\text{AlSb-InSb}}^l = 0.3$		1,115	-1.579	**	7.3	201

* Liquidus and solidus temperatures of Goryunova et al. (227).

** Liquidus temperatures of Koster and Thoma (221) and solidus temperatures of Goryunova (227).

Table 5-5. Solution model parameter estimates treating liquid as pseudobinary for the AlSb-InSb system.

Model		Liquid		Solid		Data Base	σ_0	T_c (K)
Liquid	Solid	a^1 (cal/mol)	b^1 (cal/mol K)	a^S (cal/mol)	b^S (cal/mol K)			
simple	simple	550	0.129	1,575	-1.874	*	11.4	269
regular	simple	559	0	2,061	-2.385	*	11.3	324
NRTL	simple	fixed $\alpha_{\text{AlSb-InSb}}^1 = 0.3$		1,080	-1.455	*	8.8	199
simple	simple	553	-0.591	1,212	-1.622	**	6.9	217
regular	simple	534	0	-106	-0.198	**	8.6	-
NRTL	simple	fixed $\alpha_{\text{AlSb-InSb}}^1 = 0.3$		696	-1.147	**	6.3	136

* Liquidus and solidus temperatures of Goryunova et al. (227) and liquid enthalpy of mixing of Gerdes and Predel (226).

** Liquidus temperatures of Koster and Thoma (221) and solidus temperatures of Goryunova (227) and liquid enthalpy of mixing of Gerdes and Predel (226).

Table 5-6. Solution model parameter estimates treating liquid as pseudobinary for the GaSb-InSb system.

Model		Liquid		Solid		Data Base	σ_0	$T_c(K)$
Liquid	Solid	$a^l(\text{cal/mol})$	$b^l(\text{cal/mol K})$	$a^s(\text{cal/mol})$	$b^s(\text{cal/mol K})$			
simple	simple	527	-0.582	2,146	-0.725	*	3.2	457
regular	simple	18	0	1,783	-0.309	*	3.1	416
ideal	simple	0	0	1,772	-0.311	*	3.0	413
regular	regular	18	0	1,512	0	*	3.0	380
ideal	regular	0	0	1,500	0	*	3.0	377
NRTL	simple	fixed $\alpha_{\text{GaSb-InSb}}^l = 0.3$		1,779	-0.307	*	3.3	416
simple	simple	156	-0.158	1,884	-0.425	**	2.7	428
regular	simple	154	0	1,819	-0.251	**	2.7	431
regular	regular	154	0	1,599	0	**	2.7	402
NRTL	simple	fixed $\alpha_{\text{GaSb-InSb}}^l = 0.3$		2,132	-0.688	**	2.8	455

* Liquidus and solidus temperatures of Wooley et al. (228-230) and of Blom and Plaskett (25).

** Liquidus and solidus temperatures of Wooley et al. (228-230) and of Blom and Plaskett (25) and liquid enthalpy of mixing of Gerdes and Predel (226).

the AlSb-GaSb solid solution shows a tendency toward ordering (complete miscibility) and not toward stratification (immiscibility) as suggested above. Unfortunately, there are no other studies of the thermochemical properties of this system which might be utilized for the assessment of solution models studied here. The pseudobinary phase diagram and liquid enthalpy of mixing calculated with parameters listed in Table 5-3 are displayed in Figures (5-1) and (5-2) for this system. It can be seen that the NRTL equation for the liquid solution and simple solution models for the solid solution is best able to represent the combined experimental data set (T^L , T^S , ΔH_m^L) for this system. This is expected because the standard deviation listed in Table 5-3 for this case shows a minimum. Figures 5-3 and 5-4 show the predicted enthalpy of mixing and activity of the solid solution, respectively. The results show moderate positive deviation from ideal behavior. It should be mentioned here that the solid interaction parameters for this system usually are taken to be zero in calculating the phase diagrams of the multicomponent systems because of the close lattice match between AlSb and GaSb. However, this is not true in the real situation as discussed above.

Because of the scatter in the data base, a poor fit for the AlSb-InSb system is obtained. The use of the liquidus and solidus data alone gives the results listed in Tables 5-2 and 5-4. It is seen from Table 5-4 that the parameter set is very sensitive to the liquidus data and the solution model used in the parameter estimation. When the liquidus data of Goryunova et al. (227) are used, an average value of about 18°C is obtained for σ . If the

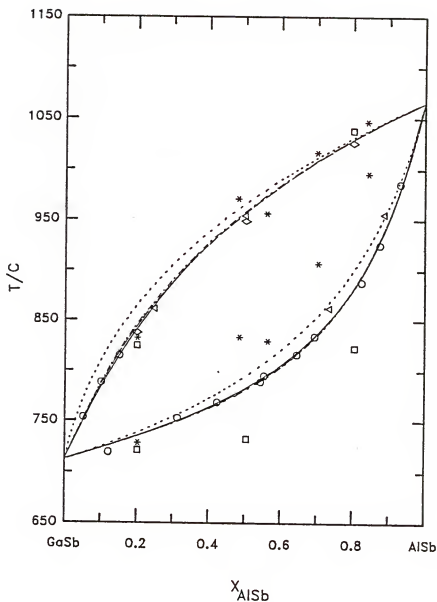


Figure 5-1. The $\text{Al}_x\text{Ga}_{1-x}\text{Sb}$ pseudobinary phase diagram calculated from a fit of the liquidus and solidus temperatures, and enthalpy of mixing. —: NRTL liquid solution and simple solid solution parameters in Table 5-3; — —: simple liquid and solid solution parameters in Table 5-3; — —: strictly regular liquid solution and simple solid solution parameters in Table 5-3; ---: ideal liquid and solid solution; o: Ref. (225); □: Ref. (222); *: Ref. (224); Δ: Ref. (223); ◇: Ref. (221).

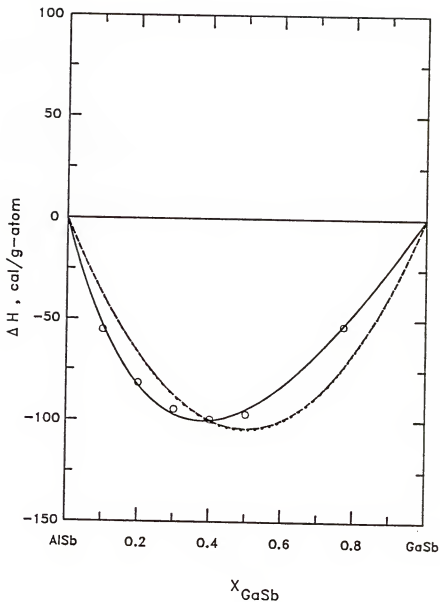


Figure 5-2. Enthalpy of mixing AlSb and GaSb in the liquid phase versus the GaSb mole fraction at 1345 K; —: calculated from NRTL liquid solution and simple solid solution parameters in Table 5-3 (data base **); ---: calculated from simple (or strictly regular) liquid and simple solid solution parameters in Table 5-3 (data base **); o: Ref. (226).

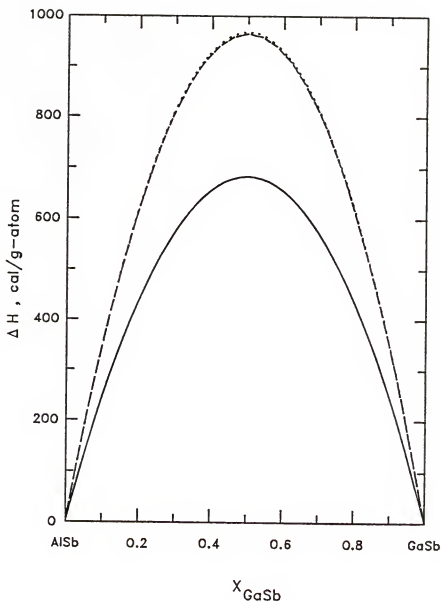


Figure 5-3. Enthalpy of mixing AlSb and GaSb in the solid phase versus the GaSb mole fraction; —: calculated from NRTL liquid solution and simple solid solution parameters in Table 5-3 (data base **); —: calculated from simple liquid and solid solution parameters in Table 5-3 (data base **); ---: calculated from strictly regular liquid and simple solid solution parameters in Table 5-3 (data base **).

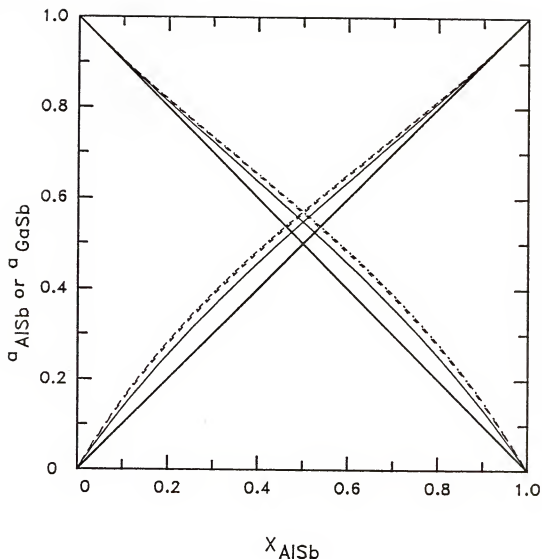


Figure 5-4. The activity of AlSb or GaSb in the solid phase versus the AlSb mole fraction at 950 K; —: calculated from NRTL liquid solution and simple solid solution parameters in Table 5-3 (data base **); ---: calculated from simple liquid solution and solid solution in Table 5-3 (data base **); —·—: calculated from strictly regular liquid and simple solid solution in Table 5-3 (data base **).

liquidus data of Koster and Thoma (221) are used, an average value for σ is reduced to about 11°C. However, the use of the NRTL equation for the liquid solution gives nearly the same σ_0 for these two data sets. In addition to the scatter in the data, the poor fit for the binary Al-Sb liquid produces a poorer fit for this system. A value of σ is over 30°C for two cases listed in Table 5-2. It would be expected that σ_0 is mainly contributed for the liquidus points because of no adjustable parameters in the liquid phase. The use of the combined liquidus, solidus and ΔH_m^1 (AlSb-InSb) measurements give the results listed in Table 5-5. As can be seen, the parameters of these fits indicate a positive enthalpy of mixing of the solid solution for each case investigated. Only when the strictly regular solution in the liquid phase was used and the solid solution assumed simple was a negative a^S obtained. The critical temperature T_C , at which the miscibility gap disappears, is found to vary between 136 K and 324 K for this system. As in the case of the AlSb-InSb system, the results presented in Table 5-5 indicate that the NRTL equation for the liquid solution and simple solution model for the solid solution provides the best fit of the combined experimental data. The pseudobinary phase diagram and liquid enthalpy of mixing calculated with best parameter set (data base *) listed in Table 5-5 are displayed in Figures (5-5) and (5-6). The predicted enthalpy of mixing and activity of the solid solution are shown in Figures 5-7 and 5-8, respectively. These results show small positive deviations from ideal behavior.

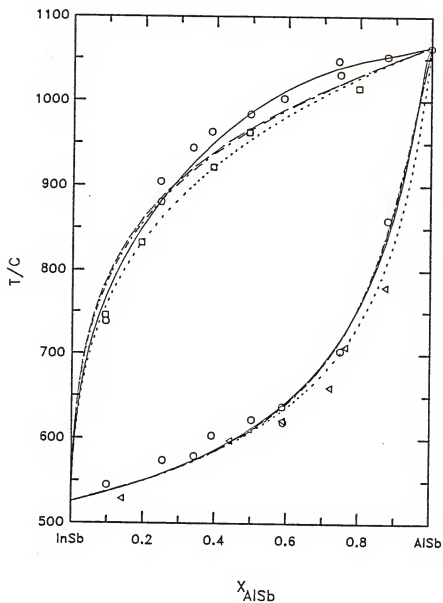


Figure 5-5. The $\text{Al}_x\text{In}_{1-x}\text{Sb}$ pseudobinary phase diagram calculated with parameters in Table 5-5 (data base *); —: NRTL liquid solution and simple solid solution; ---: simple liquid and solid solution; -·-·: strictly regular liquid and simple solid solution; ···: ideal liquid and solid solution; o: Ref. (227); Δ : Ref. (228); \square : Ref. (221).

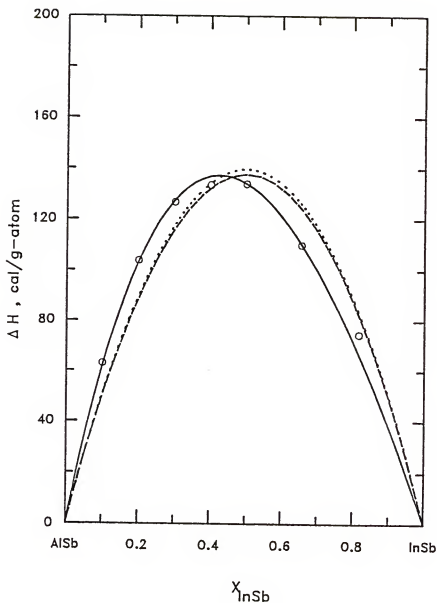


Figure 5-6. Enthalpy of mixing AlSb and InSb in the liquid phase versus the InSb mole fraction at 1345 K; —: calculated from NRTL liquid solution and simple solid solution parameters in Table 5-5 (data base *); ---: calculated from simple liquid and solid solution parameters in Table 5-5 (data base *); ···: calculated from strictly regular liquid and simple solid solution parameters in Table 5-5 (data base *); o: Ref. (226).

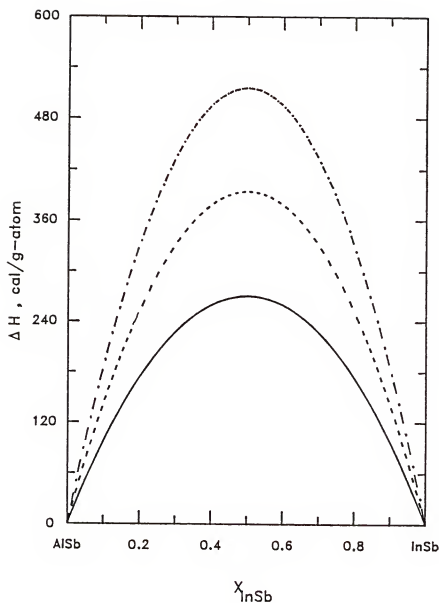


Figure 5-7. Enthalpy of mixing AlSb and InSb in the solid phase versus the InSb mole fraction; —: calculated from NRTL liquid solution and simple solid solution parameters in Table 5-5 (data base *); — —: calculated from simple liquid and solid solution parameters in Table 5-5 (data base *); - · - : calculated from strictly regular liquid and simple solid solution parameters in Table 5-5 (data base *).

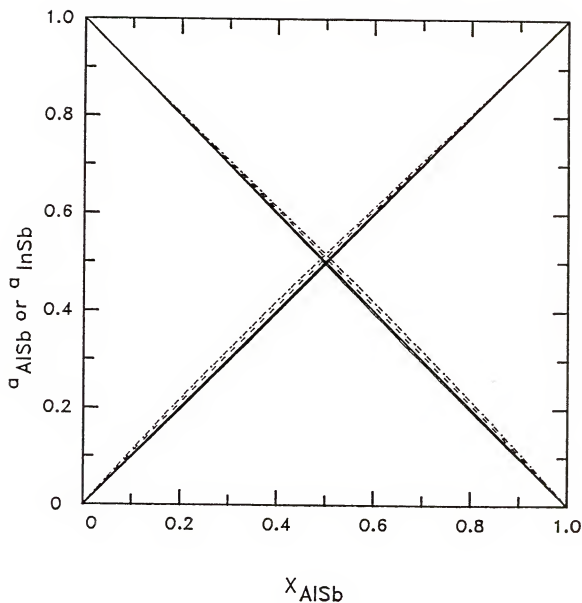


Figure 5-8. The activity of AlSb or InSb in the solid phase versus the AlSb mole fraction at 780 K; —: calculated from NRTL liquid solution and simple solid solution parameters in Table 5-5 (data base *); — — —: calculated from simple liquid and solid solution parameters in Table 5-5 (data base *); - · - : calculated from strictly regular liquid and simple solid solution in Table 5-5 (data base *).

The GaSb-InSb system is the best defined experimentally of three systems considered here. The parameter sets obtained from methods 1 and 2 are listed in Tables 5-2 and 5-6, respectively. As shown in Table 5-6, the results of these fits indicate a positive enthalpy of mixing of the solid solution for each case investigated. Only when the NRTL parameter $\alpha_{\text{GaSb-InSb}}$ in the liquid phase was fixed at a large negative value (~ -1.0) and the solid solution assumed simple was a negative a^S obtained. It is also seen that the parameter a^S for the solution is different and larger in magnitude than a^1 because of additional effects that contribute to nonideality, such as bond length and bond angle distortions, that are not present in the liquid. The excess Gibbs energy of mixing for the liquid pseudobinary solution is calculated to be nearly zero by the estimated parameters listed in Table 5-6. These results also show a miscibility gap in the 377-457°K interval. The parameters listed in Table 5-2 for this system are estimated with the same data base as those used above (liquidus and solidus temperatures). The estimated parameter a^S is opposite in sign and different in magnitude for the simple solution and strictly regular solution models. It is evident that the data base consisting of liquidus and solidus temperatures is not sufficient to permit one to discern a unique solution model. The physical interpretation of the two models with the values of the estimated parameters, however, is quite different. For example, the question of immiscibility in this solid solution is important for solid state device applications. The simple solution parameters predict complete miscibility at all temperatures, while the

assumption of strictly regular solution behavior gives a critical temperature of 433 K.

Figures 5-9 and 5-10 show the calculated pseudobinary diagrams for the $\text{Ga}_x\text{In}_{1-x}\text{Sb}$ system with methods 1 and 2, respectively. It is seen that the fit for the liquidus temperatures of Wooley et al. (230) shown in Figure 5-9 is poor. However, with the same data base, the pseudobinary phase diagram shown in Figure 5-10 is fit very well. A difference in this analysis is the presence of adjustable liquid mixture parameters. The phase diagrams calculated with NRTL equation or simple liquid solution parameter sets are nearly identical in Figure 5-10. Also shown is the phase diagram calculated assuming ideal solid and ideal ternary liquid solution behavior. Figure 5-11 shows the enthalpy of mixing the pseudobinary liquid as a function of composition. The measurements of Gerdes and Predel (226) are compared to the values calculated when the solid was assumed to be a simple mixture and the liquid phase was described by the simple solution (dashed line) or the NRTL (solid line) expression. In Figure 5-12, the a_{GaSb}^S and a_{InSb}^S in the solid solution calculated with these same parameter sets are shown. It is seen that the two liquid solution models give little difference in the predicted thermodynamic behavior of the solid solution. It is also apparent from Figures (5-10) and (5-11) that the formulation for the liquid solution treated as a pseudobinary mixture provides an excellent fit to reported phase diagram and liquid phase enthalpy of mixing.

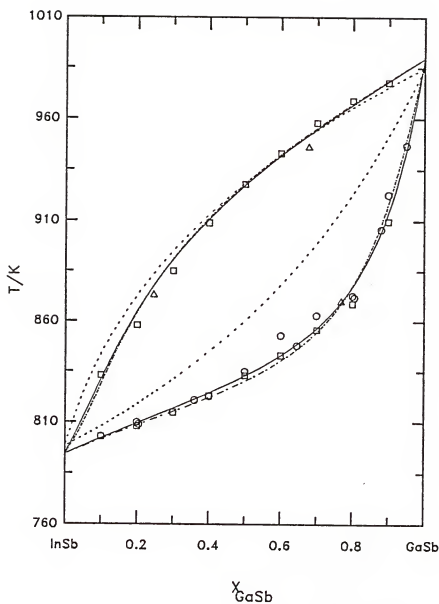


Figure 5-9. The $\text{Ga}_x\text{In}_{1-x}\text{Sb}$ pseudobinary phase diagram; —: calculated from simple liquid solution parameters in Table 5-1 and simple solid solution parameters in Table 5-6; ---: same as solid line except strictly regular solid solution; ···: calculated assuming ideal liquid and solid solution behavior; ○: Ref. (230); □: Ref. (231); Δ: Ref. (233).

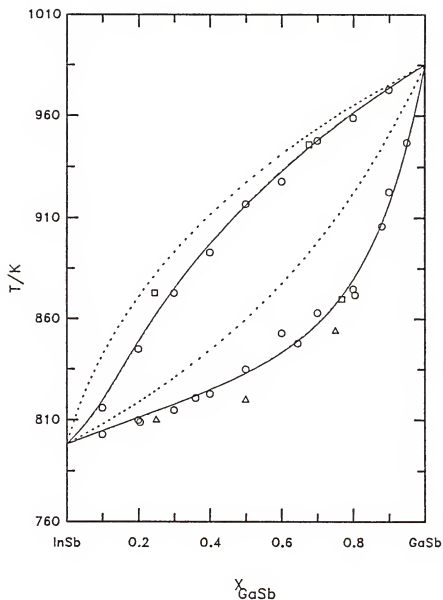


Figure 5-10. The $\text{Ga}_x\text{In}_{1-x}\text{Sb}$ pseudobinary phase diagram calculated with parameters in Table 5-6 (data base **); —: NRTL liquid solution and simple solid solution; —: simple liquid and solid solution; ---: ideal liquid and solid solution; o: Ref. (230); □: Ref. (233).

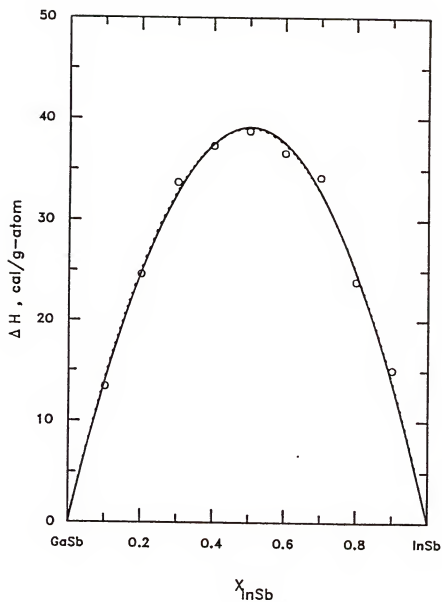


Figure 5-11. Enthalpy of mixing GaSb and InSb in the liquid phase versus the InSb mole fraction at 1022 K; —: calculated from NRTL liquid solution and simple solid solution parameters in Table 5-6 (data base **); ---: calculated from simple liquid and solid solution parameters in Table 5-6 (data base **); o: Ref. (226).

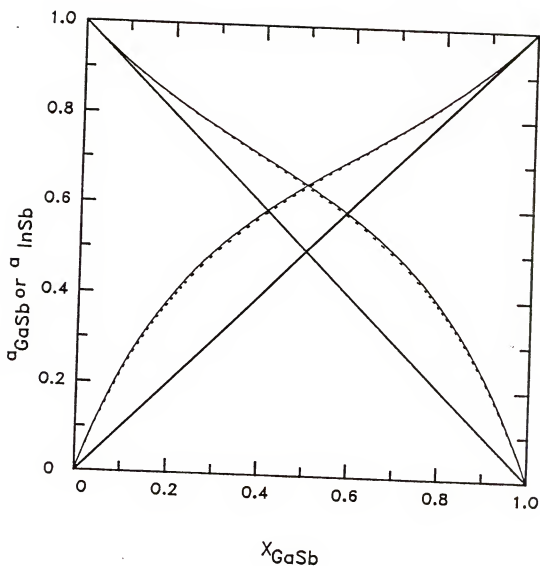


Figure 5-12. The activity of GaSb or InSb in the solid phase versus the GaSb mole fraction; —: calculated from NRTL liquid solution and simple solid solution parameters in Table 5-6 (data base **); ---: calculated from simple liquid and solid solution parameters in Table 5-6 (data base **).

The component activities and pseudobinary ΔH_m^1 for the $\text{Ga}_x\text{In}_{1-x}\text{Sb}$ system were predicted from three binary liquid parameters listed in Table 5-1. The calculated quantities are shown in Figures 5-13 and 5-14. The solid line represents the use of the NRTL equation, while the dashed line gives the result for the simple solution approximation. The NRTL equation gives excellent agreement with the ΔH_m^1 measurements of Gerdes and Predel (226), while the simple solution expression gives slightly more positive values though it retains the correct composition dependence. As shown in Figures 5-13, a_{Ga}^1 values predicted by both equations give less deviation from ideal solution behavior than those measured by Anderson (106). This is not surprising because the measurements of the viscosity, electrical resistivity, x-ray diffraction patterns and magnetic susceptibility of group III-V melts indicate that some kinds of "complexes" or "associates" must exist in the liquid state. Thus, the pseudobinary a_{Ga}^1 values predicted by the two solution models would be expected to have some discrepancy with experimentally determined values.

The parameter covariance matrix provided by the maximum likelihood algorithm allows the calculation of parameter confidence ellipses. The 87% confidence ellipses for the simple solution parameters determined by two approaches were quite narrow and elongated, indicating a high degree of correlation between the parameters a^S and b^S . The correlation coefficient between the parameters a^S and b^S for all cases studied here is over -0.99. As pointed out by the previous investigators (238), the parameters a^S and b^S

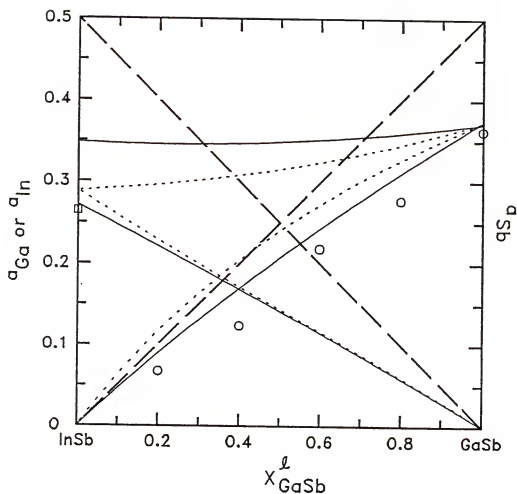


Figure 5-13. Component activities in $\text{Ga}_x\text{In}_{1-x}\text{Sb}$ liquid mixture at 1003 K versus GaSb mole fractions; —: NRTL prediction with parameters in Table 5-1; ---: simple solution prediction with parameters in Table 5-1;: ideal behavior; o: Ref. (152); □: Ref. (121).

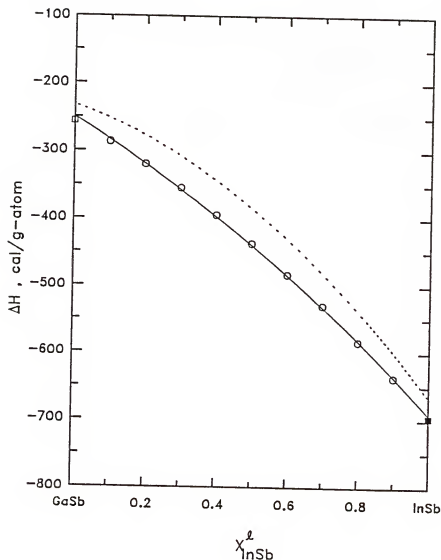


Figure 5-14. Enthalpy of mixing for $\text{Ga}_x\text{In}_{1-x}\text{Sb}$ liquid mixtures at 1022 K versus InSb mole fraction; —: NRTL prediction with parameters in Table 5-1; ---: simple solution prediction with parameters in Table 5-1; o: Ref. (226); ■: Ref. (119); □: average of values of Ref. (127) and Ref. (131).

estimated for a simple solid solution are highly correlated to each other and to the liquid solution parameter set. This same correlation between the parameters was also apparent in this study.

It can be shown that the excess Gibbs energy of mixing for a simple ternary liquid mixture at the pseudobinary composition is given by

$$\Delta G_m^{xs}[A_xB_{1-x}C(1)] = \frac{(a_{A-B}^1 + b_{A-B}^1)}{2} x_{AC}^1 (1 - x_{AC}^1) \quad (5-19)$$

Thus, for example, the binary interaction parameter given in Table 5-2 ($a_{Al-Ga}^1 + b_{Al-Ga}^1 = 598.9 - 0.318T$ (T/K)) should be twice the AlSb-GaSb interaction parameter, $a^1 + b^1T$, given in Table 5-3. The magnitude of $(a_{Al-Ga}^1 + b_{Al-Ga}^1)/2$ is 169.6 cal/mole at 1350 K and is larger than any value given in Table 5-3 by at least a factor of three. It is noted that $a^1 + b^1T$ given in Table 5-3 is negative for all cases at 1350 K. If this simple procedure of estimating the pseudobinary liquid mixture Gibbs energy were appropriate, it would also imply that the degree of nonideality of the liquid solution in the $A_xB_{1-x}P$ and $A_xB_{1-x}As$ systems might be the same as in the $A_xB_{1-x}Sb$ system. Here A and B can be Al, Ga or In. In a similar manner, it would also suggest the liquid solution behavior in the $A'_xB'_{1-x}Al$ and $A'_xB'_{1-x}Ga$ systems be the same as in the $A'_xB'_{1-x}In$ system. Here A' and B' can be P, As or Sb. An analysis of these pseudobinary phase diagrams (Panish and Ilegems (16)) indicates that this is not the situation. The treatment of the liquid as a mixture of A, B and C or as a pseudobinary solution of AC and BC gives a different

interpretation of the solid solution behavior that is obtained from a fit of the pseudobinary phase diagram.

The results for two approaches presented in this chapter have shown that, in the current formulae of the problem, the NRTL equation for liquid solution and simple solution model for solid solution provides a means of adequately representing all of the experimental data for the three pseudobinary antimonide systems, including the asymmetric enthalpy of mixing. The treatment of the liquid solution as a ternary mixture of A, B, and C gave higher standard deviations in the liquidus due to the absence of the adjustable parameters in the liquid phase. This feature is particularly prominent for the systems studied here when the melting-point difference (ΔT_f) between two pure binary III-V compounds increase. In addition, the variation of the Gibbs excess energy of the solid solution with temperature may be in opposite directions for the two different treatments of the liquid phase. It follows that the miscibility gap of the solid solution is predicted differently for each assumption. The severe departure from ideality in the solid of GaSb-InSb system is consistent with the large mismatch between the pure components, according to the pattern established in (240). The mismatch in the GaSb-InSb system of 6.3% (0.383 Å) is greatest of the systems studied here. The "best fit" solid interaction parameters obtained in this chapter with the "best fit" binary parameters in Chapter IV and with the suggested values for Θ_{IC} in Chapter III will be used to predict the ternary and quaternary phase diagrams in next two chapters.

CHAPTER VI
PREDICTIONS OF THE $\text{III}_x\text{III}_{1-x}\text{Sb}$ TERNARY PHASE DIAGRAMS

6.1 Introduction

In recent years, ternary semiconductor alloys formed from two III-V compounds have received considerable attention because the electrical and optical properties of the solid are adjustable by variation of the solid solution composition. This affords the device designer the ability to tune the electrical and optical properties of the solid to fit the particular device requirements. In some systems the compositional degree of freedom in the ternary solid solution is used to match that of the substrate (e.g., $\text{Ga}_{0.47}\text{In}_{0.53}\text{As}$ lattice matched to InP). In $\text{Al}_x\text{Ga}_{1-x}\text{V}$ systems, however, the binary compounds have nearly identical lattice parameters. For these systems, the compositional degree of freedom can then be used to vary the bandgap energy and, therefore, the optical and electrical properties. In most device applications, the first requirement to be met is matching the lattice parameter of the epitaxial film to that of the substrate. Since substrates are available only for the Ga and In binary compounds, only one composition with one bandgap energy is useful for the 15 non- $\text{Al}_x\text{Ga}_{1-x}\text{V}$ ternary alloys. This problem can be overcome by adding a fourth element to a ternary alloy to form a quaternary alloy and is discussed in the next chapter.

Many of the processing steps in the fabrication of devices containing III-V materials involve the interfacial contact of a liquid phase with a solid phase. Examples of such processes are bulk crystal growth, liquid phase epitaxy, impurity incorporation, laser annealing and melt purification (e.g., zone refining) processes. As an equilibrium boundary condition is often implied at the liquid-solid interface, knowledge of the phase diagram for the material system involved is essential in the analysis of these processes. The direct experimental determination of the possible 18 ternary phase diagrams would require considerable effort and is often compounded by the experimental difficulties of lengthy equilibration times and the rather high vapor pressures involved with the arsenides and phosphides. Because of these difficulties the development of calculational procedures for judging, interpolating, and correlating phase diagrams and thermochemical experimental information and, most importantly, for predicting these properties in systems with non-existent or minimal experimental characterization is attractive.

The description of ternary solid-liquid equilibrium in group III-V semiconductor systems has been approached by several investigators (16,24-40,248-251). Studies of the thermochemical behavior found in III-V ternary systems have been directed primarily at describing the phase diagrams by enlisting only knowledge of the contained binary phase diagram limits. The validity of a particular solution model employed is then ascertained only by its ability to reproduce known portions of the phase diagram. In this chapter, the basic equations describing chemical equilibrium between the

pseudobinary solid solution of the type $A_xB_{1-x}C$ and the ternary liquid are derived. Problems that are encountered in achieving an effective calculational procedure are also discussed.

In the two previous chapters, the use of various solution models to describe the liquid phase behavior of III-V binary systems and the solid phase behavior of the pseudobinary systems was considered. The ternary melt solution behavior can be obtained by extending these binary models to describe a ternary mixture without additional adjustable parameters. In this chapter, phase diagrams for the Al-Ga-Sb, Al-In-Sb, and Ga-In-Sb systems are presented. The best results for the binary liquid and pseudobinary solid solution parameters determined from two previous chapters in conjunction with the suggested values for θ_{IC} given in Chapter III are used to calculate the quantities Γ_{IC} and θ_{IC} necessary for the ternary phase diagram calculation. The measured phase diagrams are compared with the values calculated by an extension of the NRTL equation and simple solution model binary results to the ternary systems considered here.

6.2 Calculation of the Phase Diagram

The $A_xB_{1-x}C$ ternary III-V system consists of two elements A and B from the group III or V column and one element C from the group V or III column, respectively. The chemical formula indicates the formation of a substitutional solid solution between the A and B elements and fixed ratio of C to A and B elements. Mixing among A and B atoms involves two kinds of atoms occupying one of the sublattices. This solid solution can be considered a mixture of two

pure binary compounds AC and BC. It is obvious that x in the formulation $A_xB_{1-x}C$ is equivalent to the mole fraction X_{AC} in the solid solution. This is not the case, however, for the quaternary $A_xB_{1-x}C_yD_{1-y}$ system (discussed in Chapter II) in which mixing among solid atoms occurs on both sublattices.

The solid-liquid equilibrium state of the A-B-C ternary system is calculated by equating the temperature and pressure of each phase as well as the chemical potentials of each of the species present in both phases. In addition to these relationships, a constraint of stoichiometry is placed on the solid solution; the sum of the atom fractions of group III elements must equal the sum of the atom fractions of group V elements. As discussed above, the $A_xB_{1-x}C$ ternary system is characterized by one binary (elements A and B) and one unary (element C) sublattice. The ternary solid solution can be treated as if it were a binary solution of components AC and BC. The requirement of equal chemical potentials for each of the species present in both phases is expressed by

$$\mu_{IC}^S = \mu_I^L + \mu_C^L, \quad I = A \text{ and } B \quad (6-1)$$

where I and C refer to the liquid phase components, and IC refers to the solid phase components.

The insertion of the relation $\mu_i = \mu_i^\circ + RT \ln a_i$ defined previously for each term in Equation (6-1), followed by algebraic manipulation, results in the following implicit expressions for the liquid and solid equilibrium mole fractions of components A in the

liquid

$$x_A = \frac{\frac{1}{x_C} - (1-x_C)\Gamma_{BC}\exp(-\theta_{BC})}{\Gamma_{AC}\exp(-\theta_{AC}) - \Gamma_{BC}\exp(-\theta_{BC})} \quad (6-2)$$

and component AC in the solid solution

$$x_{AC} = \frac{x_C(1-x_C) - \frac{1}{\Gamma_{BC}}\exp(\theta_{BC})}{\frac{1}{\Gamma_{AC}}\exp(\theta_{AC}) - \frac{1}{\Gamma_{BC}}\exp(\theta_{BC})} \quad (6-3)$$

Two types of variables appear in Equations (6-2) and (6-3), θ_{IC} and Γ_{IC} . The variable θ_{IC} is a reduced standard state chemical potential difference and is defined by

$$\theta_{IC} = \frac{\mu_{IC}^{0,s} - \mu_I^{0,l} - \mu_C^{0,l}}{RT}, \quad I = A, B \quad (6-4)$$

The term Γ_{IC} is the ratio of liquid phase to solid phase activity coefficients and is given by

$$\Gamma_{IC} = \frac{\gamma_I^l \gamma_C^l}{\gamma_{IC}^s}, \quad I = A, B \quad (6-5)$$

The problem of describing the ternary III-V phase diagram is reduced to selecting the standard states, determining the temperature and pressure (negligible) dependence of θ_{IC} and determining the temperature, pressure (negligible) and composition dependence of

Γ_{IC} . Equations (6-2) and (6-3) are the same as those obtained in Chapter II by simplifying the results for the general quaternary systems.

It is noted that the effect of the point defect structure is neglected in deriving the working Equations (6-2) and (6-3). In other words, the homogeneity range of binary compound is narrow enough to produce negligible variation in the molar Gibbs energy with composition, i.e.,

$$\mu_I^S(T, P, x_I^S) + \mu_C^S(T, P, x_C^S) = \mu_{IC}^S(T, P) = \mu_{IC}^{O,S}(T, P) \quad (6-6)$$

It is obvious from the above equation that the chemical potential of component i ($i = I$ or C) in the solid can be a strong function of composition x_I^S or x_C^S along the locus of nonstoichiometry, but the sum of the chemical potentials in the binary solid is nearly constant at a given temperature and pressure. Brebrick and Strauss (117,123) have calculated the variation of the molar Gibbs energy of the solid for such nearly stoichiometric compounds HgTe and CdTe, indicating that neglecting this variation does not lead to significant errors. The maximum value of this variation would be only 0.1 Kcal/mol for HgTe and 1 cal/mol for CdTe with homogeneity range of 0.5 and 0.001 atom percent, respectively.

The values of Θ_{IC} used in this chapter are recommended in Table 3-6. As expressed by Equation (6-5), the calculation of the term Γ_{IC} involves the representation of the nonidealities in each phase with a solution model. As discussed in Chapter IV, the NRTL equation best

represents the combined data set of the group III-V binary systems, including the asymmetric and temperature dependent enthalpy of mixing. For the more symmetrical systems (e.g., Ga-Sb system), little difference was found between the models and the two-parameter simple solution model appears to be adequate. The computational procedure, however, for the simple solution model is simpler than that for the NRTL equation. For comparison, the binary results of the NRTL equation and simple solution models are extended to predict the ternary phase diagram without the use of ternary parameters. Based on the simple solution approximation, the activity coefficients for the pseudobinary solid solution are written from Equation (1-6) with $n = 2$ as

$$RT \ln \gamma_{AC} = w_{AC-BC} x_{BC}^2 \quad (6-7)$$

$$RT \ln \gamma_{BC} = w_{AC-BC} x_{AC}^2 \quad (6-8)$$

Similarly, a Wohl's expansion of the binary equation to describe a ternary liquid while retaining only binary interaction terms gives

$$RT \ln \gamma_A = w_{AC} x_C^2 + w_{AB} x_B^2 + (w_{AC} + w_{AB} - w_{BC}) x_B x_C \quad (6-9)$$

$$RT \ln \gamma_B = w_{BC} x_C^2 + w_{AB} x_A^2 + (w_{BC} + w_{AB} - w_{AC}) x_A x_C \quad (6-10)$$

$$RT \ln \gamma_C = w_{AC} x_A^2 + w_{BC} x_B^2 + (w_{AC} + w_{BC} - w_{AB}) x_A x_B \quad (6-11)$$

There exist three binary interaction parameters of the liquid

solution: w_{AB} , w_{AC} , and w_{BC} . The solid solution is described by the pseudobinary interaction parameters: w_{AC-BC} . For the NRTL equation, the corresponding ternary activity coefficient is given by

$$\ln \gamma_m = f_m / D_m + \sum_{i=1}^3 x_i g_{mi} [\tau_{mi} - f_i / D_i] / D_i, \quad m = 1, 2, 3 \quad (6-12)$$

where

$$f_i = \sum_{j=1}^3 x_j \tau_{ji} g_{ji}, \quad 1 = A, 2 = B, 3 = C \quad (6-13)$$

$$D_i = \sum_{k=1}^3 x_k g_{ki} \quad (6-14)$$

$$g_{ji} = \exp(-\alpha_{ji} \tau_{ji}) \quad (6-15)$$

The parameters α_{ij} and τ_{ij} are determined by the i - j binary system $\alpha_{ij} = \alpha_{ji}$ and $\tau_{11} = \tau_{22} = \tau_{33} = 0$.

It is noted that this treatment of the ternary liquid phase includes the assumption that the interaction parameters are independent of composition and thus the values of w , α_{ij} , and τ_{ij} determined from binary and pseudobinary systems can be used for describing the ternary liquid. Applying the Gibb's phase rule to solid-liquid equilibrium in ternary $III_x III'_{1-x} Sb$ system, the number of degrees of freedom is found to equal three. Thus, if T , P , and x_C are specified, then x_A and x_{AC} can be completely determined by these implicit equations (Equation (6-2) and (6-3)). The parameter sets determined for both the NRTL equation and the simple solution model are listed in Table 6-1 for the Al-Ga-Sb and Al-In-Sb systems and in

Table 6-1. NRTL and simple solution parameters used for calculation of the Al-Ga-Sb and Al-In-Sb plan diagram.

System	Model	a (cal/mol)	b (cal/mol-K)	c (cal/mol)	d (cal/mol-K)	α_{IC}
Al-Sb	NRTL Simple	-552 13,437	-0.244 -12.854	-75,555 -	52.251 -	-0.5 -
Ga-Sb	NRTL Simple	-3,404 3,209	12.343 -5.886	1,139 -	-6.508 -	0.242 -
In-Sb	NRTL Simple	-5,526 -4,501	7.014 0.906	2,364 -	-6.096 -	0.914 -
Al-Ga	NRTL Simple	-840 599	0.603 -0.318	1,640 -	-1.035 -	0.3 -
Al-In	Simple Regular	5,596 1,060 *	-0.705 -	- -	- -	- -
AlSb-GaSb	Simple (I) Simple (II)	3,859 2,730	-3.058 -2.139	- -	- -	- -
AlSb-InSb	Simple (I) Simple (II)	1,575 1,080	-1.874 -1.455	- -	- -	- -

* Source: Reference (16).

(I): Simple solution model for pseudobinary liquid solution.

(II): NRTL equation for pseudobinary liquid solution.

Table 6-2 for the Ga-In-Sb system. As shown above, these working equations (Equations (6-2) and (6-3)) are implicitly complex relations for T , P , x_{AC} , x_A and x_C .

6.3 Computational Procedure

A computer program which calculates the equilibrium liquid and solid composition (x_A , x_{AC}) with a given T and x_C was written in the Fortran IV language. The program solves Equations (6-2) to (6-11) simultaneously for the simple solution approach with the added requirements that in the solid

$$x_{AC} + x_{BC} = 1 \quad (6-16)$$

and in the liquid

$$x_A + x_B + x_C = 1 \quad (6-17)$$

For the NRTL equation, the program solves Equations (6-2) to (6-8) and (6-12) to (6-17) simultaneously. For simplicity, the governing Equations (6-2) and (6-3) are written as

$$f_1 = x_{AC} - \Gamma_{AC} x_A x_C \exp(-\theta_{AC}) = 0 \quad (6-18)$$

$$f_2 = x_{BC} - \Gamma_{BC} x_B x_C \exp(-\theta_{BC}) = 0 \quad (6-19)$$

Since the above implicit working equations cannot be solved analytically for $\{x_A, x_{AC}\}$, these are obtained by iteration using

Table 6-2. NRTL and simple solution parameters used for calculation of the Ga-In-Sb phase diagram.

System	Model	a(cal/mol)	b(cal/mol-K)	c(cal/mol)	d(cal/mol-K)	α_{IC}
Ga-Sb	NRTL	3647	6.016	-1415	-5.324	0.157
	Simple	-928.6	-1.394	-	-	-
	NRTL*	793.7	-3.539	-1554	1.348	-0.254
	Simple*	-982.2	-1.489	-	-	-
In-Sb	NRTL	6038	1.814	-1669	-3.622	0.315
	Simple	-2662.6	-1.708	-	-	-
	NRTL*	11367	-0.265	-9181	-3.093	0.042
	Simple*	-2658.6	-1.568	-	-	-
Ga-In	NRTL	697	-0.159	495	0.364	0.300
	Simple	1029.9	0.290	-	-	-
GaSb-InSb	Simple (I)	1884.1	-0.425	-	-	-
	Simple (II)	2131.6	-0.688	-	-	-

*: Parameter a fixed at T_m^{IC} (data base: group III component activity and enthalpy of mixing).
 (I): Simple solution model for pseudobinary liquid solution.
 (II): NRTL equation for pseudobinary liquid solution.

the Newton-Raphson method. Proper choice of initial values of x_A and x_{AC} and specified variables of T and x_C for the iterative calculation is very important to avoid divergence and excessively long computation times, so the following procedure was used: the specified variables $\{T, x_C\}$ start in the A-rich region of the binary AC limit, i.e., $\{T, (x_C)_{\min}, x_B=0\}$, and then gradually increase the C content of x_C , i.e., $\{T, (x_C)_{\min} + \Delta x_C\}$, in the ternary liquid to the B-rich binary BC limit, i.e., $\{T, (x_C)_{\max}, x_A=0\}$ or to the binary C-rich binary AC limit, i.e., $\{T, (x_C)_{\max}, x_B=0\}$. The best initial guess $\{x_A, x_{AC}\}$ for each iteration is the binary limit obtained from previous chapters. In this way, the program converges very rapidly with only three or four iterative steps typically referred for a given set of specified variables.

6.4 Results and Discussion

The working Equations (6-2) and (6-3) presented here are simple and useful for calculation of the phase diagram because the problem of quantitatively describing ternary solid-liquid equilibrium is reduced to determining the standard state properties (θ_{IC}) and the liquid and solid mixture properties (Γ_{IC}).

With the standard state for each component chosen as the pure component in the phase of interest and at the temperature of interest, four approaches for the calculation of the reduced standard state chemical potential change (θ_{IC}) have been discussed in detail in Chapter III. The recommended values listed in Table 3-6 are used in this study. The other term contained in Equations (6-2) and (6-3)

is Γ_{IC} , and its determination is discussed here. As mentioned in Chapter IV, the component activity coefficients in the liquid phase can be addressed separately from those in the solid solution by direct experimental determination or by analysis of the binary limits, since $\gamma_{IC}^S = 1$. Typically, the available binary liquidus data have been used to fix the adjustable parameters in a solution model with Θ_{IC} determined by Equation (1-1) (Vieland's method (9)). The solution model expression for the activity coefficient has been used not only to represent the component activities along the liquidus curve, but also the stoichiometric liquid phase activity product needed in Equation (1-1). The ternary melt solution behavior is then obtained by extending the binary models to describe a ternary mixture without additional adjustable parameters. The binary model parameters that are determined by a liquidus fit using method I for Θ_{IC} do not give reliable values for the enthalpy of mixing or component activity.

The parameters listed in Tables 6-1 and 6-2 were obtained by fitting the different experimental data sets. As shown in Chapter IV, the NRTL equation and simple solution model poorly describe the entire Al-Sb system because the measured AlSb phase diagram is quite asymmetric on both sides of the line compound AlSb. It is evident that the use of these solution model parameters obtained by fitting the entire phase diagram or the combined data set (liquidus, enthalpy of mixing, component activity) would cause a discrepancy between the calculated and experimental results at the binary limits. Thus, the Al-Sb interaction parameters listed in Table 6-1 for this study were

obtained by fitting the liquidus data on the Al-rich side ($x_{Al} > 0.5$) only. In a similar manner, the parameter sets listed in Table 6-1 for the Ga-Sb and In-Sb systems were obtained by fitting the liquidus data only. Note that these models can fit the entire Ga-Sb and In-Sb phase diagrams well. The parameter sets for the Al-Ga system were obtained by fitting the combined data set because the NRTL equation and simple solution model can represent the liquidus and thermochemical data well.

As mentioned in Chapter IV, the simple solution model has no ability to represent the Al-In system due to the presence of an asymmetric miscibility gap in the liquid phase. The simple solution parameters listed in Table 6-1 for the Al-In system was obtained by fitting the combined data set. The value $w_{AlIn}^1 = 1060 \text{ cal/mol}$ proposed by Panish and Ilegems (16) is also listed in this table. The predicted results for the Al-In-Sb system with these two parameter sets for the Al-In system were compared. The pseudobinary solid interaction parameters listed in Tables 6-1 and 6-2 were obtained by fitting the combined data set (liquidus, solidus, liquid enthalpy of mixing) with second approach discussed in Chapter V, for which the liquid mixture is treated as a pseudobinary liquid solution. The parameter sets listed in Table 6-2 for each of the three binary systems were obtained by fitting the combined data set consisting of liquidus temperature, enthalpy of mixing, and group III activity. The parameter values for the Ga-Sb and In-Sb systems in this table are taken from Aselage et al. (187). Also shown in Table 6-2 are the parameter sets for the Ga-Sb and In-Sb systems which were

obtained by fitting the enthalpy of mixing and group III activity with parameter a fixed at T_m^{IC} . The calculated results for the Ga-In-Sb system with these parameter sets are presented and compared with the available experimental measurements.

The importance of the Γ_{IC} term in calculating ternary ($A_xB_{1-x}C$) phase diagrams can be made apparent by examining the distribution coefficient K_{IC} , which is defined as follows:

$$K_{IC} \equiv \frac{x_{IC}}{x_I} \quad (6-20)$$

It is easily shown from Equation (6-18) or (6-19) that the distribution coefficient can be calculated by the relatively simple equation

$$K_{IC} = x_C \Gamma_{IC} \exp(-\Theta_{IC}) \quad (6-21)$$

Since Θ_{IC} is a function of temperature only, the slope of a plot of K_{IC} versus x_C along an isotherm is proportional to Γ_{IC} . This plot can be compared to the straight line that is produced when the value of Γ_{IC} is assumed equal to unity, which occurs when either the liquid and solid mixtures are both ideal solutions or the nonideality in the liquid phase ($\gamma_I^L \gamma_C^L$) is the same as that in the solid ($\gamma_I^S \gamma_C^S$). For the ideal case, the distribution coefficient is calculated by the equation

$$K_{IC}^{ideal} = x_C \exp(-\Theta_{IC}^u) \quad (6-22)$$

It is noted that the values of θ_{IC} and θ_{IC}'' are not the same.

Substituting $a_i^{S1}(T) = a_i^{S1}(T_m) = 0.5$ into Equation (3-3) or (3-6) and introducing the selected values listed in Table 3-2 into the resulting expression, we obtain

$$\theta_{AlSb}'' = -5.481 - 5.133 \times 10^{-4} T - 8261.2/T + 1.522 \ln T \quad (6-23)$$

$$\theta_{GaSb}'' = -5.184 - 7.247 \times 10^{-4} T - 7069.9/T + 1.696 \ln T \quad (6-24)$$

and

$$\theta_{InSb}'' = -5.724 - 7.061 \times 10^{-4} T - 4917.8/T + 1.656 \ln T \quad (6-25)$$

where T is the absolute temperature (K). These values are used to calculate the ideal distribution coefficient and ideal ternary phase diagrams in this study.

An experimental value for Γ_{IC} can be assigned by solving Equations (6-20) and (6-21) for Γ_{IC} and requires values for θ_{IC} , based on the experimental properties discussed previously, and liquidus and solidus data. The resulting expression is given by

$$\Gamma_{IC} = \frac{x_{IC}}{x_I x_C} \exp(\theta_{IC}) \quad (6-26)$$

Shown in Figure 6-1 is a plot of $1 - \Gamma_{GaSb}$ versus x_{Sb} along several isotherms for the Al-Ga-Sb system. It is seen that Γ_{GaSb} is nearly

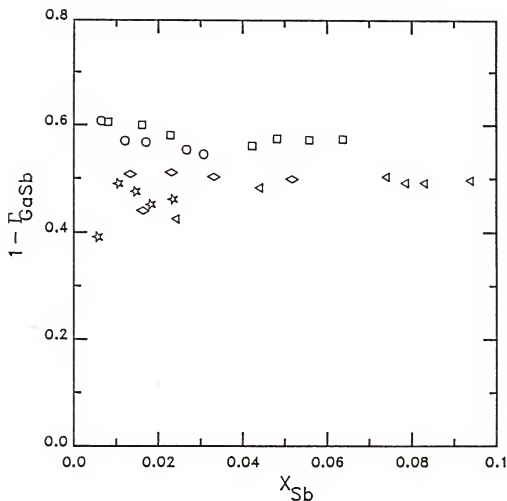


Figure 6-1. Values of $1 - \Gamma_{GaSb}$ calculated with Equation (6-26) versus the liquid phase mole fraction at various temperatures in the Al-Ga-Sb system. The calculation used the recommended value of θ_{GaSb} listed in Table 3-6 and the phase diagram determinations of Dedegkaev et al. (39): ☆, 778 K; ◇, 825 K; △, 873 K; and of Cheng and Pearson (48): o, 773 K; □, 823 K.

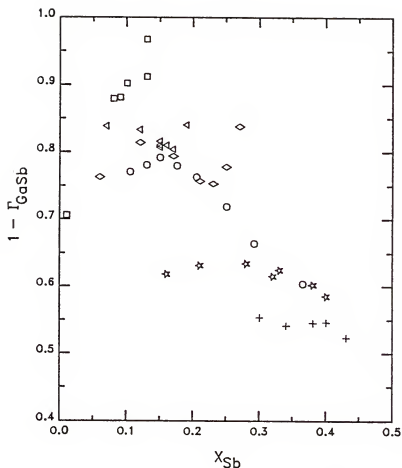


Figure 6-2. Values of $1 - \Gamma_{GaSb}$ calculated with Equation (6-26) versus the liquid phase mole fraction at various temperatures in the Ga-In-Sb system. The calculation used the recommended value θ_{GaSb} listed in Table 3-6 and the phase diagram determinations of Antypass (251): o, 773 K; and of Gratton and Woolley (24): □, 653 K; △, 703 K; ◇, 748 K; ☆, 873 K; +, 923 K.

independent of composition in the Ga-rich melts. In addition, Γ_{GaSb} varies weakly with temperature only at low values of x_{Sb} , at which the experimental uncertainty in Γ_{GaSb} is expected to be large. It is apparent from Equation (6-26) that Γ_{IC} is sensitive to the small value of x_{I} or x_{C} or both. The partial cancellation in both the composition and temperature dependence of Γ_{GaSb} is largely responsible for the ability of rather simple solution models to represent the Al-Ga-Sb ternary phase diagram. Shown in Figure 6-2 is a similar plot of $1 - \Gamma_{\text{GaSb}}$ versus x_{Sb} along six isotherms for the Ga-In-Sb system. As can be seen, the result of Γ_{GaSb} for this system shows that Γ_{GaSb} is a more complex function of both temperature and composition. This may be partly because of the large lattice mismatch (severe nonideality) between two binary compounds in the solid phase.

The solutions of Equations (6-2) and (6-3) for various liquidus isotherms determined for both the NRTL equation and simple solution model for the Al-Ga-Sb system in the Ga-rich region are shown in Figures 6-3 and 6-4, respectively, along with the available liquidus data. As shown in Figure 6-3, the results calculated with the NRTL equation appear too high for both cases considered here. However, as shown in Figure 6-4, the agreement between the calculated and experimental liquidus (48)(with the exception of the one at 773 K (248)) is excellent when the simple liquid and ideal pseudobinary solid solutions are applied. As mentioned above, this is expected because Γ_{GaSb} is nearly independent of the temperature and composition and the lattice constants of GaSb and AlSb are nearly

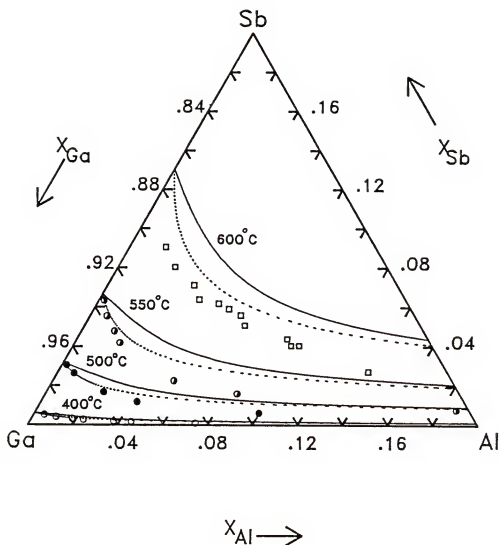


Figure 6-3. Liquidus isotherms in the Al-Ga-Sb system for Ga-rich melts: —, NRTL liquid and simple solid solution; ---, NRTL liquid and ideal solid solution; Bedair (248): □, 600°C; Cheng and Pearson (48): o, 400°C; ●, 500°C; ○, 550°C.

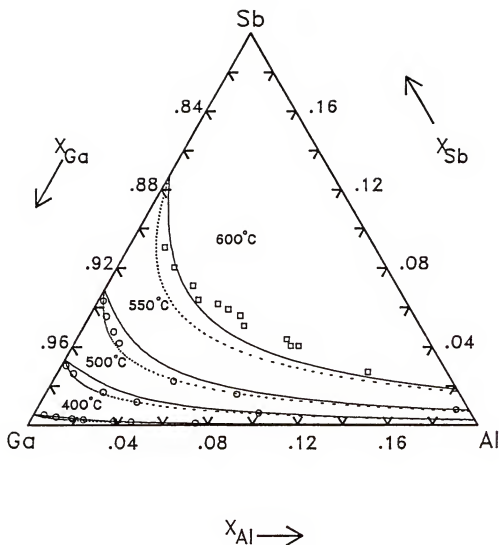


Figure 6-4. Liquidus isotherms in the Al-Ga-Sb system for Ga-rich melts at 600, 550, 500, and 400°C: —, simple liquid and solid solution; ---, simple liquid and ideal solid solution; \square , ref. (248); \circ , ref. (48).

equal (6.095 Å and 6.136 Å). The results represent a significant improvement over previous attempts to calculate the Al-Ga-Sb phase diagram. This is probably due to the improvement in the standard state property calculation as discussed in Chapter III. Figure 6-5 shows the 773 K solidus isotherm. Once again, the agreement is quite good for the case of the simple liquid and ideal solid solutions.

Plotted in Figure 6-6 are the calculated distribution coefficients as a function of x_{Sb} along the 773 K, 823 K, and 873 K isotherms for the Al-Ga-Sb system. Also shown are the data of Dedegkaev et al. (39) and Cheng and Pearson (48), and the results calculated from Equation (6-22) (the liquid and solid both behave ideally). It is apparent from Equation (6-22) that a plot of K_{AlSb} versus x_{Sb} at constant temperature should yield a straight line having a slope of $\exp(-\theta_{AlSb}^H)$. Figure 6-6 indicates that the assumption of a value of unity for Γ_{AlSb} is incorrect. Deviations from these ideal lines are an indication of the importance of the term Γ_{AlSb} . The distribution coefficients calculated with the simple liquid and ideal solid solution models are in excellent agreement with the experimental values for the 773 K isotherm, while the agreement is good over a large portion of the 823 K isotherm. The calculated distribution coefficients for the NRTL equation are smaller than the experimentally determined values because the calculated liquidus is larger than those determined by the experiment.

The calculation procedure for the generation of the Al-In-Sb ternary phase diagram is based on the simple solution model for

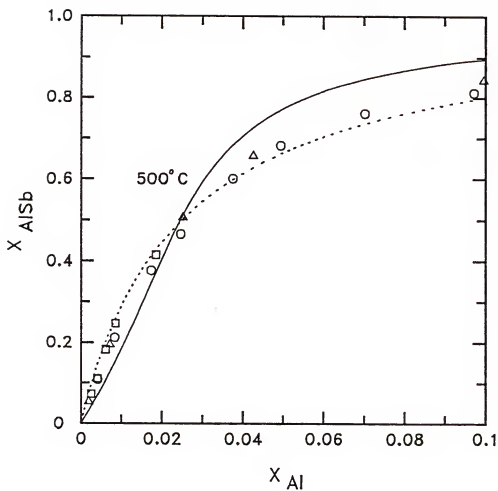


Figure 6-5. Solidus isotherm of Al-Ga-Sb system at 500°C: —, simple liquid and solid solution; ---, simple liquid and ideal solid solution; o, Ref. (18); Δ , Ref. (48); \square , Ref. (19).

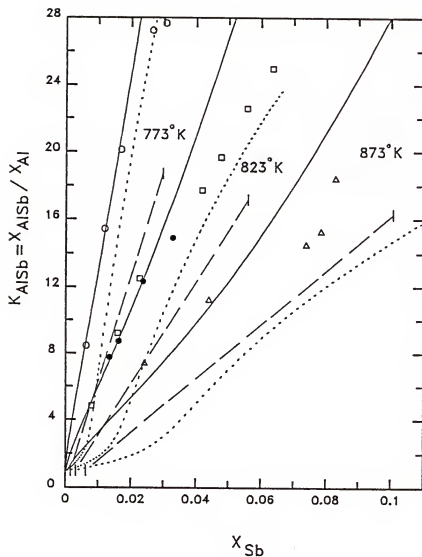


Figure 6-6. Al distribution coefficient versus antimony mole fraction in the Al-Ga-Sb system: —, simple liquid and ideal solid solution; ---, NRTL liquid and ideal solid solution; ···, ideal liquid and solid solution; o, 773 K, Ref. (48); □, 823 K, Ref. (48); ●, 823 K, Ref. (39); △, 873 K, Ref. (39).

binary and pseudobinary systems. Figures 6-7 and 6-8 show several Al-In-Sb liquidus isotherms calculated with the same parameter sets with the exception of the one for Al-In (III-III') system. It is seen that the interaction parameter w_{AlIn}^I for the Al-In system not only affects the calculated liquidus curve curvature but also shifts the calculated liquidus curve position at the pseudobinary section. In contrast comparison of Figures 6-7 and 6-8 shows that the best fit parameter $w_{AlIn}^I = 5596 - 0.705T$ (cal/mol) obtained by fitting the combined data set is too large. The better results shown in Figure 6-7 were obtained with $w_{AlIn}^I = 1060$ cal/mol proposed by Panish and Ilegems (16). As discussed by Stringfellow (79), with this large value of w_{AlIn}^I errors in this parameter make drastic changes in the calculated phase diagram. It is also seen from Figures 6-7 and 6-8 that the calculated liquidus isotherms are insensitive to the solid interaction parameter used. It should be mentioned here that the miscibility gap in the Al-In liquid extends into the Al-In-Sb ternary melts. No further attempt has been made here to calculate the detailed phase diagram because experimental data for this system is lacking. Shown in Figure 6-9 is the calculated Al distribution coefficient versus x_{Sb} along the 873 K and 1173 K isotherms. Again, these results indicates that the assumption of a value of unity for Γ_{AlSb} is clearly incorrect.

Figure 6-10 shows five Ga-In-Sb liquidus isotherms calculated with the NRTL equation and simple solution model, in which the binary solution parameters were estimated by using a data base that included experimental values of liquidus temperature, group III component

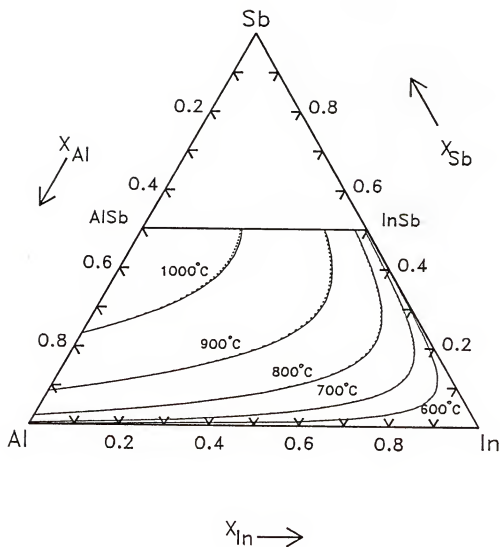


Figure 6-7. Liquidus isotherms in the Al-In-Sb system: —, calculated assuming simple liquid (except Al-In, strictly regular liquid) and solid solution; ---, simple liquid and ideal solid solution.

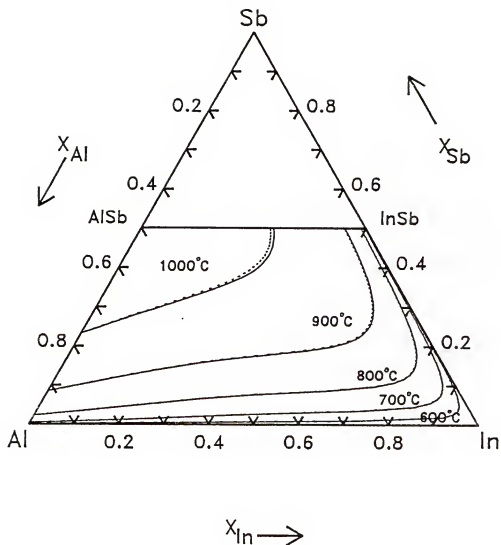


Figure 6-8. Liquidus isotherms in the Al-In-Sb system: —, calculated assuming simple liquid and solid solution; ---, calculated assuming simple liquid and ideal solid solution.

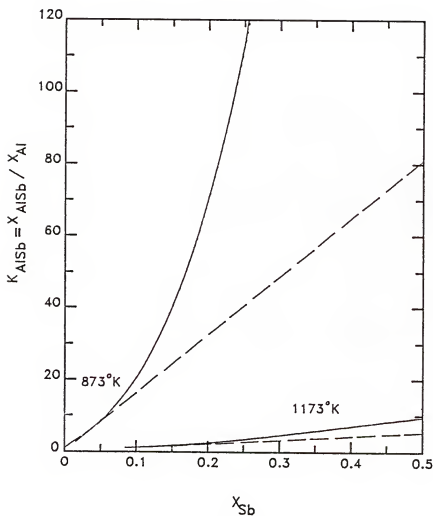


Figure 6-9. Al distribution coefficient versus antimony mole fraction in the Al-In-Sb system: —, simple liquid (Al in strictly regular liquid) and simple or solid solution; ---, ideal liquid and solid solution.

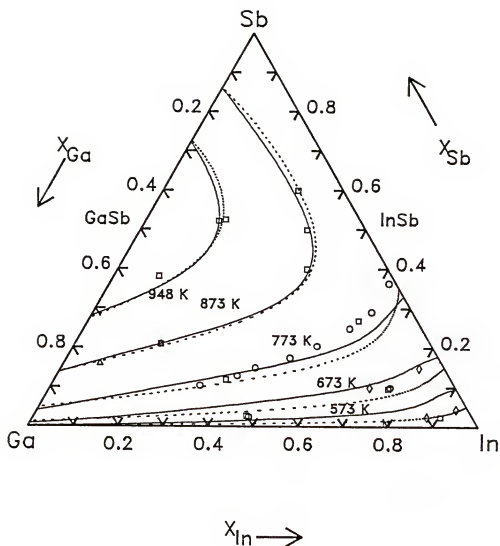


Figure 6-10. Liquidus isotherms in the Ga-In-Sb system: —, calculated assuming NRTL liquid and simple solid solution behavior; ---, calculated assuming simple liquid and solid solution behavior; □, Ref. (25); , Ref. (26); o, Ref. (251); Δ, Ref. (230).

activity, and enthalpy of mixing. The agreement is quite good for each of the isotherms predicted by the NRTL liquid and simple solid solution models with the exception of the one at 573 K. However, the use of the simple liquid and solid solution models gives better results for this low temperature. For the purpose of comparison the phase diagram was calculated under the assumption that the liquid phase behaves as the ideal solution and the solid phase behaves as the simple or ideal solution. The results of these calculation for the same temperatures as above are shown in Figure 6-11. As can be seen, the assumption of ideality is indeed poor as liquidus temperatures show disagreements of as much as 100 K. It is also shown in Figure 6-11 that the liquidus isotherm was shifted by a large amount when the solid phase was assumed to behave as an ideal solution.

Several authors (16,24-26) have used the simple solution model in conjunction with Vieland's (9) liquidus equation to calculate the ternary phase diagram for the Ga-In-Sb system. While there is little difference in the experimental and calculated liquidus isotherms for any of the investigations, the calculation of the liquid phase thermochemical properties shows a marked difference. The results of these investigations usually are in both qualitative and quantitative disagreement with the enthalpy of mixing in the binary systems. As discussed in the previous chapter, the parameter values used here have been shown to yield calculated values which are in good agreement with the thermochemical data.

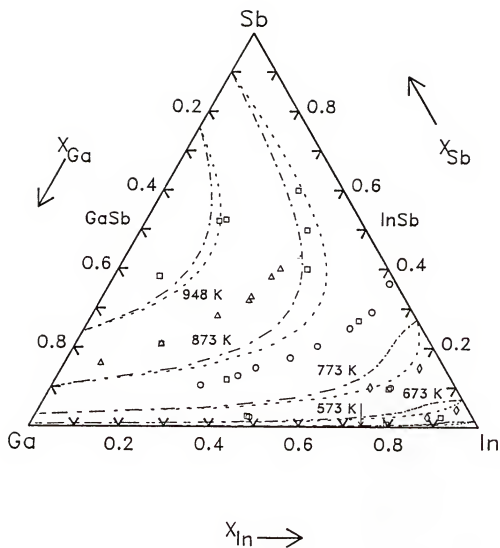


Figure 6-11. Liquidus isotherms in the Ga-In-Sb system: —, calculated assuming ideal liquid and strictly regular solid solution behavior; ---, calculated assuming ideal liquid and solid solution behavior; \square , Ref. (25); \diamond , Ref. (26); \circ , Ref. (251); Δ , Ref. (230).

Shown in Figure 6-12 is a plot of the 673 K Ga-In-Sb solidus isotherms calculated with the NRTL equation and simple solution model that account for both the liquid and solid phase deviations from ideal behavior. For comparison, the result calculated with the assumption that both the liquid and solid phases are ideal is also plotted in this figure. As was found before, marked differences exist between the real and ideal cases. Again, the results indicate that the NRTL solution model with parameters estimated from binary data provides a good description of this system. Such plots shown in Figures 6-10 and 6-12 are extremely useful to provide growth conditions in that device characteristics generally define the solid composition required. Unfortunately very little experimental information is available where both the equilibrium liquidus and solidus composition have been measured. In these studies generally one composition is measured and the other is calculated from an appropriate model.

Plotted in Figure 6-13 as the dot and solid lines is K_{GaSb} versus x_{Sb} calculated with the model studied here. For comparison the long dashed line represents the ideal values calculated with Equation (6-22). It is shown that the results calculated from the NRTL equation are better than those predicted by the simple solution model for $x_{\text{Sb}} > 0.1$, while the simple solution model gives better results for $x_{\text{Sb}} < 0.1$. As the ideal (straight) lines in this figure show, the assumption of a value of unity for Γ_{GaSb} is clearly incorrect, although it is interesting to note that the slope of the experimental data in the range $3 < K_{\text{GaSb}} < 6$ is approximately the same

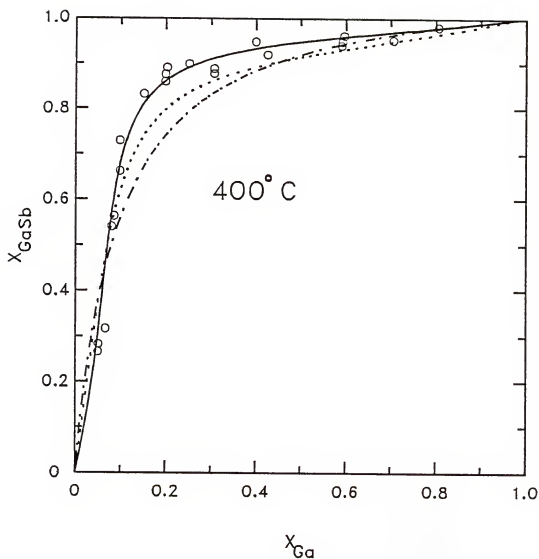


Figure 6-12. Solidus isotherm of Ga-In-Sb system at $400^{\circ}C$: —, NRTL liquid and simple solid solution; ---, simple liquid and solid solution; -.-, ideal liquid and solid solution; o, Ref. (252).

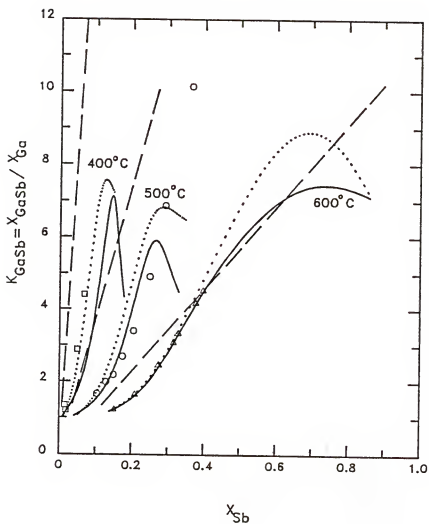


Figure 6-13. Ga distribution coefficient versus antimony mole fraction in the Ga-In-Sb system: —, NRTL liquid and simple solid solution; ---, simple liquid and solid solution; ···, ideal liquid and solid solution; Ref. (251): o, 773 K; Ref. (24): Δ, 873 K; Ref. (252): □, 673 K.

as that obtained from setting Γ_{GaSb} equal to one at the 673 K and 773 K isotherms. This means that the slope of the distribution coefficient versus mole fraction curve is determined primarily by the value of Θ_{GaSb} and thus by the temperature. In addition, this result indicates the liquid phase activity coefficients ($\gamma_{\text{I}}^{\text{L}}$) are nearly cancelled by the solid phase activity coefficients ($\gamma_{\text{I}}^{\text{S}}$). Thus model selection and parameter estimation procedures based on ternary phase diagram determinations alone can be misleading.

The liquidus composition data of Gratton and Woolley (24) were calculated rather than measured, thus the distribution coefficient derived from their data is dependent on the set of parameters used in the calculation. The experimental points for $T = 873$ K shown in Figure 6-13 were calculated using the solidus compositions measured by Gratton and Woolley (24) along with the liquidus compositions calculated using the parameters in Table 6-2. As can be seen, the distribution coefficients calculated with the NRTL equation are in excellent agreement with the experimental values for the 873 K isotherm, while the agreement is good over a large portion of the 773 K isotherm. This is not unexpected as the experimental data of Antypass (251) at low gallium mole fraction along this isotherm (773 K) are not in good agreement with the binary In-Sb liquidus of Liu and Peretti (112). This discrepancy is significant in the distribution coefficient, as the Ga mole fraction appears in the denominator of Equation (6-20).

Figures 6-14 to 6-17 show the Ga-In-Sb liquidus isotherms, solidus isotherms, and distribution coefficients calculated with

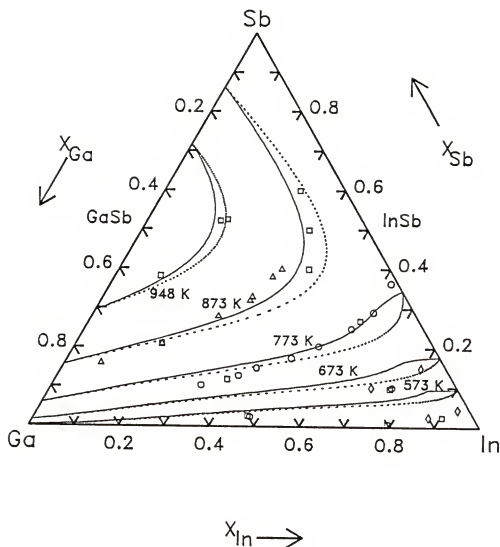


Figure 6-14. The Ga-In-Sb liquidus isotherms predicted with binary parameters determined for the combined activity and enthalpy of mixing fit: —, NRTL (parameter a^1 fixed at T_{IC}) liquid and simple solid solution; ---, NRTL liquid and ideal solid solution; \square , Ref. (25); \diamond , Ref. (26); \circ , Ref. (251); Δ , Ref. (230).

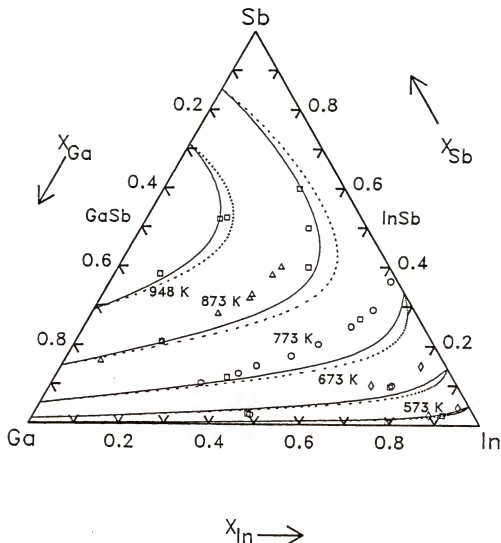


Figure 6-15. The Ga-In-Sb liquidus isotherms predicted with binary parameters (parameter a_1 fixed at T_m^{LC}) determined for the combined activity and enthalpy of mixing fit: —, simple liquid and solid solution; ---, simple liquid and ideal solid solution; □, Ref. (25); ○, Ref. (26); ◇, Ref. (251); Δ, Ref. (230).

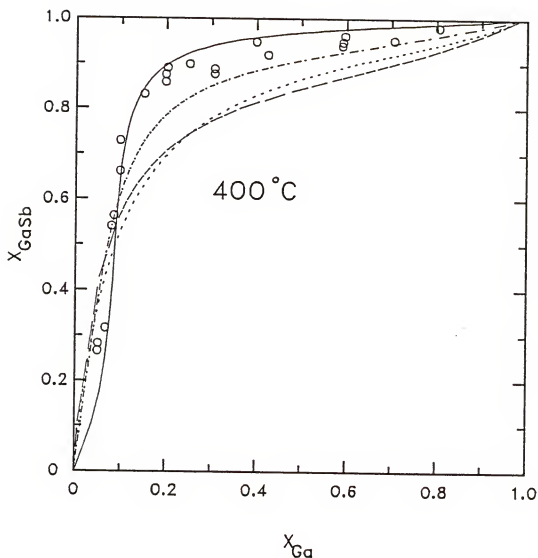


Figure 6-16. The Ga-In-Sb solidus isotherms, (400°C) predicted with binary parameters (parameter a_1 fixed at T_m^{IC}) determined for the combined activity and enthalpy of mixing fit: —, NRTL liquid and simple solid solution; ---, NRTL liquid and ideal solid solution; . . . , simple liquid and solid solution; — — —, simple liquid and ideal solid solution; o, Ref. (252).

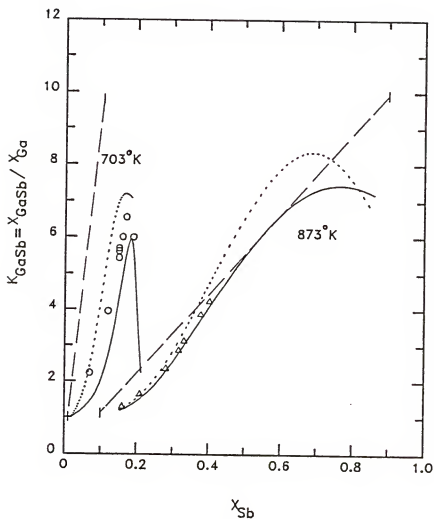


Figure 6-17. Ga distribution coefficient versus antimony mole fraction in the Ga-In-Sb system: —, NRTL (parameter a^1 fixed, activity and enthalpy of mixing data set fit) liquid and simple solid solution; ---, simple (parameter a^1 fixed, same data base) liquid and solid solution; —·—, ideal liquid and solid solution; Ref. (24): o, 703 K; Δ , 873 K.

several solution models, in which the binary solution parameters (the parameter a fixed at T_m^{IC}) were estimated by using a data base consisting of the enthalpy of mixing and group III component activity. As can be seen, the results obtained for this parameter set are similar to those obtained from the combined data set ($T^1, \Delta H_m^1, a_{III}^1$). For the purpose of comparison the phase diagrams in Figures 6-14 and 6-15 were calculated under the various situations. Once again, the NRTL equation gives better results as the Sb content x_{Sb}^1 in the liquid phase is increased. Also, the assumption of ideality for the solid phase is very sensitive to the calculation of the phase diagrams.

As mentioned previously, the lattice matching of the active layer to the substrate is necessary to produce high quality defect-free epitaxial layers. If the Vegard's law is satisfied in the $A_xB_{1-x}C$ system, the lattice constant of the $A_xB_{1-x}C$ with a composition X is expressed in the following equation:

$$a_x(\text{\AA}) = X \cdot a_{AC}(\text{\AA}) + (1 - X) \cdot a_{BC}(\text{\AA}) \quad (6-27)$$

where a_{IC} is the lattice constant of the binary compound IC. Introducing the room-temperature lattice constants $a(\text{AlSb}) = 6.1355 \text{\AA}$, $a(\text{GaSb}) = 6.09593 \text{\AA}$, and $a(\text{InSb}) = 6.47937 \text{\AA}$ given by Panish and Ilegems (16) into Equation (6-27), we obtained the lattice constants for the $\text{Al}_x\text{Ga}_{1-x}\text{Sb}$, $\text{Al}_x\text{In}_{1-x}\text{Sb}$, and $\text{Ga}_x\text{In}_{1-x}\text{Sb}$ systems as follows:

$$a_x(\text{\AA}) = 6.09593 + 0.03967X, \text{ for } \text{Al}_x\text{Ga}_{1-x}\text{Sb} \quad (6-28)$$

$$a_x(\text{\AA}) = 6.47937 - 0.34387X, \text{ for } \text{Al}_x\text{In}_{1-x}\text{Sb} \quad (6-29)$$

and

$$a_x(\text{\AA}) = 6.47937 - 0.38344X, \text{ for } \text{Ga}_x\text{In}_{1-x}\text{Sb} \quad (6-30)$$

It has been shown that the lattice constants of the $\text{Al}_x\text{Ga}_{1-x}\text{Sb}$ (253) and $\text{Ga}_x\text{In}_{1-x}\text{Sb}$ (254) systems are proportional to X , i.e., Vegard's law is satisfied in these two systems. No report is available about the lattice constant for the $\text{Al}_x\text{In}_{1-x}\text{Sb}$ system. The numerical solution of the $\text{A}_x\text{B}_{1-x}\text{C}$ solid compositions lattice-matched to the substrate for a variety of temperatures can be solved by Equations (6-16) to (6-19) with the constraint Equation (6-27).

The results presented in this chapter show that the NRTL model parameters based on the binary combined data set ($T^1, \Delta H_m^1, a_{III}^1$) and simple solution model parameters based on the pseudobinary data set ($T^S, T^1, \Delta H_m^1$) performed the best in the description of the Ga-In-Sb system due to its ability to represent the asymmetric and temperature-dependent thermodynamic properties for the binary limits. The common practice of applying the simple solution model for both phases, however, gives only fair agreement between the calculated and experimental values. The results with the assumption of $w_{\text{AlSb-GaSb}}^S = 0$ for the Al-Ga-Sb system indicate that the use of only the binary phase diagrams in the data base for the simple solution model parameter estimation gives good values for the ternary liquidus and solidus isotherms. While these simple solution model parameters provide a good representation of phase equilibrium for the

Al-Ga-Sb system, it is unable to represent the other thermodynamic properties. As an example, the liquid phase enthalpy of mixing calculated with the parameters listed in Table 6-1 was qualitatively and quantitatively incorrect for the binary group III-V systems. No report is available about the solidus isotherms for the Al-In-Sb system. The AlIn model parameters were very sensitive to the calculation of the Al-In-Sb phase diagram. This may be partly because the solution models studied here are unable to represent this system.

CHAPTER VII THERMODYNAMICS OF THE $\text{Al}_x\text{Ga}_y\text{In}_{1-x-y}\text{Sb}$ SYSTEM

Quaternary III-V alloys have been widely used in various device applications because both the energy gap and the lattice constant can be independently adjusted to values required by devices. Although there is considerable interest in these alloys, only one quaternary, GaInAsP , has been extensively studied. The phase diagram in this system is known in detail, but for most of the other quaternaries there are relatively few experimental results available.

In some of III-V and II-VI systems the presence of a miscibility gap and the volatile and highly reactive nature of the constituents makes crystal growth difficult. For example, it is expected that the growth of Al-containing alloys will encounter serious difficulties resulting from the extremely large segregation coefficient of Al. In addition, Wooley (255) showed that the preparation of single phase alloys containing Sb by simple melt and anneal technique is difficult and requires long equilibrium times. This was confirmed experimentally in the work of (256) when three months of annealing was found to be insufficient time for equilibrium to be established in $\text{Al}_x\text{Ga}_y\text{In}_{1-x-y}\text{Sb}$ alloys. Ingots of these quaternary alloys have been prepared by different bulk crystal growth methods, but strong separation effects and different phases have been observed within ingots (256).

The purpose of this chapter is to present the AlGaInSb phase diagram calculated by using the simple solution model with interaction parameters estimated from a fit of binary and pseudobinary data alone. This quaternary is expected to prove useful for longer wavelength ($\lambda = 1.24 - 2.07 \mu\text{m}$) infrared lasers with lattice matching to AlSb (257). For the $\text{Al}_x\text{Ga}_y\text{In}_{1-x-y}\text{Sb}$ system no previous work has been reported. Because of the lack of experimental data, the accuracy of the calculated quaternary phase diagrams could not be adequately tested. However, the calculation will provide an efficient guide for the future growth in the AlGaInSb system.

7.1 Calculation of the Phase Diagram

The AlGaInSb quaternary system is characterized by one ternary (atoms Al, Ga and In) and one unary (atom Sb) sublattice. Obviously, mixing among atoms involves only the three kinds of atoms occupying one of the sublattices, thus this quaternary solid solution may be imagined as the mixture of three pure binary compounds AD, BD and CD. For simplicity of notation, components Al, Ga, In and Sb in the quaternary $\text{Al}_x\text{Ga}_y\text{In}_{1-x-y}\text{Sb}$ will be denoted 1, 2, 3 and 4 in all equations for the system have been derived in Chapter 2.2 and repeated below

$$x_1^1 = \frac{\frac{1}{x_4} - r_{34}(1 - x_4^1)\exp(-\theta_{34})}{r_{14}\exp(-\theta_{14}) - r_{34}\exp(-\theta_{34})} - x_2^1 \left[\frac{r_{24}\exp(-\theta_{24}) - r_{34}\exp(-\theta_{34})}{r_{14}\exp(-\theta_{14}) - r_{34}\exp(-\theta_{34})} \right]$$

(2-138)

$$x = \frac{x_4^1(1-x_4^1) - \frac{1}{\Gamma_{34}} \exp(\theta_{34})}{\frac{1}{\Gamma_{14}} \exp(\theta_{14}) - \frac{1}{\Gamma_{34}} \exp(\theta_{34})} - x_2^1 x_4^1 \Gamma_{14} \exp(-\theta_{14}) \left[\frac{\Gamma_{24} \exp(-\theta_{24}) - \Gamma_{34} \exp(-\theta_{34})}{\Gamma_{14} \exp(-\theta_{14}) - \Gamma_{34} \exp(-\theta_{34})} \right] \quad (2-139)$$

and

$$y = \Gamma_{24} x_2^1 x_4^1 \exp(-\theta_{24}) \quad (2-140)$$

where θ_{IC} and Γ_{IC} are defined by Equations (2-49) and (2-50) with $m = n = 1$, i.e.,

$$\theta_{IC} \equiv \frac{\mu_{IC}^{0,s} - \mu_I^{0,1} - \mu_C^{0,1}}{RT} \quad ; \quad I = 1, 2 \text{ or } 3; C = 4 \quad (2-49)$$

and

$$\Gamma_{IC} \equiv \frac{\gamma_I \gamma_C}{\gamma_{IC}} \quad ; \quad IC = 14, 24 \text{ or } 34 \quad (2-50)$$

The recommended values of θ_{IC} to be used in this chapter are given in Chapter III. The calculation of the term Γ_{IC} involves the representation of the nonidealities present in each phase, as indicated by the ratio of liquid to solid phase activity coefficients, with a solution model. On the basis of the simple solution approximation, the activity coefficients for the solid can be written from equation (1-6) with $n = 3$ as

$$RT \ln \gamma_{14} = w_{14-24} y_{14-34}^2 + (w_{14-24} + w_{14-34} - w_{24-34}) y(1-x-y) \quad (7-1)$$

$$RT\ln\gamma_{24} = w_{24-34}(1-x-y)^2 + w_{14-24}x^2 + (w_{24-34} + w_{14-24} - w_{14-34})(1-x-y)x \quad (7-2)$$

$$RT\ln\gamma_{34} = w_{14-34}x^2 + w_{24-34}y^2 + (w_{14-34} + w_{24-34} - w_{14-24})xy \quad (7-3)$$

Similarly, we have for the liquid

$$RT\ln\gamma_1 = w_{12}x_2^2 + w_{13}x_3^2 + w_{14}x_4^2 + x_2x_3(w_{12} + w_{13} - w_{23}) + x_2x_4(w_{12} + w_{14} - w_{24}) + x_3x_4(w_{13} + w_{14} - w_{34}), \quad (7-4)$$

$$RT\ln\gamma_2 = w_{12}x_1^2 + w_{23}x_3^2 + w_{24}x_4^2 + x_1x_3(w_{12} + w_{23} - w_{13}) + x_3x_4(w_{23} + w_{24} - w_{34}) + x_1x_4(w_{12} + w_{24} - w_{14}), \quad (7-5)$$

$$RT\ln\gamma_3 = w_{13}x_1^2 + w_{23}x_2^2 + w_{34}x_4^2 + x_1x_2(w_{13} + w_{23} - w_{12}) + x_2x_4(w_{23} + w_{34} - w_{24}) + x_1x_4(w_{13} + w_{34} - w_{14}), \quad (7-6)$$

$$RT\ln\gamma_4 = w_{14}x_1^2 + w_{24}x_2^2 + w_{34}x_3^2 + x_1x_2(w_{14} + w_{24} - w_{12}) + x_1x_3(w_{14} + w_{34} - w_{13}) + x_2x_3(w_{24} + w_{34} - w_{23}), \quad (7-7)$$

There exists six binary interaction parameters in the liquid solution:

$$w_{12}, w_{13}, w_{14}, w_{23}, w_{24} \text{ and } w_{34}$$

The solid solution is described by three quasibinary interaction parameters:

$$w_{14-24}, w_{14-34} \text{ and } w_{24-34}$$

It is obvious that the simple solution treatment of the quaternary solutions includes the assumption that the interaction parameters are independent of composition and thus values of w determined from binary and quasibinary solutions may be used for quaternary solutions. These values taken from Chapters IV and V are listed in Table 7-1. Apparently, these working equations are implicitly complex relations for T , P , x , y , x_1 , x_2 and x_4 . As mentioned previously, the number of degrees of freedom is equal to four for a quaternary system. Thus, if T , P , x_1 and x_2 are specified, then x_4 , x and y can be completely determined by these implicit equations.

7.2 Computer Program

A computer program which calculates the equilibrium liquid and solid composition (x_4 , x and y) with a given T , x_1 and x_2 was written in the Fortran IV language and about one hundred statements in length. The program solves Equations (2-138) to (2-140) and (7-1) to (7-7) simultaneously with the added requirements that in the solid

$$x_{14} + x_{24} + x_{34} = 1 \quad (7-8)$$

and in the liquid

$$x_1 + x_2 + x_3 + x_4 = 1 \quad (7-9)$$

Table 7-1. Values of the simple solution parameters and θ_{IC} .

Component	w(cal/mole); T/K	θ_{IC} (T/K)
Al-Sb	13437.3 - 12.854 T	$-5.48 - 5.13 \times 10^{-4} T - 9176.88/T + 1.52 \ln(T)$
Ga-Sb	3208.9 - 5.886 T	$5.37 - 7950.0/T + 0.10 \ln(T)$
In-Sb	-4500.5 + 0.906 T	$-5.72 - 7.06 \times 10^{-4} T - 5902.12/T + 1.66 \ln(T)$
Al-Ga	589.9 - 0.318 T	--
Al-In	1060*	--
Ga-In	1029.9 + 0.29 T	--
AlSb-GaSb	3858.5 - 3.058 T	--
AlSb-InSb	1575.0 - 1.874 T	--
GaSb-InSb	1884.1 - 0.425 T	--

* Source: Reference (16)

System of working equations (2-138) to (2-140) can be written as:

$$f_1 = x - \Gamma_{14}x_1x_4\exp(-\theta_{14}) = 0 \quad (7-10)$$

$$f_2 = y - \Gamma_{24}x_2x_4\exp(-\theta_{24}) = 0 \quad (7-11)$$

$$f_3 = 1 - x - y - \Gamma_{34}x_3x_4\exp(-\theta_{34}) = 0 \quad (7-12)$$

Equations (7-10) to (7-12) can be obtained from Equations (2-135) to (2-127) with $m = n = 1$.

The corresponding algorithm is

- (1) Reading of the initial guess for $\{x_4, x, y\} \equiv \{U_0\}$ and the specified variables $\{T, x_1, x_2\}$.
- (2) Calculation of the recommended values θ_{IC} and interaction parameters w .
- (3) Calculation of the liquid composition $(x_3)_i$.
- (4) Calculation of the solid and liquid activity coefficients.
- (5) Computation of residual $\{f_1, f_2, f_3\} \equiv \{f_i\}$.
- (6) Calculation of the variation of solution $\{\Delta x_4, \Delta x, \Delta y\} \equiv \{\Delta U_i\}$.
- (7) Correction of solution: $\{U_i\} = \{U_{i-1}\} + \{\Delta U_i\}$.
- (8) Execute convergence test with $\|\Delta U_i\|$ or $\|f_i\|$. If the solution is not convergent, then iteration goes to step (3).
- (9) Printout of results.

Since the implicit working equations cannot be solved analytically for $\{x_4, x, y\}$, these are obtained by an iterative solution using the Newton-Raphson method. Proper choice of initial values and specified variables for the iterative calculation was

found to be important in order to avoid divergence and excessively long calculation times, so the following procedure was used: The specified variables $\{T, x_1, x_2\}$ start from the ternary, AlInSb, in the Al-rich and In-rich region, i.e., $\{T, x_1, x_2=0\}$, and then the Ga content, x_2 , is gradually increased, i.e., $\{T, x_1, x_2+\Delta x_2\}$, in the liquid to the ternary, AlGaSb, in the Al-rich and Ga-rich region. The best initial guess $\{x_4, x, y\}$ for each iteration is the ternary limit. In this way, the program converges very rapidly with only three or four iterative steps for a given initial variable set. A sample program for the calculation of the quaternary AlGaInSb system is listed in Appendix.

7.3 Results and Discussion

The AlGaInSb phase diagram was calculated by treating the quaternary liquid and solid as a simple solution in which the interaction parameters are approximated by a linear temperature dependent function. The basic equations expressing chemical equilibrium between the pseudoternary solid of the type $A_xB_yC_{1-x-y}D$ and the quaternary liquid were derived in Chapter II. These equations are simple and useful for the calculation of the phase diagram because the problem is now reduced to the calculation of two kinds of parameters θ_{IC} and Γ_{IC} . These quantities can be calculated from well characterized thermodynamic data.

The parameters used in this calculation deserve some comment because some of them were obtained by fitting different experimental data sets. In Chapter VI, it was claimed that the values of three

interaction parameters, w_{14} , w_{24} and w_{34} , which are obtained by fitting the phase diagrams only, had to be adopted to obtain the reasonable calculated phase diagram. Also, the AlSb interaction parameter w_{14} used here is only good for Al-rich side ($x_{Sb} < 0.5$) because the simple solution model cannot be used to describe the whole asymmetric system. The obvious fact of the use of the combined data set interaction parameters is the discrepancy between the calculated and experimental results at binary or ternary limits. Thus, the calculated curves can be systematically lower or higher than the experimental data. The other parameters w_{12} , w_{23} , w_{14-24} , w_{14-34} and w_{24-34} used in the calculations were obtained by fitting the combined data set because the simple solution model can represent the thermodynamic properties as well as the phase diagrams for these systems.

Information on the thermodynamic properties of the Al-In system is less reliable. The parameter w_{13} , assumed to be independent of temperature, was taken from value reported by Panish and Ilegems (16). However, this simplified representation, i.e., the regular approximation of the simple solution theory, is not fully satisfactory in the phase equilibria analysis over a wide temperature range. It is believed that this is the cause of the disagreement between the calculated results and the experimental data in AlIn-containing systems. All these values, except w_{13} , are different from those reported by previous investigators. However, it is not clear whether these parameters are useful for the present calculation of

the phase diagram or not because no experimental data are available for comparison.

Figures 7-1 and 7-2 show the calculated liquid isotherms as a function of x_{Al}^l at 600°C and 700°C, respectively. These figures indicate that the main feature of the addition of Al to the melt is to appreciably decrease the solubility of Sb in the liquid. In addition, the solubility of Sb at lower Al content decreases with increasing Ga in the liquid, while the presence of Ga has a less pronounced effect in the higher Al content region. These isotherms also indicate that the aluminum mole fraction in the liquid increases with increasing temperature. The Al compositions shown in Figures 7-1 and 7-2 may be selected to permit the growth of $Al_xGa_yIn_{1-x-y}Sb$ epitaxial layers on AlSb substrate within a reasonable temperature range. Figures 7-3 and 7-4 show calculated $Al_xGa_yIn_{1-x-y}Sb$ solid compositions in equilibrium with the quaternary liquids as a function of x_{Al}^l at 600°C and 700°C, respectively. The calculation has the trends: x increases as y decreases for a given temperature and y increases with decreasing temperature.

For those solid compositions that are lattice matched to AlSb, Vegard's law has been used to find that x and y are related by

$$x = 1 - 1.115 y, \quad 0 \leq y \leq 0.897 \quad (7-13)$$

To derive this relationship, we have used the room temperature (300°K) lattice constants (16): $a(AlSb) = 6.1355 \text{ \AA}$, $a(GaSb) = 6.0959 \text{ \AA}$, and $a(InSb) = 6.4794 \text{ \AA}$. Equation (7-13) is plotted in Figures 7-3 and 7-4 as the dashed line. We note that the lattice matching

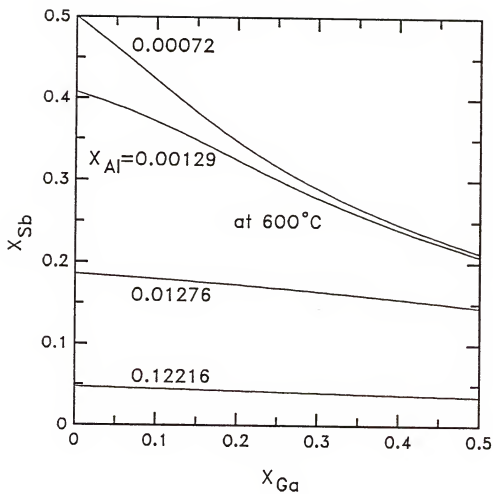


Figure 7-1. Calculated liquidus isotherms at 600°C in the AlGaInSb system as a function of x_{Al}^l .

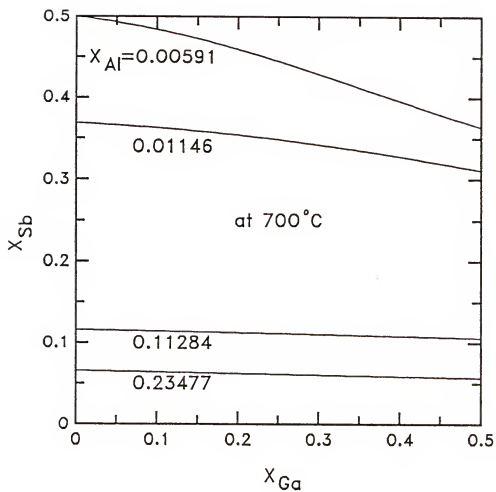


Figure 7-2. Calculated liquidus isotherms at 700°C in the AlGaInSb system as a function of x_{Al}^1 .

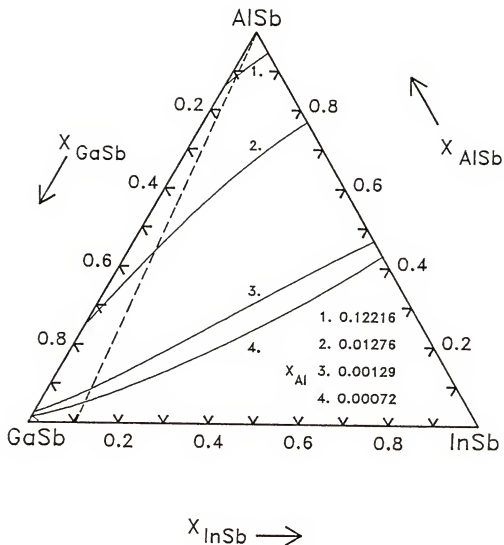


Figure 7-3. —: Calculated $Al_xGa_yIn_{1-x-y}Sb$ solid compositions in equilibrium with the quaternary liquids as a function of x_{Al} at 600°C. ---: represent compositions of the quaternary solids lattice-matched to AISb.

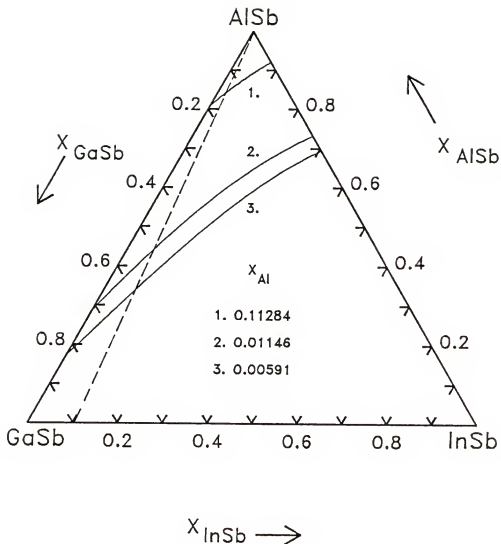


Figure 7-4. —: Calculated $\text{Al}_x\text{Ga}_y\text{In}_{1-x-y}\text{Sb}$ solid compositions in equilibrium with the quaternary liquids as a function of x_{Al} at 700°C. ---: represent compositions of the quaternary solids lattice-matched to AlSb.

conditions may differ greatly from Equation (7-13) because of the difference in the thermal expansion coefficients between the layer and the substrate. The lattice parameter values for the complete $\text{Al}_x\text{Ga}_y\text{In}_{1-x-y}\text{Sb}$ alloy system have been determined experimentally by Zbitnew and Wooley (256) and given by

$$a(x,y) = 6.4789 - 0.3433x - 0.3834y - xy(1-x-y)(4 - 3.25x - 3.25y) \text{ \AA} \quad (7-14)$$

Note that the last term in the above equation is the deviation from the result calculated by Vegard's law. Equation (7-14) serves as the lattice matching condition that must be satisfied for the quaternary solids lattice matched to the substrate with the lattice parameter $a(x,y)$. For example, the quaternary solid compositions lattice-matched to AlSb are obtained by setting $a(x,y) = a(\text{AlSb})$ in Equation (7-14)

$$x = 1 - 1.117y - xy(1-x-y)(10.195 - 9.467x - 9.467y) \quad (7-15)$$

The numerical solution of the $\text{Al}_x\text{Ga}_y\text{In}_{1-x-y}\text{Sb}$ solid compositions lattice-matched to AlSb for a variety of temperatures can be solved by Equations (7-1) to (7-12) with the constraint Equation (7-15).

Note that the solid of the type $\text{A}_x\text{B}_y\text{C}_{1-x-y}\text{D}$ is completely analogous to the pseudobinary solid. Therefore, as discussed previously, the most convenient way to compare the ideal and real solutions can be made by the use of the distribution coefficient of component I as follows:

$$K_{ID} \equiv \frac{x_{ID}^S}{x_I^L}, \quad ID = 14, 24 \text{ and } 34 \quad (7-16)$$

The distribution coefficient of component I may be calculated by the equation

$$K_{ID} = \Gamma_{ID} x_I^L \exp(-\theta_{ID}) \quad (2-132)$$

It is obvious that the term Γ_{ID} defined by the above equation is responsible for deviations from the ideal solution behavior. In the ideal case Γ_{ID} is unity and a plot of K_{ID} versus x_I^L at constant temperature should yield a straight line having a slope of $\exp(-\theta_{ID})$.

Shown in Figures 7-5 and 7-6 are the calculated distribution coefficients versus x_{Sb}^L as a function of x_{Al}^L along the 600°C and 700°C, respectively. These figures indicate that the distribution coefficients are complex functions of temperature and composition x_{Al}^L . It is clear that the assumption of a value of unity for Γ_{ID} is incorrect. The distribution coefficient becomes large with decreasing both temperature and x_{Al}^L . This result predicts the liquid solution will readily become depleted in Al at an early stage of the cooling process in LPE growth, where the solid and the liquid may be in equilibrium because of sufficiently slow cooling rate as compared with aluminum diffusion in the liquid.

As mentioned above, quaternary III-V solid solutions are important materials for the fabrication of closely lattice-matched heterojunction optoelectronic devices. In the growth of the solid

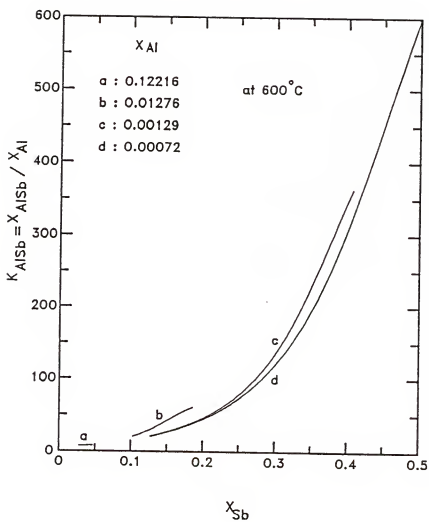


Figure 7-5. Al distribution coefficient versus antimony mole fraction as a function of x_{Al}^1 at $600^{\circ}C$.

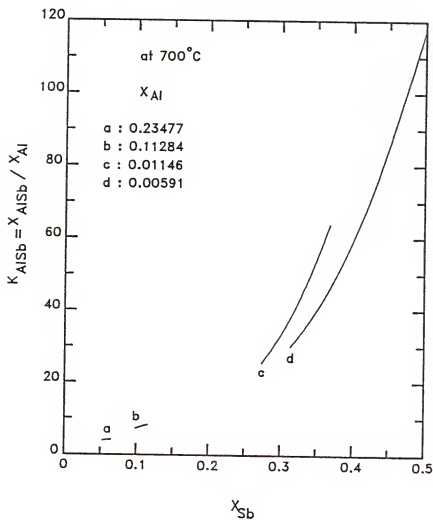


Figure 7-6. Al distribution coefficient versus antimony mole fraction as a function of x_{Al}^1 at 700°C.

solutions, however, the existence of a miscibility gap seriously limits the feasibility of obtaining uniform single-crystal epitaxial layers at a certain temperature. Onabe (87) calculated the unstable regions in type $A_xB_yC_{1-x-y}D$ III-V quaternary solid solutions with strictly regular solution approximation. The calculated spinodal isotherms for various temperatures show that the existence of miscibility gaps found on the ternary side is a common feature of these quaternaries. The unstable region of the $Al_xGa_yIn_{1-x-y}Sb$ system appears at as low as $T = 155^\circ C$ at $Ga_{0.5}In_{0.5}Sb$ for the present calculation. The experimental results (256) indicate that single phase solid solution occurs at all compositions in the quaternary system $Al_xGa_yIn_{1-x-y}Sb$; no miscibility gaps have been observed.

CHAPTER VIII
SOLID-STATE ELECTROCHEMICAL STUDY OF THE
STANDARD GIBBS ENERGY OF FORMATION OF ALUMINUM
OXIDE USING A CALCIUM FLUORIDE SOLID ELECTROLYTE

8.1 Introduction

Galvanic cells with CaF_2 as the solid electrolyte have been extensively used in measuring high temperature Gibbs energies of formation of fluorides (258), borides (259), carbides (260), phosphides (261), silicates (262), sulfides (263) and metal alloys (264). In each case, the electrode material included fluorine-containing substances. Calcium fluoride exhibits anti-Frenkel defects and conducts fluorine ions exclusively over a large range of the electrolytic domain (265,266). Some good reviews of its use and the necessary precautions required are available (106,267-269). Recently, titration experiments, d-c polarization, a-c admittance and open circuit e.m.f. measurements (270,271) have shown that CaF_2 will conduct oxygen ions at elevated temperature and thus might be suitable for aluminum-containing electrodes. While still retaining a unity transference number under the reducing conditions. As a result of the inaccessibility of Al with the use of a solid oxide electrolyte, the solid electrolyte CaF_2 was investigated here.

From a technological point of view, the use of a solid electrolyte has many clear advantages. An all solid state device does not have the contaminative problems typical of liquid solution

devices. An all solid state device is also less prone to electrochemical side reactions, e.g., hydrolytic effect, and hydration effects of aqueous systems. Furthermore, manufacturing can be simple and inexpensive since most production steps can be borrowed from the highly developed thin film and semiconductor technologies. In battery (272,273) application, solid electrolytes avoid corrosion, fabrication, and miniaturization problems encountered with many aqueous and fused-salt electrolytes. Their main drawback thus far has been a high internal resistance associated with the low specific conductivity of these materials under many conditions of interest. Other problems have been electrode polarization and trace electronic conduction.

A solid-state electrochemical technique was used to measure the standard Gibbs energy of the formation of Al_2O_3 in the temperature range from 802 to 921 K. A solid-state galvanic cell was employed, utilizing calcium fluoride (CaF_2) as the solid electrolyte, with a (Ni + NiO) mixture as the reference electrode. A linear least-square analysis of the results showed that the standard Gibbs energy of formation can be represented by

$$\Delta G_f^\circ (\text{Al}_2\text{O}_3, \text{S}, T) = -399.32 + 0.07480 T/K \pm 0.61 \text{ Kcal mol}^{-1}$$

A third-law analysis of the results showed that the standard enthalpy of formation is given by

$$\Delta H_f^\circ (\text{Al}_2\text{O}_3, \text{S}, 298 \text{ K}) = -399.47 \pm 0.71 \text{ Kcal mol}^{-1}$$

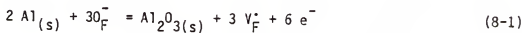
which is about 0.25% more positive than the generally accepted thermochemical value of -400.4 Kcal/mol. Comparisons with results of other studies are presented.

8.2 Theory

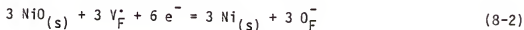
The solid-electrolyte galvanic cell employed in measuring the standard Gibbs energy of formation of $\text{Al}_2\text{O}_3(\text{s})$ can be schematically represented as



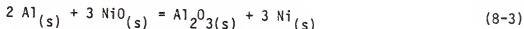
The half-cell reactions are at the anode



at the cathode



where V_{F}^+ and O_{F}^- are an anion vacancy and an oxygen ion substituted on a fluorine lattice site, respectively. The overall reaction for the cell is



At equilibrium, the Gibbs energy change for the cell reaction and the cell e.m.f. are then given by the relationship

$$\Delta G_f^\circ (\text{cell}) = \Delta G_f^\circ (\text{Al}_2\text{O}_3(\text{s})) - 3 \Delta G_f^\circ (\text{NiO}(\text{s})) \quad (8-4)$$

and

$$\Delta G_f^\circ (\text{cell}) = -6 F E \quad (8-5)$$

respectively.

Equations (8-4) and (8-5) allow one to calculate $\Delta G_f^\circ(\text{Al}_2\text{O}_3, \text{S}, \text{T})$ from the measured experimental e.m.f. and temperature and the known standard Gibbs energy of formation of nickel oxide:

$$\Delta G_f^\circ (\text{Al}_2\text{O}_3(\text{s})) = 3 \Delta G_f^\circ (\text{NiO}(\text{s})) - 6 F E \quad (8-6)$$

where F is the Faraday constant and E is the open circuit voltage measured at temperature T . $\Delta G_f^\circ(\text{NiO}(\text{s})) = -56010 + 20.37 T (\pm 0.2 \text{ Kcal})$, was taken from Richardson and Jeffes (274).

8.3 Experiment

The galvanic cell design is depicted in Figure 8-1. The graphite crucible consisted of two co-centered wells with different ID and depth. The Ni + NiO reference electrode was contained within the inner well of 1.9 cm diameter x 0.19 cm depth. The electrolyte was placed in the outer well of 2.6 cm diameter x 0.1 cm depth. The working electrode Al + Al₂O₃ was put between the electrolyte and the graphite disk. Electrical contacts were made to the graphite with 0.51 mm platinum wire. The temperature was measured with a type K (Chromel-Alumel) thermocouple.

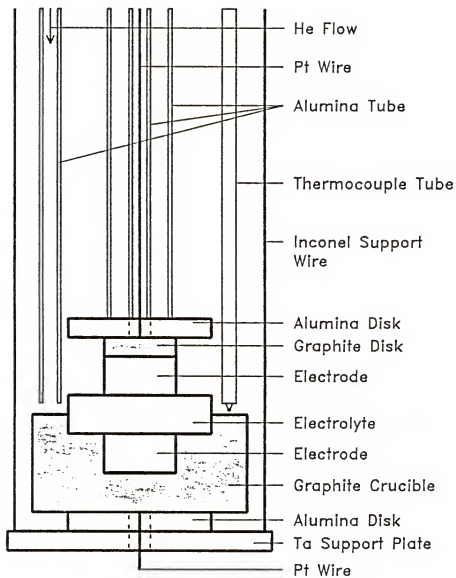


Figure 8-1. Experimental apparatus.

The cell was assembled in a 5.08 cm ID closed-end alumina tube 30.48 cm in length secured by a Viton O-ring to a water-cooled brass cell-head. The cell was suspended from this brass head with spring-loaded inconel support wires, which forced the cell against an alumina disk and tightly held an alumina push rod. In this manner, the cell components could be held in intimate contact and the electrode isolation could be achieved.

The cell was heated with a Marshall resistance-heated furnace 51 cm in length with a 6 cm bore. The temperature profile was adjusted with external shunt resistors such that a relatively constant zone ($\Delta T \leq 1.5^\circ\text{C}$) 9 cm in length existed throughout the temperature range investigated. The furnace temperature was controlled using a Lindberg digital temperature controller. The temperature of the cell was measured using a Leeds and Northrup K-5 potentiometer in conjunction with an Omega Model TRC III ice point cell. The cell e.m.f. was measured using a Cary Model 401 vibrating reed electrometer and a EG&G Model 173 potentiostat/galvanostat.

8.4 Materials

Single crystal CaF_2 disks of 2.54 cm diameter and 0.71 cm thickness were purchased from the Harshaw chemical company. The disk faces were finely ground and polished with $0.05\ \mu\text{m}$ alumina paste obtained from Union Carbide products. Before their use, the electrolyte disks were sintered overnight at 800°C under a purified helium.

Nickel and nickel oxide powders used in this study were obtained from the Atomergic Chemical Co. and had a purity of 99.99 moles percent. Aluminum powder, 99.999 moles percent pure and -325 mesh, was obtained from Orion Chemical Co. Aluminum oxide was obtained from Research Organic/Inorganic Chemical Corp. and analyzed 99.995% purity. Before assembling cell (A), the Ni and NiO were mixed in roughly equal amounts by volume and pressed in a 1.27 ID die at 12-15 tons/in² into electrode pellets of 1.27 cm diameter x 0.19 cm thickness. Similarly, Al and Al₂O₃ were mixed and pressed in a 2.54 cm ID stainless die into electrode pellets of 2.54 cm diameter x 0.22 cm thickness. The pressed Ni-NiO pellets were sintered overnight under purified helium at 800°C. The Al-Al₂O₃ pellets were sintered at 620°C overnight. As shown in Figure 8-2, pure helium for use in purging the experimental cell was prepared by passing high-purity helium through a series of molecular sieves, a furnace containing a copper-copper oxide mixture at 450°C, and finally through a furnace containing Ti sponge at 750°C. This gas was used as an inert purge around the cell during an experiment, with the purge flow rate adjusted to 20 cm³ min⁻¹.

The aluminum tubes and disks used in this study were purchased from the Coors Porcelain Co. Graphite crucibles and disks of purity greater than 99.9995% were obtained from the Ultra Carbon Corporation.

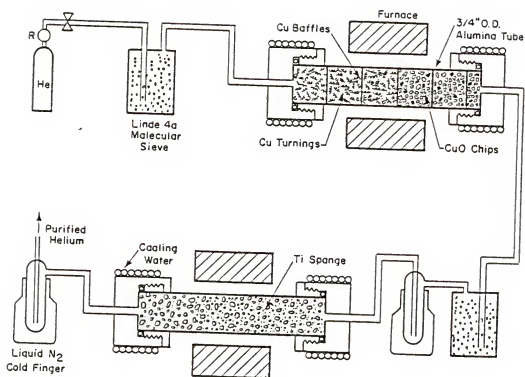


Figure 8-2. Helium purification system.

8.5 Procedure

In each of the experiments the cell was leak-checked using a vacuum system, then purged with high-purity helium. To avoid thermal shock to the electrode and electrolyte, the cell temperature was programmed to rise at 100°C/hr to the lowest measurement temperature. The cell was held at this temperature for 2 days. The approach to equilibrium was quite sluggish. The cell e.m.f. was obtained by imposing a greater e.m.f. than the equilibrium value and discharging it momentarily through an external circuit. Reversible plateau e.m.f.'s for 45-60 min duration were typically obtained. The cell temperature was then sequentially incremented and decremented throughout the experimental range, with the cell e.m.f. measured and recorded at each temperature until the complete cycle of heating and cooling had been done, at which time the cell was cooled at 100°C/hr to room temperature and disassembled.

8.6 Results

Table 8-1 shows the experimental results for the cell (A). The experimental temperature, observed open circuit e.m.f., and the Gibbs energy of formation of aluminum oxide calculated by Equation (8-6) are listed. A linear least-squares analysis of the data resulted in the following expression:

$$\Delta G_f^\circ(\text{Al}_2\text{O}_3, \text{S}, \text{T}) = -399.32 + 0.0748 \text{ T/K} \pm 0.71 \text{ Kcal mol}^{-1} \quad (8-7)$$

Table 8-1. Summary of experimental and derived results.

T/K	E/V	$-\Delta G_f^\circ (\text{Al}_2\text{O}_3)$ (Kcal/mol)
<u>Heating</u>		
802.0	1.5916	339.329
833.7	1.5886	336.976
863.9	1.5855	334.695
879.5	1.5839	333.490
889.5	1.5829	332.777
900.2	1.5819	331.985
921.3	1.5798	330.405
<u>Cooling</u>		
920.8	1.5799	330.449
895.0	1.5823	332.358
883.5	1.5838	333.269
879.5	1.5840	333.510
864.8	1.5854	334.633
835.0	1.5883	336.855
824.7	1.5893	337.623

The uncertainties given in this expression are those computed from the standard errors of the Gibbs energy of formation of NiO and cell (A). The constant term appearing in Equation (8-7) corresponds to the standard enthalpy change while the temperature coefficient represents the standard entropy change.

Shown in Figure 8-3 is the e.m.f. values of cell (A) measured in the temperature range 802-921 K. A least squares analysis of the experimental data points leads to the following expression:

$$E(V) = 1.6708415 - 0.0000988 \text{ T/K} \quad (8-8)$$

The calculated e.m.f. expression from the known values for the free energies of formation of Al_2O_3 (99) and NiO (274) is

$$E(V) = 1.67106 - 0.0000949 \text{ T/K} \quad (8-9)$$

8.7 Discussion

The first attempt to study thermodynamic properties of aluminum oxide with CaF_2 solid electrolyte was made by the following cell:



Cell (B) was heated up to 900°K for a few days. The observed e.m.f. of the cell was increasing very slowly with time and lower than the expected value. It was noted that the addition of CaF_2 about 5% by volume to the electrode can avoid this sluggish process. The reason for this is probably due to the fact that the CaF_2 directly provides more fluorine vacancies and hence changes the electronic and ionic

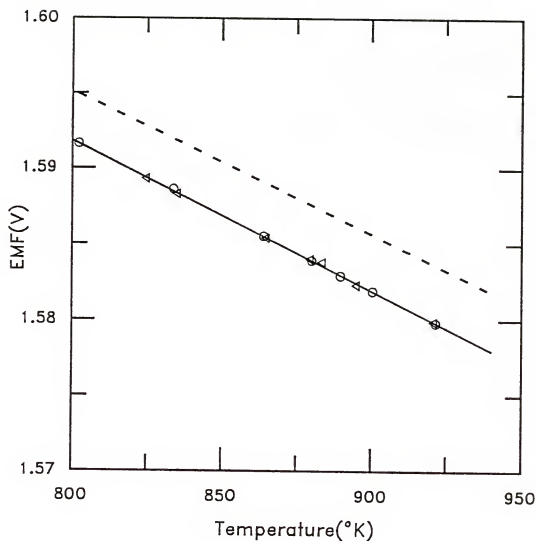
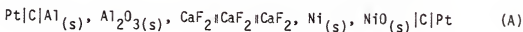


Figure 8-3. Experiment E.M.F. versus T. o: heating results; Δ: cooling results; —: calculated from Eq. (8-8); ---: calculated from Eq. (8-9).

conductivities of the electrodes. The run cell schematic is as follows:



As shown in Figure 8-1, this cell design provides three advantages: First of all, the cell helps to reduce evaporation of the volatile component during the experiment. Secondly, the cell isolates the electrode and diminishes the measured e.m.f. from the influence of the gaseous atmosphere. Finally, the cell prevents the Al electrode from reacting with Pt electrode as temperature raised higher than Al melting point to form Pt-Al alloy. The equilibrium process for the cell (A) is faster than the cell (B). The observed e.m.f. has been systematically measured over 36 or even 48 hrs at every experimental temperature by repeatedly imposing an external voltage on the cell and discharging it momentarily through an external circuit. In this way, the cell can be forced to approach equilibrium quickly, exclude non-equilibrium effects and check its reversibility. Reversible plateau e.m.f.'s curve typically obtained for 45-60 min duration.

The e.m.f. results from cell (A) are shown in Figure 8-3. Plotted in this figure as the solid line and the dash line are the results calculated from Equations (8-8) and (8-9), respectively. It can be seen that the results in this study are less than that calculated from Equation (8-9) by about 3.7 mV. A comparison of the calculated results of the Gibbs energy formation of Al_2O_3 in this study with data reported in previous studies is shown in Figure 8-4. This figure shows the experimental values of

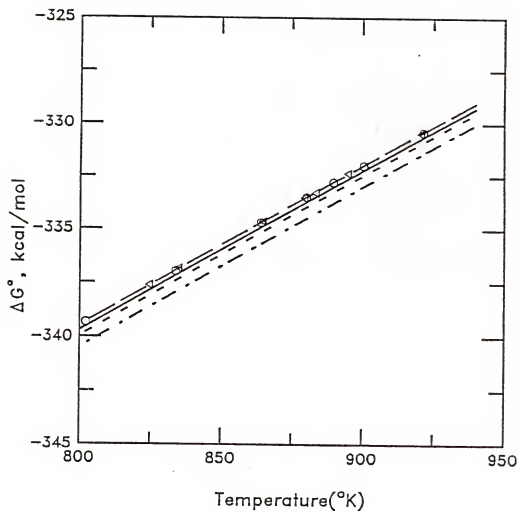


Figure 8-4. Comparison of various results for $\Delta G^\circ_f(\text{Al}_2\text{O}_3)$ as a function of temperature. o (heating), Δ (cooling), ____ (long dash), this study; —, Ref. (275); --- (short dash), Ref. (99); , Ref. (276).

$\Delta G_f^\circ(\text{Al}_2\text{O}_3, S, T)$ plotted against temperature, with the least squares straight line drawn through the points for each study. Also shown are the estimated standard Gibbs energies of formation against temperature of Coughlin (275), Kubaschewski and Alcock (99) and Pankratz and Kelley (276). In comparison with the results of other studies, the magnitude of $\Delta G_f^\circ(\text{Al}_2\text{O}_3, S, T)$ found in this study was more positive. The reasons are possible due to the sluggish equilibrium process and the alumina power which is not confirmed to be $\alpha\text{-Al}_2\text{O}_3$ employed in this study. As shown in Table 8-2, crystalline alumina (Al_2O_3) can occur in a series of different structural modifications. Among these only the α -modification is thermodynamically stable. The various metastable forms are denoted γ , δ , and κ . The conditions under which they form are not well understood. Yokokawa and Kleppa (277) indicate that all the various metastable modifications can be converted to the stable form ($\alpha\text{-Al}_2\text{O}_3$) by ignition at sufficiently high temperatures. However, the conversion process is quite sluggish.

To evaluate the internal consistency of the experimental results, and to facilitate comparison with calorimetric data, a third-law analysis was performed. The values of the standard enthalpy of formation of Al_2O_3 , $\Delta H_f^\circ(\text{Al}_2\text{O}_3, S, 298.15 \text{ K})$, were calculated from the equation:

$$\begin{aligned} \Delta H_f^\circ(\text{Al}_2\text{O}_3, S, 298.15 \text{ K}) = & \Delta G_f^\circ(\text{Al}_2\text{O}_3, S, T) - \Delta_f \{ H_f^\circ(T) - H^\circ(298.15 \text{ K}) \} \\ & + T \Delta S_f^\circ(\text{Al}_2\text{O}_3, S, 298.15 \text{ K}) + T \Delta_f \{ S^\circ(T) - S^\circ(298.15 \text{ K}) \} \end{aligned}$$

Table 8-2. The standard heat of formation, ΔH_f° 298, of various aluminum oxide.

Species	$-\Delta H_f^\circ$ 298 (Kcal mol ⁻¹)	Ref
Alpha (α)-Al ₂ O ₃	400.4 \pm 0.3	(278,279)
Kappa (κ)-Al ₂ O ₃	397.3 \pm 1.0	(280)
Delta (δ)-Al ₂ O ₃	378.3 \pm 0.6	(281)
Gamma (γ)-Al ₂ O ₃	396.0 \pm 1.5	(280)

The values of $\Delta S_f^\circ(\text{Al}_2\text{O}_3, \text{S}, 298.15 \text{ K})$, $\Delta_f[\text{H}^\circ(\text{T}) - \text{H}^\circ(298.15 \text{ K})]$ and $\Delta_f[\text{S}^\circ(\text{T}) - \text{S}^\circ(298.15 \text{ K})]$ for $\text{O}_2(\text{g})$, $\text{Al}(\text{s})$ and $\text{Al}_2\text{O}_3(\text{s})$ were taken from Stull and Prophet (280). The results of the third-law analysis are presented in Table 8-3. The overall mean value of $\Delta H_f^\circ(\text{Al}_2\text{O}_3, \text{S}, 298.15 \text{ K})$ and standard deviation from the mean were found to be -399.471 and $0.01 \text{ Kcal mol}^{-1}$, respectively. The values of $\Delta H_f^\circ(\text{Al}_2\text{O}_3, \text{S}, 298.15 \text{ K})$ calculated from the third-law analysis are compared in Figure 8-5 with the data determined by direct combustion calorimetry and to value calculated from electrochemical cells. The value derived from the present study differs by about 0.1% from the value of $-399.04 \pm 0.24 \text{ Kcal mol}^{-1}$ obtained by Snyder and Selta (282) and by 0.25% from the value of $-400.48 \pm 0.25 \text{ Kcal mol}^{-1}$ obtained by Mah (279). The calculated values of $\Delta H_f^\circ(\text{Al}_2\text{O}_3, \text{S}, 298.15 \text{ K})$ showed a temperature independence as shown in Figure 8-5. It is obvious that the standard errors involved in calculating the value of $\Delta H_f^\circ(\text{Al}_2\text{O}_3, \text{S}, 298.15 \text{ K})$ from Equation (8-10) come from the measured uncertainties of $\Delta G_f^\circ(\text{Al}_2\text{O}_3, \text{S}, \text{T})$, $\Delta S_f^\circ(\text{Al}_2\text{O}_3, \text{S}, 298.15 \text{ K})$, $\Delta_f[\text{H}^\circ(\text{T}) - \text{H}^\circ(298.15 \text{ K})]$ and $\Delta_f[\text{S}^\circ(\text{T}) - \text{S}^\circ(298.15 \text{ K})]$.

A comparison of the standard enthalpy of formation of Al_2O_3 as derived from different sources is summarized in Table 8-4. It is interesting to note that the standard enthalpy of formation is neither a monotonic function of the year of determination nor of the purity of the aluminum. Clearly, some errors, if that is the correct value, are involved. As mentioned above, there is, in fact, a number of morphological forms of aluminum oxide and hydrates thereof,

Table 8-3. Third-law analysis of the experimental results.

T/K	$-\Delta H_f^\circ(\text{Al}_2\text{O}_3, \text{S}, 298.15 \text{ K})$ (Kcal mol ⁻¹)	Deviation from mean (Kcal mol ⁻¹)
<u>Heating</u>		
802.0	399.482 (± 0.7)	-0.010
833.7	399.495	-0.024
863.9	399.469	0.003
879.5	399.449	0.013
889.5	399.462	0.009
900.2	399.469	0.002
921.3	399.465	0.006
<u>Cooling</u>		
920.8	399.472	-0.001
895.0	399.454	0.017
883.5	399.506	-0.035
879.5	399.485	0.023
864.8	399.474	-0.003
835.0	399.471	0.000
824.7	399.470	0.001

Mean = $-399.471 \pm 0.71 \text{ Kcal mol}^{-1}$

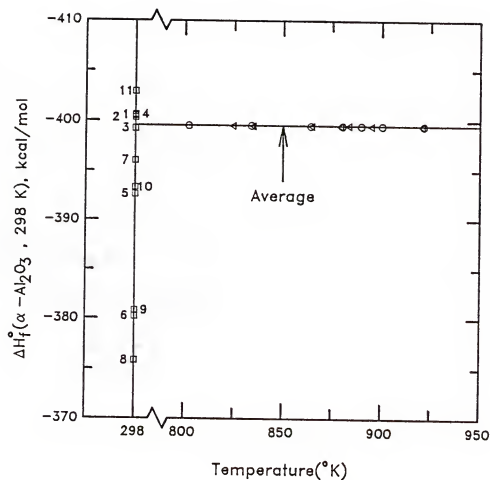


Figure 8-5. Results of the third law calculation of ΔH_{298}° versus measurement temperature. o (heating) and Δ (cooling), this study: 1: Ref. (279); 2: Ref. (278); 3: Ref. (282); 4: Ref. (283); 5: Ref. (284); 6: Ref. (285); 7: Ref. (286); 8: Ref. (287); 9: Ref. (288); 10: Ref. (289); 11: Ref. (290).

Table 8-4. Comparison of the standard enthalpy of formation of Al_2O_3 from different sources.

Method	Year	Aluminum Purity (%)	$-\Delta H_{298}^\circ$ (Kcal mol ⁻¹ Al_2O_3)	Reference
Combustion calorimetry	1901	99.6	380.2	(285)
	1919	95.0	396.0 ± 0.4	(286)
	1924	98.37	375.8 ± 0.2	(287)
	1929	99.83	380.8 ± 0.4	(288)
	1934	99.83	393.3 ± 0.4	(289)
	1940	99.83	402.9 ± 0.3	(290)
	1945	99.98	390.0 ± 0.24	(282)
	1951	99.997	400.29 ± 0.3	(278)
	1953		400.9 ± 1.5	(291)
	1954	99.99 ⁺	400.3 ± 1.4	(283)
	1957	99.998	400.48 ± 0.25	(279)
	1958		-400.0	(292)
Electrochemical cells	1977		-392.6	(284)
	1984	99.995	-399.47 ± 0.71	this study

leading to the thought that a number of these determinations may pertain to something other than pure $\alpha\text{-Al}_2\text{O}_3$.

Finally, it is mentioned that the aluminum is very sticky to the die. To obtain a good $(\text{Al} + \text{Al}_2\text{O}_3)$ electrode pellets, it would be better to use the stainless die. In addition, there were two situations which lead to unsteady e.m.f.'s in this study. One was the loose Pt lead-electrode and electrode-electrolyte interfacial contacts being poor. The other condition was a result of induction from the furnace windings. Improved interfacial contacts can be established by using pellets with prepolished smooth surfaces and by using springs to obtain intimate contacts. Possible induced electrical potential was eliminated with the use of a grounded silver sheet surrounded between the furnace bore and the outer alumina tube.

CHAPTER IX CONCLUSIONS AND RECOMMENDATIONS

9.1 Conclusions

As demands for ultra high speed, high frequency, high quantum efficiency devices and many other novel applications are placed on the semiconductor industry, the use of new device semiconductor materials other than silicon becomes necessary. The semiconducting materials formed by compounds of Groups III A and V A and Groups II B and VI A elements often have inherently improved electrical properties and there also exist degrees of freedom in the physical properties that make these materials attractive for use in new high-performance semiconductor devices when compared with the commonly used elemental Si. Many of the processing steps in the fabrication of devices with Groups III-V and II-VI materials involve the interfacial contact of a liquid phase with a solid phase, a vapor phase with a solid phase or a vapor phase with a liquid phase. The initial estimate of these processes and the effective analysis of the problems often require knowledge of the equilibrium boundary conditions at such interfaces and the phase chemistry for these semiconductor materials. For this reason, the phase diagram and thermochemical properties of these materials are presently receiving considerable investigation.

The general, rigorous and consistent thermodynamic relations that could describe phase equilibrium in quaternary systems of the types $A_xB_yC_{1-x-y}D_n$ and $(A_xB_{1-x})_m(C_yD_{1-y})_n$ were developed in this work. This formulation was applied to several Group III-V binary and ternary systems by assigning the value of m , n , x or y to one or zero. The problem of quantitatively describing the Group III-V (or II-VI) phase diagram is reduced to the simpler problems of selecting the standard states, calculating the temperature and pressure (negligible) dependence of θ_{IC} and determining the temperature, pressure (negligible) and composition dependence of Γ_{IC} , which represents the ratio of the nonidealities in the liquid phase to those in the solid phase. The liquid solution behavior can be obtained by extending the binary liquid solution models to describe the liquid mixture without additional adjustable parameters. In a similar manner, the solid solution behavior is obtained by extending the pseudobinary solid solution models without additional adjustable parameters. The existence of a solid phase immiscibility gap in ternary and quaternary systems was examined by means of the solution models investigated. The lattice constant of the ternary and quaternary systems studied here was calculated by the Vegard's law and expressed in terms of the solid compositions. The lattice matching of the active layer to the substrate is important to produce high quality defect-free epitaxial layers.

Four different methods that are solution model independent were presented to determine the reduced standard state chemical potential change and applied to the Group III antimonides and also HgTe and

CdTe systems. Each of the above four methods employs a different data base. The principal result is a suggested value for θ_{IC} with the first method most reliable at or near the melting temperature, the second method was utilized in the intermediate temperature ranges while the final technique was valuable for "pinning down" the low temperature values. It is common practice to use Vieland's equation (9) and a solution model representing the stoichiometric liquid activities to determine θ_{IC} . The solution model parameters are then estimated from a fit of the binary phase diagram only. It has been shown that this procedure can lead to large errors in the value of θ_{IC} . The errors mainly resulted from an incorrect representation of the stoichiometric liquid activities. The use of Method III, however, gave the correct temperature dependence of θ_{IC} for any (except liquidus data alone) data base studied. The inclusion of activity measurements in the data base served to pin down the value of the stoichiometric activity product at the melting point and thus replicated the recommended values of θ_{IC} .

The determination of Γ_{IC} was examined by first considering the binary liquid solution behavior in order to focus on the liquid phase nonidealities. The combined data set consisting of phase diagram, alloy enthalpy of mixing, and the Group III liquid-phase activity in conjunction with the recommended values of θ_{IC} was used in the parameter estimation for several solution models, which containing different assumptions about the solution behavior. While the improved temperature dependence and ability to represent asymmetric excess properties found in the local composition models considered in

this work, the results had shown that none of the solution models studied can simultaneously represent the combined data set (phase diagram, component activity, enthalpy of mixing) for the AlSb and AlIn systems due to highly asymmetric phase diagrams. It may be concluded that a special chemical term must be included in the models to properly describe these systems with association in the liquid phase. Little difference was found in the model calculations for the Ga-Sb, Al-Ga, and Ga-In systems. The NRTL equation (4 parameters) and simple solution model (2 parameters) are able to adequately represent the combined data well for these systems. It was also found that the NRTL equation best represents the asymmetric and temperature-dependent properties of the In-Sb system.

Attempts to use the solution models to predict a property from a fit of a different type of property were, in general, unsuccessful. The results of the use of different models to calculate properties from the fit of a single set of data or from the fit of two of the three type experimental measurements usually produced wide differences in calculated values and often strongly depended upon the model used. It was found that the problem was mainly due to the existence of the nonuniqueness of the model parameters. An improved method was proposed to predict the phase diagram by fixing one or two parameters based on the individual activity and enthalpy of mixing fits or the double data set fit of the models at the individual melting point and eutectic point or both points of the binary compound. The results showed that the prediction of the phase diagram from the activity or enthalpy of mixing data alone is

possible by the use of this technique. This prediction leads to very poor results with the original models, even when the temperature dependent parameters are introduced. The problem of parameter correlation is also discussed in this study. The correlation between the parameters was found significantly.

The solid solution behavior was normally determined from an analysis of the pseudobinary phase diagram. Two different methods for calculating the solid interaction parameters were presented in this work and applied to the AlSb-GaSb, AlSb-InSb, and GaSb-InSb systems. The simple solution model was used to describe the solid solution behavior and parameters were estimated from a fit of the data base, which including the pseudobinary phase diagram, pseudobinary liquid enthalpy of mixing, or both. The results for two approaches had shown that the NRTL equation for liquid solution and simple solution model for solid solution provides a means of adequately representing the data for these three pseudobinary antimonide systems. It was also found that the nonideality in the solid solution increases with increasing the lattice mismatch between two binary compounds. The treatment of the $A_xB_{1-x}C$ liquid solution as a ternary mixture of A, B, and C gave a higher standard deviations in the liquidus data due to the absence of the adjustable parameters in the liquid phase, for which the thermodynamic properties were estimated with binary parameters only. This discrepancy between the calculated and experimental pseudobinary liquidus measurements is particularly prominent for the system in which the melting point difference between two binary limits is large. The variation of the

excess Gibbs energy of the solid solution with temperature was also found in opposite directions for two different treatments of the liquid phase. It follows that the miscibility gap of the solid solution is predicted differently for each method. Thus, the treatment of the $A_xB_{1-x}C$ liquid as a ternary mixture of A, B, and C or as a pseudobinary solution of AC and BC may give a different interpretation of the solid solution behavior that is obtained from a fit of the pseudobinary phase diagram only.

The pseudobinary liquid phase properties for the $Ga_xIn_{1-x}Sb$ system were determined by using the solution models with only binary parameters. The NRTL equation shows excellent agreement with the ΔH_m^l experimental results of Gerdes and Predel (226), while the simple solution model gives slightly more positive values though it retains the correct composition dependence. The predicted activities of both the NRTL equation and simple solution model show significantly less from ideal behavior than do the experimental values (234). This indicates that some kinds of "associates" or "complexes" must exist in the liquid state. The results of these calculations show that the NRTL solution model with parameters estimated from binary data provides a good description of the $Ga_xIn_{1-x}Sb$ liquid solution thermodynamic properties. The common practice of applying the simple solution model to a description of the liquid phase, however, gives only fair agreement between the calculated values and the experimental measurements. On the basis of this work and a previous study (137), it is concluded that only moderate success can be expected in predicting the values of ternary liquid mixture

thermodynamic properties from analysis of the binary phase diagrams alone. Improvements in the predictive capabilities of models with parameters based on binary data were found when the data base includes measurements of the component activity or enthalpy of mixing or both.

The ability to extend the binary and pseudobinary solution parameters to calculate the ternary and quaternary phase diagrams was examined. The best results for the binary liquid and pseudobinary solid solution parameters obtained in this study in conjunction with the recommended values of θ_{IC} were used to calculate the quantities Γ_{IC} and θ_{IC} necessary for the multicomponent phase diagram calculations. Phase diagrams for the GaInSb, AlGaSb, AlInSb and AlGaInSb systems were presented. As in the case of pseudobinary systems, the NRTL equation with parameters estimated from the combined binary data set shows a good representation of the $Ga_xIn_{1-x}Sb$ liquidus isotherms, solidus isotherms and liquid solution thermodynamic properties. The use of the simple solution model for both the liquid and solid phases gives only fair agreement between the calculated and experimental values. The reason for this is apparent due to the ability of the NRTL solution model to represent the asymmetric and temperature-dependence properties for the binary limits. However, the simple solution model with parameters estimated from the binary phase diagram alone gave a good representation of the $Al_xGa_{1-x}Sb$ liquidus and solidus isotherms. While the simple solution model parameters provided a good description of phase equilibrium for AlGaSb system, it was unable to represent the other thermodynamic

properties. Because of the lack of experimental data for the AlInSb and AlGaInSb systems, the accuracy of the calculated phase diagrams could not be adequately tested. However, the calculation will provide an effective guide for the growth of these materials.

Finally, the applicability of the use of a solid state electrochemical technique employing CaF_2 as an oxygen ion conductor in high temperature Al systems was verified for the first time in this study. A solid state galvanic cell was employed to measure the standard Gibbs energy of the formation of Al_2O_3 , utilizing calcium fluoride (CaF_2) as the solid electrolyte, with a (Al+ Al_2O_3) mixture as the working electrode and a (Ni+NiO) mixture as the reference electrode. The results of this tested cell showed that the standard Gibbs energy of formation of Al_2O_3 is in good agreement with the generally accepted thermochemical value. Thus, CaF_2 is evidently suitable as a solid electrolyte for Al containing alloys studies.

9.2 Recommendations

On the basis of the results of this work the following suggestions can be made for future study, and will be briefly discussed.

9.2.1 Theory

The standard state studied in this work is quite common in low pressure vapor-liquid equilibrium correlations. Nevertheless, when the system temperature is higher than the critical temperature of a component under consideration (as is the case at high vapor pressures systems), its reference fugacity becomes a hypothetical quantity,

because under these conditions the liquid cannot exist. As an example, the pure liquid reference state provides problems for the HgTe, arsenide and phosphide systems because the mercury, arsenic and phosphorus components have very high vapor pressures even below the compound melting points or often at the system temperature of interest. The use of an infinite dilution reference state would overcome this difficulty (avoid if possible). Since the choice of reference state plays a crucial role in the study of Groups II-VI and III-V phase equilibrium, a careful study should be made in this area. The possibility of improvement in the calculation of θ_{IC} for these with the use of method III has been mentioned.

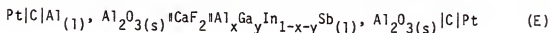
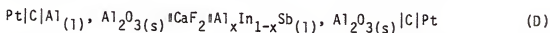
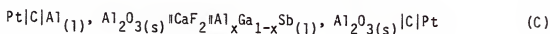
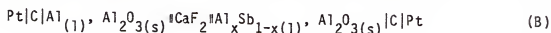
For the convenience of explanation, let us consider the phase diagram of a $A_xB_{1-x}C$ ternary system, which calculated by the simple solution model with only binary and pseudobinary parameters (i.e., w_{A-C}^1 , w_{B-C}^1 , w_{A-B}^1 and w_{AC-BC}^S). These parameters play a different role in the calculation of the phase diagram. The parameters w_{A-C}^1 and w_{B-C}^1 serve to "pin down" the liquidus surface at binary limits, while the parameter w_{AC-BC}^S fixes the pseudobinary portion of the phase field. The parameter w_{A-B}^1 has an effect on the curvature of the liquidus surface. Once these parameters are well characterized, it would be expected that the ternary phase diagram should be well defined. As mentioned above, no solution models considered here have ability to represent highly asymmetric systems. Thus, further consideration of the calculation of the multicomponent phase diagrams containing highly asymmetric binary systems should take into account possible chemical association of the components of the binary

limits. This effect is not included in the models studied here but some of them could easily be modified.

Further numerical calculation is desired to obtain the lattice matching condition that must be satisfied for the $\text{Al}_x\text{Ga}_y\text{In}_{1-x-y}\text{Sb}$ quaternary solids lattice matched to the desired substrate to produce high quality defect-free crystal.

9.2.2 Experiments

The standard Gibbs free energy of formation of $\text{AlSb}_{(s)}$ and the liquid aluminum activity in the binary and multicomponent systems studied in this work can be measured with the galvanic cells employing a CaF_2 solid electrolyte and a $\text{Al}+\text{Al}_2\text{O}_3$ mixture as the reference electrode. The cells are represented schematically as follows:



As shown in Figure 9-1, the cell set-up for these liquid III-V cells will be simple and analogous to that already used in this work. In a similar manner, the following cells will be used to determine the AlSb activity in the AlSb-GaSb , AlSb-InSb , and AlSb-GaSb-InSb solid solutions and the GaSb activity in the GaSb-InSb solid solution:

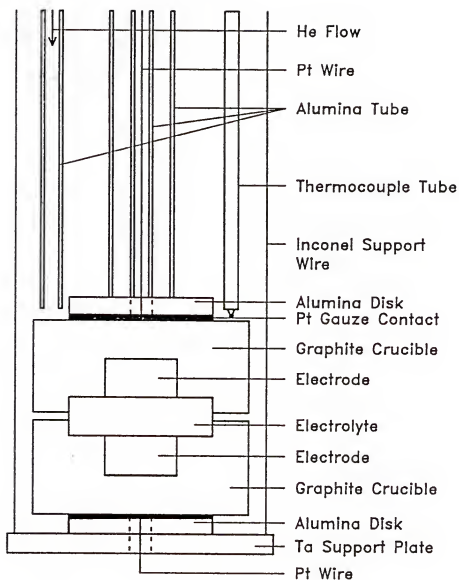
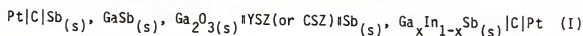
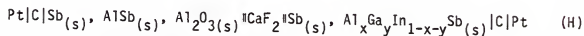
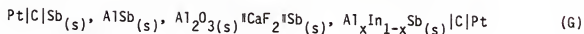
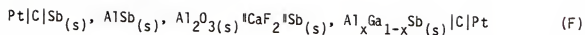


Figure 9-1. Experimental Apparatus



Here the solid electrolyte material yttria-stabilized zirconia (YSZ) and calcium-stabilized zirconia (CSZ) usually are used in the study of the Ga-In-Sb system. The performance of these cells is strongly influenced by the following factors:

1. Is the solid or liquid solution mixed completely?
2. Do the electrochemical cells reach the equilibrium condition?
3. Does vapor phase short the circuit?

The results of the measurements provide a means of verifying the validity of the use of the solution models based on a fit of the binary and pseudobinary phase diagrams to predict the multicomponent phase diagram and thermochemical properties. Especially, such measurements for the solid solutions would couple the thermodynamic data base for each ternary system studied here. Using this complete data set, a variety of the solution models can be compared for the liquid and solid phases. The best fit parameters for the model are then used to calculate phase diagrams and to predict the solid phase immiscibility gap. Finally, the technique with a modification of the solid state cells considered here might also be extended to the direct measurement of component activity in the volatile systems (e.g., HgTe, arsenide and phosphide systems). The results of such a

study would be independent of any assumptions about the hypothetical reference of the volatile components.

APPENDIX
SAMPLE PROGRAM FOR CALCULATING Al-Ga-In-Sb PHASE DIAGRAM

```

implicit real*8 (a-h,o-z)
real*8 x1(100),x40(100),x3(100),x4(100,x2(100)
er=1,0d-5
do 10 i=1,101
x40(i)=0.489394
x0=0.818098
y0=0.181902
20 x1(i)=0.0277357
x2(i)=0.00504408*(i-1)
x3(i)=1.0-x1(i)-x2(i)-x40(i)
t=1073.
w14=13437.29-12.85393*t
w24=3208.964-5.886396*t
w34=-4500.5+0.9064179*t
w12=598.9409-0.3178501*t
w13=1060
w23=1029.9+0.29T
w1424=3858.539-3.057946*t
w1434=1574.993-1.874394*t
w2434=1884.091-0.4248481*t
t14=-5.4806483-0.0005133*t-9176.8767/t
++1.5218923*dlog(t)
t24=5.37-7950./t+0.1*dlog(t)
t34=-5.7237-0.0007061*t-5902.119/t+1.65576*dlog(t)
r14=dexp((w1424*y0**2+w1434*(1.-x0-y0)**2+
+ w1434+w1424-w2434)*y0*(1.-x0-y0))/(1.9872*t))
r24=dexp((w2434*(1.-x0-y0)**2+w1424*x0**2t(
+ w2434+w1424-w1434)*x0*(1.-x0-y0))/(1.9872*t))
r34=dexp((w1434*x0**2 w2434*y0**2+(w1434+w2
+434-w1424)*x0*y0)/(1.9872*t))
r1=dexp((w12*x2(i)**2+w13*x3(i)**2+w14*x40(i)**2
++(w12+w13-w23)*x2(i)*x3(i)+(w13+w14-w34)*x3(i)*
+x40(i)+(w12+w14-w24)*x2(i)*x40(i))/(1.9872*t))
r2=dexp((w12*x1(i)**2+w23*x3(i)**2+w24*x40(i)**2
++(w23+w24-w34)*x3(i)*x40(i)+(w24+w12-w14)*x1(i)*
+x40(i)+(w12+w23-w13)*x1(i)*x3(i))/(1.9872*t))
r3=dexp((w34*x40(i)**2+w13*x1(i)**2+w23*x2(i)**2
++(w34+w13-w14)*x1(i)*x40(i)+(w13+w23-w12)*x1(i)*
+x2(i)+(w23+w34-w24)*x2(i)*x40(i))/(1.9872*t))
r4=dexp((w14*x1(i)**2+w24*x2(i)**2+w34*x3(i)**2
++(w14+w24-w12)*x1(i)*x2(i)+(w24+w34-w23)*x2(i)*
+x3(i)+(w34+w14-w13)*x1(i)*x3(i))/(1.9872*t))

```

```

g14=r1*r4/r14
g24=r2*r4/r24
g34=r3*r4/r34
f1=x0-g14*x1(i)*x40(i)*dexp(-t14)
t2=y0-g24*x2(i)*x40(i)*dexp(-t24)
f3=1.-x0-y0-g34*x3(i)*x40(i)*dexp(-t34)
a1=(-2.*w13*x3(i)+2.*w14*x40(i)-x2(i)*(w12+w13-w23)+x2(i)
+*(w12+w14-w24)+(w13+w14-w34)*(x3(i)-x40(i)))/(1.9872*t)
a2=(-2.*w23*x3(i)+2.*w24*x40(i)-x1(i)*(w12+w23-w13)+x1(i)
+*(w12+w24-w14)+(w23+w24-w34)*(x3(i)-x40(i)))/(1.9872*t)
a3=(2.*w34*x40(i)+x2(i)*(w23+w34-w24)+x1(i)*(w13+w34-w14))
+/(1.9872*t)
a4=(-2.*w34*x3(i)-x1(i)*(w14+w34-w13)-x2(i)*(w24+w34-w23))
+/(1.9872*t)
a5=(-2.*w1434*(1.-x0-y0)-y0*(w1434+w1424-w2434))/1.9872/t
a6=(-2.*w2434*(1.-x0-y0)+2.*w1434*x0+(1.-2.*x0-y0)*
+(w2434+w1424-w1434))/(1.9872*t)
a7=(-2.*w1434*x0+y0*(w1434+w2434-w1424))/(1.9872*t)
a8=(2.*w1424*y0-2.*w1434*(1.-x0-y0)+(w1434+w1424-w2434)*
+(1.-x0-2.*y0))/(1.9872*t)
a9=(-2.*w2434*(1.-x0-y0)-x0*(w2434+w1424-w1434))/(+1.9872*t)
a10=(2.*w2434*y0+x0*(w1434+w2434-w1424))/(1.9872*t)
f1x=-g14*x1(i)*dexp(-t14)+(f1-x0)*(a1+a4)
f1y=1.+(x0-f1)*a5
f1z=(x0-f1)*a8
f2x=-g24*x2(i)*dexp(-t24)+(f2-y)*(a2+a4)
f2y=(y0-f2)*a6
f2z=(1.+(y0-f2)*a9
f3x=(x40(i)-x3(i))*g34*dexp(-t34)+(f3-1.+x0+y0)*(a3+a4)
f3y=-1.+(1.-x0-y0-f3)*a7
f3z=-1.+(1.-x0-y0-f3)*a10
a=f1*f2y*f3z+f1y*f2z*f3+f1z*f2*f3y-f1z*f2y*f3-
+f1*f2z*f3y-f1y*f2*f3z
b=f1x*f2*f3z+f1*f2z*f3x+f1z*f2x*f3-f1z*f2*f3x-
+f1x*f2z*f3-f1*f2x*f3z
c=f1x*f2y*f3+f1y*f2*f3x+f1*f2x*f3y-f1*f2y*f3x-
+f1x*f2*f3y-f1y*f2x*f3
d=f1x*f2y*f3z+f1y*f2z*f3x+f1z*f2x*f3y-f1z*f2y*f3x-
+f1x*f2x*f3y-f1y*f2x*f3z
dr=-a/d
ds=-b/d
dt=-c/d
if (dmax1(abs(dr),abs(ds),abs(dt),dabs(f1),dabs(f2),
+dabs(f3)),1t.er) go to 40
x40(i)=x40(i)+dr
x0=x0+ds
y0=y0+dt
go to 20
40 write(6,50)x1(i),x2(i),x3(i),x40(i)x0,y0
50 format(6d13,5)
10 continue
stop
end

```

REFERENCES

1. Ghandi, S. K., in VLSI Fabrication Principles, Silicon and Gallium Arsenide, John Wiley & Sons, New York (1983).
2. Einspruch, N. G., in VLSI Electronics Microstructure Science, 3, Academic Press, New York (1982).
3. Streetman, B. G., in Solid State Electronic Devices, Prentice-Hall, Englewood Cliffs, N. J. (1980).
4. Melngailis, I., and Harman, T. C., in Semiconductors and Semimetals, 5, Academic Press, New York (1970).
5. Sirota, N. N., in Semiconductors and Semimetals, eds. R. K. Willardson and A. C. Beer, 4, Academic Press, New York (1968).
6. Van Vechten, J. A., J. Electrochem. Soc., 122, 423 (1975).
7. Hurle, D. T. J., J. Phys. Chem. Solids, 40, 613 (1979).
8. Edelin, G., and Mathiot, D., Philosophical Magazine B, 42, 95 (1980).
9. Vieland, L. J., Acta. Met., 11, 137 (1963).
10. Hall, R. N., J. Electrochem. Soc., 110, 385 (1963).
11. Thurmond, C. D., J. Phys. Chem. Solids, 26, 785 (1965).
12. Arthur, J. R., J. Phys. Chem. Solids, 28, 2257 (1967).
13. Nougaret, P., and Potier, A., J. Chim. Phys., 66, 764 (1969).
14. Ilegems, M., and Panish, M. B., J. Chem. Thermodyn., 5, 291 (1973).
15. Panish, M. B., J. Crystal Growth, 27, 6 (1974).
16. Panish, M. B., and Ilegems, M., in Progress in Solid State Chemistry, ed. J. O. McCaldin, 7, Pergamon Press, New York (1972).
17. Nguyen Van Mau, A., Ance, C., and Bougnot, G., J. Crystal Growth, 36, 273 (1976).

18. Anderson, S. J., School, F., and Harris, J. S., in Proc. 6th Int. Symp. on GaAs and Related Compounds, St. Louis, Mo., 346 (1976).
19. Joullie, A., and Gautier, P., J. Crystal Growth, 47, 100 (1979).
20. Foster, L. M., and Woods, J. F., J. Electrochem. Soc., 118, 1175 (1971).
21. Wu, T. Y., and Pearson, G. L., J. Phys. Chem. Solids, 33, 409 (1972).
22. Gorelenok, A. T., Mdivani, V. N., Moskvina, P. P., Sorokin, V. S., and Usikov, A. S., Russian J. Phys. Chem., 56, 1481 (1982).
23. Brebrick, R. F., and Panlener, R. J., J. Electrochem. Soc., 121, 932 (1974).
24. Gratton, M. F., and Woolley, J. C., J. Electrochem. Soc., 125, 657 (1978).
25. Blom, G. M., and Plaskett, T. S., J. Electrochem. Soc., 118, 1831 (1971).
26. Joullie, A., Dedies, R., Chevrier, J., and Bougnot, G., Rev. Phys. Appl., 9, 455 (1974).
27. Ilegems, M., and Pearson, G. L., Proc. Symp. on GaAs, 3 (1968).
28. Mabbitt, A. W., J. Materials Science, 5, 1043 (1970).
29. Blom, G. M., J. Electrochem. Soc., 118, 1834 (1971).
30. Panish, M. B., and Ilegems, M., Proc. Symp. on GaAs, 67 (1970).
31. Kajiyama, K., Japan. J. Appl. Phys., 10, 561 (1971).
32. Sugiura, T., Sugiura, H., Tanaka, A., and Sukegawa, T., J. Crystal Growth, 49, 559 (1980).
33. Antypas, G. A., J. Electrochem. Soc., 117, 1393 (1970).
34. Tomlinson, J. L., Naval Ocean Systems Center, Technical Note 386, San Diego, Ca. (1978).
35. Tanaka, A., Sugiura, T., and Sukegawa, T., J. Crystal Growth, 60, 120 (1982).
36. Gratton, M. F., and Woolley, J. C., J. Electrochem. Soc., 127, 55 (1980).

37. Ilegems, M., and Panish, M. B., *J. Crystal Growth*, 20, 77 (1973).
38. Doi, A., Hirao, M., and Ito, R., *Japan. J. Appl. Phys.*, 17, 503 (1978).
39. Dedegkaev, T. T., Kryukov, I. I., Lideikis, T. P., Tsarenkov, B. V., and Yakovlev, Y. P., *Sov. Phys. Tech. Phys.*, 23, 350 (1978).
40. Nguyen Van Mau, A., Ance, C., and Bougnot, G., *J. Crystal Growth*, 36, 273 (1976).
41. Onabe, K., *J. Phys. Chem. Solids*, 43, 1071 (1982).
42. Nakajima, K., Kusunoki, T., Akita, K., and Kotani, T., *J. Electrochem. Soc.*, 125, 123 (1978).
43. Ilegems, M., and Panish, M. B., *J. Phys. Chem. Solids*, 35, 409 (1974).
44. Gorelenok, A. T., Mdivani, V. N., Moskvina, P. P., Sorokin, V. S., and Usikov, A. S., *J. Crystal Growth*, 60, 355 (1982).
45. Alavi, K. T., Perea, E. H., and Fonstad, C. G., *J. Electronic Materials*, 10, 591 (1981).
46. Perea, E. H., and Fonstad, C. G., *J. Appl. Phys.*, 51, 331 (1980).
47. Henry, Y., and Moulin, M., *J. Crystal Growth*, 51, 387 (1981).
48. Cheng, K. Y., and Pearson, G. L., *J. Electrochem. Soc.*, 124, 753 (1977).
49. Rao, M. V., and Tiller, W. A., *J. Phys. Chem. Solids*, 31, 191 (1970).
50. Knobloch, G., Butter, E., and S. Reiffarth, *Z. Phys. Chemie*, 259, 667 (1978).
51. Knobloch, G., *Kristall U. Technik*, 10, 605 (1975).
52. Peuschel, G. P., Apelt, R., Knobloch, G., and Butter, E., *Kristall U. Technik*, 14, 409 (1979).
53. Peuschel, G. P., Knobloch, G., Butter, E., and Apelt, R., *Crystal Research and Technology*, 16, 13 (1981).
54. Ilegems, M., Panish, M. B., and Arthur, J. R., *J. Chem. Thermodyn.*, 6, 157 (1974).
55. Panish, M. B., *J. Crystal Growth*, 27, 6 (1974).

56. Stringfellow, G. B., and Greene, P. E., J. Phys. Solids, 30, 1779 (1969).
57. Stringfellow, G. B., and Greene, P. E., J. Electrochem. Soc., 117, 1075 (1970).
58. Brebrick, R. F., Met. Trans., 8, 403 (1977).
59. Kaufman, L., Nell, J., Taylor, K., and Hayes, F., CALPHAD, 5, 185 (1981).
60. Esdaile, J. D., The Metallurgical Soc. of AIME, 13(B), 213 (1982).
61. Bale, C. W., and Pelton, A. D., Metall. Trans., 5, 2323 (1974).
62. Darken, L. S., Trans. TMS-AIME, 239, 80 (1967).
63. Eckert, C. A., Smith, J. S., Irwin, R. B., and Cox, K. R., AICHE Journal, 28, 325 (1982).
64. Jordan, A. S., Metall. Trans., 1, 239 (1970).
65. Osamura, K., and Predel, B., Trans. JIM, 18, 765 (1977).
66. Osamura, K., and Murakami, Y., J. Phys. Chem. Solids, 36, 931 (1975).
67. Kharif, Y. L., Kovtunenکو, P. V., and Maier, A. A., Russ. J. Phys. Chem., 56(1), 34 (1982).
68. Liao, P.-K., Su, C.-H., Tung, T., and Brebrick, R. F., CALPHAD, 6, 141 (1982).
69. Liao, P.-K., Su, C.-H., and Brebrick, R. F., CALPHAD, 7, 207 (1983).
70. Foster, L. M., and Woods, J. F., J. Electrochem. Soc., 119, 504 (1972).
71. Foster, L. M., Scardefield, J. E., and Woods, J. F., J. Electrochem. Soc., 119, 765 (1972).
72. Foster, L. M., Scardefield, J. E., and Woods, J. F., J. Electrochem. Soc., 119, 1426 (1972).
73. Foster, L. M., in Electrochemical Society Extended Abstracts, Houston Meeting, 147 (1972).
74. Phillips, J. C., and Van Vechten, J. A., Phys. Rev., B2, 2147 (1970).

75. Hildebrand, J. H., and Scott, R. L., in The Solubility of Nonelectrolytes, Dover Publications, New York (1964).
76. Gordy, W., Phys. Rev., 69, 604 (1946).
77. Gordy, W., and Thomas, J. O., J. Chem. Phys., 25, 439 (1956).
78. Stringfellow, G. B., Mat. Res. Bull., 6, 371 (1971).
79. Stringfellow, G. B., J. Phys. Chem. Solids, 33, 665 (1972).
80. Stringfellow, G. B., J. Crystal Growth, 27, 21 (1974).
81. Phillips, J. C., Phys. Rev. Lett., 20, 550 (1968).
82. Fedders, P. A., and Muller, M. W., J. Phys. Chem. Solids, 45, 685 (1984).
83. Nakajima, K., Yamazaki, S., and Akita, K., J. Crystal Growth, 56, 547 (1982).
84. Szapiro, S., J. Phys. Chem. Solids, 41, 279 (1980).
85. Ilegems, M., and Panish, M. B., J. Phys. Chem. Solids, 35, 409 (1974).
86. Jordan, A. S., and Ilegems, M., J. Phys. Chem. Solids, 36, 329 (1975).
87. Onabe, K., J. Phys. Chem. Solids, 43, 1071 (1982).
88. Weast, R. C., and Astle, M. J., eds., CRC Handbook of Chemistry and Physics, 56th Ed., CRC Press, Boca Raton, Fl. (1980-1981).
89. Wager, C., Acta. Met., 6, 309 (1958).
90. Vieland, L. J., Acta. Met., 11, 137 (1963).
91. Ilegems, M., Ph. D. Thesis, Stanford University (1969).
92. Brebrick, R. F., Met. Trans., 2, 1657 (1971).
93. Jordan, A. S., Met. Trans., 2, 1559 (1971).
94. Brebrick, R. F., Met. Trans., 2, 3377 (1971).
95. Jordan, A. S., and Weiner, M. E., J. Phys. Chem. Solids, 36, 1335 (1975).
96. Furukawa, Y., and Thurmond, C. D., J. Phys. Chem. Solids, 26, 1535 (1965).

97. Panish, M. B., and Sumski, S., J. Phys. Chem. Solids, 30, 129 (1969).
98. Tung, T., Su, C.-H., Liao, P.-K., and Brebrick, R. F., J. Vac. Sci. Technol., 21, 117 (1982).
99. Kubaschewski, O., and Alock, C. B., in Metallurgical Thermochemistry, 5th Ed., Pergamon Press, Ltd., New York (1979).
100. Rosa, C. J., Rupf-Bolz, N., Sommer, F., and Predel, B., Z. Metallkde, 71, 320 (1980).
101. Richman, D., and Hockings, E. F., J. Electrochem. Soc., 112, 461 (1965).
102. Lichter, L. D., and Sommelet, P., Trans. Met. Soc. AIME, 245, 99 (1969).
103. Predel, B., and Schallner, U., Mater. Sci. Eng., 5, 210 (1970).
104. Anderson, T. J., and Donaghey, L. F., J. Electrochem. Soc., 131, 3006 (1984).
105. Anderson, T. J., Aselage, T., and Donaghey, L. F., accepted J. Chem. Thermodynamics.
106. Anderson, T. J., Ph. D. Thesis, University of California, Berkeley (1978).
107. Predel, B., and Stein, D. W., J. Less Comm. Met., 24, 391 (1971).
108. Rosa, C. J., Rupf-Bolz, N., Sommer, F., and Predel, B., Z. Metallkde, 71, 320 (1980).
109. Tung, T., Gdonka, and Brebrick, R. F., J. Electrochem. Soc., 128, 1601 (1981).
110. Blachnik, R., and Schneider, A., Anorg. Allgem. Chem., 372, 314 (1970).
111. Hultgren, R., Desai, P. D., Hawkins, D. T., Gleizer, M., and Kelley, K. K., in Selected Values of the Thermodynamic Properties of the Binary Alloys, American Society for Metals, Metals Park, Oh. (1973).
112. Liu, T. S., and Peretti, E. A., Trans. Amer. Soc. Metals, 44, 539 (1952).
113. Steininger, J., Strauss, A. J., and Brebrick, R. F., J. Electrochem. Soc., 117, 1305 (1970).

114. Tung, T., Su, C., Liao, P., and Brebrick, R. F., J. Vac. Sci. Technol., 21, 117 (1982).
115. Kelley, J. D., Martin, B. G., Szofran, F. R., and Lehoczy, S. L., J. Electrochem. Soc., 129, 2360 (1982).
116. Lorenz, M. R., J. Phys. Chem. Solids, 23, 939 (1962).
117. Brebrick, R. F., and Strauss, A. J., J. Phys. Chem. Solids, 26, 989 (1965).
118. Hultgren, R., Desai, P. D., Hawkins, D. T., Gleizer, M., and Kelley, K. K., in Selected Values of the Thermodynamic Properties of the Elements, American Society for Metals, Metals Park, Oh. (1973).
119. Garbato, L., and Ledda, F., Thermochimic Acta, 14, 267 (1977).
120. Terpilowski, J., and Trzebiatowski, W., Bull. Acad. Polon. Sci., Ser. Sci. Chim., 8, 95 (1960).
121. Kleppa, O. J., J. Am. Chem. Soc., 77, 897 (1955).
122. Schwartz, J. P., Tung, T., and Brebrick, R. F., J. Electrochem. Soc., 128, 438 (1981).
123. Brebrick, R. F., and Strauss, A. J., J. Phys. Chem. Solids, 25, 1441 (1964).
124. Su, C., Liao, P., Tung, T., and Brebrick, R. F., High Temperature Sci., 14, 181 (1981).
125. Steininger, J., J. Electronic Mat., 5, 299 (1976).
126. Samokhval, V. V., and Vecher, A. A., Russ. J. Phys. Chem., 42 (1968).
127. Vecher, A. A., Geiderikh, V. A., and Gerasimov, Y. I., Russ. J. Phys. Chem., 39, 144 (1965).
128. Marina, L. I., Nashel'skii, A. Y., and Sakharov, B. A., in Chemical Bonds in Semiconductors and Solids, ed. N. N. Sirato, Consultants Bureau, New York (1972).
129. Samokhval, V. V., Vecher, A. A. and Panko, E. P., in Chemical Bonds in Semiconductors and Solids, ed. N. N. Sirato, Consultants Bureau, New York (1972).
130. Abbasov, A. S., Nikol'skaya, and Gerasimov, A. V., Ya. I., Doklady Akad. Nauk SSSR, 156, 1399 (1964).

131. Sirota, N. N., and Yushkevich, N. N., in Chemical Bonds in Semiconductors and Solids, ed. N. N. Sirota, Consultants Bureau, New York (1967).
132. Nikol'skaya, A. V., Geiderikh, V. A., and Gerasimov, Ya. I., Dokl. Akad. Nauk SSSR, 130, 1074 (1959).
133. Abbasov, A. S., and Mamedov, K. N., Izv. Akad. Nauk, Azerb. SSSR, Ser, Fiz. Mat. Itekh. Nauk, 3, 86 (1970).
134. Scottky, W. F., and Bever, M. B., Acta. Met., 6, 320 (1958).
135. Drowart, J., and Goldfinger, P., J. Chim. Phys., 55, 721 (1958).
136. Jena, A. K., Bever, M. B., and Banus, M. D., Trans. Met. Soc. AIME, 239, 725 (1967).
137. McAteer, J. H., and Seltz, H., J. Amer. Chem. Soc., 58, 2081 (1936).
138. Goldfinger, P., and Jeunehomme, M., Trans. Faraday Soc., 59, 851 (1963).
139. Korneeva, I. V., Belyaev, A. V., and Novoselova, A. V., Russ. J. Inorg. Chem., 5, 1 (1960).
140. Terpilowski, J., Arch. Hutn., 4, 355 (1959).
141. Predel, B., and Oehme, G., Z. Metallkde., 67, 826 (1976).
142. Mechkovskii, L. A., Savitskii, A. A., Skums, V. F., and Vecher, A. A., Russ. J. Phys. Chem., 45, 1143 (1971).
143. Glazov, V. M., and Petrv, D. A., Izv. Akad. Nauk SSSR, Otd. Tekhn. Nauk, 4, 125 (1958).
144. Cox, R. H., and Pool, M. J., J. Chem. Eng. Data, 12, 247 (1967).
145. Gadzhiev, S. N., and Sharifov, K. A., Dokl. Akad. Nauk SSSR, 136, 1339 (1961).
146. Lundin, C. E., Pool, M. J., and Sullivan, R. W., Denver Research Inst. Final Report No. AFORL-63-156 (1963).
147. Maslov, P. G., and Maslov, Yu. P., in Chemical Bonds in Semiconductors and Solids, ed. N. N. Sirota, Consultant Bureau, New York (1972).
148. Hoshino, H., Nakamura, Y., Shimoji, M., and Niwa, K., Ber. Bunsenges, Phys. Chem., 69, 114 (1965).

149. Welker, H., *Physica*, 20, 893 (1954).
150. Yazawa, A., Kawashima, T., and Itagaki, K., *J. Japan Inst. Metals*, 32, 1288 (1968).
151. Gerasimenko, L. N., Kirichenko, I. V., Lozhkin L. N., and Morachevskii, A. G., *Zashchitn. Metal i Oksidyne Pokrytiya, korroziya Metal. i Issled. V Obl. Elektrokhim.*, Akad. Nauk SSSR, Otd. Ob Shch, i Tekhn. Khim. Sb. Statei, 236 (1965).
152. Cunnell, F. A., Edmond, J. T., and Richards J. L., *Proc. Phys. Soc. (London)*, 1367, 848 (1954).
153. Sirota, N. N., and Yushkevich, N. N., *Khim. Svyas V Poluprov. i Tverd. Telakh, Inst. Fiz. Tverd. Tela i Poluprov.*, Akad. Nauk Belorusok. SSR, 122 (1965).
154. Maglione, M. H., and Potier, A., *J. Chim. Phys.*, 65, 1595 (1968).
155. Gambino M., and Bros, J. P., *J. Chem. Thermodynamics*, 7, 443 (1975).
156. Hildebrand, J. H., *Proc. Nat. Acad. Sci.*, 13, 267 (1927).
157. Hildebrand, J. H., and Scott, R. L., in The Solubility of Non-Electrolytes, Reinhold Publishing Corp., New York (1950).
158. Hildebrand, J. H., and Scott, R. L., in Regular Solutions, Prentice-Hall, Englewood Cliffs, N.J. (1962).
159. Scatchard, G., and Hamer, W., *J. Am. Chem. Soc.*, 57, 1805 (1935).
160. Scatchard, G., and Hamer, W., *J. Am. Chem. Soc.*, 57, 1809 (1935).
161. Guggenheim, E. A., Mixtures, Oxford University Press, London (1952).
162. Wilson, G. M., *J. Am. Chem. Soc.*, 86, 127 (1964).
163. Renon, H., and Prausnitz, J. M., *A.I.Ch.E. Journal*, 14, 135 (1968).
164. Abrams, D. S., and Prausnitz, J. M., *A.I.Ch.E. Journal*, 21, 116 (1975).
165. Prigogine, I., in The Molecular Theory of Solutions, North-Holland Publishing Co., Amsterdam (1957).

166. Hill, T. L., in An Introduction to Statistical Thermodynamics, Addison-Wesley Publishing Company, Inc., Reading, Ma. (1960).
167. Prausnitz, J. M., in Molecular Thermodynamics of Fluid Phase Equilibria, Prentice-Hall, Englewood Cliffs, N. J. (1969).
168. Wohl, K., Trans. A.I.Ch.E., 42, 215 (1946).
169. van Laar, J. J., Z. Phys. Chem., 83, 599 (1913).
170. Dolezalek, F., Z. Phys. Chem., 64, 727 (1908).
171. Lacmann, R., Z. Phys. Chem. (N.F.), 23, 313 (1960).
172. Lacmann, R., Z. Phys. Chem. (N.F.), 23, 324 (1960).
173. Lacmann, R., Z. Phys. Chem. (N.F.), 35, 86 (1962).
174. Flory, P. J., J. Chem. Phys., 9, 660 (1941).
175. Flory, P. J., J. Chem. Phys., 10, 51 (1942).
176. Huggins, M. L., J. Phys. Chem., 9, 440 (1941).
177. Huggins, M. L., Ann. N. Y. Acad. Sci., 43, 1 (1942).
178. Orye, R. V., and Prausnitz, J. M., Ind. Eng. Chem., 57(5), 18 (1965).
179. Hala, E., Collect. Czech. Chem. Commun., 37, 2817 (1972).
180. Scott, R. L., J. Chem. Phys., 25, 193 (1956).
181. Urasov, G. G., Izv. Inst. Fiz., Khim. Anal., 1, 461 (1921).
182. Guertler, W., and Bergman, A., Z. Metallk., 25, 81 (1933).
183. Linnebach, R., and Benz, K. W., J. Crystal Growth, 53, 579 (1981).
184. Linnebach, R., and Benz, K. W., J. Crystal Growth, 55, 531 (1981).
185. Glazov, V. M., and Petrov, D. A., Isv. Akad. Nauk. SSSR, Otd. Tekhn. Nauk, 4, 125 (1958).
186. Dix, E. M., Keller, F., and Willey, L. A., Trans. AIME, 93, 396 (1931).
187. Asefage, T. L., Chang, K. M., and Anderson, T. J., CALPHAD, 9, 221 (1985).

188. Chatterji, D., and Smith, J. V., J. Electrochem. Soc., 120, 770 (1973).
189. Predel, B., and Stein, D. W., J. Less-Common Metals, 17, 377 (1969).
190. Danilin, V. N., and Yatsenko, S. P., J. Appl. Chem. USSR, 41, 1396 (1968).
191. Zoller, H., Metall., 11, 378 (1957).
192. Clare, J. W. H., J. Inst. Metals, 86, 431 (1957/58).
193. Pusin, N. A., and Micic', O.D., Z. Anorg. Chem., 234, 233 (1937).
194. Shunk, F. A., in Constitution of Binary Alloys, Second Supplement, McGraw-Hill Book Company, New York (1969).
195. Jenckel, E., Z. Metallkunde, 26, 249 (1934).
196. Lee, Y. K., and Yazawa, A., J. Japan Inst. Metals, 33, 323 (1969).
197. Batalin, G. I., Fesenko, P. L., Geskina, Zh. Ya., Ryabokon, L. I., and Novostroinyi, S. V., Russ. J. Phys. Chem., 45, 1103 (1971).
198. Predel, V. B., and Schallner, U., Z. Metallkde, 60, 869 (1969).
199. Eslami, H., de Franceschi, J., Gambino, M., and Bros, J. P., Z. Naturforsch, 34, 810 (1979).
200. Svirbely, W. J., and Selis, S. M., J. Phys. Chem., 42, 33 (1954).
201. Denny, J. P., Hamilton, J. H., and Lewis, J. R., Trans. AIME, 194, 39 (1952).
202. French, S. J., Saunders, D. J., and Ingle, G. W., J. Phys. Chem., 42, 265 (1937).
203. Heubner, U., and Wincierz, P., Metall., 20, 703 (1966).
204. Hayes, F. H., and Kubaschewski, O., J. Inst. Metals, 97, 381 (1969).
205. Rao, M. V., and Tiller, W. A., J. Mat. Sci., 7, 14 (1972).
206. Bros, J. P., Compt. Rend. C., 263, 977 (1966).

207. Bross, J. P., Castanet, R., and Laffite, M., *Compt. Rend. C.*, 264, 184 (1967).
208. Klinedinst, K. A., Rao, M. W., and Stevenson, D. A., *J. Electrochem. Soc.*, 119, 1261 (1972).
209. Pong, R., and Donaghey, L. F., *J. Chem. Eng. Data*, 21, 370 (1976).
210. Svirbely, W. J., and Read, S. M., *J. Phys. Chem.*, 66, 658 (1962).
211. Macur, G. J., Edwards, R. K., and Wahlbech, P. G., *J. Phys. Chem.*, 72, 1047 (1968).
212. Massart, G., Durand, F., and Bonnier, E., *Compt. Rend.*, 262, 185 (1966).
213. Predel, B., *Z. Metallk.*, 56, 791 (1965).
214. Campbell, A. N., and Wagemann, R., *Can. J. Chem.*, 14, 657 (1966).
215. Wittig, F. E., and Keil, G., *Z. Metallkde*, 54, 576 (1963).
216. Raub, E., and Engel, M., *Z. Metallkde*, 37, 148 (1946).
217. Valentiner, S., and Puzieha, I., *Z. Metallforsch.*, 2, 127 (1947).
218. Skjold-Jørgensen, S., Rasmussen, P., and Fredenslund, A., *Chemical Engineering Science*, 35, 2389 (1980).
219. Hanks, R. W., O'Neill, T. K., and Christensen, J. J., *Ind. Engng. Chem. Proc. Des. Dev.*, 18, 408 (1979).
220. Meyer, S. L., in *Data Analysis for Scientists and Engineers*, John Wiley & Sons, Inc., New York (1975).
221. Koster, W., and Thoma B., *Z. Metallk.*, 46, 293 (1955).
222. Burdijan, I. I., and Borshevskii, A. S., *Zh. Tekn. Fiz.*, 28, 2684 (1958).
223. Miller, J. F., Goering, H. L., and Himes, R. C., *J. Electrochem. Soc.*, 107, 527 (1960).
224. Borshevskii, A. S., Burdijan, I. I., Lubenskaya, E. Yu., and Sokolova, E. V., *Russ. J. Inorg. Chem.*, 4, 1306 (1959).
225. Aulombard, R. L., and Joullie, A., *Mat. Res. Bull.*, 14, 349 (1979).

226. Gerdes, F., and Predel, B., J. Less-Common Metals, 64, 285 (1979).
227. Goryunova, N. A., in The Chemistry of Diamond Like Semiconductors, MIT Press, Cambridge, Ma. (1965).
228. Wooley, J. C., and Smith, B. A., Proc. Phys. Soc., 72, 214 (1958).
229. Wooley, J. C., Smith, B. A., and Lees, D. G., Proc. Phys. Soc., 69B, 1339 (1956).
230. Wooley, J. C., and Lees, D. G., J. Less-Common Metals, 1, 192 (1959).
231. Ufimtsev, V. B., Timoshin, A. S., and Kostin, G. V., Neorg. Mat., 7, 2090 (1971).
232. Gorshkov, I. Ye., and Goryunova, N. A., Zh. Neorg. Khim, 3, 668 (1958).
233. Blom, G. M., and Plaskett, T. S., J. Electrochem. Soc., 118, 1831 (1971).
234. Chang, K. M., Coughanowr, C. A., and Anderson, T. J., accepted to Chem. Eng. Comm. (1985).
235. Ansava, I., Gambino, M., and Bros, J. P., J. Crystal Growth, 32, 101 (1976).
236. Vecher, A. A., Voronova, F. I., Mechkovskii, L. A., and Skoropanov, A. S., Russ. J. Phys. Chem., 48, 584 (1974).
237. Mechkovskii, L. A., Savitskii, A. A., Skums, V. F., and Vecher, A. A., Russ. J. Phys. Chem., 45, 1143 (1971).
238. Cho, S. A., Z. Metallk., 67, 479 (1976).
239. Steininger, J., J. Appl. Phys., 41, 2713 (1970).
240. Osamura, K., Nakajima, K., and Murakami, Y., J. Jap. Inst. Metals, 36, 744 (1972).
241. Kuznetsov, V. V., and Sorokin, V. S., Russ. J. Inorg. Mat., 16, 1417 (1980).
242. Kuhn, G., and Leonhardt, A., Kristall und Technik, 7, K57 (1972).
243. Nebauer, E., and Schneider, M., Phys. Stat. Sol. (a), 23, 485 (1974).

244. Bublik, V. T., Karman, M. B., Kleptsin, V. F., and Leikin, V. M., *Phys. Stat. Sol. (a)*, 32, 631 (1975).
245. Fedders, P. A., and Muller, M. W., *J. Phys. Chem. Solids*, 45, 685 (1984).
246. Mikkelsen, J. C., *J. Electrochem. Soc.*, 132, 500 (1985).
247. Marbeuf, A., and Guillaume, J. C., *Revue Phys. Appl.*, 19, 311 (1984).
248. Bedair, S. M., *J. Electrochem. Soc.*, 122, 1150 (1975).
249. Yordanova, I., Pramatarova, L., and Tretyakov, D., *Crystal Research and Technology*, 16, 46 (1981).
250. Gontcharova, T. S., Konnikov, S. G., Riabtsev, N. G., Tret'yakov, D. N., and Alexandrova, T. P., *Izv. Vyssh. Ucheb. Zaved. Fiz.*, 16, 146 (1973).
251. Antypas, G. A., *J. Crys. Growth*, 16, 181 (1972).
252. Miki, H., Segawa, K., Otsubo, M., Shirahata, K., and Fujibayashi, K., *Jap. J. App. Phys.*, 17, 2079 (1978).
253. Sonomura, H., Nishimura, T., and Miyauch, T., *Phys. Stat. Sol. (a)*, 61, K51 (1980).
254. Auvergne, D., Gamassel, J., Mathieu, H., and Joullie, A., *J. Phys. Chem. Solids*, 35, 133 (1974).
255. Woolley, J. C., in *Compound Semiconductors*, eds. R. K. Willardson and H. L. Goering, Reinhold, New York (1962).
256. Zbitnew, K., and Woolley, J. C., *J. Appl. Phys.*, 52, 6611 (1981).
257. Casey, H. C., Jr., and Panish, M. B., in *Heterostructure Lasers*, Academic Press, New York (1978).
258. Heus, R. J., and Egan, J. J., *Z. Phys. Chem.*, 49, 38 (1966).
259. Aronson, S., and Auskern, A., *Thermodynamics*, IAEA, Vienna, 1, 165 (1965).
260. Aronson, S., *AIME*, 10, 247 (1964).
261. Gingerich, K. A., and Aronson, S., *J. Phys. Chem.*, 70, 2517 (1966).
262. Benz, R., and Wagner, C., *J. Phys. Chem.*, 65, 1308 (1961).

263. Aronson, S., J. Inorg. Nucl. Chem., 29, 1611 (1967).
264. Samokhval, V. V., and Vetcher, A. A., Zh. Fiz. Khim., 42, 644 (1968).
265. Ure, R. W., J. Chem. Phys., 26, 1363 (1957).
266. Hinze, J. W., and Patterson, J. W., J. Electrochem. Soc., 120, 96 (1973).
267. Rapp, R. A., and Shores, D. A., in Physicochemical Measurements in Metal Research, 4(Part 2), ed. R. A. Rapp, Interscience, New York, 123 (1970).
268. Hladik, J., ed., in Physics in Electrolytes, Academic Press, London (1972).
269. Subbarao, E. C., ed., in Solid Electrolytes and Their Applications, Plenum Press, New York (1980).
270. Ramanarayanan, T. A., Narula, M. L., and Worrell, W. L., J. Electrochem. Soc., 126, 1360 (1979).
271. Chou, S. F., and Rapp, R. A., J. Electrochem. Soc., 130, 506 (1983).
272. Lehovic, K., and Broder, J., J. Electrochem. Soc., 101, 208 (1954).
273. Mrgudich, J. N., J. Electrochem. Soc., 107, 475 (1960).
274. Richardson, F. D., and Jeffes, J. H. E., J. Iron Steel Inst., 160, 261 (1948).
275. Coughlin, J. P., U.S. Bureau of Mines Bull. 542 (1954).
276. Pankyatz, L. B., and Kelley, K. K., U.S. Bureau of Mines Rep. Invest. 6198 (1963).
277. Yokokawa, T., and Kleppa, O. J., J. Phy. Chem., 68, 3246 (1964).
278. Holley, C. E., and Huber, E. J., J. Amer. Chem. Soc., 73, 5577 (1951).
279. Mah, A. D., J. Phys. Chem., 61, 1572 (1957).
280. Stull, D. R., and Prophet, H., in JANAF Thermochemical Tables, NSRDS-NBS 37, U.S. Bureau of Standards, Washington, D.C. (1971); Revised (1976).

281. Yokokawa, T., and Kleppa, O. J., J. Phys. Chem., 68, 3246 (1964).
282. Snyder, P. E., and Seltz, H., J. Amer. Chem. Soc., 67, 683 (1945).
283. Schneider, A., and Gattow, G., Z. Anorg. Allg. Chem., 277, 40 (1954).
284. Ghosh, D., and Kay, D. A. R., J. Electrochem. Soc., 124, 1836 (1977).
285. Berthelot, M., Ann. Chim. Phys., 22, 479 (1901).
286. Wartenberg, H., and Witzel, G., Z. Electrochem., 25, 209 (1919).
287. Moose, J. E., and Parr, S. W., J. Am. Chem. Soc., 46, 2656 (1924).
288. Roth, W. A., and Muller, F., Z. Phys. Chem., A144, 253 (1929).
289. Meichsuer, A., and Roth, W. A., Z. Electrochem., 40, 19 (1934).
290. Roth, W. A., Wolf, U., and Fritz, O., Z. Electrochem., 46, 42 (1940).
291. Glemser, O., and Schroder, H., Z. Anorg. Allg. Chem., 271, 293 (1953).
292. Karapet'yants, M. K., and Karapet'yants, M. L., in Fundamental Thermodynamic Constants of Inorganic and Organic Compounds, Izd. Khimiya, Moscow (1968).

BIOGRAPHICAL SKETCH

Kow-Ming Chang was born on July 1, 1954, in Kaohsiung, Taiwan, Republic of China. After graduating from the Tainan Second Senior High School in Tainan, Taiwan, he attended National Central University in Chung-Li, Taiwan, in September, 1973. In June, 1977, he received the degree of Bachelor of Science in chemical engineering.

On completion of his military service in the Chinese Army, he went back to N.C.U., and served as a full time teaching assistant for a year. Kow-Ming joined the graduate program at the University of Florida in September, 1980, and received the Master of Science degree in August, 1981. He continued his work toward the Ph.D. in Chemical Engineering under the direction of T.J. Anderson.

After graduation, Kow-Ming is going to National Chiao Tung University in Hsin-Chu, Taiwan, to be an assistant professor in the Department of Electrons Engineering and Institute of Electronics and in the Department of Applied Chemistry. His research interests include electrochemical technology, semiconductor process technology, semiconductor physics and devices theory, and mathematic modelling.

His hobbies include gardening, fishing, camping, badminton, and volleyball. He is married to Yu-Fen Chang and has a daughter, Jennifer, born July 14, 1984. He is a member of Phi Tau Phi, the Electrochemical Society, AIChE, AAAS, and ACS.

I certify that I have read this study and that in my opinion it conforms to acceptable standards of scholarly presentation and is fully adequate, in scope and quality, as a dissertation for the degree of Doctor of Philosophy.

Timothy J. Anderson

Timothy J. Anderson, Chairman
Associate Professor of Chemical
Engineering

I certify that I have read this study and that in my opinion it conforms to acceptable standards of scholarly presentation and is fully adequate, in scope and quality, as a dissertation for the degree of Doctor of Philosophy.

Lewis E. Johns

Lewis E. Johns
Professor of Chemical Engineering

I certify that I have read this study and that in my opinion it conforms to acceptable standards of scholarly presentation and is fully adequate, in scope and quality, as a dissertation for the degree of Doctor of Philosophy.

John P. O'Connell

John P. O'Connell
Professor of Chemical Engineering

I certify that I have read this study and that in my opinion it conforms to acceptable standards of scholarly presentation and is fully adequate, in scope and quality, as a dissertation for the degree of Doctor of Philosophy.

Robert T. Dehoff

Robert T. Dehoff
Professor of Materials Science
and Engineering

This dissertation was submitted to the Graduate Faculty of the College of Engineering and to the Graduate School, and was accepted as partial fulfillment of the requirements for the degree of Doctor of Philosophy.

December, 1985

Herbert A. Bawi
Dean, College of Engineering

Dean, Graduate School